Reactive Poly(ionic liquid)s (PILs) and Nanostructures from PIL-based Block Copolymers

Paul Coupillaud

THÈSE EN COTUTELLE PRÉSENTÉE

POUR OBTENIR LE GRADE DE

DOCTEUR DE

L'UNIVERSITÉ DE BORDEAUX

AND THE BASQUE COUNTRY UNIVERSITY

ÉCOLE DOCTORALE DES SCIENCES CHIMIQUES UBX

SPÉCIALITÉ: POLYMÈRES

Par Paul COUPILLAUD

Reactive Poly(ionic liquid)s (PILs) and Nanostructures from PIL-based Block Copolymers

Sous la direction de : Prof. Daniel TATON et Prof. David MECERREYES

Soutenue le 20 novembre 2014

Membres du jury :

M. HADZIIOANNOU, Georges	Professeur, Université de Bordeaux	Président
M. VIDAL, Frédéric	Professeur, Université de Cergy-Pontoise	rapporteur
M. BOUTEILLER, Laurent	Professeur, Université Pierre et Marie Curie	rapporteur
M. DROCKENMULLER, Éric	Professeur, Université Lyon 1	Examinateur
M. MECERREYES, David	Professeur, University of the Basque Country	Directeur de thèse
M. TATON, Daniel	Professeur, Université de Bordeaux	Directeur de thèse

AVANT-PROPOS

Les travaux de thèse décrits dans ce manuscrit ont été effectués dans le cadre d'une cotutelle internationale entre l'université de Bordeaux et l'université du Pays Basque à Saint-Sébastien en Espagne. Une grande partie du travail a été effectué au Laboratoire de Chimie des Polymères Organiques (LCPO, Pessac, France) sous la direction du Prof. D. Taton. Plus ponctuellement, quelques séjours ont été effectués au laboratoire POLYMAT en Espagne, sous la supervision du Prof. D. Mecerreyes. Cette thèse a été financée par le Ministère de l'Enseignement Supérieur et de la Recherche Français sur une durée de 3 ans (01/10/11-30/09/14).

Ce manuscrit est composé de trois chapitres et a été entièrement rédigé en anglais. L'objectif de cette thèse a été de développer des polymères liquides ioniques réactifs (PILs en anglais) et des nanostructures issues de l'auto-assemblage de copolymères à blocs dérivés.

Le chapitre 1 présente un état de l'art des polymères liquides ioniques à base d'unités imidazolium en général et, de manière plus approfondie, décrits les différents copolymères à blocs contenant un tel bloc PIL. Leurs voies de synthèse, leurs propriétés d'auto-assemblage en masse et en solution, ainsi que leurs applications potentielles sont discutées en détail.

Le chapitre 2 décrit la synthèse de nouveaux PILs de type imidazolium et leur utilisation comme précurseurs à la fois à des fins de catalyse organique et pour la modification chimique par post-polymérisation.

Le chapitre 3 concerne le développement d'une nouvelle famille de copolymères à blocs contenant un bloc PIL de type imidazolium par polymérisation radicalaire contrôlée fondée sur une chimie à base de complexes de cobalt (CMRP en anglais). La capacité à s'auto-assembler de tels copolymères à blocs, en masse comme en solution pour diverses applications potentielles, seront discutées.

PUBLICATIONS

P. Coupillaud, J. Vignolle, D. Mecerreyes, D. Taton. "Post-polymerization Modification and Organocatalysis using Reactive Statistical Poly(Ionic Liquid)-Based Copolymers." *Polymer* **2014**, *55*, 3404.

P. Coupillaud, D. Kuzmicz, Y. Men, J. Vignolle, G. Vendraminetto, M. Ambrogi, D. Taton, J. Yuan. "Mesoporous poly(ionic liquid)-based copolymer monoliths: from synthesis to catalysis and microporous carbon production." *Polymer* **2014**, *55*, 3423.

A. Panniello, C. Ingrosso, P. Coupillaud, M. Tamborra, E. Binetti, M-L. Curri, D. Taton, M. Striccoli. "A novel nanocomposite based on luminescent colloidal nanocrystals and polymeric ionic liquids towards optoelectronic applications." *Materials* **2014**, *7*, 591.

P. Coupillaud, M. Fèvre, A-L. Wirotius, K. Aissou, G. Fleury, A. Debuigne, C. Detrembleur, D. Mecerreyes, J. Vignolle, D. Taton. "Precision Synthesis of Poly(Ionic Liquid)-Based Block Copolymers by Cobalt-Mediated Radical Polymerization and Preliminary Study of Their Self-Assembling Properties." *Macromol. Rapid Comm.* **2013**, *35*, 422.

P. Coupillaud, J. Pinaud, N. Guidolin, J. Vignolle, M. Fèvre, E. Veaudecrenne, D. Mecerreyes, D. Taton. "Poly(ionic liquid)s based on imidazolium hydrogen carbonate monomer units as recyclable polymer-supported *N*-heterocyclic carbenes: Use in organocatalysis." *J. Polym. Sci. Part. A. Polym. Chem.* **2013**, *51*, 4530.

M. Fèvre, P. Coupillaud, J. Vignolle, D. Taton. "Imidazolium Hydrogen Carbonates *Versus* Imidazolium Carboxylates as Organic Pre-catalysts for Room Temperature *N*-Heterocyclic Carbene-Catalyzed Reactions." *J. Org. Chem.* **2012**, *77*, 10135.

C. Detrembleur, A. Debuigne, M. Hurtgen, C. Jérome , J. Pinaud, M. Fèvre, P. Coupillaud, J. Vignolle, D. Taton. "Synthesis of 1-Vinyl-3-Ethylimidazolium-Based Ionic Liquid (Co)polymers by Cobalt-Mediated Radical Polymerization." *Macromolecules* **2011**, *43*, 6397.

BOOK CHAPTER

P. Coupillaud, D. Taton "Imidazolium-Based Poly(ionic Liquid) Block Copolymers" in *Handbook of Ionic Liquids&Polymers*, Editor-in-chief: D. Mecerreyes, Springer, Heidelberg, 2014, *in press*.

TABLE OF CONTENTS

Chapter 2. Poly(ionic liquid)s (PILs): Reactive Platforms for a use in Organocatalysis and Post-polymerization Modification

Chapter 3. Poly(ionic liquid)-based Block Copolymers by Cobalt-Mediated Radical Polymerization: Synthesis, Self-Assembly and Applications

Titre : Polymères Liquides Ioniques (PIL) Réactifs et Nanostructures à Partir de Copolymères à Blocs Composés d'un Bloc PIL

Résumé : Au cours de la dernière décennie, la combinaison des propriétés singulières des liquides ioniques moléculaires (conductivité ionique, stabilité thermique, solubilité modulable et stabilité chimique) avec les propriétés intrinsèques des polymères (formation de films, possibilités de former des assemblages à l'échelle mésoscopique) a permis un développement croissant des polymères liquides ioniques (PILs en anglais). Les PILs sont caractérisés par la présence d'un groupement chargé sur chaque unité monomère liée au squelette polymère, formant une structure macromoléculaire. Ils peuvent être aussi bien des polycations, combinés à des contre-anions mobiles, que des polyanions avec un contre-cation mobile sur chaque unité monomère ; des polyzwitterions portants un anion et un cation sur leur structure, avec divers contre-ions représentent également une autre catégorie de PILs.

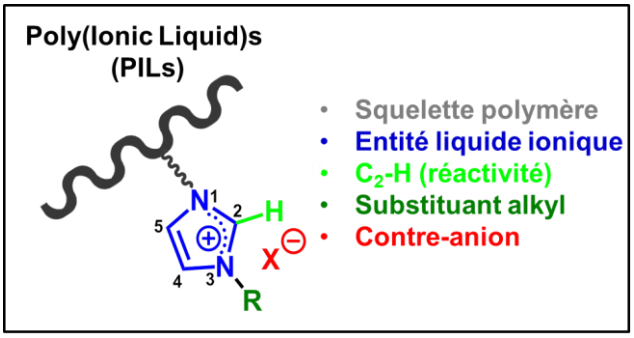

Dans la large gamme de PIL, un réel intérêt a été porté aux PILs contenant l'entité imidazolium. L'objectif de ce travail de thèse a été de développer l'ingénierie des polymères liquides ioniques (PILs) de type imidazolium ainsi qu'une nouvelle famille de copolymères à blocs apparentés.

Des PILs type imidazolium ont été utilisés en tant que polymères réactifs pour la catalyse organique et la modification chimique par post-polymérisation.[1-3] Divers composés (homopolymères, copolymères statistiques de type styrénique, polymères réticulés) stables à

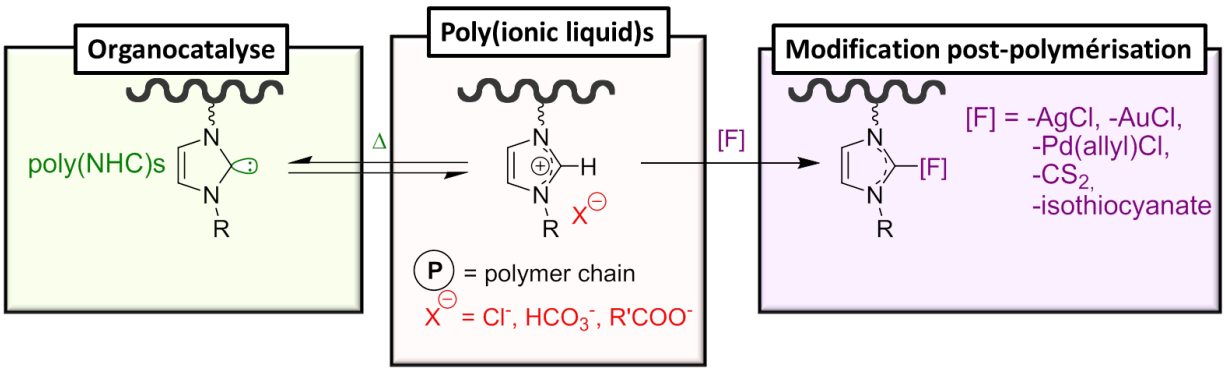

l'air, portant divers contre-anions (bromures, hydrogénocarbonates, carboxylates), ont été spécialement conçus *via* des stratégies de synthèse relativement simples. La génération de

carbènes *N*-hétérocycliques supportés sur polymères (poly(NHC)s) a permis de comparer les performances catalytiques de tous ces précurseurs à travers des réactions de référence de la catalyse organique. Spécifiquement, les copolymères statistiques type styrénique peuvent également être fonctionnalisés de manière stœchiométrique par post-polymérisation avec différents substrats électrophiles (*e.g.* CS_2, isothiocyanate, métaux de transition).

Une nouvelle famille de copolymère à blocs contenant un bloc poly(acétate de vinyle) et un bloc de type poly(bromure de *N*-vinyl-3-alkylimidazolium), a été synthétisé par « Cobalt Mediated Radical Polymerization » (CMRP).[4-5] La capacité de ces composés à s'auto-assembler en diverses mésostructures en masse comme en solution a ensuite été démontrée. Des mesures de conductivité ionique ont montré l'influence de la préparation des échantillons et des conditions de mesures sur les valeurs obtenues. Le comportement en solution par la réactivité ionique du bloc PIL et la modification chimique du bloc hydrophobe poly(acétate de vinyle) en hydrophile poly(alcool vinylique) ont permis la formation de différentes nanostructures micellaires pour la synthèse de nanoparticules d'or *via* l'utilisation d'un contre-anion jouant le rôle de réducteur.

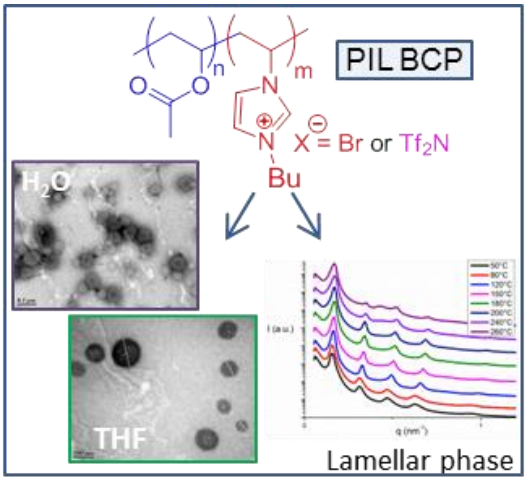

Ce travail de thèse ouvre de nombreuses perspectives pour ces PILs type imidazolium réactifs et leurs copolymères à bloc apparentés *via* l'exploitation de la réactivité de l'entité imidazolium et la modularité des nombreux paramètres tels que la structure chimique du polymère, le substituant alkyl et le contre-anion.

Mots clés : Polymères liquides ioniques, Copolymères à blocs, Imidazolium, catalyse organique, Modification post-polymérisation, Auto-assemblage, Conductivité ionique, nanoparticules d'or.

Références

[1]P. Coupillaud, J. Pinaud, N. Guidolin, J. Vignolle, M. Fèvre, E. Veaudecrenne, D. Mecerreyes, D. Taton *J. Polym. Sci. Part. A. Polym. Chem.* 2013, *51*, 4530.
[2]P. Coupillaud, J. Vignolle, D. Mecerreyes, D. Taton *Polymer* 2014, *55*, 3404.
[3]P. Coupillaud, D. Kuzmicz, Y. Men, J. Vignolle, G. Vendraminetto, M. Ambrogi, D. Taton, J. Yuan *Polymer* 2014, *55*, 3423.
[4]C. Detrembleur, A. Debuigne, M. Hurtgen, C. Jérome , J. Pinaud, M. Fèvre, P. Coupillaud, J. Vignolle, D. Taton *Macromolecules* 2011, *43*, 6397.
[5]P. Coupillaud, M. Fèvre, A-L. Wirotius, K. Aissou, G. Fleury, A. Debuigne, C. Detrembleur, D. Mecerreyes, J. Vignolle, D. Taton *Macromol. Rapid Comm.* 2013, *35*, 422.

List of Abbreviations

ADMET: acyclic diene metathesis polymerization
AIBN: Azobis(2-methylpropionitrile)
AN: acrylonitrile
ATRP: atom transfer radical polymerization
BCP: block copolymer
C/LP: controlled/living polymerization
CMRP: cobalt-mediated radical polymerization
CNT: carbon nanotube
$Co(acac)_2$: *bis*(acetylacetonato)cobalt(II)
coPIL: copoly(ionic liquid)
CTA: chain transfer agent
~~*Đ*~~: dispersity
DLS: dynamic light scattering
DMAPN: Dimethylaminopropionitrile
DMF: dimethyl formamide
DMSO: dimethyl sulfoxide
DOSY: diffusion ordered spectroscopy
DSC: differential scanning calorimetry
DT: degenerative transfer
EIS: electrochemical impedance spectroscopy
Et_2O: diethyl ether
FRP: free radical polymerization
FTIR: Fournier transform infrared spectroscopy
GISAXS: grazing-incidence small-angle X-ray scattering
Hex: hexagonal compact cylinder
HMA: hexylmethacrylate
I: initiator
IL: ionic liquid
$KHCO_3$: potassium hydrogen carbonate
KHMDS: Potassium bis(trimethylsilyl)amide
KPF_6: potassium hexafluorophosphate
KPS: potassium persulfate
Lam: Lamellar
LiTFSI: lithium bis(trifluorosulfonyl) imide
MALDI-ToF: matrix-assisted laser desorption ionization time-of-flight
M_n: number average molar mass
$NaBF_4$: sodium tetrafluoroborate
$NaBH_3CN$: sodium cyanoborohydride
NHC: *N*-heterocyclic carbene
NHC-CO_2: azolium-2-carboxylate
[NHC(H)][HCO_3]: azolium hydrogen carbonate
NMP: nitroxide mediated polymerization
NMR: nuclear magnetic resonance
P2VP: poly(2-vinylpyrridine)
PAm: polyacrylamide
PANI: polyaniline
PBuA: poly(*n*-butyl acrylate)

PBuMa: poly(*n*-butyl methacrylate)
PDMA: poly(*N,N*-dimethylacrylamide)
PEDOT: poly(3,4-ethylenedioxythiophene)
PEO: poly(ethylene oxide)
PHMAm: poly(histaminemethacrylamide)
PIL: poly(ionic liquid)
PILPN: poly(ionic liquid)-based porous network
PMAA: poly(methacrylic acid)
PMMA: poly(methyl methacrylate)
PNIPAM: poly(*N*-isopropylacrylamide)
Poly(NHC): poly(*N*-heterocyclic carbene)
Poly(NHC-CO_2): poly(*N*-heterocyclic carbene-carboxylate) adduct
Poly[NHC(H)][HCO_3]: poly(*N*-vinyl-3-alkylimidazolium hydrogen carbonate)
PPO: poly(propylene oxide)
PPy: polypyrrole
PS: poly(styrene)
P(STFSILi): poly(4-styrenesulfonyl (trifluoromethylsulfonyl) imide lithium)
PVA: poly(vinyl alcohol)
PVAc: poly(vinyl acetate)
PVBnCl: poly(4-vinylbenzyl chloride)
PVRImBr: poly(*N*-vinyl-3-alkylimidazolium bromide)
P(VDF-HFP): poly(vinylidene fluoride-*co*-hexafluoropropylene)
RAFT: reversible addition fragmentation chain transfer
RCOOK: potassium carboxylate
RDRP: reversible deactivation radical polymerization
RH: relative humidity
R_H: hydrodynamic radius
ROMP: ring-opening mediated polymerization
RT: room temperature
SANS: small-angle neutron scattering
SAXS: small-angle X-ray scattering
SEC: size exclusion chromatography
*t*BuOK: potassium *tert*-butoxide
TEM: transmission electron microscopy
TEMPO: 2,2,6,6-tetramethylpiperidine-1-oxyl
TFSI: bis(trifluorosulfonyl) imide
T_g: glass transition temperature
TGA: thermogravimetric analysis
THF: tetrahydrofuran
TMSCN: trimethylsilyl cyanide
TOF: turnover frequency
UV: ultraviolet
V-501: 4,4'-Azobis(4-cyanovaleric acid)
V-70: 2,2'-azobis(4-methoxy-2,4-dimethyl valeronitrile)
VAc: vinyl acetate
VFT: Vogel-Fulcher-Tammann
VIm: *N*-vinylimidazole
WL: weight loss
XRD: X-ray diffraction

General Introduction

Ionic liquids (ILs) are organic or inorganic salts possessing a melting point generally lower than 100 °C and that are characterized by a high chemical and thermal stability, a negligible volatility and inflammability, a high CO_2 permeability, an adjustable solubility, and a high ionic conductivity. Due to these specific properties, ILs have been regarded as organic green solvents, but they have been expanded to an increasing number of applications in various areas such as catalysis, electrochemistry, organic and polymer synthesis, energy, nano- and biotechnology. In the past decade, ILs have been introduced as true building blocks into polymeric structures, leading to a unique class of polyelectrolytes referred to as "poly(ionic liquid)s", also called "polymerized ionic liquids" (PILs).[1–6]

PILs are attracting an increasing interest by combining the inherent features of ILs mentioned above, with specific properties of polymers, such as mechanical stability, film formation and processability.

PILs are characterized by the presence of charged groups in each monomer unit connected to a polymeric backbone, forming a macromolecular structure. PILs can be either polycations, *i.e.* carrying a cation in their backbone, and a mobile counter-anion, or polyanions with fixed anionic monomer unit and a mobile counter-cation; polyzwitterions carrying both an anion and a cation in their structure, with various counterions, represents another category of PILs.

In the wide PIL range, those based on the imidazolium moiety have received an increasing attention in the past two decades. In this context, our group at LCPO, in collaboration with D. Mecerreyes at POLYMAT in San–Sebastian, designed well-defined imidazolium-based PILs and related block copolymers (BCPs). To this end, the reversible addition fragmentation chain transfer (RAFT) polymerization of methacrylamido- or methacrylate IL-type monomers was employed. These PIL BCPs could be further manipulated and made to self-assemble in a selective solvent into a variety of micelle-like structures, by exchanging the bromide (Br^-) counter-anion of PIL blocks for bis(trifluorosulfonyl) imide ($(CF_3SO_2)_2N^-$).[7,8]

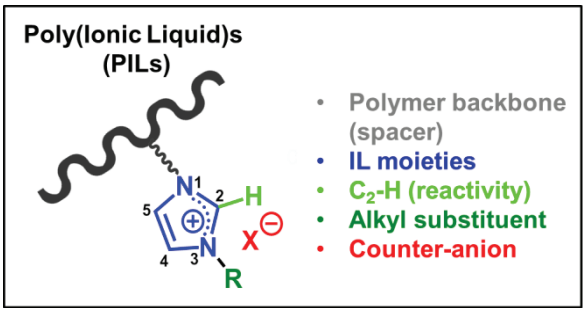

In a subsequent work at LCPO, PILs deriving from *N*-vinyl-3-alkylimidazolium bromide monomers were shown to serve as recyclable precursors of polymer-supported *N*-heterocyclic carbenes, referred as poly(NHC)s.[9]

In this PhD thesis, we propose new innovations in this field of engineered PILs. The main aim of this work is to expand the scope of the imidazolium-based PILs, by exploiting, the intrinsic reactivity of the C_2-H group of the imidazolium moiety for organocatalysis and for post-chemical modification. Secondly, a new class of PIL BCPs consisting of *N*-vinyl-3-alkylimidazolium units has been also developed by a particular controlled radical polymerization named cobalt-mediated radical polymerization (CMRP). Investigations into the self-assembling properties both in solution and at the solid state of these PIL BCPs are also described.

Chapter 1 is an overview of imidazolium-based PILs, with a special focus on PIL BCPs including related synthetic strategies and identification of nanostructures formed by self-assembly in bulk or in solution. Potential applications of PILs and PIL BCPs will be also briefly discussed.

Chapter 2 describes the use of the imidazolium-based PILs as true reactive polymers for organocatalysis, in the one hand, and, on the other hand, for post-chemical modification.

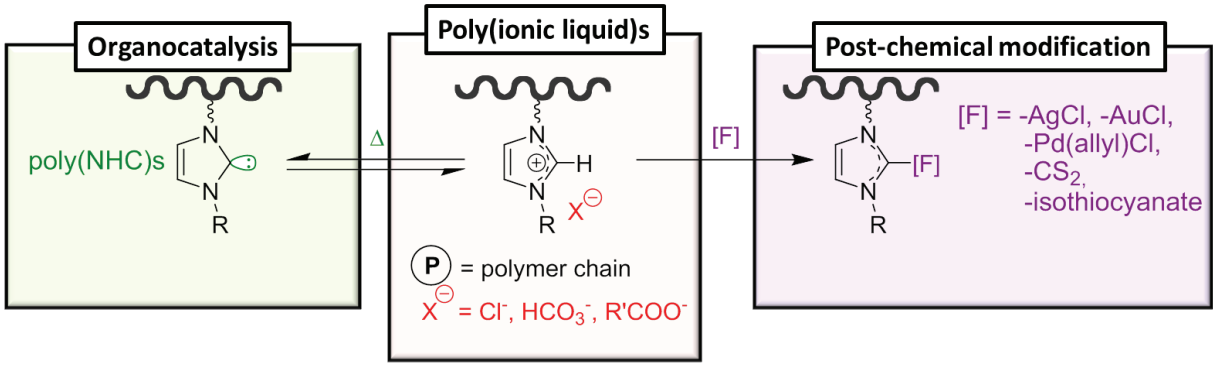

Miscellaneous PIL derivatives featuring various counter-anions (*e.g.* Br^-, HCO_3^-, $R'COO^-$), including homopolymers, statistical copolymers of styrenic-type and crosslinked polymer networks have been specifically designed by free radical (co)polymerization, most often following simple synthetic strategies. The catalytic performances of these different (co)PILs will be first evaluated and compared in selected organocatalyzed reactions (*e.g.* benzoin condensation, transesterification, cyanosilylation, cycloaddition of carbon dioxide and propylene oxide) according to their polymer structure. In addition specific polystyrene-based coPILs have been derivatized by post-chemical modification in presence of different

electrophilic substrates (*e.g.* CS_2, isothiocyanates, or metallic complexes) which transforms, in each case, the PIL precursor into a new polymeric compound.

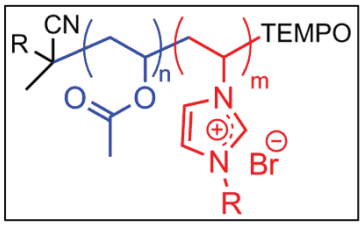

Chapter 3 is dedicated to the development of a novel family of imidazolium-based PIL BCPs, namely poly(vinyl acetate)-*b*-poly(*N*-vinyl-3-alkylimidazolium bromide)s. The synthesis can be readily achieved by sequential cobalt-mediated radical polymerization (CMRP). The ability of these compounds to self-assemble into various types of mesostructures, either at the solid state or in solution, is described in details. The ionic conductivity of some self-assembled compounds is presented. Interestingly, self-assembly can be manipulated not only thanks to the ionic responsiveness of the PIL block, but also by post-chemical modification of the PVAc block that can indeed be transformed into poly(vinyl alcohol) (PVA). Preliminary studies utilizing double hydrophilic block copolymer based on PVA and PIL with the cyanoborohydride counter-anions as copolymeric stabilizer and reducing agent to achieve gold nanoparticles in aqueous solution is also described.

References:

1. Green, O.; Grubjesic, S.; Lee, S.; Firestone, M. A. *Polym. Rev.* **2009**, *49*, 339–360.
2. Lu, J.; Yan, F.; Texter, J. *Prog. Polym. Sci.* **2009**, *34*, 431–448.
3. Green, M. D.; Long, T. E. *Polym Rev* **2009**, *49*, 291–314.
4. Mecerreyes, D. *Prog. Polym. Sci.* **2011**, *36*, 1629–1648.
5. Yuan, J.; Mecerreyes, D.; Antonietti, M. *Prog. Polym. Sci.* **2013**, *38*, 1009–1036.
6. Shaplov, A. S.; Lozinskaya, E. I.; Vygodskii, Y. S. In *Electrochemical Properties and Applications of Ionic Liquids*; A. A. J. Torriero; M. J. A. Shiddiky, Eds.; **2011**; pp. 203–298.
7. Vijayakrishna, K.; Jewrajka, S. K.; Ruiz, A.; Marcilla, R.; Pomposo, J. A.; Mecerreyes, D.; Taton, D.; Gnanou, Y. *Macromolecules* **2008**, *41*, 6299–6308.
8. Vijayakrishna, K.; Mecerreyes, D.; Gnanou, Y.; Taton, D. *Macromolecules* **2009**, *42*, 5167–5174.
9. Pinaud, J.; Vignolle, J.; Gnanou, Y.; Taton, D. *Macromolecules* **2011**, *44*, 1900–1908.

Chapter 1

Bibliographic Study: Imidazolium-based Poly(ionic liquid)s and Related Block Copolymers

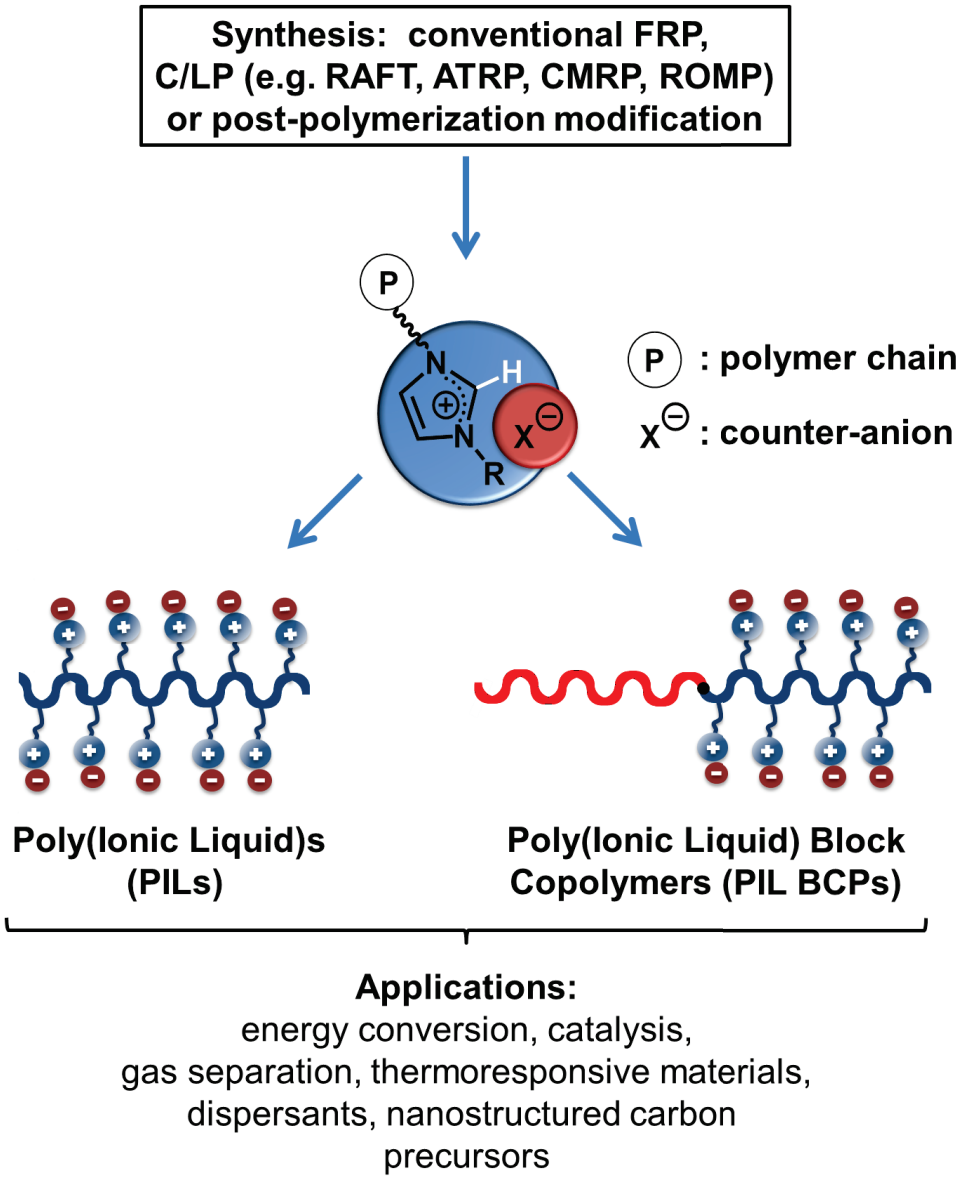

Keywords: Poly(ionic liquid)s, Block copolymers, Imidazolium, Polymerization, Self-assembly.

Abstract. Synthesis, physico-chemical properties and potential applications of imidazolium-based poly(ionic liquid) (PILs) block copolymers (BCPs) are described in this chapter. The first part gives a short introduction to the field of PILs that are a special class of polyelectrolytes characterized by the combined properties of ionic liquids (*e.g.* high chemical and thermal stability, negligible volatility and inflammability, high ionic conductivity) with those of polymer materials, such as processability, mechanical properties, film formation, etc. Synthetic strategies, including chain-growth polymerization –controlled or not-, step-growth polymerization and/or post-chemical modification of preformed polymers, are briefly discussed. Potential applications of PILs for energy, gas separation or for the preparation of nanostructured carbons are also highlighted.

The second part is specifically devoted to PIL BCPs that combine the specific properties of PILs, such as responsiveness to ion exchange, ionic conductivity and/or gas transport, with the self-assembling properties in solution or at the solid state of BCPs. A wide range of robust ionic nanostructured morphologies can thus be accessed. Synthetic strategies to PIL BCPs utilizing "controlled/living" polymerization methods and/or post-chemical modification of preformed copolymers, as well as their self-assembling properties in a selective solvent and in bulk are discussed. Finally, potential applications of this emerging class of ionic nanostructured materials, for instance, in energy conversion devices or in gas separation membranes, are highlighted.

This bibliographic chapter corresponds in large parts to the book chapter that will appear in "Handbook of ionic liquids&polymers", Editor-in-Chief: D. Mecerreyes, Springer, Heidelberg, 2014, in press.

Chapter 1.

Bibliographic Study : Imidazolium-based Poly(ionic liquid)s and Related Block Copolymers

Table of Contents

Introduction

Ionic liquids (ILs) are defined as organic/inorganic salts with a melting point lower than 100 °C. They are characterized by a high chemical and thermal stability, negligible volatility and inflammability, and a high ionic conductivity.[1–6] Originally, ILs have been used as organic solvents for green chemistry,[7] but they have been expanded to an increasing number of applications such as catalysis,[8] electrochemistry,[9,10] organic and polymer chemistry,[2,11] analytical chemistry,[12] energy,[13] nano-[14] and biotechnology.[15]

In the past decade, ILs have been also introduced as building blocks of polymeric structures, leading to a new class of polyelectrolytes, referred to as "poly(ionic liquid)s" (PILs), also called "polymerized ionic liquids" (Figure 1).[1–5,16]

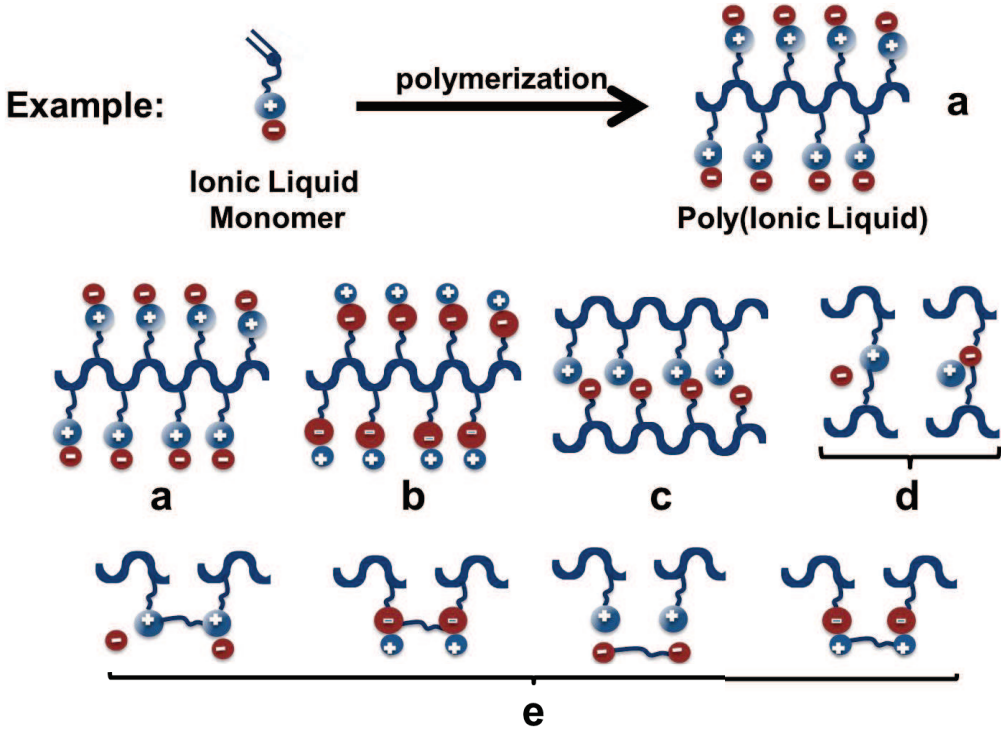

Figure 1. Illustration of poly(ionic liquid)s (PILs) and the five basic PIL structures.

PILs are attracting an increasing interest by combining inherent features of ILs, including thermal stability, high solid state ionic conductivity, high CO_2 permeability and adjustable solubility, with specific properties of polymers, such as film formation and processability. Initially, PILs appeared to play a purely complementary role towards the amplification of the IL functions, delivering performance that could not readily be afforded by ILs. For example, development of membranes for gas separation required the use of polymeric materials

providing mechanical properties and film formation, which proved of a high efficiency for CO_2 capture.[1–5]

Usual PIL chemical structures are illustrated in Figure 2. They include imidazolium **1**, 1,2,3-triazolium **2**, pyridinium **3**, tetraalkylammonium **4** or phosphonium **5** as cationic PILs, and perfluorosulfonyl imides **6**, sulfate cyanides **7**, sulfonates **8**, phosphonates **9** and carboxylates **10**, as anionic PILs, featuring various counterions. Synthesis, properties and applications of PILs have been reviewed by several groups in recent years.[1–6,16,17]

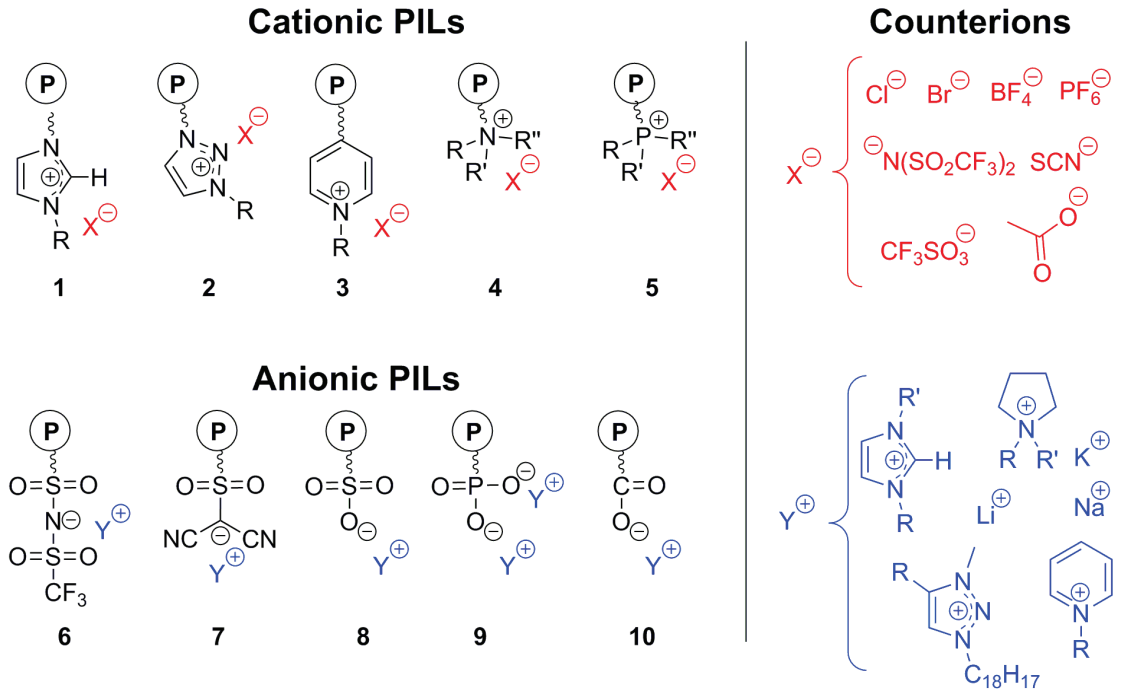

Figure 2. Classic PIL chemical structures and their counterions.

This chapter briefly covers recent achievements mainly regarding imidazolium-based PILs **1** (Figure 2), including their synthetic strategies and their potential applications. This will be followed by an overview of PIL block copolymers (PIL BCPs) based on the imidazolium (or pyridinium ring in one case), associated with various counter-anions. Synthetic strategies of PIL BCPs by controlled/living polymerization (C/LP), as well as their self-assembling properties both in solution and in bulk will be discussed. In contrast, BCPs that are issued from alkylation of tertiary amino-containing units, *i.e.* quaternization reaction of *e.g.* dialkylaminoethyl (meth)acrylate, will not be covered here; information regarding such materials can be found elsewhere.[18–20]

1. Poly(ionic liquid)s

1.1. Definition and main features

Although there is no clear definition of PILs, these polyelectrolytes are characterized by the presence of charged groups in each monomer repeating unit, connected through a polymeric backbone to form a macromolecular structure. An IL monomer is defined as an IL compound bearing a polymerizable group in its chemical structure (Figure 1). PILs can be of cationic-type, that is, a cationic moiety fixed to the polymer backbone with a mobile counter-anion of each monomer unit, or of anionic- or zwitterionic-type. In the latter case, the polymer backbone carries both a cationic and anionic functionality.

Different types of IL-based copolymers (random, alternating, block) and branched macromolecular architectures are potentially accessible. The number of PILs that can be derived is eventually high, due to all possible combinations between cations, anions and different polymer backbones and architectures. The five common forms of PIL are illustrated in Figure 1. These include polycations (Figure 1a), polyanions (Figure 1b), and crosslinked PIL network composed of polycations and polyanions (Figure 1c). IL monomer units can also be covalently linked by an alkyl chain spacer to form various crosslinked PIL networks (Figure 1d-e). Currently, IL monomers possessing a single polymerizable unit on the cation (Figure 1a) dominates the PIL research. In this chapter, we will mainly discuss PILs consisting of imidazolium cationic units (Figure 2, **1**).

In sharp contrast to regular polyelectrolytes, PILs can be made soluble not only in water, but also in polar organic solvents, depending on the anion/cation combination. Their solubility in organic solvents is due to the hydrophobic character of the constitutive counter-anions, and the reduced columbic interactions. Solubility of cationic PILs is indeed mainly governed by the anion that can be adjustable by the anion metathesis reaction (Scheme 1).

Additionally to hydrophilic halide anions (Cl^-, Br^-, I^-), hydrophobic anions can be introduced in PILs, which includes tetrafluoroborate (BF_4^-), hexafluorophosphate (PF_6^-), bis(perfluoroethylsulfonyl) imide ($(CF_3CF_2SO_2)_2N^-$) and bis(trifluoromethanesulfonyl) imide ($(CF_3SO_2)_2N^-$, also referred as TFSI or Tf_2N^-) which is a highly stable and a non-coordinating counter-anion.[21–23]

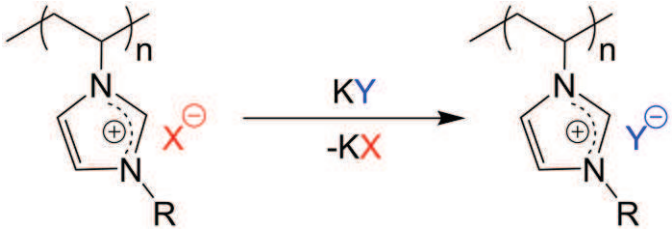

Scheme 1. Anion metathesis reaction on imidazolium-based PILs, here poly(*N*-vinyl-3-alkylimidazolium).

More generally, counterions play a crucial role in governing the physical properties of PILs. For instance, a broad range of values of the glass transition temperature (T_g) has been reported for PILs consisting of imidazolium units.[1–5] Contrary to "conventional" polyelectrolytes, PILs can exhibit a T_g as low as -60 °C.[24]

The question that can arise is can PILs be liquid compounds, like most of their IL counterparts? It turns out that PILs are most often amorphous, excepting some cases having liquid/fluidic properties at room temperature.[1–5,16] At the solid state, PILs can be easily manipulated for film formation *via* spin-coating, electrospinning or extrusion.

One major interest of PILs is their use as solid polymer electrolytes in energy application, by taking advantage of their rather high ion-conductivity.[16] Their polymeric character yet endows PILs with a low ion mobility, and a decrease of roughly 2-4 orders of magnitude between PILs and corresponding IL monomers (or molecules) has been reported.[1–5,16,25] For example, *N*-vinyl-3-ethylimidazolium bis(trifluoromethanesulfonyl) imide shows an ionic conductivity of 6 x 10^{-3} S.cm^{-1} and of 5 x 10^{-5} S.cm^{-1}, at 30 °C, before and after polymerization, respectively.[25,26] Hence, a proper balance has to be found to engineer PILs with an optimal ion conductivity. With a cationic polymer backbone, only the free counter-anion mobility is taken into account, and is limited by the interstitial space or free volume of polymeric chains.[4,25,27]

1.2. Synthetic strategies to imidazolium-based PILs

PIL synthesis is mainly achieved by direct chain growth polymerization of IL monomers, or by post-chemical modification of preformed polymers (Scheme 2). Imidazolium-based PILs can also be obtained by step-growth polymerization, as illustrated in route C, Scheme 2. These two synthetic strategies can be implemented by different polymerization techniques, such as conventional free- and "controlled/living" polymerization (reversible addition fragmentation chain transfer (RAFT),[28–31] atom transfer radical polymerization (ATRP),[32–34]

cobalt-mediated radical polymerization (CMRP),[35] nitroxide-mediated polymerization (NMP)[36] or ring-opening metathesis polymerization (ROMP)).[37]

Post-polymerization modification is typically carried out by quaternization between the *N*-alkylimidazole building block and a polymer carrying an alkyl halide handles (*e.g.* poly(4-vinylbenzyl chloride) (route B in Scheme 2).

Note that the determination by direct methods of both imidazolium-type PIL molar masses and dispersity in general, *e.g.* by size exclusion chromatography (SEC) or by matrix-assisted laser desorption ionization time-of-flight mass spectrometry (MALDI ToF), is most often inconclusive. This is due to interactions of these polyelectrolytes with SEC columns. Very recently, however, Matyjaszewski *et al.* proposed a "universal" method to analyze imidazolium-based PILs with TFSI counter-anions, by employing THF as eluent in presence of LiTFSI (*i.e.* the same anion) .[38]

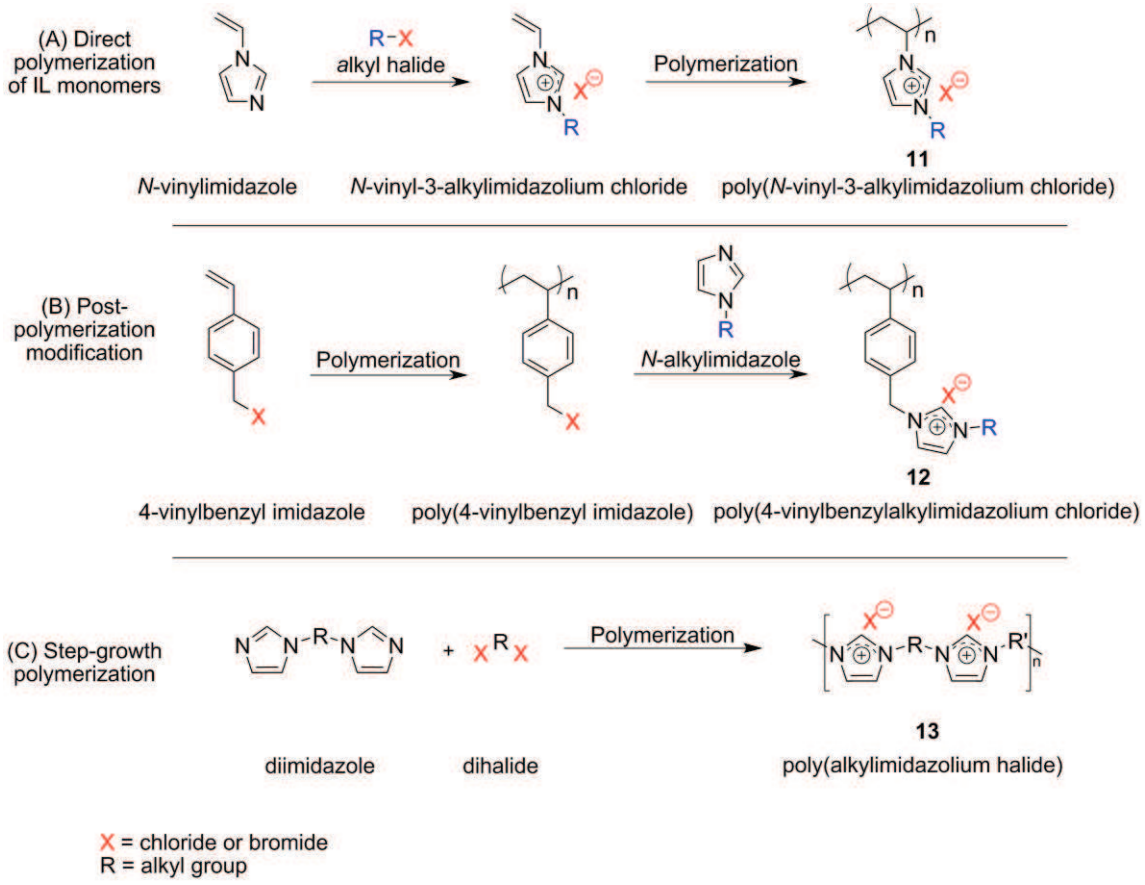

Scheme 2. Main synthetic strategies to imidazolium-based PILs.

Method A (Scheme 2) most often requires the synthesis (and purification) of the IL monomer prior to its polymerization. Post-chemical modification (method B, Scheme 2) can sometimes facilitate the control of the molecular weight of the polymer precursor, or the

synthesis of random copolymers. One limitation, however, is the anion exchange reaction that may be incomplete. Method C (Scheme 2) is an example of the step-growth polymerization that will be discussed further.[39,40]

1.2.1. Polymerization of imidazolium-based IL monomers

Typical PILs constituted of an imidazolium moiety are shown in Figure 3 (**11-12** and **14-20**). The polymer backbone can derive from a vinyl (**11**),[41–45] or a styrenic (**12**),[46–48] or a (meth)acrylic or (meth)acrylamide (**14**),[49–52] or a vinyl ether (**15**),[53] or a glycidyl ether (**16**), or a norbornenyl monomers (**17**) (Figure 3).[54]

Other cations such as tetraalkyl ammonium,[47,55,56] pyridinium,[27,57,58] pyrrolidonium,[59] guanidinium,[60] piperidinium,[61] or tetraalkyl phosphonium[62] with vinyl, styrenic and methacrylic-type have also been synthesized, but these will not be discussed here.

Polymerizations are usually carried out in bulk or in solution (*e.g.* in DMF, CH_3OH…). A few examples of water-borne emulsion or in dispersed media polymerization of IL monomers have also been reported.[63–66]

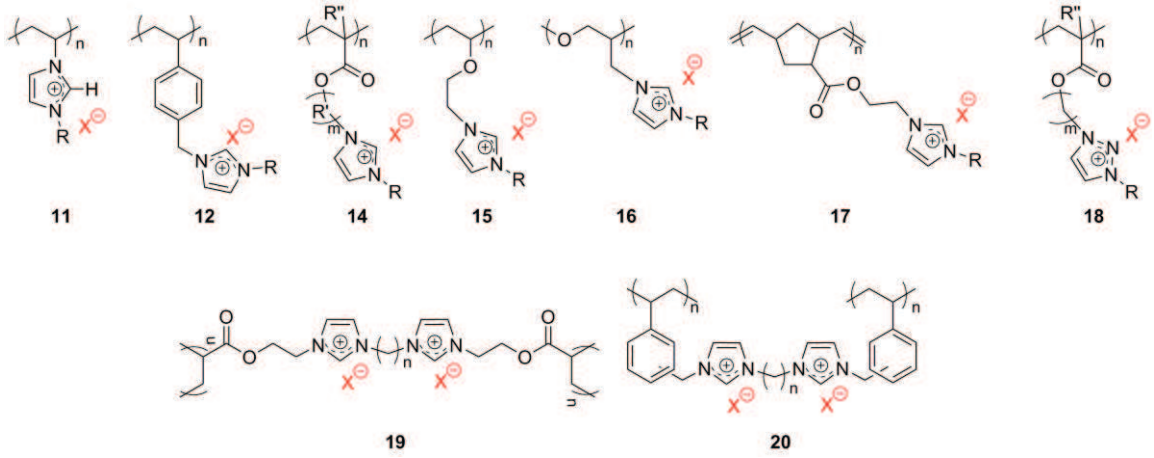

Figure 3. Chemical structure of cationic PILs synthesized by chain-growth polymerization.

1.2.1.1. Free radical polymerization

Many examples of PIL synthesis by free-radical polymerization (FRP) have been reported (**11, 12, 14, 18,** Figure 3).[1–5] FRP can be readily implemented using conventional radical sources (*e.g.* AIBN or azoinitiators such as V-501 or V-70) and is tolerant to many functional groups.

In addition to linear polymers, crosslinked PIL networks (**19-20**) have also been obtained by FRP, using bi- or trifunctional acrylate- or styrenic-type IL monomers (Figure 3).[66–69] Linear PILs can bear a large variety of counter-anions such as halides, tetrafluoroborate, hexafluorophosphate, triflate, nitrate, bis(trifluoromethane)sulfonyl imide, alkylsulfonate, dicyanoamide, iron tetrachloride and perchlorate (see Figure 2). In contrast, most of PIL networks reported so far mainly consist of halide and bis(trifluoromethane)sulfonyl imide counter-anions. Generally, IL monomers with halides counter-anions are first polymerized, which is followed by anion metathesis.

One also resorts to FRP to achieve copolymers consisting of both IL and nonionic monomer units.[70–72] This synthetic strategy enables to dilute the charge density, and/or to increase the distance between IL monomer units on the polymer backbone. For example, a random copolymer of hexylmethacrylate (HMA) and a methacryloyl-based imidazolium IL monomer, 1-[2-methacryloyloxy)ethyl]-3-butylimidazolium tetrafluoroborate, was synthesized *via* free radical copolymerization.[72] Interestingly, a significant amount of nonionic monomer allowed increasing the ionic conductivity over an order of magnitude. Indeed, the presence of HMA units decreased the glass transition temperature of the copolymer and thus increased the ion mobility.

Obviously, (co)polymers obtained by FRP are polydisperse compounds which is not yet an issue for applications such as gas separation *via* synthesis of porous materials, for example. However, it does not allow comparing efficiency of PILs in terms of molar masses for mechanical properties, for example. Consequently, more precise synthetic methods have been developed to achieve well-defined PILs and related block copolymers.

1.2.1.2. Precise synthesis by controlled/living polymerization

In the last two decades, "controlled/living" polymerization methods have attracted a considerable attention.[29–34,37,73–75] These techniques have been recently applied to the polymerization of imidazolium-based monomers. The possibility to design well-defined macromolecular architectures from these methods has also opened avenue for a use of "controlled PILs" and related block copolymers in various areas, such as catalysis, energy, gas separation, etc. (see section 1.3 and 2.4)

Polymerization by atom transfer radical polymerization (ATRP)[32–34] of imidazolium-based styrenic[76] and acrylate[49] monomers (**12** and **14**, Figure 3), with tetrafluoroborate as

counter-anions was first attempted in 2004 by Shen *et al.*. The nature of both the copper catalyst, initiator and solvent were shown to have a strong influence on the ATRP outcomes. For example, the polymerization of IL acrylate monomers carried out in acetonitrile at 60 °C was very fast but uncontrolled using CuBr complex as catalyst, whereas the CuCl catalyst led to a high conversion with a good control (<1.3).[49,76]

Recently, Matyjaszewski *et al.* showed the impact of the presence of salts/couterions such as halides, TFSI, BF_4^- and PF_6^- (Figure 2) on the ATRP process.[77] Controlled polymerization was possible, but a proper choice of conditions was required, with an appropriate combination of copper catalyst, initiator, solvent and counterion. The nature and relative amounts of salts were found to significantly affect the polymerization rate. For instance, the polymerization rate was slow with halide counter-anion, in contrast to TFSI. Use of BF_4^- and PF_6^- caused significant side reactions at high conversions, which was ascribed to the presence of trace amounts of hydrogen fluoride generated from the degradation of the counterions.

The reversible addition-fragmentation chain transfer polymerization method (RAFT)[29–31,73] was also applied to control the molecular weight of PILs. Main chain transfer agents (CTA's) used in the RAFT process to achieve imidazolium-based PILs and related BCPs are shown in Figure 4. A typical synthesis of PIL by RAFT is illustrated in Scheme 3.

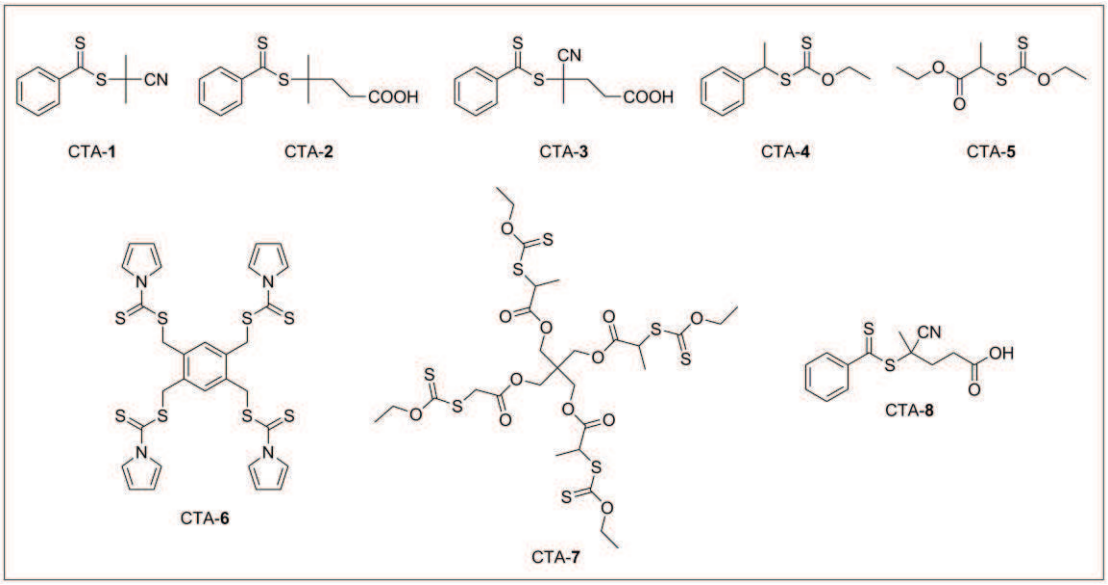

Figure 4. Chain transfer agents (CTA's) used for PIL and related BCP synthesis by RAFT polymerization.[52,78–85]

The first example was reported by Mecerreyes, Taton, Gnanou *et al.* in 2008.[52] Methacrylamido- and methacrylate-type monomers were purposely designed to this end. RAFT polymerization of these monomers was conducted in methanolic solutions at 70 °C, in

the presence of either 2-cyanopropyl dithiobenzoate (CTA-**1**) or (4-cyanopentanoic acid)-4-dithiobenzoate (CTA-**2**), and a radical source such as azobis(2-methylpropionitrile) (AIBN) or 4,4'-Azobis(4-cyanovaleric acid) (V-501).

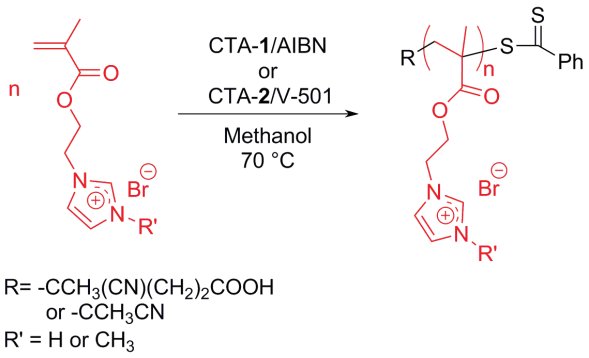

Scheme 3. First example of imidazolium-based PIL synthesis by RAFT polymerization.[52]

Polymers did exhibit molar masses predetermined by the initial molar ratio of the monomer to the dithioester precursor, as evidenced by ^{1}H NMR spectroscopy from polymer chain end analysis. Polyacrylamide (PAm) and poly(methacrylic acid) (PMAA) were also pre-synthesized by RAFT to serve as macro-CTA's for block copolymer synthesis.[52,78]

Other well-defined block copolymers with PIL block were also prepared thanks to the controlled character of the RAFT method, as discussed further.[52,78,79,81–87]

For instance, Endo, Mori *et al.* synthesized PILs based on *N*-vinylimidazolium (Figure 3, **11**) and related PIL BCPs using xanthates (CTA-**4** and CTA-**5**, Figure 4) as CTAs, with a reasonably good control ($Đ$ < *1.56)*.[81] It is worth pointing out that controlled radical polymerization of *N*-vinylimidazolium IL monomers is more challenging, due to the generated radical species that are highly reactive due to their nonconjugated nature.[28–31,88,89]

Cobalt-mediated radical polymerization (CMRP) developed by the group in Liège is yet a powerful method to control the polymerization of conjugated vinyl monomers, including acrylonitriles or acrylates, and nonconjugated vinyl monomers as well, such as vinyl acetate or *N*-vinylpyrrolidone.[74] In 2011, Detrembleur, Taton *et al.* polymerized *N*-vinylimidazolium IL monomers using a preformed alkyl-cobalt(III) adduct as the mediating agent. Excellent control over molecular weights and dispersities ($Đ$ ~1.05-1.06) was achieved.[90]

In 2003, Barrett *et al.* reported the synthesis of imidazolium-based polymers (Figure 3, **17**) *via* ring-opening metathesis polymerization (ROMP) (Scheme 4).[37,75] Obviously, imidazolium-based PILs deriving from norbornene monomers have been scarcely studied as polyelectrolytes.[91,92] PIL BCPs (see further) synthesized *via* ROMP have been reported by

Gin, Bailey *et al.*, not only for conductivity measurements, but also to achieve membrane for gas separation in collaboration with Noble *et al.*.[93–96]

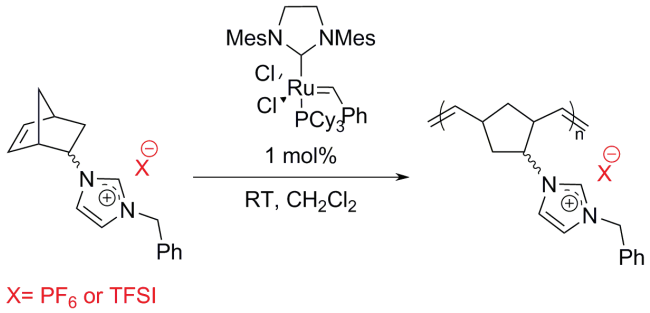

Scheme 4. Example of imidazolium-based PIL synthesis by ROMP.[75,91–96]

1.2.2. Post-polymerization modification

The post-polymerization modification method is also largely employed to design PILs. It consists in converting pre-existing nonionic polymers into PILs. As discussed previously, polymerization of some IL monomers is very challenging, hence chemical modification of pre-formed polymers made by "controlled/living polymerization" and that can be easily characterized may be convenient. This technique is also useful for PIL block copolymer synthesis with at least one PIL block (see Scheme 2).

This method has been mainly applied to imidazolium-based PILs with styrenic, (meth)acrylic and norbornene polymer backbones, following two routes (Figure 3, **12**, **14-16**). The first one involves the quaternization of *N*-alkylimidazole of a pre-polymer carrying an alkyl halide substituent along the polymer backbone (route B, Scheme 2).[97,98] Oppositely, halo-alkanes can readily quaternize imidazole-containing polymer precursors (Scheme 5).[99] The first route is the most used due to the number of halogen-containing polymers. A typical example is the quaternization of poly(4-vinylbenzyl chloride) (PVBnCl) with 1-alkylimidazole (route B, Scheme 2). Well-defined PVBnCl synthesis can also be easily achieved by RAFT or by NMP.[97,98,100–104] Quaternization of PVBnCl is quantitative in DMF at 80 °C, forming the corresponding PIL. This strategy allows achieving PIL BCPs and random copolymers as well.[97,98,100–104]

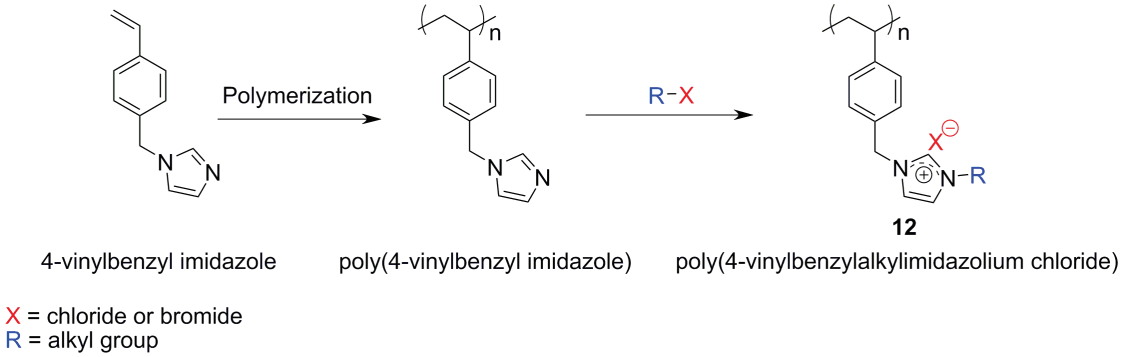

Scheme 5. Example of post-polymerization modification to synthesize imidazolium-based PILs (see also route B, Scheme 2).

Recently, Drockenmuller *et al.* reported the synthesis of cationic poly(acrylate)s with pendant 1,2,3-triazolium monomer units (Figure 3, **18**).[105] The latter moieties were obtained *via* the copper-catalyzed azide-alkyne cycloaddition, followed by quaternization. The easy formation and abundance of structures carrying 1,2,3-triazole units and their versatile conversion to 1,2,3-triazolium analogues by a simple quaternization thus adds to the synthetic toolbox for building new macromolecular architectures.

1.2.3. Step-growth polymerization

Step-growth polymerization has been more rarely employed for the synthesis of PILs. [1–5,16] This technique does not allow a precise control over chain length and dispersity, in contrast to chain-growth polymerization method proceeding by RAFT, ATRP, CMRP or ROMP. Nevertheless, main-chain imidazolium- or 1,2,3-triazolium-based PILs can be achieved. Generally, subsequent anion metathesis leads to the targeted PIL. Four different main strategies can eventually be implemented:

- The most direct method is by direct quaternization of a dihalide-containing monomer precursor with a diimidazole monomer, which leads to a main-chain imidazolium-based PILs (**13**) (Scheme 6, A).[39,40]
- Polymerization by hydroboration of diallylimidazolium IL derivatives was also reported (**21**) (Scheme 6, B).[106]
- Polymerization of click chemistry α-azido, ω-alkyne AB-type monomers, followed by quaternization was implemented to access main-chain 1,2,3-triazolium-based PILs (**22**) (Scheme 6, C).[107–109]

- The acyclic diene metathesis polymerization (ADMET) process allowed synthesizing ionic polyolefins substituted with pendant ILs (**23**) (Scheme 6, D).[110]

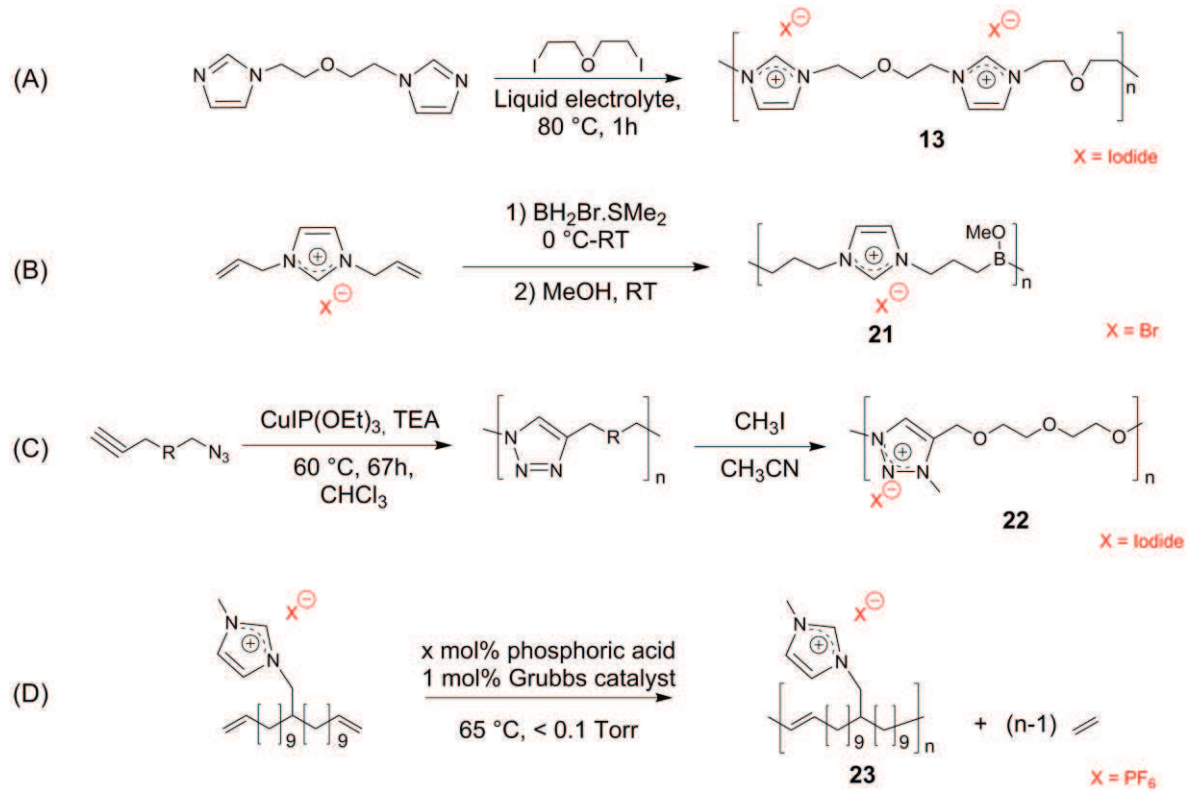

Scheme 6. Examples of cationic PILs synthesized by step-growth polymerization.

1.3. Potential applications of PILs

Due to their combined properties emanating from the IL units and their intrinsic polymeric nature, PILs have emerged as a new class of polyelectrolytes finding potential applications in various areas, such as energy, analytical chemistry, biotechnology, catalysts, gas separation, or dispersants (see Figure 5). Use of PILs in all these applications has been recently reviewed and will not be covered here in details.[1–5]

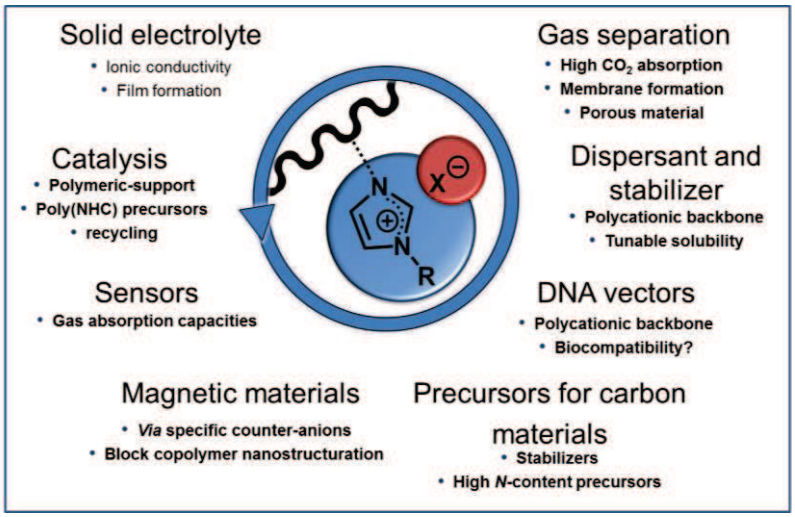

Figure 5. Potential applications of PILs (for a review see references 1-6)

1.3.1. PILs for energy devices

Interest in PILs as solid-state polymer electrolytes is linked to their high ionic conductivity combined with their mechanical stability, safety and simple processing.[3,16,60,111–122] Obviously, PIL ionic conductivities are most often below that of their molecular IL counterparts, generally over two or three orders of magnitude,[16,251] PILs ionic conductivities being in the range of 10^{-3} to 10^{-6} S.cm^{-1} or less.

However, it is important to note some essential points to compare PILs as solid conductive materials. Synthetic strategy, purification, sample preparation and measurements can differ significantly, it questioning the obtained results.

For example, the ionic conductivity of poly(*N*-vinyl-3-ethylimidazolium bis(trifluoromethanesulfonyl) imide) was determined by three different research teams. The group of Ohno reported a value of 6.3 x 10^{-7} S.cm^{-1} at 25 °C,[123] whereas Mecerreyes *et al.* indicated a value of 5.0 x 10^{-5} S.cm^{-1} at 30 °C,[26] and Vygodkii measured a conductivity of 2.5 x 10^{-11} S.cm^{-1} at 25 °C.[124] All PIL compounds were actually not purified by the same way and the presence of residual monomers and/or exogenous salts could strongly influence the measurement. Anion exchange, from bromide to TFSI, was achieved before or after polymerization, and no precise information about the polymer molar masses was provided. It is therefore difficult to draw clear conclusions about the ionic conductivity of PILs at a given temperature.

Besides the fine tuning of their mechanical properties, appropriate counter-anions can be selected to engineer PILs for a targeted application utilizing their ion conduction. In this

regard, the bis(trifluoromethane)sulfonyl imide ($(CF_3SO_2)_2N^-$, referred to as TFSI) anion appears the more efficient, not only owing to its large size decreasing significantly the glass transition temperature, but also to the strong delocalization of the minus charge providing a weak coordinating nature to the anion.

Interestingly, PILs can be doped with exogenous molecular ILs so as to enhance the ionic conductivity.[26,99,125]

1.3.2. PILs for separation devices

Another active field utilizing PILs is gas separation and sorption. This increasing interest is explained by the significantly higher CO_2 absorption capacity of PILs compared to that of their IL homologues, and by a complete reversibility of these reactions for cycles.[126] CO_2 molecules can indeed penetrate into the free volume of the PIL matrix.[127] The type of ion pairing and the polymer backbone dramatically influence the kinetic and efficiency of the CO_2 absorption capacities.[128,129] The chemical structure has been optimized for the cation accessibility and the CO_2 mobility.[127]

PILs have been employed for separation of light gases, such as nitrogen and methane.[69] This requires processing PILs into membranes for simultaneous high CO_2 flux, selectivity and stability, at processing temperatures and pressures.[46,68] However, the solid nature and physically resistance to high pressure of PILs reduced the CO_2 permeability. A blend system of ILs and PILs has been purposely designed so as to improve the CO_2 permeability.[69,130,131] Current studies are focusing on understanding the influence of various chemical structures on the performance on the blend system.[132]

PILs have also been used in analytical chemistry. Due to the increase of IL viscosity at high temperature, PILs are excellent alternatives for a use in solid phase extraction and chromatography.[133,134] Crosslinked PIL networks made from cationic divinylimidazolium IL monomers, for instance, were used as supports to enhance chromatographic efficiency.[156] Interest in porous materials lies in the possibility to make use of IL species as reacting sites.

1.3.3. PILs for catalysis

PILs can also be used as polymer-supported catalysts or pre-catalysts for various molecular reactions. The main interest in using PILs for catalysis is to facilitate the recycling and reuse of the polymer-support. For intance, crosslinked PIL nanoparticles exhibiting a

high-surface-to-volume ratio were employed for the cycloaddition of carbon dioxide and epoxide with high activity and selectivity.[135]

PILs can complex and stabilize metallic compounds and metal oxide nanoparticles, such as rhodium nanoparticles.[136] Imidazolium-based PILs can also serve as polymeric precursors of poly(*N*-heterocyclic carbene)s, as illustrated in Figure 6, this aspect will be exploited in this PhD work (see chapter 2).[137]

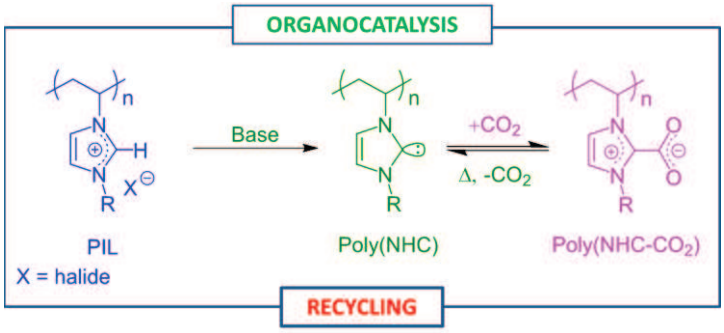

Figure 6. Imidazolium-based PILs as precursors of poly(*N*-heterocyclic carbene)s for further organocatalysis adapted from reference 137.

1.3.4. PILs as dispersants and stabilizers

Imidazolium-based PILs have been successfully applied as polymeric dispersants for the synthesis of π-conductive polymers and for nanomaterials in aqueous and organic solutions.[138] Polypyrrole (PPy), polyaniline (PANI) and poly(3,4-ethylenedioxythiophene) (PEDOT) organic dispersions have indeed been prepared using PIL stabilizers with proper selected anions. For example, EDOT can be polymerized in an aqueous dispersion of poly(*N*-vinylimidazolium bromide). Anion exchange from bromide to TFSI can be applied on the PIL stabilizer that precipitates in water and trapped the conducting polymer microparticles.[139] Thus, the recovered powders can be easily dispersed in various organic solvents through the solubility of the PILs. The PIL/PEDOT mixture is currently used in electrochemical devices.[140–142]

1.3.5. PILs as precursors for carbon materials

Imidazolium-based ILs and PILs have been reported as an interesting class of precursors for functional carbon-based nanomaterials and for nitrogen doped carbons as well. PILs are especially useful to produce nitrogen-doped carbons fibers and membranes by electrospinning.[82,143–145]

Carbon hollow spheres possessing a high surface-to-volume ratio, high thermal stability, low apparent density and low percolation threshold have also been prepared from PILs.[146] More recently, Antonietti *et al.* reported the use of a mesoporous PIL network for carbonization in the presence of $FeCl_2$, so as to obtain graphitic carbon nanostructures with a high electric conductivity.[147]

In addition, aromatic carbon nanostructures (single-wall carbon nanotubes (CNTs), multi-wall carbon nanotubes or graphene sheets) can interact with the nitrogen-containing five-membered cation ring of the imidazolium-based PILs by cation-π interactions.[138] PILs can dispersed such carbon nanostructures. Alternatively, IL monomers can be polymerized *in situ* in the IL/CNT mixture, generating a polymeric gel with a high content of CNTs and a high electrical conductivity.[148]

1.3.6. Other applications

Similar to ILs, several groups have investigated the preparation of cellulose/PIL composites thanks to the cellulose solubility in IL monomers.[48,149,150] Another interesting application of PILs comes to their potential to be an organic-inorganic hybrid materials induced by the use of counter-anion such as $FeCl_4^-$ which gives some magnetic properties.[126] Recently, others fields such as microwave absorbing materials,[126] sensors[151] and DNA vectors[152] have been investigated utilizing PILs.

2. Poly(ionic liquid) block copolymers

Block copolymer (BCP) engineering is a major item of polymer science, spanning aspects of macromolecular chemistry through the molecular design of active species, to theoretical and physicochemical studies.[153–156] Currently, some neutral (nonionic) BCPs are practically used in our daily life as specialty polymers, *e.g.* as dispersants,[157] adhesives, in microelectronics[158–161] or drug delivery systems.[162–165]

The success of neutral BCPs is due to their self-assembling properties, either at the solid state or in a selective solvent of one block, which provides a wide range of morphologies in the submicron size range.[166–171] Miscellaneous BCP architectures and compositions can be achieved by resorting to “controlled/living polymerization” (C/LP) techniques, which can be combined with modern synthetic tools, such as “click chemistry”,[172] post-polymerization

modification of preformed and reactive (co)polymers,[173–175] or supramolecular chemistry.[176,177]

In recent years, ionic liquids (ILs) have been introduced as doping agents in nonionic (nonconducting) BCPs as a means to tune nanostructured morphologies and impart ionic conductivity or gas transport in nanodomains.[131,178–186] This is because ILs exhibit a high intrinsic CO_2 solubility as well as a high ion conductivity as emphasized in the sections above.[22,179,187–190]

For instance, ionic nanodomains of continuous morphology prove more conductive than morphologies in which grain boundaries impede ion mobility.[100,191] An anisotropic ionic conductivity can be achieved from IL-doped BCPs exhibiting a lamellar mesophase,[192] while BCPs with a three-dimensional network morphology can lead to a direction-independent ionic conductivity, due to well-connected ion-conducting pathways.[184]

However, blends between an exogenous ionic liquid electrolyte and a polymer matrix are prone to electrolyte leakages. To alleviate this problem, one solution may be to resort to PILs instead of molecular ILs. In the past five-six years, design and self-assembling properties of BCPs constituted of a PIL block have been the topic of detailed studies. This novel family of BCPs combines the attributes of PILs, such as ionic sensitivity, with the self-assembling properties of BCPs, which provides access to a range of nanostructured morphologies in solution and at the solid state (Figure 7). In bulk, ionic and non-ionic blocks generally segregate in highly ordered nanodomains, due to the strong incompatibility of the two blocks.[93] This is expected to impart complementary features to these ion-conducting materials, such as structural stability and bulk mechanical properties, while affording tunable transport performances.[99,193]

The next sections will describe synthetic methods to achieve imidazolium-type PIL BCPs, their self-assembling properties in solution and in bulk. Potential applications of these compounds will be discuss in the last section.

This topic is obviously still in its infancy, and concerns roughly fifty papers that were published in the past five-six years (in fact the first paper on imidazolium-type PIL BCP dates back to 2003).

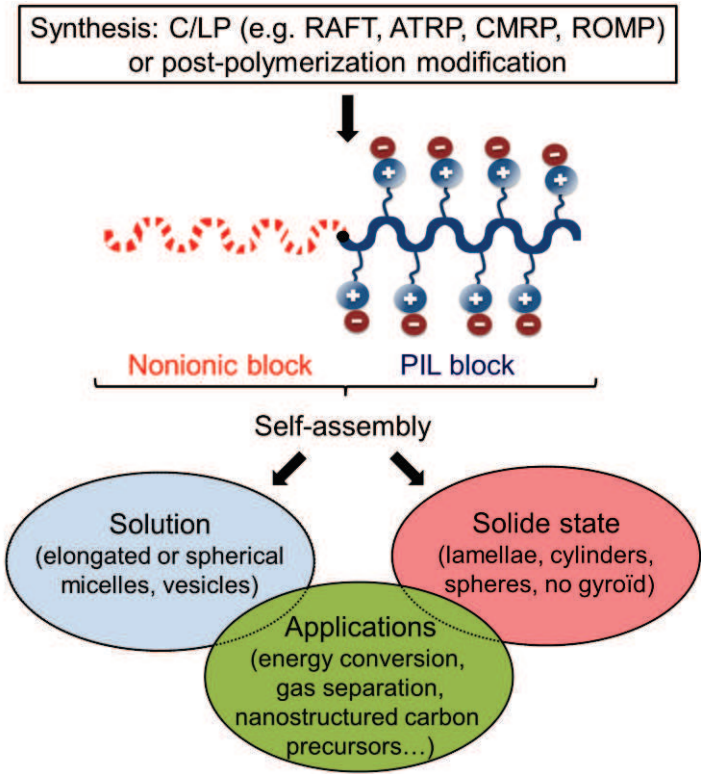

Figure 7. Poly(ionic liquid) block copolymers (PIL BCPs) and their self-assembly potential for a use in various applications.

2.1. Synthesis of poly(ionic liquid)-based block copolymers

The traditional synthetic route to linear AB-type BCPs is by sequential addition of monomers. Various PIL BCPs have been directly synthesized by C/LP of imidazolium-type IL monomers featuring a halide counter-anion (see Table 1), which includes not only radical methods by RAFT, ATRP, NMP, and CMRP, but also ROMP.[52,78–85,90,93–96,194–196]

Besides direct sequential polymerization, PIL BCPs can be accessed by post-polymerization modification of preformed BCP precursors (Scheme 7).[172,175,197] First examples based on imidazolium units were actually made in this way, as reported by Waymouth, Gast *et al*. in 2003.[97] The resulting compounds were found to self-assemble in toluene into elongated micelles with PIL blocks at the core (see also further).

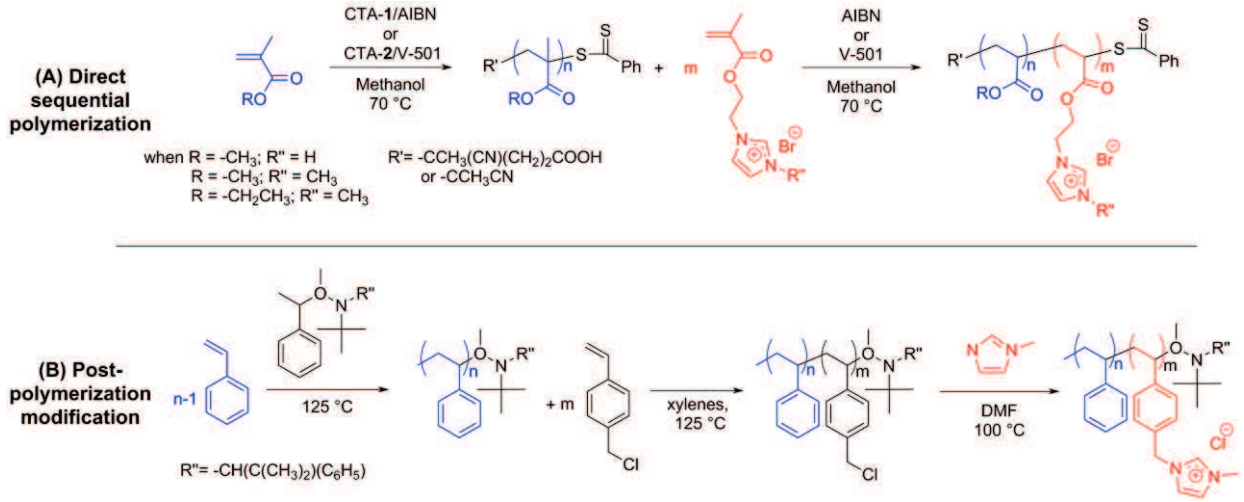

Scheme 7. Synthesis of PIL BCPs. Route A: Direct sequential polymerization by RAFT.[52] Route B: Sequential polymerization by NMP followed by a quaternization.[97]

Table 1 gathers the different imidazolium-based PIL BCP structures that were reported so far, including the nature of the anions and that of the alkyl chains on the imidazole ring, as well as the associated synthetic methods. In this section are described the synthetic aspects, while following sections will discuss the self-assembling properties in solution and at the solid state of these materials.

2.1.1. Reversible addition fragmentation chain transfer (RAFT)

As previously mentioned, the first example of PIL BCP synthesis by RAFT was reported by Mecerreyes, Taton, Gnanou *et al.* in 2008 (Route A, Scheme 7).[52] Polyacrylamide (PAm) and poly(methacrylic acid) (PMAA) were pre-synthesized by RAFT to serve as macro-CTA's for block copolymer synthesis.[52,78] Chain extension experiments were carried out in aqueous or in alcoholic solutions, affording double hydrophilic PIL BCPs with bromide anions (PMAA-*b*-PIL(Br) and PAm-*b*-PIL(Br); Entries 1 and 2, Table 1). These compounds were further manipulated and made to self-assemble in micelle-like structures, either by anion exchange or by chemical modification of PMAA.

Sequential RAFT polymerization was also employed to achieve copolymers based on PIL and poly(*N*-isopropylacrylamide) (PNIPAM), thus exhibiting both an ionic and a thermal responsiveness (Entry 3, Table 1).[79] Dithioester CTA-**3** was used and the length of the PIL block was kept constant, while that of PNIPAM was varied ($\overline{M}_n$ values from 5500-38600 g.mol^{-1}, with $Đ$ < 1.13). The selected PIL, namely, poly(2-(1-butylimidazolium-3-yl)ethyl

methacrylate tetrafluoroborate) was insoluble in water (anion exchange from bromide (Br^-) to tetrafluoroborate (BF_4^-) was carried out with the IL monomer prior to RAFT polymerization).

Synthesis of RAFT-derived BCPs based on PIL and PNIPAM (Entry 4, Table 1) were previously reported by Endo, Mori *et al.* who employed xanthates as RAFT agents (CTA-**4** and CTA-**5**, Figure 4).[81] Polymerization of the *N*-vinylimidazolium salt was accomplished from a xanthate-functionalized PNIPAM, leading to a reasonably well-defined PIL BCP ($Đ$ < 1.5). The same group also synthesized four-armed star block copolymer homologues, using tetrafunctional dithiocarbamate CTAs (CTA-**6** and CTA-**7**, Figure 4; Entry 5, Table 1).[86] Two types of star-block compounds were prepared: one consisting of PNIPAM blocks forming the core, surrounded by the PIL layer, and the other with the reverse structure. A lower dispersity was noted when using a four-armed PIL as macro-CTA: $Đ$ < 1.22 *vs.* 1.57, when starting by RAFT polymerization of NIPAM.

Antonietti and Yuan also resorted to the xanthate chemistry to derive a series of double hydrophilic PIL BCPs ($Đ$ ~ 1.20-2.19; Entry 6, Table 1), from four different *N*-vinylimidazolium IL monomers possessing different alkyl substituents and anions.[82] PNIPAM or poly(*N,N*-dimethylacrylamide) (PDMA) was selected as the nonionic polymer associated with the PIL block. Use of dicyanamide, $(CN)_2N^-$, as counter-anion was found to favor ion pair dissociation (increasing the distance between the imidazolium and the dicyanamide ions). However, polymerization of corresponding IL monomers proved energetically unfavorable (conversion ~ 10%), in contrast to monomers featuring other anions. Hence, reactivity of *N*-vinylimidazolium IL monomers might be adjusted by a proper selection of this structural parameter.

PNIPAM and PIL segments were also associated in BCP architectures obtained by sequential RAFT in the works by Wu *et al.* (Entry 7, Table 1).[83] Self-assembling properties in solution were studied by dynamic FTIR, which evidenced the occurrence of interactions by H-bonding.

Recently, Tauer *et al.* in collaboration with Yuan developed a series of PIL BCPs based on poly(3-*n*-tetradecyl-1-vinylimidazolium bromide) as PIL block by sequential RAFT, with second nonionic block being PNIPAM, poly(butyl acrylate), poly(butyl methacrylate), or poly(styrene) (Entry 8, Table 1).[198] The colloidal behavior and stimuli-responsive properties of these PIL BCPs were then studied after self-assembly.

Elabd *et al.* described the synthesis of a series of well-defined PIL BCPs based on poly(methyl methacrylate) (PMMA), with various PIL compositions ($\overline{M}_n$ values from 16100-25700 g.mol^{-1} with 4.3-15.7 mol% PIL, $Đ$ < 1.6; Entry 9, Table 1).[84,85,87] The aim of this study was to provide an understanding of the influence of morphology on ion transport after anion exchange, from bromide to TFSI or hydroxide (HO^-), as discussed further.

Wang *et al.* developed a synthetic strategy to ABA-type triblock copolymers ($\overline{M}_n$ values from 21-29 kg.mol^{-1} with 6.8-13.5 mol% PIL; Entry 10, Table 1).[195] A telechelic poly(vinylidene fluoride-*co*-hexafluoropropylene) [P(VDF-HFP)] macro-RAFT agent was first designed, before polymerization of the methacrylate-type imidazolium monomer. No microphase separation was observed with this particular triblock PIL BCPs, presumably owing to some compatibility of the PIL and the fluoropolymer matrix.

2.1.2. Atom transfer radical polymerization (ATRP)

As mentioned above, only a very few examples of PILs and PIL BCPs were prepared by ATRP. In 2012, Texter *et al.* reported the synthesis of ABA-type symmetric triblock copolymers with a central poly(propylene oxide) block and poly(1-[11-acryloylundecyl]-3-methyl-imidazolium: $\overline{M}_n$ ~ 9600 g.mol^{-1}, $Đ$ ~ 1.5), after chemical modification of a telechelic PPO precursor (Entry 11, Table 1).[194]

2.1.3. Nitroxide-mediated polymerization (NMP)

Recently, Armand, Gigmes *et al.* elaborated PIL BCPs consisting of a polyanionic backbone with lithium as counter-cation (Entry 12, Table 1).[193] A series of BAB triblock, poly(4-styrenesulphonyl(trifluoromethylsulphonyl) imide lithium)-*b*-poly(ethylene oxide)-*b*-poly(4-styrenesulphonyl(trifluoromethylsulphonyl) imide lithium), denoted as P(STFSILi)-*b*-PEO-*b*-P(STFSILi), with 10 to 40 wt% P(STFSILi) were designed by NMP.

2.1.4. Cobalt-mediated radical polymerization (CMRP)

In 2011, Detrembleur, Taton *et al.* introduced a new family of PIL BCPs based on poly(*N*-vinyl-3-ethylimidazolium bromide) (PVEtImBr) and poly(vinyl acetate) (PVAc), the synthesis of which was achieved by sequential CMRP (see Scheme 8, Route A; Entry 13, Table 1).[74,90] Polymerizations were typically carried out either in dimethylformamide or in

methanol solution, using a pre-formed alkyl-cobalt(III) adduct as both the polymerization initiator and controlling agent upon dissociation. Excellent control over molar masses and dispersities (*Đ* ~ 1.05-1.06) were achieved in MeOH. Substituting methanol for DMF induced much faster polymerization process, even under quite high dilute conditions. Well-defined PVAc-*b*-PVEtImBr PIL BCPs were synthesized from a CMRP-derived PVAc-$Co(acac)_2$ macroinitiator, in a mixture of DMF and MeOH (2/1: v/v) at 30 °C. Finally cobalt-mediated radical coupling of such PIL BCPs, in the presence of isoprene, readily led to PVAc-*b*-PVEtImBr-*b*-PVAc symmetrical triblock copolymers.

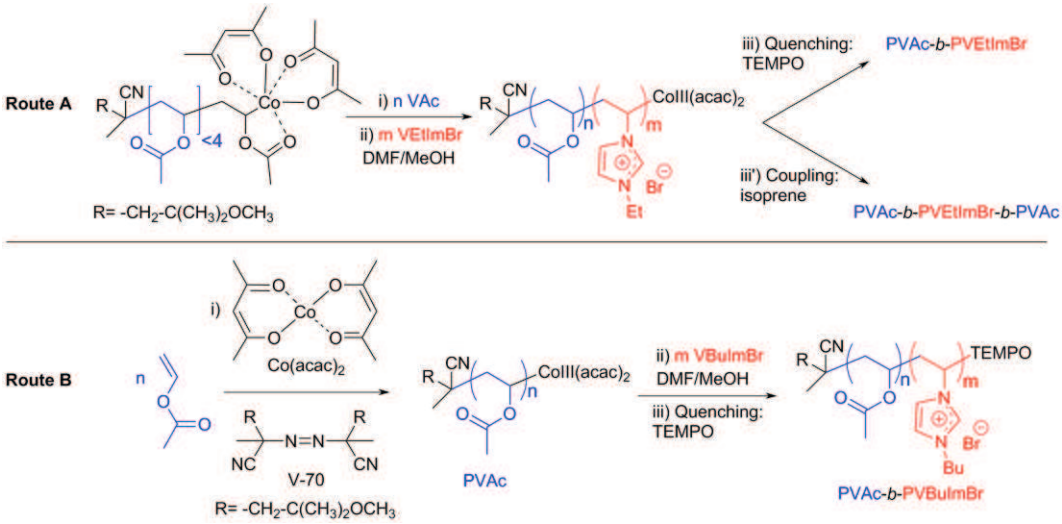

Scheme 8. Route A. Synthesis of PVAc-*b*-PVEtImBr and PVAc-*b*-PVEtImBr-*b*-PVAc by sequential CMRP using alkyl-cobalt(III) adduct as a mediating agent.[90] Route B. Synthesis of PVAc-*b*-PVBuImBr by sequential CMRP using Co(acac)2 and V-70.[196]

Though straightforward, this method required the prior synthesis of the alkyl-cobalt(III) adduct. In this PhD work, we will report on an alternative strategy to CMRP-derived PIL BCPs, by using a commercially available controlling agent, namely, *bis*(acetylacetonato)cobalt(II) ($Co(acac)_2$) in conjunction with 2,2'-azobis(4-methoxy-2,4-dimethylvaleronitrile) (V-70) (Entry 13, Table 1).[196] This work will be discussed in Chapter 3 of this manuscript.

2.1.5. Ring-opening metathesis polymerization (ROMP)

In a series of papers, Gin, Bailey *et al.* investigated the synthesis and self-assembling properties in bulk of PIL BCPs obtained by ROMP of norbornenyl-type monomers, using Grubbs' first generation catalyst (Entry 14, Table 1).[93,94] Control over the ROMP process

allowed the authors to vary the relative volume fraction of the poly(norbornene dodecyl ester) block (f_{DOD} = 0.42-0.96) and the overall molar masses of their compounds ($\overline{M}_n$ values from 5000-20100 g.mol^{-1}). As an indirect evidence for the formation of copolymers with no apparent homopolymer contaminant, analysis by NMR DOSY showed only one room-temperature diffusion coefficient in CD_2Cl_2, whereas a physical blend of the two homopolymers gave rise to two distinct diffusion coefficients.

The same team also reported the synthesis of ABC-type triblock copolymers by sequential ROMP (Entry 15, Table 1).[95,96] Triblock copolymers of similar composition (mass fraction: 26.4 wt% for the hydrophobic block A, 46.1 wt% for the PIL block B and 27.5 wt% for the hydrophilic block C), and total chain length ($\overline{M}_n$ values from 20.8-22.8 kg.mol^{-1}), but with different block sequences (ABC, CAB, ACB) were designed in this way. The ABC- and CAB-type sequenced compounds were used as membranes in gas permeation application.

2.1.6. Chemical modification of preformed block copolymers

As mentioned above, first PILs arranged in a BCP architecture were synthesized in this way, as reported in 2003 by Waymouth, Gast *et al*. (Entry 16, Table 1).[97,98] This was achieved from neutral polystyrene-*b*-poly(4-vinylbenzyl chloride) (PS-*b*-PVBnCl) BCPs ($Đ$ < 1.2) obtained by NMP,[36,199] followed by functionalization with 1-methylimidazole (Route B, Scheme 7). The obtained PIL BCPs were then subjected to anion exchange using sodium tetrafluoroborate ($NaBF_4$).

Later on, a few groups employed similar NMP-derived PS-*b*-PVBnCl precursors, to achieve PIL BCPs of different composition and study their self-assembling properties in bulk. For instance, Elabd *et al.* described a series of poly(styrene-*b*-4-vinylbenzyl-alkylimidazolium bis(trifluorosulfonyl) imide) (PS-b-PVBn-(alkyl)-ImTFSI) of various compositions ($\overline{M}_n$ ranging from 20000-25000 g.mol^{-1} with 2.7-17.0 mol% PIL, $Đ$ < 1.26), and carrying different alkyl groups (CH_3, *n*-C_4H_9, *n*-C_6H_{13}) (Entry 17, Table 1).[100] Balsara *et al.* synthesized PS-*b*-PVBnBuImCl BCPs, with molar masses varying from 4 to 60 kg.mol^{-1} ($Đ$ ~ 1.09-1.45), and that were further quaternized with *n*-butylimidazole (Entry 18, Table 1).[101]

By combining NMP and post-polymerization modification, Long *et al.* reported a series of papers on ABA-type triblock copolymer synthesis, with PIL as the mid-block, with a view at developing electromechanical transducers. For instance, imidazole groups of poly(styrene-*b*-[vinylbenzyl imidazole-*co*-*n*-butyl acrylate]-*b*-styrene) triblock copolymer were quaternized

to introduce the IL units (Entry 19, Table 1).[102] The charge content was varied so as to tune the glass transition temperature (T_g) and the Young modulus of the material. Another example concerned the prior synthesis of difunctional poly(VBIm) ($\overline{M}_n$ value = 204 kg.mol^{-1}, $Đ$ ~ 1.2) from a difunctional NMP initiator. This was followed by the quaternization with an alkyl imidazole (Entry 20, Table 1).[99] After anion exchange, from Br^- to TFSI, chain extension of this PIL precursor with styrene produced the targeted ABA triblock copolymer.

Elabd *et al.* quaternized poly(styrene-*b*-1-((2-acryloyloxy)ethyl)-3-butyl bromide) (PS-*b*-PBrEA) made by RAFT polymerization, into poly(styrene-*b*-1-((2-acryloyloxy)ethyl)-3-butylimidazolium bis(trifluorosulfonyl) imide) (poly(S-*b*-AEBIm-TFSI) with *n*-butylimidazole (Entry 21, Table 1), which was followed by anion exchange.[103] $\overline{M}_n$ values of the resulting PIL BCPs ranged from 9950-18800 g.mol^{-1} with 6.6-23.6 mol% PIL, $Đ$ < 1.31).

Combination of RAFT polymerization and post-chemical modification also allowed Lodge *et al.* to derive ABA triblock copolymers. PS-*b*-PBrEA-*b*-PS copolymers, with BrEA corresponding to 2-bromoethyl acrylate, were first synthesized using a difunctional CTA.[104] The quaternization reaction was then performed using *n*-butylimidazole to introduce the IL groups (Entry 22, Table 1). The final PS-*b*-PIL-*b*-PS triblock copolymers were characterized by an overall molar mass of 260 kg.mol^{-1} and a dispersity index of 1.21.

Segalman *et al.* modified an ATRP-derived poly(styrene-*b*-histamine methacrylamide) (PS-*b*-PHMA; $\overline{M}_n$ in the range 24000-53000 g.mol^{-1}, $Đ$ < 1.3) with trifuoroacetic acid, so as to generate a protic PIL (PS-*b*-PIL) featuring trifluoroacetate counter-anions, for a use as ion-conducting materials (Entry 23, Table 1).[200]

As for Garcia *et al.*, they chemically modified poly(styrene-*b*-2-vinylpyridine) (PS-*b*-P2VP; $Đ$ = 68600 g.mol^{-1} with a dispersity of 1.09; Entry 24, Table 1) by partial quaternization of the P2VP block with ethyl bromide.[201] Note that in this case, the resulting PIL BCP is a nonimidazolum-type compound. The same was true for the post-chemical modification of poly(2-vinylpyridine)-*b*-poly(methyl methacrylate) P2VP-*b*-PMMA (Entry 25, Table 1), grown by anionic polymerization and whose degree of substitution was varied.[202] The extent of quaternization of resulting compounds, denoted as [(P2VP-*r*-poly(1-ethyl-2-vinylpyridinium bromide)]-*b*-PMMA, were in the range 7.5-37%. Adding a methanolic solution of $FeBr_3$ onto the latter PIL BCPs led to paramagnetic materials, [(P2VP-*r*-poly(1-ethyl-2-vinylpyridinium $Fe_3Br_{10}^-$)]-*b*-PMMA.

Table 1. Representative PIL BCP structures, related synthetic and characterization methods, morphologies observed at the solid state, and ionic conductivity. Note that Entries 11 and 23-24 correspond to nonimidazolium PIL BCPs.

Entry	Structure	X^- = Anion	R-groups	Polym. Method	Charact.	S.A. in solution	S.A. in bulk	Morph.[a]	Conductivi-ty range ($S.cm^{-1}$)	Ref.
1	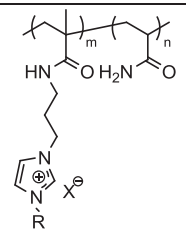	Br^-	$-CH_2CH_3$	RAFT	^1H NMR, SEC in THF	DLS, SLS, TEM	n.i.[b]	n.i.[b]	n.i.[b]	52
2	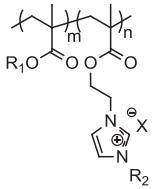	Br^-	$R_1 = H$; $R_2 = CH_3$, $R_1 = CH_3$; $R_2 = CH_3$, $R_1 = CH_3$; $R_2 = CH_2CH_3$	RAFT	^1H NMR, SEC in THF	DLS, SLS, TEM	n.i.[b]	n.i.[b]	n.i.[b]	78
3	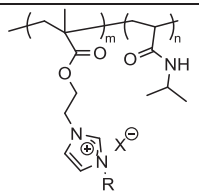	BF_4^-	$-(CH_2)_3CH_3$	RAFT	^1H NMR, SEC	DLS, cryoTEM, fluorometry	n.i.[b]	n.i.[b]	n.i.[b]	79

4	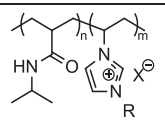	Br^-	$-(CH_2)_3-(C_6H_5)$	RAFT	^1H NMR, SEC in acetonitrile/ water (1:1)	n.i.[b]	n.i.[b]	n.i.[b]	n.i.[b]	81
5	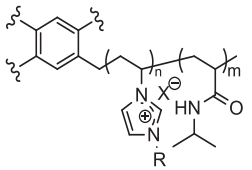	Br^-	$-CH_2CH_3$	RAFT	^1H NMR, ^{13}C NMR, SEC in acetonitrile/ water (1:1), FTIR	DLS, AFM	n.i.[b]	n.i.[b]	n.i.[b]	86
6	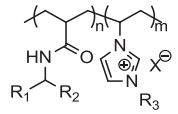	Br^-, $(CN)_2N^-$	R_1 = -H, $-CH_3$ R_2 = $-CH_3$, $-CH(CH_3)_2$ R_3 = $-CH_2CH_3$, $-CH_2CN$, $-(CH_2)_3CN$	RAFT	^1H NMR, SEC in NMP, FTIR, UV, TGA, DSC	AUC, TEM, XRD, FT-IR, nitrogen sorption	n.i.[b]	n.i.[b]	n.i.[b]	82
7	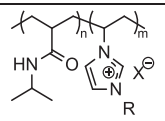	Br^-	$-(CH_2)_3CH_3$	RAFT	^1H NMR, FTIR	DLS	n.i.[b]	n.i.[b]	n.i.[b]	83
8	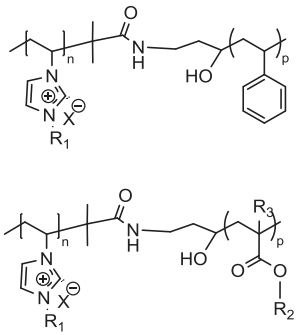	Br^-	R_1 = $-(CH_2)_{13}CH_3$ R_2 = $-(CH_2)_3CH_3$ R_3 = -H, $-CH_3$	RAFT	^1H NMR, FTIR	DLS, TEM	n.i.[b]	n.i.[b]	n.i.[b]	198

	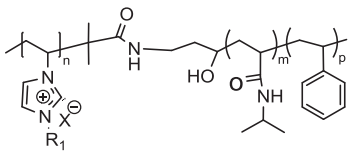 Styrene or BMA or BA as third block									
9	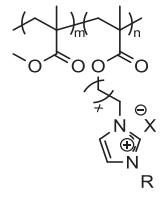 x = 1 or 10	Br^-, Tf_2N^-, HO^-	$-(CH_2)_3CH_3$	RAFT	^{1}H NMR, DSC, TGA, FTIR, Elemental analysis	n.i.[b]	TEM, SAXS EIS, Dynamic vapor sorption (DVS)	Lam	10^{-4}-10^{-7}; 64.85 x 10^{-3}-2.5 x 10^{-2} until 90% of relative humidity	84,85, 87
10	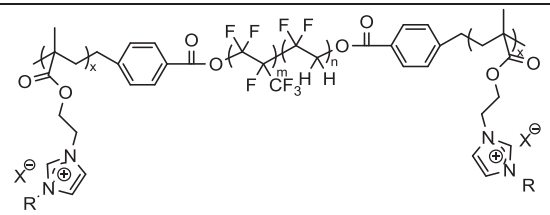	BF_4^-, Tf_2N^-	$-(CH_2)_3CH_3$	RAFT	^{1}H NMR, SEC in THF, TGA, DSC	n.i.[b]	WAXS, SAXS, dielectric relaxation spectroscopy (DRS)	Unord	10^{-12}-10^{-4}	195
11	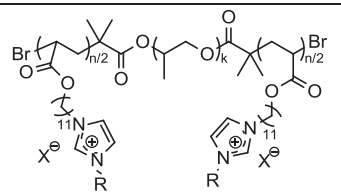	Br^-	$-CH_3$	ATRP	^{1}H NMR, SEC in HFIP, FTIR, UV, TGA, DSC	Dynamic contact angle	n.i.[b]	n.i.[b]	n.i.[b]	194

12	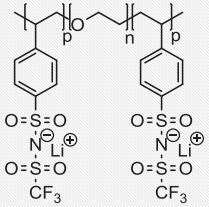	-	-	NMP	^{1}H NMR, SEC in H_2O + acetonitrile, TGA, DSC, DMA	n.i.[b]	EIS	n.i.[b]	2×10^{-8} - 5×10^{-5}	193
13	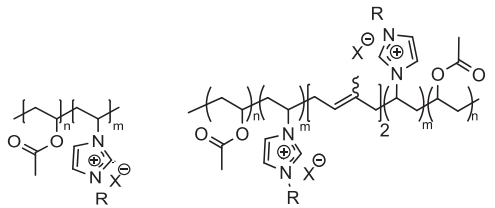	Br-	$-CH_2CH_3$, $-(CH_2)_5CH_3$	CMRP	^{1}H, ^{13}C and DOSY NMR , SEC in DMF or THF/LiTFSI (10 mM), TGA, DSC	DLS, TEM	TEM, SAXS	Lam; Hex	8×10^{-10} - 8×10^{-5} at 30 °C	90,196
14	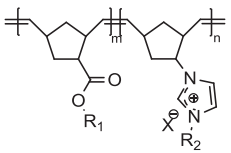	Tf_2N^-	$R_1 = -(CH_2)_{11}CH_3$ $R_2 = -(CH_2)_5CH_3$	ROMP	^{1}H NMR, DOSY NMR, SEC in THF, DSC, TGA, Dynamic mechanical spectro.	n.i.[b]	SAXS	Lam; Hex; Lam+ Hex; S_{BCC}; LLP	n.i.[b]	93,94
15	Several sequences : ABC, CAB and ACB 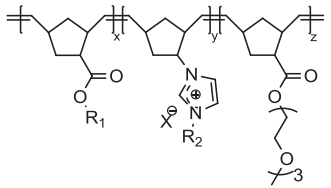	Tf_2N^-	$R_1 = -(CH_2)_{11}CH_3$ $R_2 = -(CH_2)_5CH_3$	ROMP	^{1}H NMR, DOSY NMR, SEC in THF, DSC, TGA, Dynamic mechanical spectro.	n.i.[b]	Synchroton SAXS, SEM, Gas Transport Properties	Lam; Hex; S_{BCC}	n.i.[b]	95,96

16	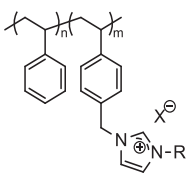	Cl^-, BF_4^-	$-CH_3$	NMP + Post modif.	^1H NMR, ^{13}C NMR, SEC in THF, Elemental analysis	DLS, SANS, Neutron contrast matching, Karl Fischer water content testing	n.i.[b]	n.i.	n.i.[b]	97,98
17	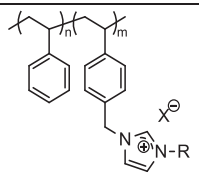	Tf_2N^-	$-(CH_2)_3CH_3$	NMP + Post modif.	^1H NMR, SEC in THF, DSC	n.i.[b]	SAXS, TEM, EIS	Lam; Hex; Lam + Hex	6.3×10^{-8}-3.2×10^{-4}	100
18	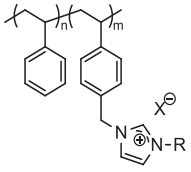	Cl^-, HO^-	$-(CH_2)_3CH_3$	NMP + Post modif.	^1H NMR, SEC in DMF, TGA, DSC	n.i.[b]	SAXS, EIS, galvanodyna.	Lam	$1.8\text{-}3.2 \times 10^{-3}$	101
19	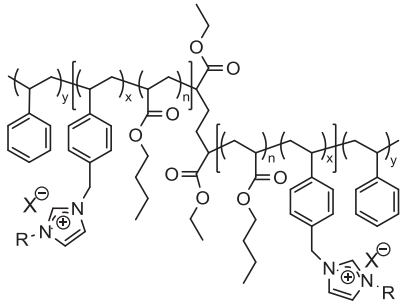	Br^-	$-CH_2CH_3$	NMP + Post modif.	^1H NMR, SEC in THF, DSC, TGA, DMA, EIS	n.i.[b]	SAXS, TEM	See Fig. 5	$1.2\text{-}4.9 \times 10^{-3}$ (doped BCPs)	102

20	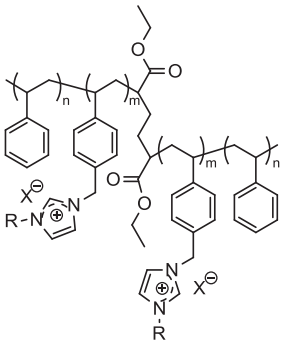	Tf_2N^-	$-CH_2CH_3$	NMP + Post modif.	^{1}H NMR, SEC in THF, DSC, TGA, DMA	n.i.[b]	EIS	unord	5×10^{-7}-5×10^{-4}; 8×10^{-5}-2×10^{-2} (doped BCPs)	99
21	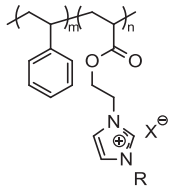	Br^-, Tf_2N^-	$-(CH_2)_3CH_3$	RAFT + post modif.	^{1}H NMR, SEC in THF, TGA, DSC	n.i.[b]	SAXS, TEM, EIS	Hex; Lam + Net; Unord; Lam	10^{-6}-10^{-3}	103
22	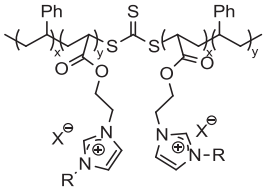	Cl^-, TFSA	$-(CH_2)_3CH_3$	RAFT + post modif.	^{1}H NMR, SEC in THF, elemental analysis	n.i.[b]	n.i.[b]	n.i.[b]	n.i.[b]	104
23	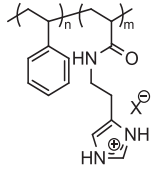	CF_3COO^-		ATRP + Post modif.	^{1}H NMR, SEC in THF	n.i.[b]	SAXS, TEM	Hex; Lam	5×10^{-4}-1.2×10^{-2}	200

24	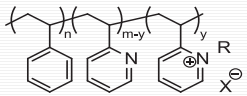	Br^-, Tf_2N^-, $CF_3(CF_2)_3\text{-}SO_3^-$	$-CH_2CH_3$	Anionic + Post modif.	^{1}H NMR, SEC in DMF, TGA, FTIR	n.i.[b]	AFM, TEM	Lam	n.i.[b]	201
25	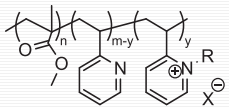	Br^-, $Fe_3Br_{10}^-$	$-CH_2CH_3$	Anionic + post modif.	^{1}H NMR, SEC in THF, TGA, DSC, FTIR	n.i.[b]	TEM, Osmometry, Magnetic charact.	n.i.[b]	n.i.[b]	202

[a] Morphology abbreviations: Lam: Lamellae; Hex: hexagonally packed cylinders; Lam + Hex: coexisting Lam + Hex; S_{BCC}: spheres on a body-centered cubic lattice; LLP: liquid-like packing; Unord: unordered separated microphase; Net: network. [b] n.i.: not investigated.

2.2. Self-assembly in solution

Only a handful of studies have focused on the self-assembly in solution of PIL BCPs. Use of a selective solvent of one block gives rise to micelle-like nanostructures. Interestingly, self-assembly of PIL BCPs can be triggered by a simple ion exchange, which relates to the ionic sensitivity of PILs.[4,41]

Pioneer works by Waymouth, Gast *et al.* evidenced the formation of elongated micelles in dilute toluene solution, from styrenic-based PIL BCPs shown in Entry 16. The PIL block was found to arrange in a cylindrical morphology at the core.[4,41,97,98] This was investigated both by small-angle neutron scattering (SANS) and dynamic light scattering (DLS). As the length of the IL core-forming block was increased, the conformation of the PS shell changed, from a starlike to a brushlike arrangement, as depicted in Figure 8. It was also shown that these micelles could sequester a few water molecules for each IL repeating unit.

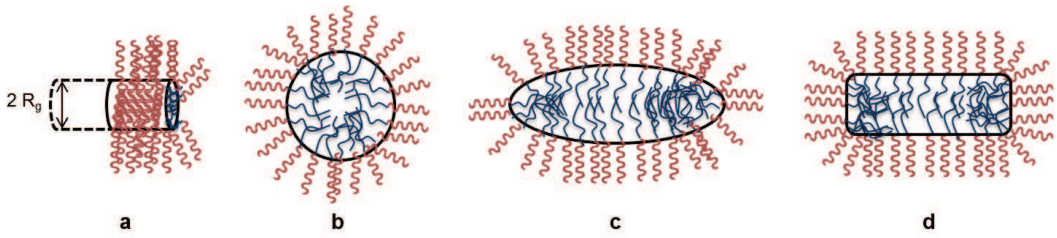

Figure 8. Nanoassemblies obtained from PIL BCP (Entry 16, Table 1; PIL in red, PS in blue): (a) PS-PIL elongated micelles with (b) circular, (c) ellipsoidal, or (d) tablet-shaped cross sections; adapted from reference 98.

Gnanou, Taton *et al.* investigated in details the self-assembly in solution of PIL BCPs shown in Entries 1 and 2 (Table 1).[52,78] Anion exchange, from Br^- to TFSI, turned the solution properties of PIL blocks from hydrophilic to hydrophobic, forming water-soluble micellar aggregates. Studies by ^1H NMR, dynamic light scattering and transmission electron microscopy (TEM) evidenced that compounds consisting of a hydrophilic mass fraction (f) around 35±10 self-organized into direct or reverse polymersomes (= polymeric vesicles), as a function of the selective solvent used (water, methanol or THF). Hydrodynamic radius of polymersomes ranged from 17 to 150 nm, depending on the composition of the copolymer. Compounds with f > 45 self-assembled into polymeric spherical micelles.

For instance, anion exchange of the PIL block, from Br^- to TFSI led to a vesicular morphology consisting of TFSI-based PIL blocks as the hydrophobic membrane stabilized by water-soluble PAm (or PMAA). The PAm_{135}-*b*-$(PIL\text{-}TFSI)_{12}$ sample possessing a hydrophilic

mass fraction higher than 45, was found to self-assemble into spherical polymeric micelles. All these observations were consistent with the empirical classification of Discher and Eisenberg regarding the type of nanoparticles obtained by self-assembly of amphiphilic block copolymers of coil-coil type, as a function of the hydrophilic mass fraction.[203]

Interestingly, this variation in solubility due to anion exchange was found to occur reversibly, so that a given self-assembled morphology could be unassembled and/or reassembled into another nanostructure.

Moreover, chemical modification of the hydrophilic PMAA block allowed generating a hydrophobic PMMA, offering another means to manipulate nanostructures, not only in water but also in organic media, through a proper selection of the selective solvent of one block (Figure 9).

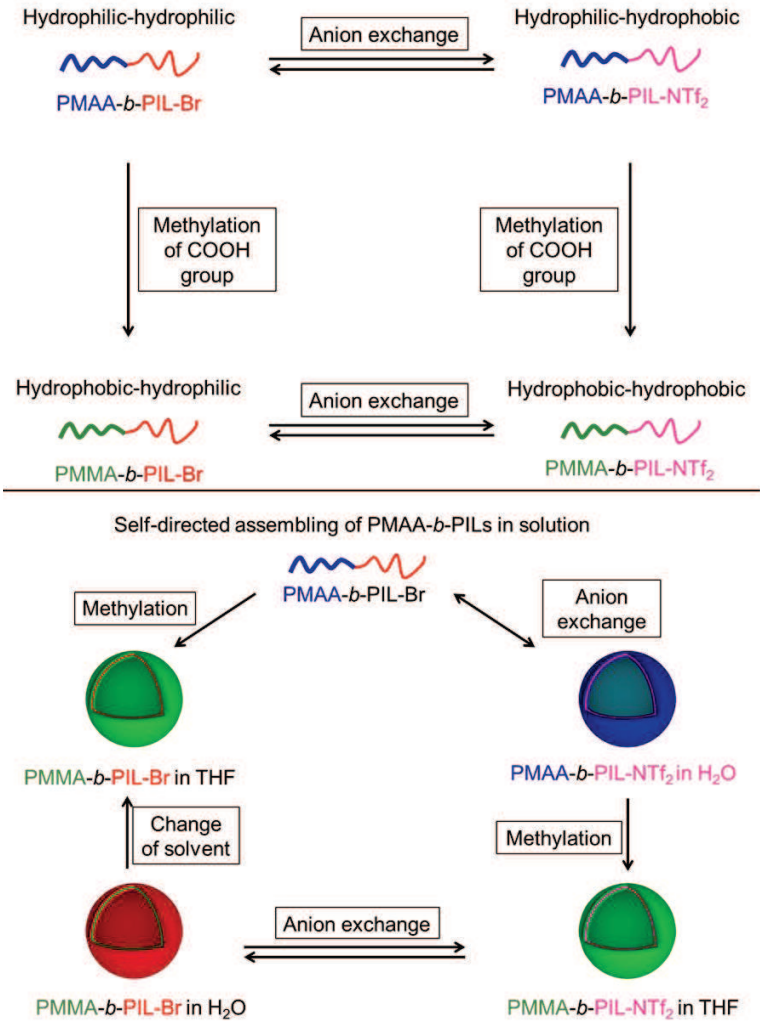

Figure 9. Chemical manipulation either by anion exchange or by chemical modification of the PMAA block of PIL BCPs (Entries 1-2, Table 1); adapted from reference 78.

The first example of a doubly responsive PIL/PNIPAM BCP was reported by Endo, Mori *et al.* (Entry 4, Table 1).[81] As expected, introduction of poly(1-(2-ethoxyethyl)-3-vinylimidazolium bromide) (PEtOEVI-Br) hydrophilic segment increased the LCST of the compound. In contrast, BCP containing hydrophobic blocks, such as poly(1-(3-phenylpropyl)-3-vinylimidazolium bromide) (PPVI-Br) or poly(1-(6-ethoxycarbonylhexyl)-3-vinylimidazolium bromide) (PEHVI-Br), were insoluble in water at room temperature. The amphiphilic $PNIPAM_{91}$-*b*-$PPVI\text{-}Br_9$ BCP was found to self-organize into micelles consisting of a hydrophobic PIL core and hydrophilic shell of PNIPAM. In contrast, no detectable micelle was observed from the double hydrophilic PNIPAM-*b*-PEtOEVI-Br sample.

The same team evidenced that the star-block architecture shown in Entry 5 (Table 1) could form spherical micelles that aggregated into dehydrated clusters at temperature above the LCST of PNIPAM.[86] The thermally induced phase separation behavior and self-assemblies in aqueous solution were found to depend on the sequence of each block (location of the thermoresponsive segment) along the arm star.

The ATRP-derived ABA-type symmetric PIL BCP reported by Texter *et al.* (Entry 11, Table 1) also exhibited both an ionic and a thermal responsive behavior, emanating from the PIL and the pluronic block, respectively.[194] In addition to exhibit "classical" surface activity, the amphiphilic compound also immunized colloids against coagulation induced by electrostatic screening. It was also used as a wetting additive and was found to form a thermoreversible gel, with a LCST ranging from 0 to 50 °C (Figure 10).

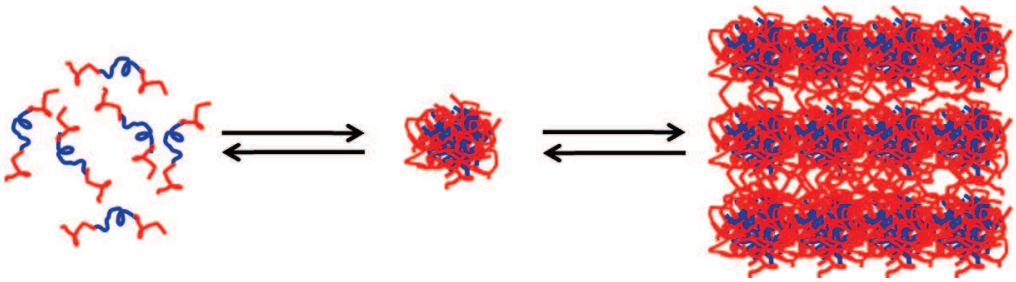

Figure 10. Multi-stimuli responsive micelle-like structures obtained from poly(ILBr-*b*-PO-*b*-ILBr) triblock copolymer; adapted from reference 194.

In the same vein, Tehnu *et al.* investigated the self-assembly in solution of their linear PIL BCPs shown in Entry 3 (Table 1).[79] These compounds were not water soluble due to the bulky hydrophobic counter-anion. Core-shell micelles formed in pure water from amphiphilic samples featuring BF_4^- counterions, while double-hydrophilic compounds with Br^-

counterions showed a partial structural inversion in aqueous $NaBF_4$, upon the thermal collapse of PNIPAM.

Investigations by DLS and turbidity measurements into the self-assembling properties of $PNIPAM_{50}$-*b*-$PBVImBr_{17}$ (Entry 7, Table 1) was reported by Wu *et al.*.[83] Furthermore, FTIR in combination with two-dimensional correlation spectroscopy (2Dcos) and the perturbation correlation moving window (PCMW) technique allowed studying the micro-dynamics of micelle-like structures. Micelle formation consisting of a core of PBVImBr and a shell of PNIPAM was again evidenced. The increase of the phase transition temperature was attributed to the dehydration of alkyl chains of the PIL. A greater hysteresis was also observed during the heating–cooling cycle. This was explained by the existence of hydrogen bonds among the micelles (inter-micellar interactions) formed upon heating and that could be hardly disrupted. Hence, the recovery hydration process involving C–H groups upon cooling was prevented, due to the compact micellar structure. Intra-micellar hydrogen bonding developing at room temperature was also suggested.

Another example of self-assembly from doubly responsive PIL/PNIPAM BCP was reported by Yuan, Antonietti *et al.* (Entry 6, Table 1).[82] The authors took benefit of the $(CN)_2N^-$ counter-anion generated by anion exchange from parent bromide-containing PIL, and made use of the resulting dicyanamide-containing PIL as carbon precursor. With this counter anion, indeed, the polymeric carbon framework was better preserved at elevated temperatures during the carbonization step.

Tauer *et al.* discussed the colloidal behavior of PIL BCPs that contain poly(3-*n*-tetradecyl-1-vinylimidazolium bromide) as PIL block and PNIPAM, or PS, or PBuA, or PBuMA as a nonionic block (Entry 8, Table 1).[198] They evidenced PIL dispersion formation and used these compounds as electrostatic stabilizers for heterophase polymerization of hydrophobic monomers. Zeta potential measurements established the amphiphilic character of these PIL BCPs.

2.3.Self-assembly at the solid state and related transport properties

As already mentioned, PIL BCPs enable to access a range of nanostructured morphologies at the solid state, where the ion-transporting and the non-ionic blocks segregate in ordered nanodomains. In this regard, PILs behave as single-ion conductors with IL moieties as pendant groups and mobile counterions, making PILs good candidates as solid

polymer electrolytes.[3,16] For instance, strong microphase separation and large nanodomain width (lower number of interfaces) are expected to favor high conductivity. However, optimal properties require that a balance between ionic conductivity and mechanical strength can be found.

The ion conduction behavior of PS-*b*-poly(1-(4-vinylbenzyl)-3-alkylimidazolium TFSI; Entry 17, Table 1), as a function of morphology in the microphase separated structure, was studied by Elabd, Mahanthappa *et al.*[100] Morphologies at the solid state were examined both by temperature-dependent synchrotron small-angle X-ray scattering (SAXS) and TEM. These PIL BCPs were found to self-assemble into a hexagonally packed cylindrical morphology for a composition in PIL lower than 7.1 mol%. A lamellar morphology was observed above 17.0 mol%, and a blend of cylinders and lamellae were evidenced between these two compositions. Comparable values of ionic conductivity (1.0×10^{-4} S.cm^{-1} at 150 °C) were determined by electrochemical impedance spectroscopy (EIS), regardless of the imidazolium alkyl substituent. However, ionic conductivity increased by an order of magnitude when the PIL content increased from 8.6 mol% to 17.0 mol%. Another 5-fold conductivity enhancement was noted for higher mol. fraction in PIL.

The conductivity dropped off by more than an order of magnitude, from the lamellar sample (1.0×10^{-6} S.cm^{-1} at 90 °C) to the sample showing the coexistence of lamellae + hexagonally packed cylinders (3.2×10^{-7} S.cm^{-1} at 90 °C; 8.6 mol% in PIL). This was explained by the lack of connectivity of the discontinuous cylindrical mesophase, where grain boundaries might act as morphological defects impeding conductivity. Values were also dramatically dependent on BCP processing method; solvent casting providing well-ordered morphologies *vs.* melt pressing giving rise to more poorly ordered mesophases.

Similar PIL BCPs, but with chloride as counter-anion, *i.e.* PS-*b*-poly(1-(4-vinylbenzyl)-3-butylimidazolium chloride) (Entry 18, Table 1), were investigated by Balsara *et al.*.[101] These compounds were also compared with PS-*b*-poly(1-(4-vinylbenzyl)-3-trimethylammonium chloride) compounds. All samples exhibited a lamellar organization, regardless of the volume fraction (φ), which ranged from 0.35 to 0.60. The authors observed that the scaling of domain size with chain length was weakly dependent on the nature of the bound cation (trimethylammonium *vs.* butylimidazolium). Slightly higher conductivity values were determined compared to PIL BCPs studied by Elabd *et al.*[100] For a given sample ($\overline{M}_n$, PS = 27 kg.mol^{-1} and $\overline{M}_n$, PIL = 21 kg.mol^{-1}), the conductivity increased with time and temperature,

from 1.8 x 10^{-3} S.cm^{-1} at 22 °C to 3.1 x 10^{-3} S.cm^{-1} at 40 °C. Exchange from chloride to hydroxide anions allowed increasing the conductivity of PIL BCP membranes by a factor of 10. This result was explained by a higher diffusion of hydroxide ions (ratio of diffusion coefficients of HO^- and Cl^- in water: $D_{HO^-}/D_{Cl^-} \approx 3$), and also likely to some differences of condensation and hydration of counterions. However, some degradation was noted with PIL BCPs with the hydroxide ions, presumably owing to the formation of bicarbonate ions (HCO_3^-) formed in contact with atmospheric CO_2.

Long *et al.* also evidenced microphase separation at the solid state for their poly(Sty-*b*-[EVBIm-*co*-*n*BA]-*b*-Sty) ABA-type triblock copolymers (Entry 19, Table 1). A rather limited long-range order was yet noted, which was attributed to a relatively high dispersity value ($Đ \sim 1.40$).[102] PS-type external A blocks allowed for mechanical reinforcement, while the central statistical copolymer B block provided ionic conductivity. These properties could also be tuned by doping the material with 20 mol% of an exogenous molecular IL. Ionic conductivity values were in the range 5 x 10^{-4} – 5 x 10^{-6} S.cm^{-1} at 90 °C. Observation of a second scattering peak at $q \sim 1.8$ nm^{-1} was ascribed to aggregation phenomena occurring between ion-rich domains. The proposed morphology is shown in Figure 11.

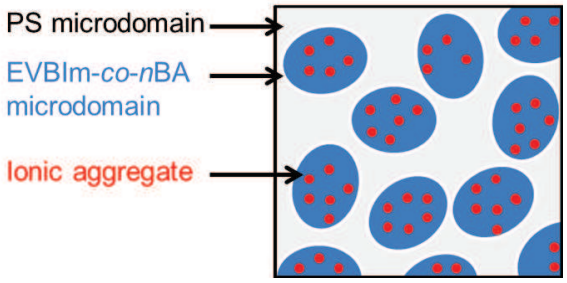

Figure 11. Proposed morphology of the self-assembled poly(Sty-b-[EVBIm$_{25\%}$-co-nBA$_{75\%}$]-b-Sty) triblock copolymer; adapted from reference 102.

The same team designed the poly(styrene-*b*-[vinylbenzyl imidazolium TFSI]-*b*-styrene) triblock copolymer (Entry 20, Table 1) for a use as electromechanical transducer.[99] A modulus of approximately 100 MPa at 23 °C was determined by dynamic mechanical analysis for this PIL BCP. Addition of 1-ethyl-3-methylimidazolium triflate, as molecular exogenous IL, allowed reducing the T_g of the central block, and increasing ionic conductivity by an order of magnitude for 20 wt%, and an additional order of magnitude for 40 wt% IL (a value of 1 x 10^{-2} S.cm^{-1} at 90 °C was determined in the latter case). In addition, actuator testing revealed superior curvature relative to Nafion®. It was found, however, that the presence of both

homoPIL and diblock copolymer limited precise and long-range ordered microstructure formation.

With both PMMA-*b*-PIL BCPs having TFSI anions (Entry 9, Table 1), and random copolymer homologues, Elabd, Winey *et al.* studied the effect of the weak microphase separation in ion transport.[84] SAXS and TEM analyses evidenced a microphase-separated morphology for the PIL BCP, but with no long-range order, likely owing to the partial affinity between the PIL and the PMMA blocks. The interdomain distances were 18 nm and 21 nm, for BCPs made of 13.4 and 15.7 mol% in PIL, respectively. In contrast, random copolymer homologues did not show any microphase separation, as expected. At similar PIL compositions, the ionic conductivity of the PIL BCPs was almost 2 orders of magnitude higher than that of the random copolymers (6.3×10^{-6} *vs.* 1.0×10^{-7} $S.cm^{-1}$ at 150 °C), demonstrating that local confinement of conducting ions in nanoscale ionic domains –despite a weak segregation regime- can favor ion transport.

In another contribution, the same PIL BCPs were evaluated for hydroxide (HO^-) conductivity.[85] Parent compounds carrying bromide anions were employed to this end. A nanoscale morphology was observed at 30 °C, in both dry and relative humidity conditions (from 30 to 90% RH). Hydroxide-exchanged PIL BCPs showed only two broader scattering peaks, compared to the bromide counterparts exhibiting four peaks. The HO^- conductivity (25×10^{-3} $S.cm^{-1}$ at 80 °C, 90% RH) was one order of magnitude higher, not only than that of the random copolymer analog, but also than that of the homoPIL analog with the same IL composition and water content. This was again explained by the ion-water confinement in nanodomains that might accelerate transport.

More recently, Elabd *et al.* synthesized similar PMMA-*b*-PIL BCPs with bromide as counter-anions, but having long alkyl side-chain length between the acrylate and the imidazolium groups.[87] Interestingly, at 80 °C with 90% RH, this PIL BCP exhibited a high bromide ion conductivity (64.85×10^{-3} $S.cm^{-1}$) which is an order of magnitude higher than a similar PIL BCP with shorter alkyl side chain length and three times than its analogous PIL homopolymer. In addition, this PMMA-*b*-PIL BCP was transparent and showed a high mechanical strengh (0.74 GPa modulus) and a PIL block glass transition temperature around 24 °C.

The same group showed that, at comparable PIL composition, acrylate-based poly(Sty-*b*-AEBIm-TFSI) PIL BCPs (Entry 21, Table 1) strongly microphase separated. In addition,

these compounds exhibited ~ 1.5−2 orders of magnitude higher ionic conductivity than their methacrylate-based homologues with weak microphase separation described above.[103] Hence, a higher degree of incompatibility between the low-T_g PIL and the nonionic PS block improved ion transport properties. Hexagonally packed cylinders, lamellae, and coexisting lamellae and network morphologies were observed, as a function of PIL composition (6.6−23.6 PIL mol%). The measured interdomain distances of the lamellar morphology were in the range of 25-30 nm. These morphologies were also found sensitive to casting conditions. Increasing the PIL content increased the ionic conductivity, owing to a morphological transition, from hexagonally packed cylinders with 1-D conducting pathways to lamellae with 2-D conducting pathways. In addition, the transition from 2-D lamellar morphology to coexisting 2-D lamellae and 3-D continuous conducting network structures further increased ionic conductivity (88 x 10^{-5} S.cm^{-1} at 150 °C in the latter case, corresponding to 23.6 PIL mol%). Overall, these acrylate-based PIL BCPs exhibited better conducting performances than PS-based PIL BCPs, highlighting the importance of the chemical nature of PIL.

Gin, Bailey *et al.* investigated in details the self-assembling properties in bulk of 16 ROMP-derived copolymers (Entry 14, Table 1) with variable volume fraction of the poly(norbornene dodecyl ester) block (f_{DOD} = 0.42-0.96; $\overline{M}_n$ values ranging from 5000-20100 g.mol^{-1}).[93,94] SAXS and rheological measurements at 25 °C showed the classic equilibrium self-assembled BCP morphologies, including lamellae, hexagonally packed cylinders, and spheres on a body-centered-cubic lattice. Even PIL BCPs having relatively low molecular weights exhibited a long-range ordered and stable morphology showing diffraction patterns with numerous higher order reflections by SAXS.

However, the bicontinuous gyroid phase occupying that region with traditional BCPs – and often sought for transport-related applications- was not observed in any sample. Instead, coexistence of cylinders and lamellae were identified at the intersection of hexagonal and lamellar regions. Poorly defined liquid-like packing of spheres was also noted in most asymmetric samples. The absence of the bicontinuous gyroid morphology, and difficulties in accessing order-to-disorder transitions were attributed to the strong microphase separation of such PIL BCPs.

The first examples of self-assembled ABC-type triblock copolymers (A: hydrophobic block, B: PIL block and C: hydrophilic block; Entry 15, Table 1) were described by Gin *et al.*[95] SAXS analysis of these samples verified phase-separation on the nanoscale and formation of different ordered morphologies, depending on block sequence and compositions.

ABC- and ACB-type triblock compounds were found to self-assemble into a lamellar phase, while the CAB-type BCP generated a hexagonally packed cylinder morphology. Interdomain spacings for the three compounds were very similar (*i.e.*, ABC: 26.2 nm, CAB: 28.6 nm, ACB: 24.7 nm).

PIL BCPs reported by Segalman *et al.* were prepared by deprotonation of histidine moieties of nonPIL precursors based on PS and poly(histaminemethacrylamide) (PHMAm) with trifluoroacetic acid.[200] SAXS and TEM analyses evidenced that, after thermal annealing above T_g (210 °C) under vacuum, hexagonally packed PHMAm cylinders formed from the precursor materials containing between 8 to 20 wt% PHMAm, while lamellar morphologies were observed for BCPs between 32 and 54 wt% PHMAm. A change of domain sizes was noted after chemical modification with TFA, resulting in PIL BCPs shown in Entry 23 (Table 1). This was ascribed to a higher incompatibility between the PS and the PIL blocks, likely due chain stretching of histidinium-type chains, as well as to an increase in volume fraction of the as-derivatized PHMAm. A higher water affinity of conducting blocks was also noted. While PS-*b*-PHMAm membranes had conductivities up to 2 x 10^{-4} S.cm^{-1} at room temperature, conductivities resulting from PIL BCPs increased by an order of magnitude, presumably owing to a higher mobility of PIL chains.

In order to vary the lamellar interdomain sizes of their self-assembled pyridinium-type PIL BCPs (Entry 24, Table 1), Garcia *et al.* exploited the anion exchange method (see Figure 12).[201] Neutral PS-*b*-P2VP BCPs were first partially quaternized (20 mol% of the 2-VP units) with 1-bromoethane, and Br^- anions were exchanged with larger sized anions, such as TFSI or $CF_3(CF_2)_3SO_3^-$. All compounds, with Br^-, $TFSI^-$ and $CF_3(CF_2)_3SO_3^-$ anions, exhibited a lamellar morphology, the lamellar domain size of which varied from 34 nm to 48 nm and further to 73 nm, from the Br^- to the TFSI to $CF_3(CF_2)_3SO_3^-$ BCP compound, respectively.

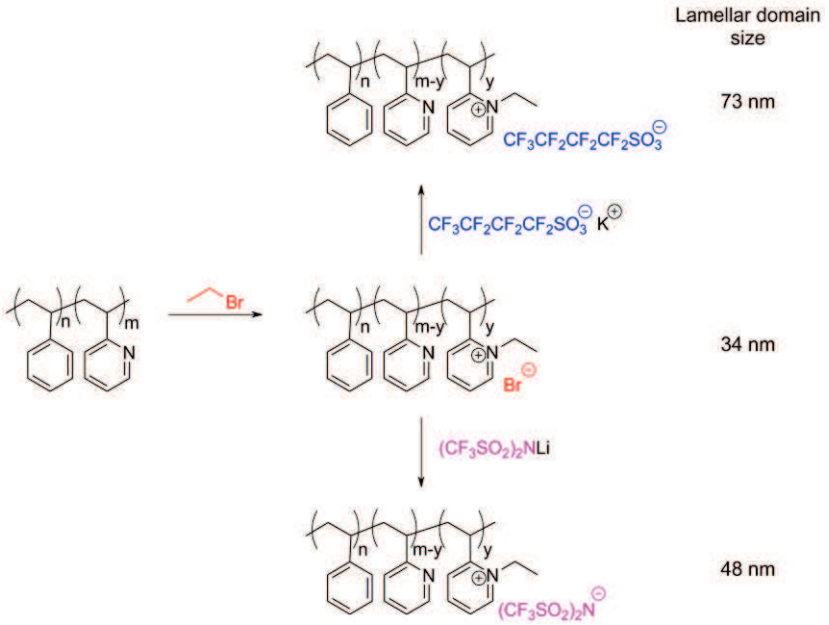

Figure 12. Modification of lamellar domain sizes in pyridinium-based PIL BCP *via* anion exchange; adapted from reference 201.

In another contribution, Garcia *et al.* used the same strategy by using $FeBr_3$ to obtain a paramagnetic [(P2VP-*r*-poly(1-ethyl-2-vinylpyridinium $Fe_3Br_{10}^-$)]-*b*-PMMA (Entry 25, Table 1).[202] This other nonimidazolium precursor was then blended with an epoxy resin (30 wt% relative to epoxy) and cured, which resulted in a spherical nanostructure, with sphere sizes of approximately 16 nm (by TEM). This led to the formation of a magnetic nanostructured thermoset material free of any kind of metal oxide or metal magnetic nanoparticles. The magnetic properties were measured by superconducting quantum interference device (SQUID). The spherical nanostructuration combined with confinement of magnetic anions (Figure 13) allowed promoting strong dipolar interactions between the magnetic entities and the observed ferromagnetic ordering.

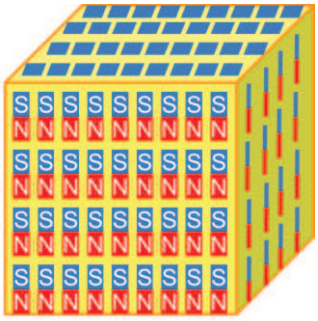

Figure 13. Schematic representation of the thermoset magnetic material based on PIL BCP; adapted from reference 202.

2.4. Potential applications of PIL BCPs

As already emphasized, PILs and related BCPs have emerged as a versatile family of polyelectrolytes showing multiple advantages, such as tunable solubility, adjustable chain flexibility, relatively high ionic conductivity, or ionic-responsiveness. This section briefly discusses the very few and preliminary investigations regarding PIL BCPs' applications in selected fields, such as energy harvesting, gas separation, or as precursors for magnetic or nanostructured carbon materials.

2.4.1. Energy conversion devices

Due to their relatively high ionic conductivity, which can be tuned by a proper selection of both the alkyl substituent on the imidazolium ring and the counter-anion, PILs are promising materials as solid polymer electrolytes for various electrochemical devices (actuators, transducers, fuel cells, ion-conducting membranes, or solar cells).[111,114–119,204,205] Ion-conducting membranes are key components in energy conversion devices, since they not only enable the transport of ionic species across physically separated reaction sites, but they also provide structural stability and barrier properties to the device. As previously discussed, microphase separated PIL BCPs represent a promising method to develop mechanically robust nanostructured materials (*via* the non-ionic block, preferentially of high T_g), while the PIL domains can form connecting paths for ion conduction (this is particularly favored with low T_g PILs). However, specific nanodomains (*e.g.* hexagonally packed cylinders) impede ionic conductivity due to grain boundaries,[100] whereas larger size nanodomains (*e.g.* in lamellar morphologies) favor ion transport. Other parameters can influence conductivity of PIL BCPs, such as the type of couterion, relative humidity, temperature, or use of an exogenous IL. In different cases, the temperature dependence of the ionic conductivity was well described by the Vogel-Tamman-Fulcher (VFT) model, indicating a strong correlation between ion conduction and polymer segmental dynamics.[84,85,87,99–103,200]

Armand, Gigmes *et al.* integrated their P(STFSILi)-*b*-PEO-*b*-P(STFSILi)s, BAB triblock copolymers (Entry 12, Table 1) as solid polymer electrolytes in real lithium batteries.[193] Corresponding devices exhibited unprecedented performances in this application: the best ionic conductivity of 1.3×10^{-5} S.cm^{-1} was obtained at about 20 wt% P(STFSILi) (molar ratio [EO]/[Li] = 30) at 60 °C, and the mechanical properties was significantly improved compared to a neutral PS-*b*-PEO-*b*-PS triblock copolymer electrolyte (10 MPa *vs.* 1 MPa at 40 °C,

respectively). This work opens avenue for the development of energy device-based on PIL BCPs discussed in this section.

2.4.2. PIL BCPs for gas separation

ILs and PILs represent promising materials for CO_2 capture, storage and conversion, and for gas separation applications in general.[46,68,187–189,206,207] These features combined with the potential of nanophase-separation on transport properties make PIL BCPs potential candidates for gas separation. Lodge *et al.* evaluated the separation performance of their triblock copolymer ion gel, PS-*b*-PBrEA-*b*-PS (Entry 22, Table 1) on a microporous PVDF membrane (0.45 μm pore sire, 75 % porosity), at room temperature.[104] The pores of the PVDF membranes were filled with ion gels containing 15 wt% of the triblock to form a dense, dry membrane. The BCP ion gel showed a permselectivity of 19 for CO_2/CH_4 and 39 for CO_2/N_2 gas pairs. The permeability of each gas (CO_2, N_2, CH_4) was roughly the same in presence or in absence of another gas (Example: CO_2 = 985 ± 29 *vs.* CO_2 in presence of N_2 = 1030 ± 24 *vs.* CO_2 in presence of CH_4 = 1040 ± 23).

Gas transport through phase-separated ROMP-derived PIL BCPs (71, 42, 31 and 18 wt% IL units respectively; entry 15, Table 1) was also investigated by Gin, Noble *et al.*.[95] Preparation of defect-free, thin film membrane composites, with a 3–20 μm thick nanostructured top layer of the BCP, could be achieved. The composition of the BCP top layer was found to impact the CO_2 permeability that could be increased by 2 orders of magnitude up to a value of 9300 barrers. This beneficial effect on the CO_2 permeability was attributed to a higher gas diffusion coefficient of the ordered nanostructures arising from PIL BCPs, compared to amorphous BCP compounds. However, the selectivity was not improved since the diffusion of both CO_2 and N_2 was favored by the nanostructuration. Use of an additional molecular IL might be helpful to gain in selectivity.

The same group reported the first example of membrane nanocomposites issued from ABC PIL-based triblock copolymer (Entry 15, Table 1).[96] Only the ABC- and CAB-type sequences were successfully coated onto the surface of a commercial porous poly(acrylonitrile) membrane support, forming hybrid membranes, the potential of which for CO_2/light gas separations was examined on a series of four gases (*i.e.*, CO_2, N_2, CH_4, H_2). The two phase-separated systems showed different gas permeability values, but similar selectivity

values (Table 2). This was ascribed to different polymer nanostructures and/or nanodomain orientation.

Table 2. Gas permeabilities (in barrers) and selectivities of ABC- and CAB-type triblock copolymer composite membranes. Thickness of the active layers were respectively 12.4 μm and 12.6.[96]

	Perm (CO_2) [Barrers]	Perm (N_2) [Barrers]	Perm (CH_4) [Barrers]	Perm (H_2) [Barrers]	α(CO_2/ N_2)	α(CO_2/ CH_4)	α(CO_2/ H_2)
ABC	2340	230	820	740	10.2	2.9	3.2
CAB	410	30	100	140	13.7	4.1	2.9

2.4.3. As precursors for nanostructured carbon

Imidazolium-based ILs and PILs have been reported as effective precursors for functional carbon-based nanomaterials.[144,146,147] Incorporation of molecular ILs into porous templates, without the need for high pressure, can be easily achieved owing to the liquid state and the highly thermostability of ILs.

Antonietti *et al.* reported that PIL BCPs (Entry 6, Table 1) could serve as efficient precursors for the preparation of mesoporous graphitic nanostructures in the presence of metal salts.[82] The carbonization step was carried out in the presence of 10 wt% of $FeCl_2.4H_2O$ or $CrCl_3.6H_2O$, leading to porous carbon products, after 2h at 1000 °C under N_2 atmosphere. Compounds prepared with $FeCl_2.4H_2O$ and $CrCl_3.6H_2O$ exhibited a surface area of 150 and 175 m^2/g respectively. TEM images revealed layered graphitic nanostructures, constructed from the stacking of graphene sheets with a *d* spacing of 0.34 nm. XRD characterizations revealed the existence of iron carbide phases as nanoparticles with a size range of 10-80 nm within the mesoporous graphitic carbon products. Same observations were made using chromium carbide. These mesoporous graphitic nanostructures are promising candidates for electrochemical applications.

Conclusion

In the past decade, the field of polyelectrolytes has been widely expanded by the introduction of poly(ionic liquid)s that exhibit specific properties such as relatively high CO_2 solubility, ionic conductivity, thermal and chemical stability and tunable solubility, thanks to ion exchange, with the intrinsic properties of polymers.

From a synthetic viewpoint, PILs can be achieved by free radical polymerization, or by "controlled/living" polymerization (*e.g.* RAFT, ATRP, RAFT, ROMP), or by step-growth polymerization of IL-type monomers. Post-chemical modification enabling the introduction of IL units side groups onto a preformed polymer is an alternative synthetic strategy to obtain PILs and related PIL BCPs. These synthetic tools allow fine-tuning composition, IL content, type of couterion and alkyl chain. Both the thermomechanical properties and the ionic conductivity can thus be tailored by a judicious selection of these parameters.

Introduction of ILs and PIL segments into BCPs has also emerged in the past five years. PIL BCPs combine properties of PILs with the ordered phase-separated nanostructures formed by self-assembly of BCPs.

The possibility to achieve multiresponsive, robust, and stable nanostructures from PIL BCPs in solution opens avenues for their use in areas, such as micellar catalysis and drug delivery systems. On the other hand, several studies have evidenced that transport properties of PIL BCPs correlate with their nanostructured morphologies resulting from their self-assembly at the solid state. As for traditional self-assembled materials, processing conditions (*e.g.*, solvent casting *vs.* melt casting) influence phase segregation and resulting size and nature domains, which can have a significant impact on ionic conductivity and/or gas transport. Higher conductivities may be reached by increasing the size of the conducting channels, *e.g.* in lamellar domains where PIL chains can adopt a stretched conformation. In contrast, PIL BCPs self-assembling into hexagonally packed cylinders may exhibit a rather poor ionic conductivity, owing to defects and grain boundaries of this peculiar morphology. None of the studies reported so far has established the existence of the bi-continuous gyroid morphology, which would be of particular interest for gas or ion transport-related applications. This is presumably due to the strong microphase segregation regime resulting from the covalent association of nonionic and PIL blocks that have been so far considered. However, further efforts may be needed to achieve such co-continuous morphology, for instance, using specific solvent and/or thermomechanical treatments.

The field of PIL BCPs is still in its infancy, and pioneer works described in this chapter may help for an optimization of their transport and mechanical properties. There is still plenty of room to design and engineer novel compounds and, for instance, to introduce new functionalities *via* the PIL and/or the uncharged blocks towards a specific applications. One can thus expect that this field will blossom in the next few years.

In this PhD work, and as discussed in the two following chapters, we have expanded the use of PILs by exploiting the potential reactivity of the imidazolium units, for the purpose of catalysis and post-chemical modification. In particular, we have designed novel PILs that can generate poly(*N*-heterocyclic carbene)s (chapter 2).

We have also developed a specific synthetic strategy to PIL BCP based on PVAc and poly(*N*-vinyl-3-alkylimidazolium) (PVAc-*b*-PIL) featuring different alkyl chains counter-anions. The ionic conductivity of this PIL BCPs induced by their self-assembling property at the solid state will be discussed in chapter 3. Meanwhile their self-assembling properties in solution are studied with various counter-anions. The use of PIL BCPs as stabilizers and reducing agents *via* the counter-anion for the synthesis of gold nanoparticles will be also described in chapter 3.

References

1. Green, O.; Grubjesic, S.; Lee, S.; Firestone, M. A. *Polym. Rev.* **2009**, *49*, 339–360.
2. Lu, J.; Yan, F.; Texter, J. *Prog. Polym. Sci.* **2009**, *34*, 431–448.
3. Green, M. D.; Long, T. E. *Polym Rev* **2009**, *49*, 291–314.
4. Mecerreyes, D. *Prog. Polym. Sci.* **2011**, *36*, 1629–1648.
5. Yuan, J.; Mecerreyes, D.; Antonietti, M. *Prog. Polym. Sci.* **2013**, *38*, 1009–1036.
6. Nishimura, N.; Ohno, H. *Polymer* **2014**, *55*, 3289–3297.
7. Rogers, R.; Seddon, K.; Volkov, S.; editors. New-York: Springer-Verlag, **2003**; p. 545.
8. Pârvulescu, V. I.; Hardacre, C. *Chem. Rev.* **2007**, *107*, 2615–2665.
9. Ohno, H. *Electrochemical aspects of ionic liquids.*; John Wiley& Sons, Inc;, **2005**.
10. Armand, M.; Endres, F.; MacFarlane, D. R.; Ohno, H.; Scrosati, B. *Nat Mater* **2009**, *8*, 621–629.
11. Yuan, J.; Antonietti, M. *Polymer* **2011**, *52*, 1469–1482.
12. Soukup-Hein, R. J.; Warnke, M. M.; Armstrong, D. W. *Annu. Rev. Anal. Chem.* **2009**, *2*, 145–168.
13. Wishart, J. F. *Energy Environ. Sci.* **2009**, *2*, 956–961.
14. Dupont, J.; Scholten, J. D. *Chem. Soc. Rev.* **2010**, *39*, 1780–1804.
15. Roosen, C.; Müller, P.; Greiner, L. *Appl. Microbiol. Biotechnol.* **2008**, *81*, 607–614.
16. Shaplov, A. S.; Lozinskaya, E. I.; Vygodskii, Y. S. In *Electrochemical Properties and Applications of Ionic Liquids*; A. A. J. Torriero; M. J. A. Shiddiky, Eds.; **2011**; pp. 203–298.
17. Jangu, C.; Long, T. E. *Polymer* **2014**, *55*, 3298–3304.
18. Jaeger, W.; Bohrisch, J.; Laschewsky, A. *Prog. Polym. Sci.* **2010**, *35*, 511–577.
19. Alhoranta, A. M.; Lehtinen, J. K.; Urtti, A. O.; Butcher, S. J.; Aseyev, V. O.; Tenhu, H. J. *Biomacromolecules* **2011**, *12*, 3213–3222.
20. Massignani, M.; LoPresti, C.; Blanazs, A.; Madsen, J.; Armes, S. P.; Lewis, A. L.; Battaglia, G. *Small* **2009**, *5*, 2424–2432.
21. Shaplov, A. S.; Lozinskaya, E. I.; Ponkratov, D. O.; Malyshkina, I. A.; Vidal, F.; Aubert, P.-H.; Okatova, O. V; Pavlov, G. M.; Komarova, L. I.; Wandrey, C.; Vygodskii, Y. S. *Electrochim. Acta* **2011**, *57*, 74–90.
22. Lewandowski, A.; Świderska, A. *Solid State Ionics* **2004**, *169*, 21–24.
23. Shaplov, A. S.; Vlasov, P. S.; Lozinskaya, E. I.; Ponkratov, D. O.; Malyshkina, I. A.; Vidal, F.; Okatova, O. V; Pavlov, G. M.; Wandrey, C.; Bhide, A.; Schönhoff, M.; Vygodskii, Y. S. *Macromolecules* **2011**, *44*, 9792–9803.
24. Washiro, S.; Yoshizawa, M.; Nakajima, H.; Ohno, H. *Polymer* **2004**, *45*, 1577–1582.
25. Ohno, H. *Macromol. Symp.* **2007**, *249-250*, 551–556.
26. Marcilla, R.; Alcaide, F.; Sardon, H.; Pomposo, J. A.; Pozo-Gonzalo, C.; Mecerreyes, D. *Electrochem. commun.* **2006**, *8*, 482–488.
27. Marcilla, R.; Blazquez, J. A.; Fernandez, R.; Grande, H.; Pomposo, J. A.; Mecerreyes, D. *Macromol. Chem. Phys.* **2005**, *206*, 299–304.
28. Destarac, M. *Polym. Rev.* **2011**, *51*, 163–187.
29. Perrier, S.; Takolpuckdee, P. *J. Polym. Sci. Part A Polym. Chem.* **2005**, *43*, 5347–5393.
30. Moad, G.; Rizzardo, E.; Thang, S. H. Living Radical Polymerization by the RAFT Process – A Third Update. *Australian Journal of Chemistry*, **2012**, *65* , 985–1076.
31. Moad, G.; Rizzardo, E.; Thang, S. H. *Polym. Int.* **2011**, *60*, 9–25.
32. Matyjaszewski, K.; Xia, J. *Chem. Rev.* **2001**, *101*, 2921–2990.
33. Matyjaszewski, K. *Macromolecules* **2012**, *45*, 4015–4039.

34. Kato, M.; Kamigaito, M.; Sawamoto, M.; Higashimura, T. *Macromolecules* **1995**, *28*, 1721–1723.
35. Debuigne, A.; Caille, J.-R.; Detrembleur, C.; Jérôme, R. *Angew. Chemie Int. Ed.* **2005**, *44*, 1101–1104.
36. Hawker, C. J.; Bosman, A. W.; Harth, E. *Chem. Rev.* **2001**, *101*, 3661–3688.
37. Bielawski, C. W.; Grubbs, R. H. *Prog. Polym. Sci.* **2007**, *32*, 1–29.
38. He, H.; Zhong, M.; Adzima, B.; Luebke, D.; Nulwala, H.; Matyjaszewski, K. *J. Am. Chem. Soc.* **2013**, *135*, 4227–4230.
39. Li, F.; Cheng, F.; Shi, J.; Cai, F.; Liang, M.; Chen, J. *J. Power Sources* **2007**, *165*, 911–915.
40. Zhang, Y.; Zhao, L.; Patra, P. K.; Hu, D.; Ying, J. Y. *Nano Today* **2009**, *4*, 13–20.
41. Marcilla, R.; Alberto Blazquez, J.; Rodriguez, J.; Pomposo, J. A.; Mecerreyes, D. *J. Polym. Sci. Part A Polym. Chem.* **2004**, *42*, 208–212.
42. Hirao, M.; Ito, K.; Ohno, H. *Electrochim. Acta* **2000**, *45*, 1291–1294.
43. Batra, D.; Seifert, S.; Varela, L. M.; Liu, A. C. Y.; Firestone, M. A. *Adv. Funct. Mater.* **2007**, *17*, 1279–1287.
44. Patachia, S.; Savin, G.; Luca, C.; Beldie, C. *Eur. Polym. J.* **2002**, *38*, 1121–1127.
45. Zhang, G.; Liu, X.; Li, B.; Bai, Y. *J. Appl. Polym. Sci.* **2009**, *112*, 3337–3340.
46. Bara, J. E.; Lessmann, S.; Gabriel, C. J.; Hatakeyama, E. S.; Noble, R. D.; Gin, D. L. *Ind. Eng. Chem. Res.* **2007**, *46*, 5397–5404.
47. Tang, J.; Tang, H.; Sun, W.; Radosz, M.; Shen, Y.; Plancher, H. *Polymer* **2005**, *46*, 3325–3327.
48. Kadokawa, J.; Murakami, M.; Kaneko, Y. *Compos. Sci. Technol.* **2008**, *68*, 493–498.
49. Ding, S.; Tang, H.; Radosz, M.; Shen, Y. *J. Polym. Sci. Part A Polym. Chem.* **2004**, *42*, 5794–5801.
50. Yu, B.; Zhou, F.; Hu, H.; Wang, C.; Liu, W. *Electrochim. Acta* **2007**, *53*, 487–494.
51. Batra, D.; Hay; Firestone, M. A. *Chem. Mater.* **2007**, *19*, 4423–4431.
52. Vijayakrishna, K.; Jewrajka, S. K.; Ruiz, A.; Marcilla, R.; Pomposo, J. A.; Mecerreyes, D.; Taton, D.; Gnanou, Y. *Macromolecules* **2008**, *41*, 6299–6308.
53. Seno, K.-I.; Kanaoka, S.; Aoshima, S. *J. Polym. Sci. Part A Polym. Chem.* **2008**, *46*, 5724–5733.
54. Vygodskii, Y. S.; Shaplov, A. S.; Lozinskaya, E. I.; Lyssenko, K. A.; Golovanov, D. G.; Malyshkina, I. A.; Gavrilova, N. D.; Buchmeiser, M. R. *Macromol. Chem. Phys.* **2008**, *209*, 40–51.
55. Mineo, P. G.; Livoti, L.; Giannetto, M.; Gulino, A.; Lo Schiavo, S.; Cardiano, P. *J. Mater. Chem.* **2009**, *19*, 8861–8870.
56. Sato, T.; Marukane, S.; Narutomi, T.; Akao, T. *J. Power Sources* **2007**, *164*, 390–396.
57. Watanabe, M.; Yamada, S.; Ogata, N. *Electrochim. Acta* **1995**, *40*, 2285–2288.
58. Xiao, S.; Lu, X.; Lu, Q. *Macromolecules* **2007**, *40*, 7944–7950.
59. Pont, A.-L.; Marcilla, R.; Meatza, I. De; Grande, H.; Mecerreyes, D. *J. Power Sources* **2009**, *188*, 558–563.
60. Li, M.; Yang, L.; Fang, S.; Dong, S. *J. Memb. Sci.* **2011**, *366*, 245–250.
61. Ogihara, W.; Washiro, S.; Nakajima, H.; Ohno, H. *Electrochim. Acta* **2006**, *51*, 2614–2619.
62. Cheng, S.; Beyer, F. L.; Mather, B. D.; Moore, R. B.; Long, T. E. *Macromolecules* **2011**, *44*, 6509–6517.
63. Marcilla, R.; Sanchez-Paniagua, M.; Lopez-Ruiz, B.; Lopez-Cabarcos, E.; Ochoteco, E.; Grande, H.; Mecerreyes, D. *J. Polym. Sci. Part A Polym. Chem.* **2006**, *44*, 3958–3965.

64. Yan, F.; Texter, J. *Chem. Commun.* **2006**, 2696–2698.
65. Yu, S.; Yan, F.; Zhang, X.; You, J.; Wu, P.; Lu, J.; Xu, Q.; Xia, X.; Ma, G. *Macromolecules* **2008**, *41*, 3389–3392.
66. Yuan, J.; Antonietti, M. *Macromolecules* **2011**, *44*, 744–750.
67. Nakajima, H.; Ohno, H. *Polymer* **2005**, *46*, 11499–11504.
68. Bara, J. E.; Hatakeyama, E. S.; Gabriel, C. J.; Zeng, X.; Lessmann, S.; Gin, D. L.; Noble, R. D. *J. Memb. Sci.* **2008**, *316*, 186–191.
69. Bara, J. E.; Hatakeyama, E. S.; Gin, D. L.; Noble, R. D. *Polym. Adv. Technol.* **2008**, *19*, 1415–1420.
70. Bezdushna, E.; Ritter, H. *Macromol. React. Eng.* **2009**, *3*, 516–521.
71. Chen, H.; Choi, J.-H.; la Cruz, D.; Winey, K. I.; Elabd, Y. A. *Macromolecules* **2009**, *42*, 4809–4816.
72. Matsumoto, K.; Talukdar, B.; Endo, T. *Polym. Bull.* **2010**, *66*, 199–210.
73. Moad, G.; Rizzardo, E.; Thang, S. H. Living Radical Polymerization by the RAFT Process. *Australian Journal of Chemistry*, **2005**, *58* , 379–410.
74. Debuigne, A.; Poli, R.; Jérôme, C.; Jérôme, R.; Detrembleur, C. *Prog. Polym. Sci.* **2009**, *34*, 211–239.
75. Årstad, E.; Barrett, A. G. M.; Tedeschi, L. *Tetrahedron Lett.* **2003**, *44*, 2703–2707.
76. Tang, H.; Tang, J.; Ding, S.; Radosz, M.; Shen, Y. *J. Polym. Sci. Part A Polym. Chem.* **2005**, *43*, 1432–1443.
77. He, H.; Zhong, M.; Luebke, D.; Nulwala, H.; Matyjaszewski, K. *J. Polym. Sci. Part A Polym. Chem.* **2014**, DOI: 10.1002/pola.27229.
78. Vijayakrishna, K.; Mecerreyes, D.; Gnanou, Y.; Taton, D. *Macromolecules* **2009**, *42*, 5167–5174.
79. Karjalainen, E.; Chenna, N.; Laurinmaki, P.; Butcher, S. J.; Tenhu, H. *Polym. Chem.* **2013**, *4*, 1014–1024.
80. Mori, H.; Müller, A. H. E. *Prog. Polym. Sci.* **2003**, *28*, 1403–1439.
81. Mori, H.; Yahagi, M.; Endo, T. *Macromolecules* **2009**, *42*, 8082–8092.
82. Yuan, J.; Schlaad, H.; Giordano, C.; Antonietti, M. *Eur. Polym. J.* **2011**, *47*, 772–781.
83. Wang, Z.; Lai, H.; Wu, P. *Soft Matter* **2012**, *8*, 11644–11653.
84. Ye, Y.; Choi, J.-H.; Winey, K. I.; Elabd, Y. A. *Macromolecules* **2012**, *45*, 7027–7035.
85. Ye, Y.; Sharick, S.; Davis, E. M.; Winey, K. I.; Elabd, Y. A. *ACS Macro Lett.* **2013**, 575–580.
86. Mori, H.; Ebina, Y.; Kambara, R.; Nakabayashi, K. *Polym J* **2012**, *44*, 550–560.
87. Nykaza, J. R.; Ye, Y.; Elabd, Y. A. *Polymer* **2014**, *55*, 3360–3369.
88. Guinaudeau, A.; Mazieres, S.; Wilson, D. J.; Destarac, M. *Polym. Chem.* **2012**, *3*, 81–84.
89. Guinaudeau, A.; Coutelier, O.; Sandeau, A.; Mazières, S.; Nguyen Thi, H. D.; Le Drogo, V.; Wilson, D. J.; Destarac, M. *Macromolecules* **2014**, *47*, 41–50.
90. Detrembleur, C.; Debuigne, A.; Hurtgen, M.; Jérôme, C.; Pinaud, J.; Fèvre, M.; Coupillaud, P.; Vignolle, J.; Taton, D. *Macromolecules* **2011**, *44*, 6397–6404.
91. Vygodskii, Y. S.; Shaplov, A. S.; Lozinskaya, E. I.; Filippov, O. A.; Shubina, E. S.; Bandari, R.; Buchmeiser, M. R. *Macromolecules* **2006**, *39*, 7821–7830.
92. Zheng, L.; Chen, F.; Xie, M.; Han, H.; Dai, Q.; Zhang, Y.; Song, C. *React. Funct. Polym.* **2007**, *67*, 19–24.
93. Scalfani, V. F.; Wiesenauer, E. F.; Ekblad, J. R.; Edwards, J. P.; Gin, D. L.; Bailey, T. S. *Macromolecules* **2012**, *45*, 4262–4276.

94. Wiesenauer, E. F.; Edwards, J. P.; Scalfani, V. F.; Bailey, T. S.; Gin, D. L. *Macromolecules* **2011**, *44*, 5075–5078.
95. Wiesenauer, E. F.; Nguyen, P. T.; Newell, B. S.; Bailey, T. S.; Noble, R. D.; Gin, D. L. *Soft Matter* **2013**, *9*, 7923–7927.
96. Nguyen, P. T.; Wiesenauer, E. F.; Gin, D. L.; Noble, R. D. *J. Memb. Sci.* **2013**, *430*, 312–320.
97. Stancik, C. M.; Lavoie, A. R.; Schütz, J.; Achurra, P. A.; Lindner, P.; Gast, A. P.; Waymouth, R. M. *Langmuir* **2003**, *20*, 596–605.
98. Stancik, C. M.; Lavoie, A. R.; Achurra, P. A.; Waymouth, R. M.; Gast, A. P. *Langmuir* **2004**, *20*, 8975–8987.
99. Green, M. D.; Wang, D.; Hemp, S. T.; Choi, J.-H.; Winey, K. I.; Heflin, J. R.; Long, T. E. *Polymer* **2012**, *53*, 3677–3686.
100. Weber, R. L.; Ye, Y.; Schmitt, A. L.; Banik, S. M.; Elabd, Y. A.; Mahanthappa, M. K. *Macromolecules* **2011**, *44*, 5727–5735.
101. Sudre, G.; Inceoglu, S.; Cotanda, P.; Balsara, N. P. *Macromolecules* **2013**, *46*, 1519–1527.
102. Green, M. D.; Choi, J.-H.; Winey, K. I.; Long, T. E. *Macromolecules* **2012**, *45*, 4749–4757.
103. Choi, J.-H.; Ye, Y.; Elabd, Y. A.; Winey, K. I. *Macromolecules* **2013**, *46*, 5290–5300.
104. Gu, Y.; Lodge, T. P. *Macromolecules* **2011**, *44*, 1732–1736.
105. Sood, R.; Obadia, M. M.; Mudraboyina, B. P.; Zhang, B.; Serghei, A.; Bernard, J.; Drockenmuller, E. *Polymer* **2014**, *55*, 3314–3319.
106. Matsumi, N.; Sugai, K.; Miyake, M.; Ohno, H. *Macromolecules* **2006**, *39*, 6924–6927.
107. Dimitrov-Raytchev, P.; Beghdadi, S.; Serghei, A.; Drockenmuller, E. *J. Polym. Sci. Part A Polym. Chem.* **2013**, *51*, 34–38.
108. Mudraboyina, B. P.; Obadia, M. M.; Allaoua, I.; Sood, R.; Serghei, A.; Drockenmuller, E. *Chem. Mater.* **2014**, *26*, 1720–1726.
109. Obadia, M. M.; Mudraboyina, B. P.; Allaoua, I.; Haddane, A.; Montarnal, D.; Serghei, A.; Drockenmuller, E. *Macromol. Rapid Commun.* **2014**, *35*, DOI: 10.1002/marc.201400075.
110. Aitken, B. S.; Lee, M.; Hunley, M. T.; Gibson, H. W.; Wagener, K. B. *Macromolecules* **2010**, *43*, 1699–1701.
111. Qiu, B.; Lin, B.; Si, Z.; Qiu, L.; Chu, F.; Zhao, J.; Yan, F. *J. Power Sources* **2012**, *217*, 329–335.
112. Lin, B.; Qiu, L.; Lu, J.; Yan, F. *Chem. Mater.* **2010**, *22*, 6718–6725.
113. Qiu, B.; Lin, B.; Qiu, L.; Yan, F. *J. Mater. Chem.* **2012**, *22*, 1040–1045.
114. Deavin, O. I.; Murphy, S.; Ong, A. L.; Poynton, S. D.; Zeng, R.; Herman, H.; Varcoe, J. R. *Energy Environ. Sci.* **2012**, *5*, 8584–8597.
115. Luo, Y.; Guo, J.; Wang, C.; Chu, D. *ChemSusChem* **2011**, *4*, 1557–1560.
116. Li, W.; Fang, J.; Lv, M.; Chen, C.; Chi, X.; Yang, Y.; Zhang, Y. *J. Mater. Chem.* **2011**, *21*, 11340–11346.
117. Chen, X.; Zhao, J.; Zhang, J.; Qiu, L.; Xu, D.; Zhang, H.; Han, X.; Sun, B.; Fu, G.; Zhang, Y.; Yan, F. *J. Mater. Chem.* **2012**, *22*, 18018–18024.
118. Ran, J.; Wu, L.; Varcoe, J. R.; Ong, A. L.; Poynton, S. D.; Xu, T. *J. Memb. Sci.* **2012**, *415–416*, 242–249.
119. Azaceta, E.; Marcilla, R.; Sanchez-Diaz, A.; Palomares, E.; Mecerreyes, D. *Electrochim. Acta* **2010**, *56*, 42–46.
120. Wang, G.; Zhuo, S.; Lin, Y. *J. Appl. Polym. Sci.* **2013**, *127*, 2574–2580.

121. Kim, J.-K.; Niedzicki, L.; Scheers, J.; Shin, C.-R.; Lim, D.-H.; Wieczorek, W.; Johansson, P.; Ahn, J.-H.; Matic, A.; Jacobsson, P. *J. Power Sources* **2013**, *224*, 93–98.
122. Choi, U. H.; Ye, Y.; de la Cruz, D.; Liu, W.; Winey, K. I.; Elabd, Y. A.; Runt, J.; Colby, R. H.; Salas de la Cruz, D. *Macromolecules* **2014**, *47*, 777–790.
123. Ohno, H. *Electrochim. Acta* **2001**, 1407–1411.
124. Vygodskii, Y. S.; Mel'nik, O. A.; Lozinskaya, E. I.; Shaplov, A. S.; Malyshkina, I. A.; Gavrilova, N. D.; Lyssenko, K. A.; Antipin, M. Y.; Golovanov, D. G.; Korlyukov, A. A.; Ignat'ev, N.; Welz-Biermann, U. *Polym. Adv. Technol.* **2007**, *18*, 50–63.
125. Hamedi, M.; Herlogsson, L.; Crispin, X.; Marcilla, R.; Berggren, M.; Inganäs, O. *Adv. Mater.* **2009**, *21*, 573–577.
126. Tang, J.; Radosz, M.; Shen, Y. *Macromolecules* **2008**, *41*, 493–496.
127. Tang, J.; Shen, Y.; Radosz, M.; Sun, W. *Ind. Eng. Chem. Res.* **2009**, *48*, 9113–9118.
128. Wilke, A.; Yuan, J.; Antonietti, M.; Weber, J. *ACS Macro Lett.* **2012**, *1*, 1028–1031.
129. Xiong, Y.-B.; Wang, H.; Wang, Y.-J.; Wang, R.-M. *Polym. Adv. Technol.* **2012**, *23*, 835–840.
130. Bara, J. E.; Noble, R. D.; Gin, D. L. *Ind. Eng. Chem. Res.* **2009**, *48*, 4607–4610.
131. Bara, J. E.; Camper, D. E.; Gin, D. L.; Noble, R. D. *Acc. Chem. Res.* **2009**, *43*, 152–159.
132. Tomé, L. C.; Mecerreyes, D.; Freire, C. S. R.; Rebelo, L. P. N.; Marrucho, I. M. *J. Memb. Sci.* **2013**, *428*, 260–266.
133. Qiu, H.; Mallik, A. K.; Takafuji, M.; Liu, X.; Jiang, S.; Ihara, H. *J. Chromatogr. A* **2012**, *1232*, 116–122.
134. Qi, M.; Armstrong, D. W. *Anal. Bioanal. Chem.* **2007**, *388*, 889–899.
135. Xiong, Y.; Wang, Y.; Wang, H.; Wang, R.; Cui, Z. *J. Appl. Polym. Sci.* **2012**, *123*, 1486–1493.
136. Mu, X.; Meng, J.; Li, Z.-C.; Kou, Y. *J. Am. Chem. Soc.* **2005**, *127*, 9694–9695.
137. Pinaud, J.; Vignolle, J.; Gnanou, Y.; Taton, D. *Macromolecules* **2011**, *44*, 1900–1908.
138. Fukushima, T.; Kosaka, A.; Ishimura, Y.; Yamamoto, T.; Takigawa, T.; Ishii, N.; Aida, T. *Sci.* **2003**, *300* , 2072–2074.
139. Marcilla, R.; Ochoteco, E.; Pozo-Gonzalo, C.; Grande, H.; Pomposo, J. A.; Mecerreyes, D. *Macromol. Rapid Commun.* **2005**, *26*, 1122–1126.
140. Marcilla, R.; Pozo-Gonzalo, C.; Rodríguez, J.; Alduncin, J. A.; Pomposo, J. A.; Mecerreyes, D. *Synth. Met.* **2006**, *156*, 1133–1138.
141. Pozo-Gonzalo, C.; Marcilla, R.; Salsamendi, M.; Mecerreyes, D.; Pomposo, J. A.; Rodríguez, J.; Bolink, H. J. *J. Polym. Sci. Part A Polym. Chem.* **2008**, *46*, 3150–3154.
142. Kim, T.; Suh, M.; Kwon, S. J.; Lee, T. H.; Kim, J. H. J. E.; Lee, Y. J.; Hong, M.; Suh, K. S. *Macromol. Rapid Commun.* **2009**, *30*, 1477–1482.
143. Chen, H.; Elabd, Y. A. *Macromolecules* **2009**, *42*, 3368–3373.
144. Yuan, J.; Marquez, A. G.; Reinacher, J.; Giordano, C.; Janek, J.; Antonietti, M. *Polym. Chem.* **2011**, *2*, 1654–1657.
145. Pan, C.; Qiu, L.; Peng, Y.; Yan, F. *J. Mater. Chem.* **2012**, *22*, 13578–13584.
146. Bo, X.; Bai, J.; Ju, J.; Guo, L. *J. Power Sources* **2011**, *196*, 8360–8365.
147. Yuan, J.; Giordano, C.; Antonietti, M. *Chem. Mater.* **2010**, *22*, 5003–5012.
148. Hong, S. H.; Tung, T. T.; Huyen Trang, L. K.; Kim, T. Y.; Suh, K. S. *Colloid Polym. Sci.* **2010**, *288*, 1013–1018.
149. Murakami, M.; Kaneko, Y.; Kadokawa, J. *Carbohydr. Polym.* **2007**, *69*, 378–381.
150. Prasad, K.; Mine, S.; Kaneko, Y.; Kadokawa, J. *Polym. Bull.* **2010**, *64*, 341–349.

151. Huang, J.; Tao, C.; An, Q.; Zhang, W.; Wu, Y.; Li, X.; Shen, D.; Li, G. *Chem. Commun.* **2010**, *46*, 967–969.
152. Zhang, Y.; Chen, X.; Lan, J.; You, J.; Chen, L. *Chem. Biol. Drug Des.* **2009**, *74*, 282–288.
153. Bates, F. S.; Hillmyer, M. A.; Lodge, T. P.; Bates, C. M.; Delaney, K. T.; Fredrickson, G. H. *Science* **2012**, *336*, 434–440.
154. Whitesides, G. M.; Grzybowski, B. *Science* **2002**, *295*, 2418–2421.
155. Giacomelli, C.; Schmidt, V.; Aissou, K.; Borsali, R. *Langmuir* **2010**, *26*, 15734–15744.
156. Hadziioannou, G.; Patel, S.; Granick, S.; Tirrell, M. *J. Am. Chem. Soc.* **1986**, *108*, 2869–2876.
157. Okhapkin, I.; Makhaeva, E.; Khokhlov, A. In *Conformation-Dependent Design of Sequences in Copolymers I*; Khokhlov, A., Ed.; Springer Berlin Heidelberg, **2006**; Vol. 195, pp. 177–210.
158. Ruokolainen, J.; Mäkinen, R.; Torkkeli, M.; Mäkelä, T.; Serimaa, R.; Brinke, G. ten; Ikkala, O. *Science* **1998**, *280*, 557–560.
159. Ruiz, R.; Kang, H.; Detcheverry, F. A.; Dobisz, E.; Kercher, D. S.; Albrecht, T. R.; de Pablo, J. J.; Nealey, P. F. *Science* **2008**, *321*, 936–939.
160. Bates, F. S.; Fredrickson, G. H.; Hucul, D.; Hahn, S. F. *AIChE J.* **2001**, *47*, 762–765.
161. Gamys, C. G.; Schumers, J.-M.; Mugemana, C.; Fustin, C.-A.; Gohy, J.-F. *Macromol. Rapid Commun.* **2013**, *34*, 962–982.
162. Pan, D.; Turner, J. L.; Wooley, K. L. *Chem. Commun.* **2003**, 2400–2401.
163. Lin, Y.; Boker, A.; He, J.; Sill, K.; Xiang, H.; Abetz, C.; Li, X.; Wang, J.; Emrick, T.; Long, S.; Wang, Q.; Balazs, A.; Russell, T. P. *Nature* **2005**, *434*, 55–59.
164. Meng, F.; Zhong, Z.; Feijen, J. *Biomacromolecules* **2009**, *10*, 197–209.
165. Gohy, J.-F.; Zhao, Y. *Chem. Soc. Rev.* **2013**, *42*, 7117–7129.
166. Helfand, E.; Wasserman, Z. R. *Macromolecules* **1976**, *9*, 879–888.
167. Leibler, L. *Macromolecules* **1980**, *13*, 1602–1617.
168. Klok, H. A.; Lecommandoux, S. *Adv. Mater.* **2001**, *13*, 1217–1229.
169. Bates, F. S.; Fredrickson, G. H. *Phys. Today* **1999**, *52*, 32–38.
170. Yu, B.; Li, B.; Sun, P.; Chen, T.; Jin, Q.; Ding, D.; Shi, A.-C. *J. Chem. Phys.* **2005**, *123*, 234902–234908.
171. Ding, J.; Liu, G.; Yang, M. *Polymer* **1997**, *38*, 5497–5501.
172. Hawker, C. J.; Wooley, K. L. *Science* **2005**, *309*, 1200–1205.
173. Theato, P.; Klok, H.-A. *Functional Polymers by Post-Polymerization Modification: Concepts, Guidelines, and Applications*; Wiley-VCH Verlag GmbH & Co. KGaA: University of Hamburg, Institute for Technical and Macromolecular Chemistry, Bundesstrasse 45, 20146 Hamburg, Germany., **2013**.
174. Odian, G. In *Principles of Polymerization*; John Wiley & Sons, Inc., **2004**.
175. Roth, P. J.; Wiss, K. T.; Theato, P. In *Polymer Science: A Comprehensive Reference*; Matyjaszewski, K.; Möller, M., Eds.; Elsevier: Amsterdam, **2012**; pp. 247–267.
176. Lee, C. C.; Grenier, C.; Meijer, E. W.; Schenning, A. P. H. J. *Chem. Soc. Rev.* **2009**, *38*, 671–683.
177. Zayed, J. M.; Nouvel, N.; Rauwald, U.; Scherman, O. A. *Chem. Soc. Rev.* **2010**, *39*, 2806–2816.
178. Lodge, T. P. *Science* **2008**, *321*, 50–51.
179. He, Y.; Boswell, P. G.; Bühlmann, P.; Lodge, T. P. *J. Phys. Chem. B* **2006**, *111*, 4645–4652.
180. Hoarfrost, M. L.; Segalman, R. A. *Macromolecules* **2011**, *44*, 5281–5288.
181. Simone, P. M.; Lodge, T. P. *Macromolecules* **2008**, *41*, 1753–1759.

182. Virgili, J. M.; Hexemer, A.; Pople, J. A.; Balsara, N. P.; Segalman, R. A. *Macromolecules* **2009**, *42*, 4604–4613.
183. Kim, S. Y.; Kim, S.; Park, M. J. *Nat Commun* **2010**, *1*, 88.
184. Gwee, L.; Choi, J.-H.; Winey, K. I.; Elabd, Y. A. *Polymer* **2010**, *51*, 5516–5524.
185. Kim, S. Y.; Yoon, E.; Joo, T.; Park, M. J. *Macromolecules* **2011**, *44*, 5289–5298.
186. Hoarfrost, M. L.; Tyagi, M. S.; Segalman, R. A.; Reimer, J. A. *Macromolecules* **2012**, *45*, 3112–3120.
187. Muldoon, M. J.; Aki, S. N. V. K.; Anderson, J. L.; Dixon, J. K.; Brennecke, J. F. *J. Phys. Chem. B* **2007**, *111*, 9001–9009.
188. Raeissi, S.; Peters, C. J. *Green Chem.* **2009**, *11*, 185–192.
189. Camper, D.; Bara, J.; Koval, C.; Noble, R. *Ind. Eng. Chem. Res.* **2006**, *45*, 6279–6283.
190. He, Y.; Lodge, T. P. *Chem. Commun.* **2007**, 2732–2734.
191. Wanakule, N. S.; Virgili, J. M.; Teran, A. A.; Wang, Z.-G.; Balsara, N. P. *Macromolecules* **2010**, *43*, 8282–8289.
192. Simone, P. M.; Lodge, T. P. *ACS Appl. Mater. Interfaces* **2009**, *1*, 2812–2820.
193. Bouchet, R.; Maria, S.; Meziane, R.; Aboulaich, A.; Lienafa, L.; Bonnet, J.-P.; Phan, T. N. T.; Bertin, D.; Gigmes, D.; Devaux, D.; Denoyel, R.; Armand, M. *Nat Mater* **2013**, *12*, 452–457.
194. Texter, J.; Vasantha, V. A.; Crombez, R.; Maniglia, R.; Slater, L.; Mourey, T. *Macromol. Rapid Commun.* **2012**, *33*, 69–74.
195. Chanthad, C.; Masser, K. A.; Xu, K.; Runt, J.; Wang, Q. *J. Mater. Chem.* **2012**, *22*, 341–344.
196. Coupillaud, P.; Fèvre, M.; Wirotius, A.-L.; Aissou, K.; Fleury, G.; Debuigne, A.; Detrembleur, C.; Mecerreyes, D.; Vignolle, J.; Taton, D.; Fevre, M. *Macromol. Rapid Commun.* **2014**, *35*, 422–430.
197. Gauthier, M. A.; Gibson, M. I.; Klok, H.-A. *Angew. Chemie Int. Ed.* **2009**, *48*, 48–58.
198. Tauer, K.; Yu, R. *Polym. Chem.* **2014**, DOI: 10.1039/C4PY00458B.
199. Nicolas, J.; Guillaneuf, Y.; Lefay, C.; Bertin, D.; Gigmes, D.; Charleux, B. *Prog. Polym. Sci.* **2013**, *38*, 63–235.
200. Schneider, Y.; Modestino, M. A.; McCulloch, B. L.; Hoarfrost, M. L.; Hess, R. W.; Segalman, R. A. *Macromolecules* **2013**, *46*, 1543–1548.
201. Carrasco, P. M.; Ruiz de Luzuriaga, A.; Constantinou, M.; Georgopanos, P.; Rangou, S.; Avgeropoulos, A.; Zafeiropoulos, N. E.; Grande, H.-J.; Cabañero, G.; Mecerreyes, D.; Garcia, I. *Macromolecules* **2011**, *44*, 4936–4941.
202. Carrasco, P. M.; Tzounis, L.; Mompean, F. J.; Strati, K.; Georgopanos, P.; Garcia-Hernandez, M.; Stamm, M.; Cabañero, G.; Odriozola, I.; Avgeropoulos, A.; Garcia, I. *Macromolecules* **2013**, *46*, 1860–1867.
203. Discher, D. E.; Eisenberg, A. *Science* **2002**, *297*, 967–973.
204. Jin, X.; Tao, J.; Yang, Y. *J. Appl. Polym. Sci.* **2010**, *118*, 1455–1461.
205. Chi, W. S.; Koh, J. K.; Ahn, S. H.; Shin, J.-S.; Ahn, H.; Ryu, D. Y.; Kim, J. H. *Electrochem. commun.* **2011**, *13*, 1349–1352.
206. Carlisle, T. K.; Bara, J. E.; Lafrate, A. L.; Gin, D. L.; Noble, R. D. *J. Membr. Sci.* **2010**, *359*, 37–43.
207. Samadi, A.; Kemmerlin, R. K.; Husson, S. M. *Energy & Fuels* **2010**, *24*, 5797–5804.

Chapter 2

Poly(ionic liquid)s (PILs): Reactive Platforms for a Use in Organocatalysis and Post-polymerization Modification

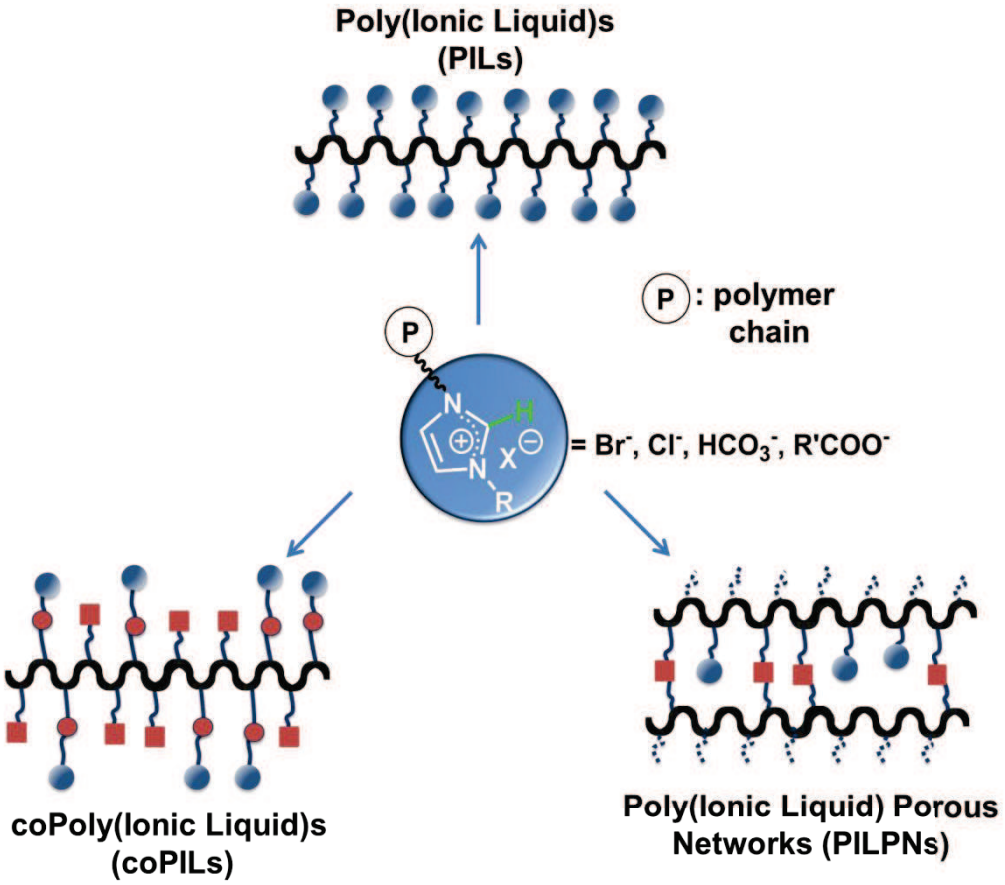

Keywords: Poly(ionic liquid)s, Statistical copolymers, Mesoporous copolymer networks, Imidazolium, Organocatalysis, Post-polymerization modification, *N*-heterocyclic carbenes, Reactivity.

Abstract: In this chapter, the intrinsic reactivity of the imidazolium units of PILs has been exploited for the purpose of catalysis and for post-chemical modification as well.

Synthesis of novel poly(ionic liquid)s, namely, poly(*N*-vinyl-3-alkylimidazolium hydrogen carbonate)s, denoted as poly([NHC(H)][HCO_3])s or PVRImHCO_3, where R is an alkyl group (R = ethyl, butyl, phenylethyl, dodecyl), is first described. All poly([NHC(H)][HCO_3])s salts prove air stable and can be manipulated without any particular precautions. They can subsequently serve as polymer-supported pre-catalysts to generate polymer-supported *N*-heterocyclic carbenes, referred to as poly(NHC)s, formally by a loss of "H_2CO_3" (H_2O +CO_2) in solution. This is demonstrated through selected organocatalyzed reactions of molecular chemistry, namely benzoin condensation, transesterification and cyanosilylation. Organocatalyzed reactions can be performed with excellent yields, even after five catalytic cycles.

Synthesis of poly(*N*-vinyl-3-butylimidazolium bromide-*co*-*N*-vinyl-3-butylimidazolium carboxylate), denoted as poly([NHC(H)][Br]-*co*-[NHC(H)][R'COO]); R' = 1-adamantyl, 10-undecyl, is also described. IL monomers with halide counter-anions are first polymerized by free radical polymerization using AIBN as initiator, which is followed by anion metathesis substituting the $R'COO^-$ for the Br^- anion. Nevertheless, these $R'COO^-$ counter-anion-containing PILs can serve as pre-catalysts. Catalytic efficiencies prove better in this case than with the poly([NHC(H)][HCO_3])s.

In addition, statistical copoly(ionic liquid)s, denoted as coPILs, based on poly(styrene)-*co*-poly(4-vinylbenzylbutylimidazolium) are used for the same organocatalyzed molecular reactions. In comparison with the *N*-vinylimidazolium-based PILs mentioned above, imidazolium units are statistically distributed along the polymer backbone decreasing the catalytic density. Poly(styrene)-*co*-poly(4-vinylbenzylbutylimidazolium chloride or hydrogen carbonate) precursors, denoted as PS-*co*-PVBnBuIm(Cl or HCO_3), are thus synthesized by statistical free radical copolymerization of styrene and 4-vinylbenzyl chloride, followed by quaternization with butylimidazole, and anion exchange using $KHCO_3$. The two polymers (with Cl^- and HCO_3^- anions) exhibit excellent catalytic activities for the carbonatation reaction between CO_2 and propylene oxide, and the benzoin condensation *via* the generation of the corresponding NHC units, respectively.

Novel mesoporous polymer monoliths are also elaborated by a facile solvothermal copolymerization route. Such IL-type mesoporous polymers are successfully applied as polymer-supported organic (pre)catalysts either for the cyclocarbonatation of propylene oxide or for the benzoin condensation and cyanosilylation, *via* generation of NHC units by

deprotonation with a strong base. The insolubility of mesoporous copoly(ionic liquid)s enables to easily recycle the monolithic precursor up to three cycles, with excellent yields in all cases, attesting to the efficient catalytic activity.

The latter coPILs are also employed as reactive polymer precursors for post-polymerization modification, in this case, in stoichiometric transformations with small electrophilic antagonist molecules. CoPILs are, for instance, shown to react not only with organic substrates, such as CS_2 or isothiocyanate affording the corresponding polybetaines, but also with transition metals, such as Pd or Au, yielding corresponding poly(NHC-Met) complexes.

A number of results presented in this chapter have been published in the following papers:

- *P. Coupillaud, J. Pinaud, N. Guidolin, J. Vignolle, M. Fèvre, E. Veaudecrenne, D. Mecerreyes, D. Taton. "Poly(ionic liquid)s based on imidazolium hydrogen carbonate monomer units as recyclable polymer-supported N-heterocyclic carbenes: Use in organocatalysis." J. Polym. Sci. Part. A. Polym. Chem.,* ***2013****, 51, 4530-4540.*
- *P. Coupillaud, J. Vignolle, D. Mecerreyes, D. Taton. "Post-polymerization Modification and Organocatalysis using Reactive Statistical Poly(Ionic Liquid)-Based Copolymers." Polymer* ***2014****, 55, 3404-3414.*
- *P. Coupillaud, D. Kuzmicz, Y. Men, J. Vignolle, G. Vendraminetto, M. Ambrogi, D. Taton, J. Yuan. "Mesoporous poly(ionic liquid)-based copolymer monoliths: from synthesis to catalysis and microporous carbon production." Polymer* ***2014****, 55, 3423-3430.*

Chapter 2

Poly(ionic liquid)s (PILs): Reactive Platforms for a Use in organocatalysis and Post-polymerization Modification

Table of Contents

Introduction

As emphasized in chapter 1 of this document, poly(ionic liquid)s (PIL)s have emerged as a special class of polyelectrolytes combining the inherent features of ionic liquids (ILs), such as thermal and chemical stability, high solid ionic conductivity, or adaptable solubility, with the intrinsic properties of polymers, including mechanical stability and processability.[1–6]

In this PhD work, we have expanded the use of PILs by exploiting their potential reactivity for the purpose of catalysis, and for post-chemical modification of the imidazolium units as well. Some ILs[7–9] and PILs[10,11] have already been demonstrated to behave as efficient catalysts (or pre-catalysts) in selected reactions. In particular, both imidazolium-based ILs and PILs can generate *N*-heterocyclic carbenes (NHCs) and poly(NHCs), respectively, for the purpose of organocatalysis.[12–17]

NHCs are not only being employed as ligands for transition metals,[18–20] but also as true organocatalysts in various molecular transformations.[21–23] More recently, NHCs have also served as organocatalysts or building blocks in metal-free polymer synthesis.[24–26] Steric and/or electronic properties of NHCs can be finely tuned through variation of their substituent pattern, which allows modulating their overall reactivity (*e.g.* nucleophilicity and/or basicity) towards various substrates.[27,28] However, their poor stability when exposed to air makes NHCs difficult to handle.[29–31] To circumvent this limitation, various masked NHCs have proved of practical use as pre-catalysts both in molecular and macromolecular reactions.[22,26]

The common route to *in situ* generate NHCs or poly(NHCs) is the deprotonation by a strong base of the acidic proton of imidazol(in)ium IL units.[26] However, NHCs can be masked in the form of NHC-Ag(I) complexes[32,33] or 2-alkoxy,[34] trichloromethyl,[35] pentafluorophenyl,[35] isothiocyanate,[36] carboxylic acid,[36,37] and NHC-CO_2 adducts.[38,39]

The latter zwitterionic azol(in)ium-2-carboxylates usually result from the carboxylation of free carbenes most often prepared separately with CO_2.[4,6–9,40] Progressive hydrolysis of NHC-CO_2 adducts, forming imidazol(in)ium hydrogen carbonates, denoted as [NHC(H)][HCO_3], has yet been reported.[12,41] Hence, it would be highly desirable to develop air-stable NHC precursors that could be of practical usage for the purpose of organocatalysis or organometallic chemistry.[12,17,42–50]

Our group at LCPO has reported that [NHC(H)][HCO_3] salts can serve as a genuine source of NHCs, under very mild conditions, formally by a loss of "H_2CO_3" (H_2O +CO_2).[12,13]

In addition, synthesis of [NHC(H)][HCO_3] precursors can be readily achieved in one pot, by anion exchange from commercial imidazol(in)ium halides ([NHC(H)][X]; X= Br or Cl), in the presence of $KHCO_3$ in methanol.

In the first part of this chapter, we provide synthetic developments to imidazolium-based PIL precursors as genuine sources of poly(NHC)s:

i. First, the easy synthesis of air-stable and recyclable polymeric versions of imidazolium hydrogen carbonates, poly([NHC(H)][HCO_3])s, and their use in organocatalysis will be described. Interestingly, these salt precursors can be readily synthesized following two distinct routes that do not require the prior formation of poly(NHC)s. These particular PILs can be subsequently used as a source of poly(NHC)s, by analogy with their molecular versions, for selected organocatalyzed molecular reactions.[12,13] Re-carboxylation at the completion of each tested reaction allow us to recycle the poly([NHC(H)][HCO_3]) precursors (Scheme 1), while maintaining excellent yields, even after five catalytic cycles.

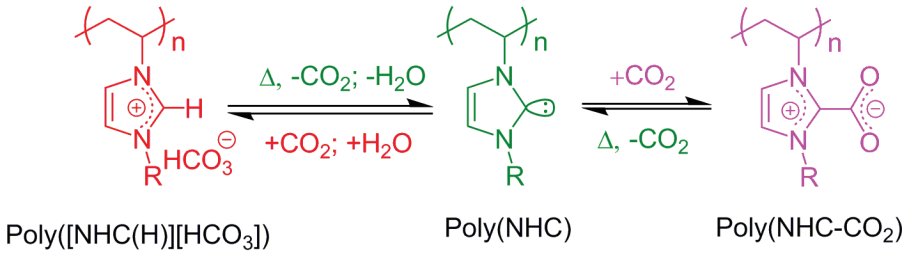

Scheme 1. Reversible generation of poly(NHC)s from poly([NHC(H)][HCO_3]) salts and poly(NHC-CO_2) adducts.

ii. Alternatively, specific PILs with carboxylate counter-anions have been investigated as precursors of poly(NHC)s (Scheme 2). Recently, it has been evidenced, indeed, that some counter-anions showing some high basicity (*e.g.* amino salts or weak organic acids such as acetic acid) allow for a proton transfer in the imidazolium moiety.[51–55] Increasing the basicity of the counter-anion thus enables tuning the relative stability of the [cation…anion] pair *via* hydrogen bonding. The generation of NHCs from imidazolium salts with sufficiently basic counter-anions has been evidenced experimentally by carbene-type reaction employing elemental sulfur,[54] and for the benzoin condensation reaction as well.[55] We report here, for the first time, the synthesis of polymeric versions of imidazolium with carboxylate counter-anions, referred to poly([NHC(H)][R'COO])s, for a use in organocatalysis.

The poly([NHC(H)][R'COO])s can be readily synthesized *via* a simple anion exchange reaction from the halide-containing corresponding precursors, again not requiring the prior synthesis of poly(NHC)s. Poly(NHC)s can be generated then, from these poly(vinylimidazolium) salts featuring carboxylate counter-anions and used for organocatalyzed molecular reactions (Scheme 2).

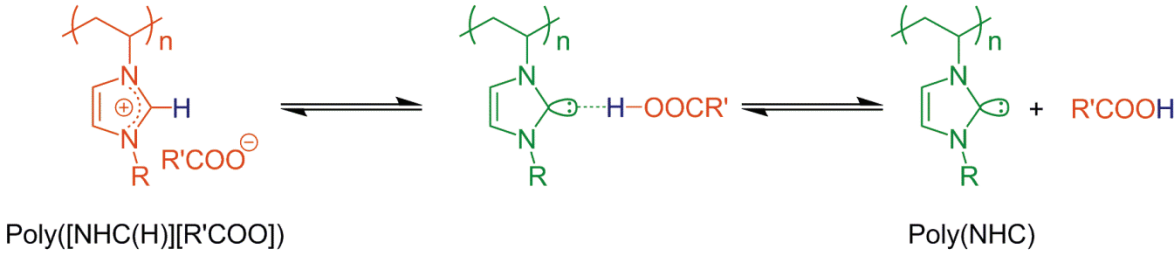

Scheme 2. Generation of poly(NHC)s from poly[NHC(H)][R'COO]**.**

Their catalytic performance will be compared with the other polymer pre-catalysts described in this chapter.

iii. Statistical copoly(ionic liquid)s (coPILs) PS-*co*-PVBnBuImCl and PS-*co*-PVBnBuImHCO_3, based on poly(styrene)-*co*-poly(4-vinylbenzylbutylimidazolium) with different anions (Cl^- or HCO_3^-) will be also described. These coPILs have served as reactive polymers both for the post-polymerization modification and organocatalysis. The catalytic activity of coPIL will be examined in cyclic carbonate formation, by reaction between CO_2 and propylene oxide and in the benzoin condensation reaction by the generation of NHC units.

iv. Finally, we will evidence that poly(ionic liquid)-based porous networks (PILPNs) can serve as monoliths for organocatalysis. This part of my PhD work was conducted in collaboration with Dr. Jayin Yuan at the Max Planck Institute of Colloids and Interfaces (Potsdam, Germany). PILPNs have been prepared by copolymerization of an imidazolium-based IL monomer with divinylbenzene (DVB) as crosslinker, under solvothermal conditions.

The second part of this chapter will describe the use of PS-type coPILs as reactive precursors for post-chemical modification. In other words, we have here exploited the inherent reactivity of the C_2-H group of the imidazolium moiety towards various electrophilic substrates (*e.g.* CS_2, isothiocyanates, or metallic complexes, Scheme 3). In the latter case, reactivity of PILs involves a stoichiometric (noncatalytic) addition reaction, transforming the PIL precursor into a new polymeric compound.

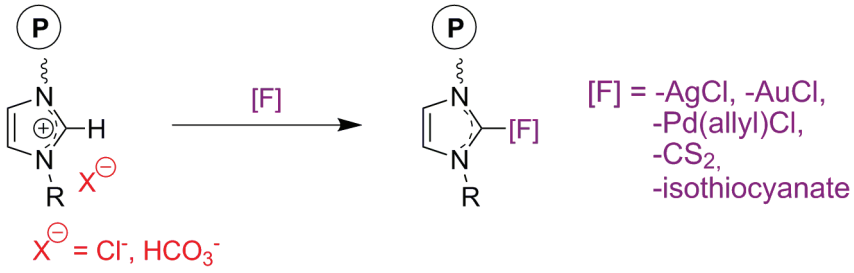

Scheme 3. Post-polymerization modification of imidazolium-based PILs.

1. Novel imidazolium-based PILs as polymer-supported catalysts

Catalyst recycling is obviously of prime importance in catalyzed processes,[56–61] including molecular reactions by an organocatalytic pathway.[62] In a previous work from our group, the synthesis of polymeric analogues of both NHCs and NHC-CO_2 adducts, denoted as poly(NHC)s and poly(NHC-CO_2) adducts were described (Route A, Scheme 4).[46] When used as polymer-supported pre-catalysts for metal-free transesterification and benzoin condensation reactions, poly(NHC-CO_2) adducts did prove easier to handle and could be more easily recycled than their "bare" poly(NHC) counterparts. One limitation of this approach, however, was the need for the prior synthesis of related air sensitive poly(NHC) intermediates.[63] This was achieved by deprotonation of PIL possessing halide anions, at low temperature and in the presence of a strong base. We now provide a new synthetic access to air-stable and recyclable PILs for facile organocatalysis.

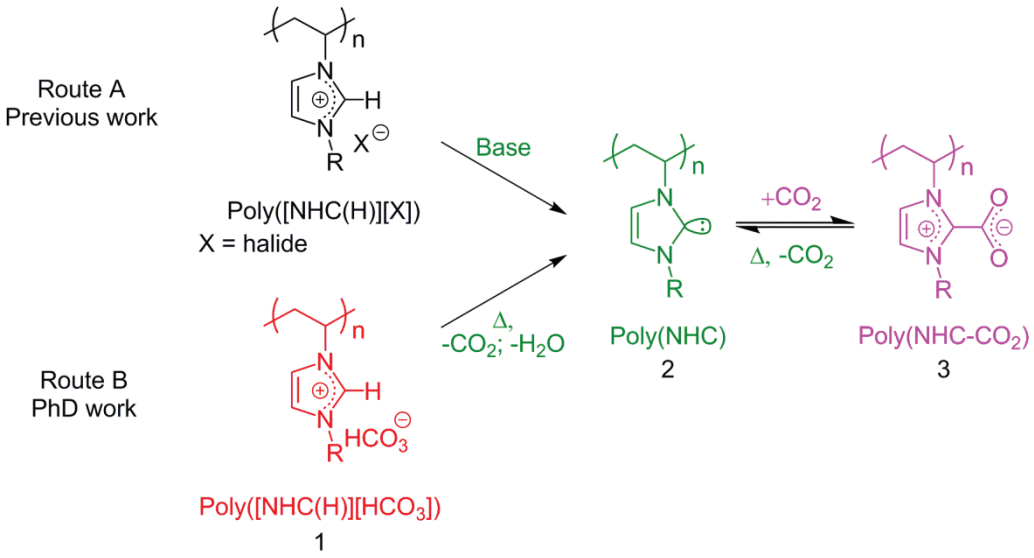

Scheme 4. Route A. Generation of poly(NHC)s from poly([NHC(H)][halide]) salts by deprotonation with a strong base and reversible generation of poly(NHC)s from poly(NHC-CO_2) adducts.[46] Route B. Reversible generation of poly(NHC)s from poly([NHC(H)][HCO_3]) salts and poly(NHC-CO_2) adducts.

1.1. *N*-vinyl-3-alkylimidazolium-based PILs with hydrogen carbonate counter-anions as polymer-supported *N*-heterocyclic carbenes

1.1.1. Synthesis of poly(*N*-vinyl-3-alkylimidazolium hydrogen carbonate)s

Poly(*N*-vinyl-3-alkyl imidazolium hydrogen carbonate)s **1** synthesized in this work, denoted as poly(VRImHCO_3)s or poly([NHC(H)][HCO_3])s, where R is an alkyl substituent (R = ethyl, butyl, phenylethyl, dodecyl), represent novel poly(ionic liquid)s (PILs).[1,2,4–6,64,65] As depicted in Scheme 5, synthesis of these PILs could be achieved following two distinct routes.[46]

The first synthetic method is based on the free-radical polymerization (FRP) of *N*-vinyl-3-alkylimidazolium monomers featuring a hydrogen carbonate (HCO_3^-) counter-anion, denoted as VRImHCO_3 (Scheme 5, path a). The latter monomers were readily synthesized by alkylation of *N*-vinylimidazole (VIm) that is commercially available, followed by direct anion exchange of *N*-vinyl-3-alkylimidazolium bromide (VRImBr) monomers, using potassium hydrogen carbonate ($KHCO_3$) in methanol, at room temperature, following a procedure described in our group.[12]

This method could be generalized to VRImBr monomers carrying various alkyl substituents in 3-position. Four different VRImBr monomers **4a-d** were thus synthesized by quaternization of VIm, using various alkyl (ethyl, *n*-butyl, 1-phenylethyl, and *n*-dodecyl) bromides.[46,66–68]

The four $VRImHCO_3$ monomers **5a-d** (R= ethyl, *n*-butyl, 1-phenylethyl and *n*-dodecyl) were next obtained by anion exchange.[12,13,41,69] The novel $VRImHCO_3$ monomers were characterized by ^1H and ^{13}C NMR spectroscopy.

Figure 1 and Figure 2 show, for instance, the NMR spectra of the $VBuImHCO_3$ **2b** compound. Analysis by ^1H NMR in CD_3OD did not allow stating on the quantitative anion exchange, from bromide to hydrogen carbonate (Figure 1); chemical shifts of protons of the imidazolium backbone were indeed similar to those of the starting material **4b**. In contrast, the characteristic signals of both the N_2CH carbon and the HCO_3^- quaternary carbon atoms were observed by ^{13}C NMR at 136.0 and 161.1 ppm, respectively (Figure 2). All other signals observed both on the ^1H and ^{13}C NMR spectra were consistent with data reported on molecular imidazolium hydrogen carbonate homologues.[12]

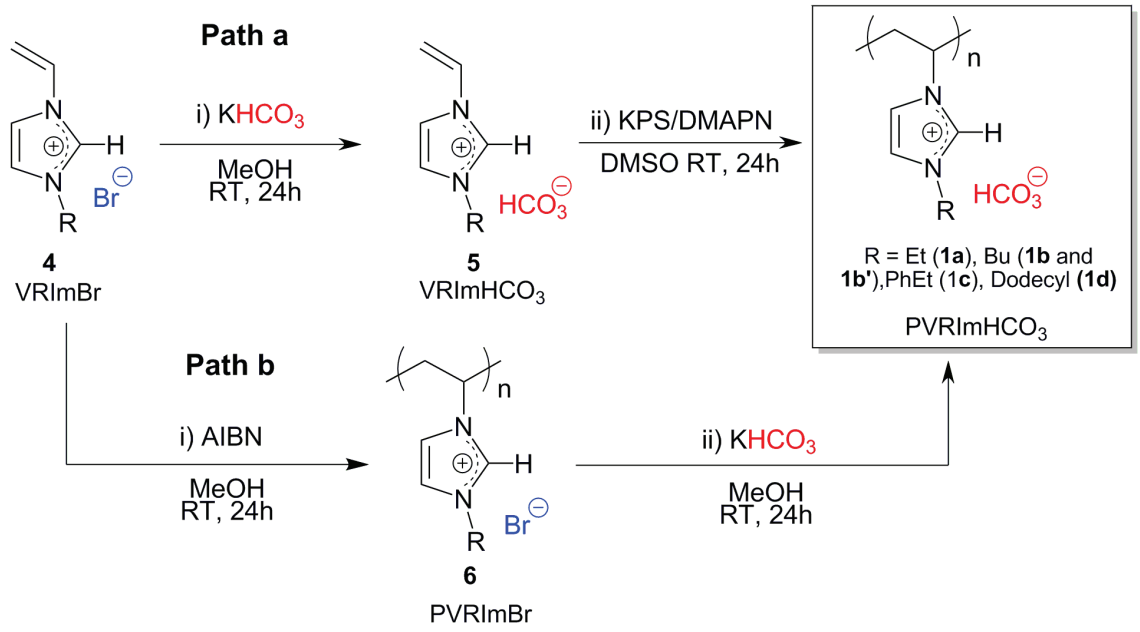

Scheme 5. Synthesis of $PVRImHCO_3$ **1a-d** by anion exchange of VRImBr **4a-d**, followed by FRP of $VRImHCO_3$ **5a-d** (path a) and synthesis of $PVRImHCO_3$ **1b'** by FRP of VRImBr **4b** followed by anion exchange exchange of PVRImBr **6b** (path b).

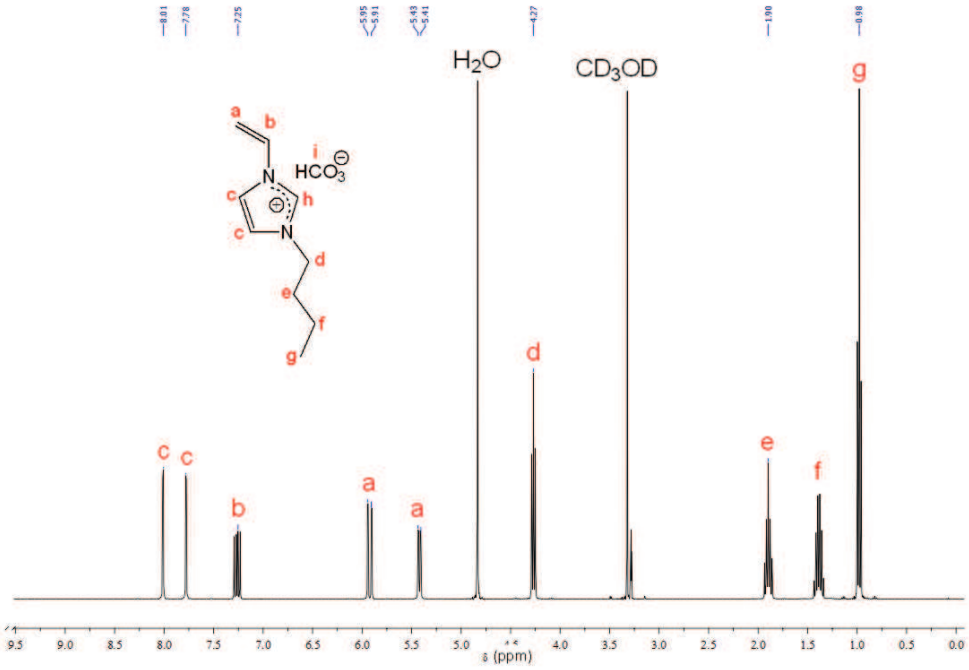

Figure 1. ^{1}H NMR spectrum of *N*-vinyl-3-butylimidazolium hydrogen carbonate **5b** in CD_3OD.

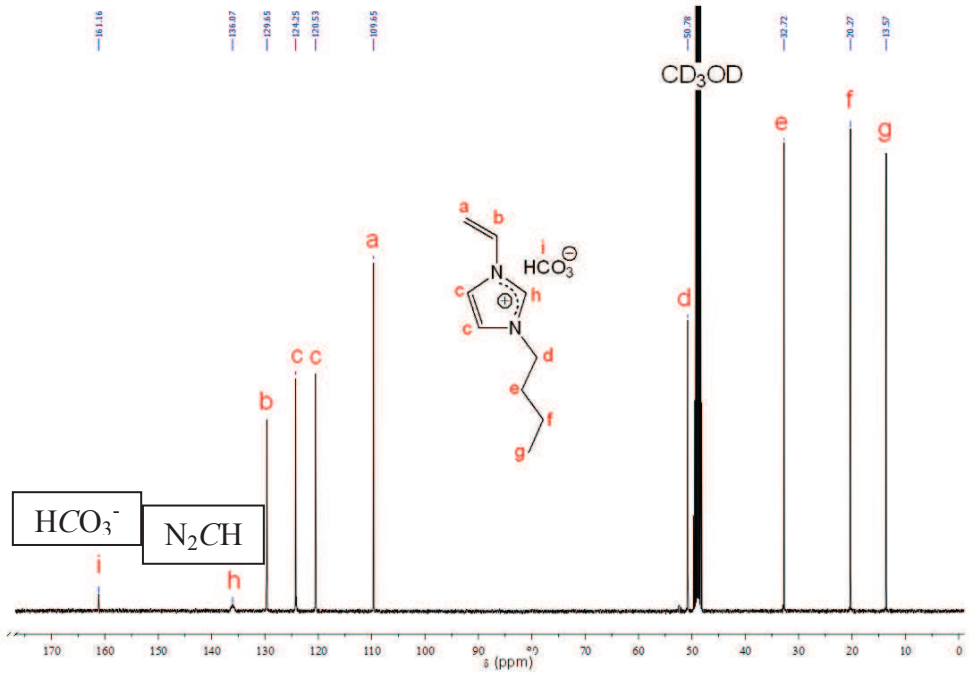

Figure 2. ^{13}C NMR spectrum of *N*-vinyl-3-butylimidazolium hydrogen carbonate **5b** in CD_3OD.

Synthesis of PILs by free-radical polymerization (FRP) of *N*-vinyl-3-alkylimidazolium is well-documented.[1,2,4–6,64,65] FRP of $VRImHCO_3$ monomers **5a-d** was investigated under different conditions, as summarized in Table 1. For instance, attempts to polymerize **5b** using

either azobis(2-methylpropionitrile) (AIBN) or 4,4'-azobis(4-cyanovaleric acid) (V-501) as a radical source, at 80 °C, were not successful, neither in DMSO nor in MeOH as solvent (entry 1, Table 1). We hypothesized that a too high temperature (80 °C) could lead to the premature degradation of VRImHCO$_3$ monomers **5**. 2,2'-Azobis(4-methoxy-2,4-dimethyl valeronitrile) (V-70) was thus employed as initiator at 40 °C, which enabled the polymerization to proceed, albeit with a low conversion after a reaction time of 72h (entry 2, Table 1). In contrast, the redox initiating system utilizing potassium persulfate (KPS) and dimethylaminopropionitrile (DMAPN) at room temperature (RT) enabled quantitative conversion of monomer **5b** in DMSO, after 18h (entry 4, Table 1), whereas a low conversion was noted in MeOH, likely owing to the poor solubility of KPS in the latter solvent (entry 5, Table 1). All monomers **5a-d** were thus efficiently polymerized in DMSO at RT in the presence of KPS/DMAPN, providing polymers, PVRImHCO$_3$ **1a-d**, in near quantitative yields (Table 1). Although the possibility of anion exchange between KPS and PVRImHCO$_3$ cannot be ruled out, this metathesis reaction could not be evidenced.

Characterization of polymers **1a-d** by ^{1}H NMR spectroscopy confirmed the expected structure. In particular, the signal corresponding to the C*H* proton of the imidazolium moiety could be clearly identified at 9-10 ppm. In addition, signals due to the vinylic protons of monomers at 5.4-6 ppm completely vanished, while protons of monomer units C*H*-CH$_2$ were observed at 4-4.3 ppm (Figure 3-Figure 4 and Figure S1-Figure S6). While all signals were broadened after polymerization, that corresponding to the H*C*O$_3^-$ carbon atom at 160.0 ppm was found as sharp as in the ^{13}C NMR spectrum of monomer **5** (Figure 2).

Table 1. Free-radical polymerization of VRImHCO$_3$ monomers **5**.

Entry	Monomer	Initiator[a]	T (°C)	Solvent	Time (h)	Conv. (%)[b]	$\overline{M_n}$ (g.mol^{-1})[c]	$Đ$[c]
1	**5b (R=Bu)**	AIBN or V-501	80	DMSO or MeOH	144	0	-	-
2	**5b (R=Bu)**	V-70	40	DMSO	72	30	-	-
3	**5a (R=Et)**	KPS/DMAPN	R.T.	DMSO	18	85	29000	2.30
4	**5b (R=Bu)**	KPS/DMAPN	R.T.	DMSO	18	98	26200	1.78
5	**5b (R=Bu)**	KPS/DMAPN	R.T.	MeOH	18	40	-	-
6	**5c (R=EtPh)**	KPS/DMAPN	R.T.	DMSO	18	95	-[d]	-[d]
7	**5d (R=Dod)**	KPS/DMAPN	R.T.	DMSO	18	68	-[d]	-[d]

[a]A [Monomer]/[Initiator] ratio equal to 60 : 1 was used. [b]Conversion was calculated by ^{1}H NMR from the disappearance of the signal at 7.2 ppm and appearance of signal at 0.8 ppm corresponding to the polymer. [c]Molecular weight and dispersity were determined by SEC in water/formic acid (0.3 M) calibrated with poly(2-vinyl pyridine). [d]Molecular weight and dispersity were not determined due to the insolubility of the polymer in aqueous solvent used for SEC.

Characterization of PILs by size exclusion chromatography (SEC) is challenging owing to interactions of these polylectrolytes with SEC columns.[70] Recently, however, Matyjaszewski *et al.* reported a "universal" method to analyze well-defined PILs based on imidazolium-based with bis(trifluoromethanesulfonyl)imide (TFSI) counter-anions.[70] THF was employed as the eluent in presence of the same TFSI anion. In the present work, analysis of some polymers (PVBuImBr **6b**, PVEtImHCO$_3$ **1a** and PVBuImHCO$_3$ **1b**) by aqueous SEC (that was realized before aforementioned paper by Matyjaszewski *et al.* came out) showed a unimodal molecular weight distribution in each case (Figure 5), with a dispersity between 1.4 and 2.3. Due to the nonsolubility of polymers **1c** and **1d** in water, analysis of these polymers by aqueous SEC could not be carried out.

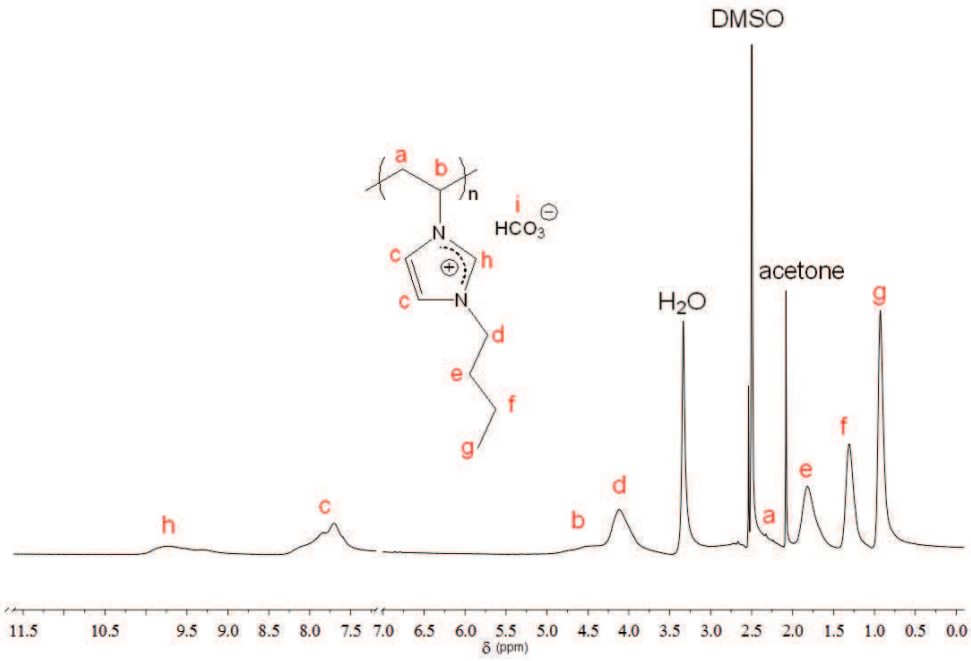

Figure 3. [1]H NMR spectrum of poly(*N*-vinyl-3-butylimidazolium hydrogen carbonate) salt **1b** in DMSO-d_6.

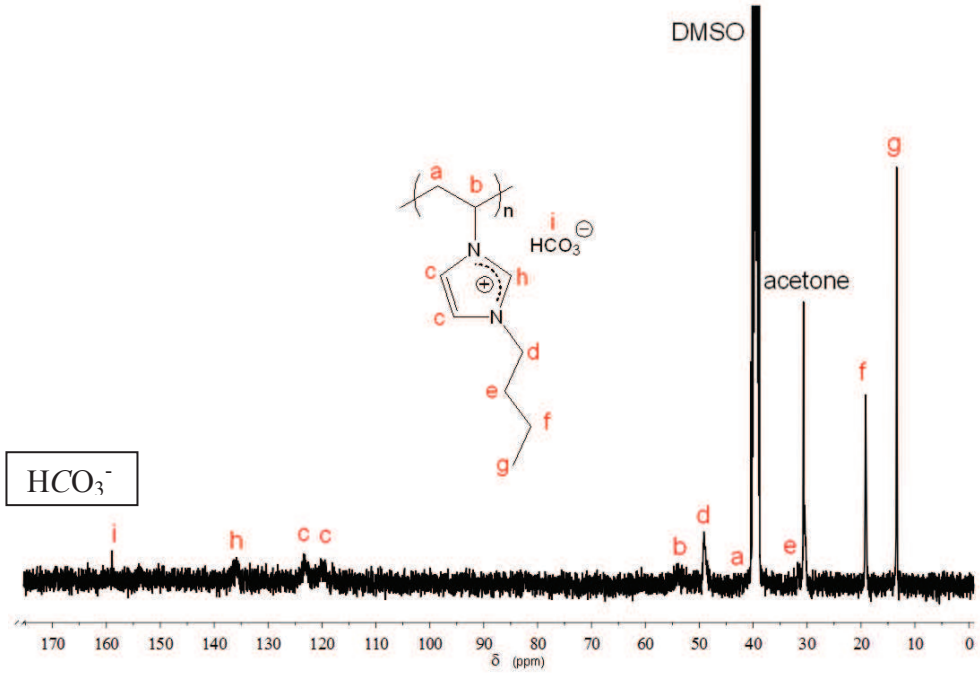

Figure 4. [13]C NMR spectrum of poly(*N*-vinyl-3-butylimidazolium hydrogen carbonate) salt **1b** in DMSO-d_6.

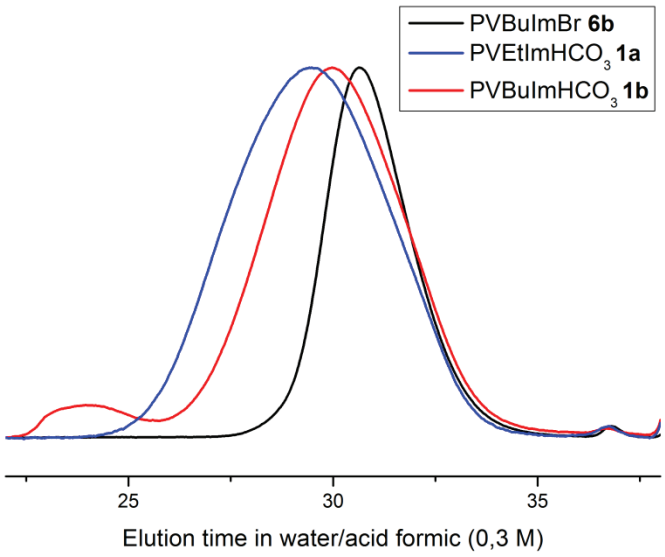

Figure 5. Aqueous SEC traces of PVBuImBr **6b**, PVEtImHCO$_3$ **1a** (entry 3, Table 1) and PVBuImHCO$_3$ **1b** (entry 4, Table 1) obtained by free radical polymerization in DMSO at RT.

An alternative synthetic route to PVRImHCO$_3$ **1** consisted in applying the same anion exchange method described above to FRP-derived poly(*N*-vinyl-3-alkylimidazolium bromide)s, PVRImBr **6** (Scheme 5, path b). The FRP of VRImBr monomers **4** was already reported.[3–5,46,71] For instance, PVBuImBr **6b** was synthesized in methanol using AIBN as a radical source at 80 °C. Characterization of PIL **6b** by ^{1}H NMR spectroscopy confirmed the expected structure (see annex Figure S7). Corresponding PVBuImHCO$_3$ **1b'** was obtained by anion exchange of **6b** with KHCO$_3$ in methanol at RT for 24h (see Scheme 5). A similar yellowish powder to **1b** (path a) was obtained, with identical ^{1}H and ^{13}C NMR spectra.

Thus synthesis of novel *N*-vinyl-3-alkylimidazolium-based PILs with hydrogen carbonate as counter-anion could be readily achieved, following two distinct routes both relying on a simple and direct anion exchange, from Br^- to HCO_3^-.

1.1.2. Use of poly(*N*-vinyl-3-alkylimidazolium hydrogen carbonate)s in organocatalysis

The potential of poly(vinylimidazolium hydrogen carbonate) salts **1a-d** and **1b'** (see Scheme 5) as polymer-supported pre-catalysts was then explored. Here we provide our preliminary results regarding their catalytic potential, without a complete investigation into the optimization of their catalytic efficiency. It is well-established, indeed, that polymer-supported catalysts with optimized catalytic properties requires a specific design and a systematic and logical approach, from the precise understanding of the mechanism of

elementary catalytic reactions.[72] Various parameters can be manipulated, including the nature of the polymer support, the nature of the linker, catalyst density along the polymer support, and the nature of the connectivity of the catalyst to the support.

Here polymers **1a-d** and **1b'** were expected to *in situ* generate poly(NHC)s **2**, by formal loss of H_2O and CO_2, as illustrated in Scheme 1, and by analogy with their molecular versions.[46] In this regard, **1a-d** and **1b'** are also denoted as poly[NHC(H)][HCO_3]s.

Three different organocatalyzed reactions of molecular chemistry were implemented, namely, transesterification,[46,73–75] benzoin condensation[17,46,75,76] and cyanosilylation of aldehydes,[77,78] all known as being efficiently catalyzed by both molecular NHCs and ([NHC(H)][HCO_3]) salt precursors.[13] Mechanisms of the three tested molecular reactions catalyzed by NHCs are depicted in the annex (See Scheme S1-S3).

Similar experimental conditions were used for all organocatalytic tests: reagents and polymer salt precursors **1** (5 or 10 mol%) were mixed in THF and stirred at 80 °C for 1, 2 or 24h, depending on the implemented reaction. It is worth pointing out, however, that **1** were not soluble under such conditions, organocatalyzed reactions taking place heterogeneously, except in the case of precursor **1d** carrying the dodecyl group on the imidazolium ring. Moreover, access to the NHC catalytic sites -generated from [NHC(H)][HCO_3] units- might be reduced because of the close vicinity of NHCs to the polymer backbone (short linker) and the steric hindrance brought by the alkyl group on the imidazole ring. It is therefore likely that the *in situ* generation of poly(NHC)s from poly[NHC(H)][HCO_3] **1a-d** and **1b'** was not complete. This also explained why a catalytic amount of up to 10 mol% of these polymer-supported pre-catalysts was employed, while molecular versions, [NHC(H)][HCO_3], required only 0.1-1 mol% at room temperature for the same reactions.[13]

Of particular interest, addition of CO_2 at RT at the completion of each tested reaction, allowed retrieving polymer-supported pre-catalysts, presumably co-existing in the form of a mixture of poly[NHC(H)][HCO_3] **1** and poly[NHC-CO_2] adducts **3** (see Scheme 1). The as-recovered polymers could thus be filtered off and recycled, for next runs of catalysis.

1.1.2.1. Transesterification reaction

In a typical transesterification reaction, benzyl alcohol (BnOH) and vinyl acetate (VAc) were added to a THF solution containing poly[NHC(H)][HCO_3] salts **1**, and the reaction was stirred for 2h (Scheme 6). Analysis by ^{1}H NMR spectroscopy of the filtrate confirmed the

formation of benzyl acetate, and the conversion could thus be determined (see Figure S8-S10 in the annex).

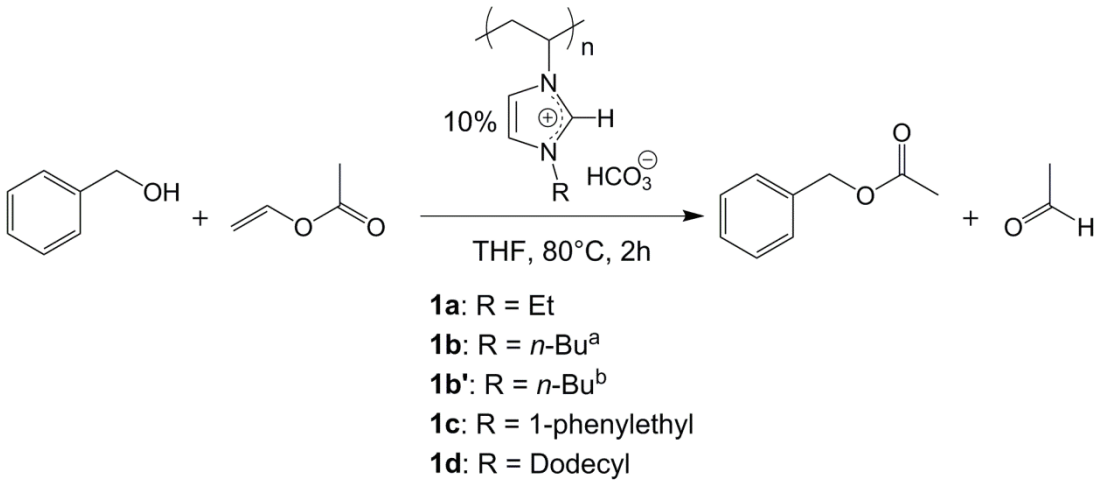

Scheme 6. Use of poly([NHC(H)][HCO_3]) **1** as polymer-supported pre-catalysts of transesterification between vinyl acetate and benzyl alcohol (see also Scheme 1).

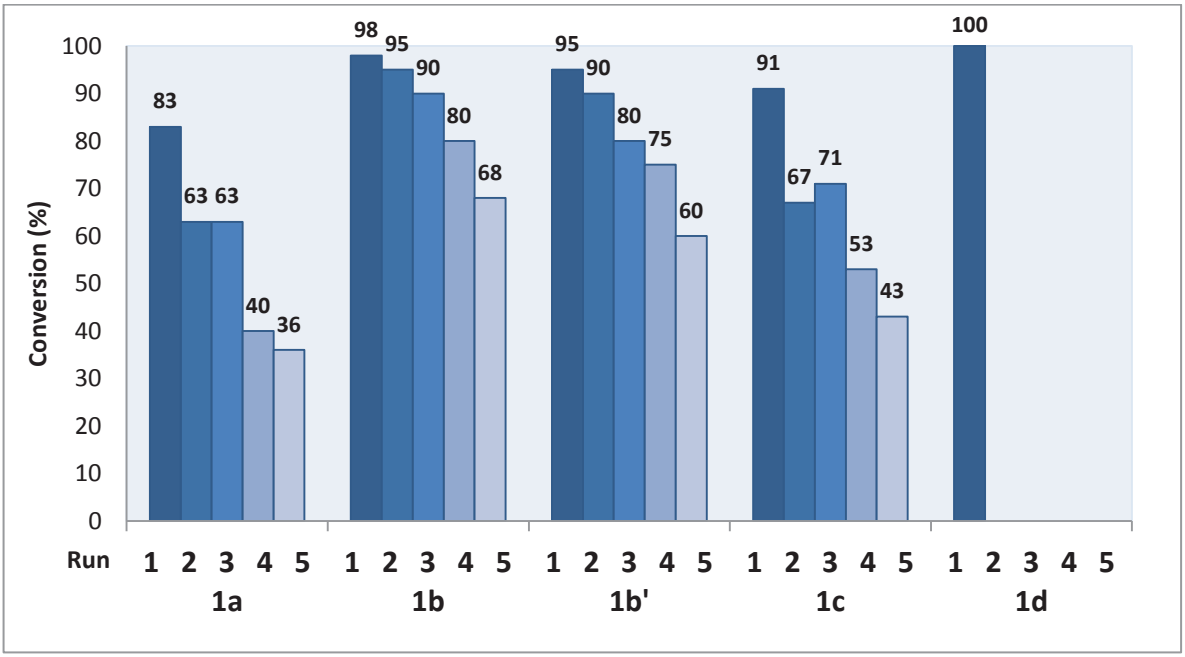

Figure 6. Results of the transesterification of benzyl alcohol (1 eq.) and vinyl acetate (1.2 eq.) in THF at 80 °C for 2h in the presence of poly([NHC(H)][HCO_3]) **1**.

All poly([NHC(H)][HCO_3]) salts exhibited an excellent catalytic activity at the first run, providing excellent conversion of benzyl acetate (83-100%), irrespective of the nature of the alkyl substituent on the imidazolium ring (Figure 6). This indicated that free poly(NHC)s **2** were efficiently generated at 80 °C, at least partially, from the poly([NHC(H)][HCO_3]) salt

precursors, formally by loss of "H_2CO_3". In contrast, the same precursors did not show any catalytic activity at all at RT., evidencing their latent character for catalysis.

Fairly good conversions (63-98%) were achieved with **1a-c** and **1b'** over 3 runs of organocatalysis (See Figure 6), attesting to an efficient recycling with no significant loss of catalytic activity. Precursors **1b** and **1b'**, obtained from path a and path b, respectively (Scheme 5), showed roughly the same catalytic efficiency for this transesterification reaction, indicating that the structure of both polymers was likely very similar.

The poly([NHC(H)][HCO_3]) precursor **1d** allowed reaching a complete conversion in benzyl acetate after the first run (Figure 6). However, **1d** (or **3d**, Scheme 1) could not be recovered by re-carboxylation due to its solubility in THF, unlike **1a-c** (or **3a-c**). The catalytic efficiency of the latter precursors however decreased progressively with the number of cycles, which might be explained by incomplete re-incorporation of CO_2 and/or of partial deactivation of *in situ* generated poly(NHC)s **2a-c**.

1.1.2.2. Cyanosilylation reaction

Precursors **1a-d** were then investigated as polymer-supported pre-catalysts for the cyanosilylation of benzaldehyde with trimethylsilyl cyanide (TMSCN), another NHC-catalyzed molecular reaction.[77,78] Only one report previously described the use of polymer-supported version of NHCs for this reaction (1 mol% of catalyst, RT., 10 min).[79] Results of the cyanosilylation of benzaldehyde with TMSCN catalyzed by 5 mol% of **1a-d** in THF for 1h (Scheme 7) are presented in Figure 7.

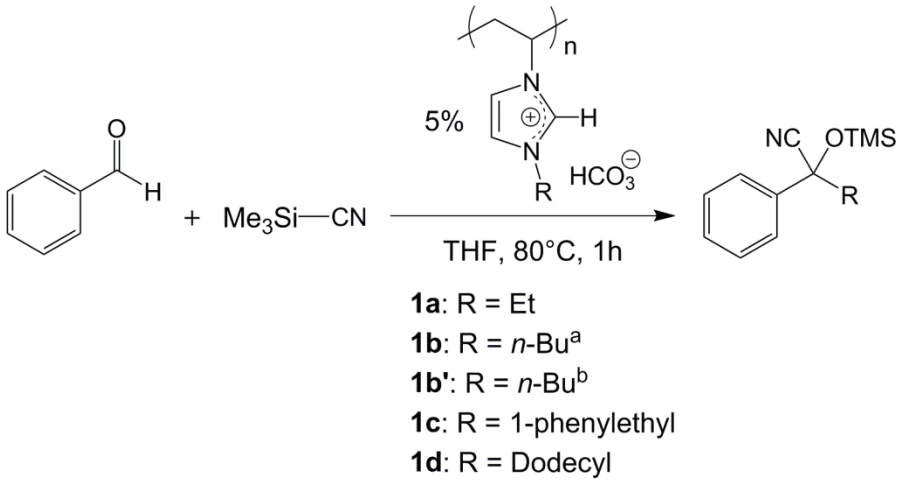

Scheme 7. Use of poly([NHC(H)][HCO_3]) **1** as polymer-supported pre-catalysts of the cyanosilylation of benzaldehyde with trimethylsilyl cyanide (see also Scheme 1).

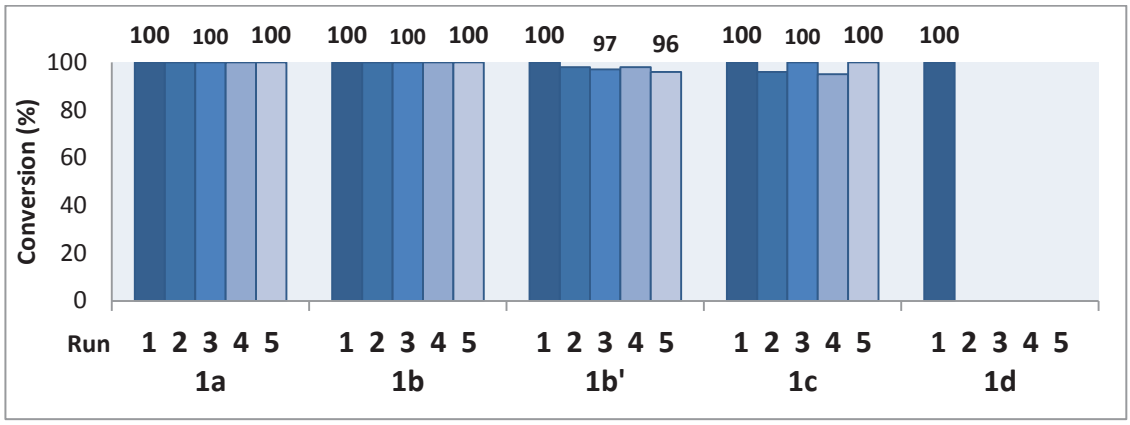

Figure 7. Results of the cyanosilylation of benzaldehyde and trimethylsilyl cyanide performed in THF at 80 °C for 1h in the presence of poly([NHC(H)][HCO_3]) **1**.

Excellent yields were obtained with **1a-c** and **1b'** up to five catalytic cycles (See Figure 7), meaning that all polymer-supported NHC precursors could be readily recycled after carboxylation, without any significant loss of catalytic activity (Figure 7). For the same reason mentioned above, the THF soluble precursor **1d**/**3d** could not be recycled, though also providing a quantitative conversion after the first run of organocatalysis.

1.1.2.3. Benzoin condensation reaction

Then, we examined the catalytic potential of poly([NHC(H)][HCO_3])s **1** for the benzoin condensation, a NHC-catalyzed self-condensation of benzaldehyde forming a β-keto alcohol called benzoin.[17,46,75,76] Reactions were carried out in THF for 24h at 80 °C, in the presence of 10 mol% of **1** (Scheme 8).

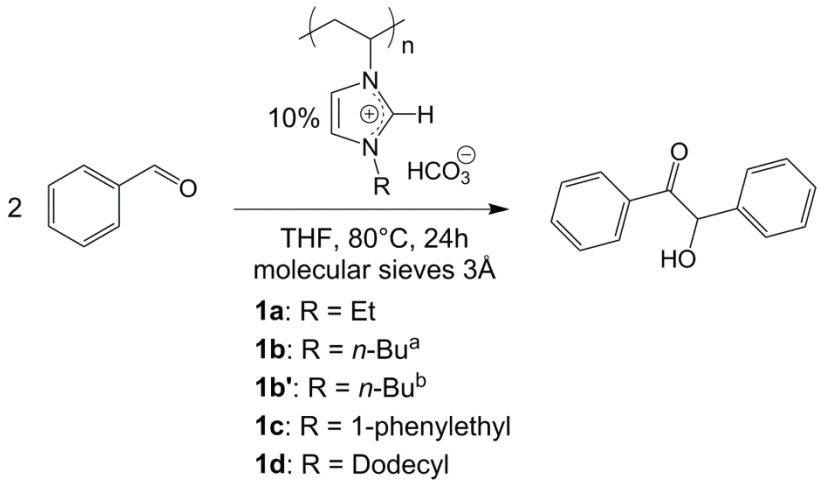

Scheme 8. Use of poly([NHC(H)][HCO_3]) **1** as polymer-supported pre-catalysts of the benzoin condensation of benzaldehyde (see also Scheme 1).

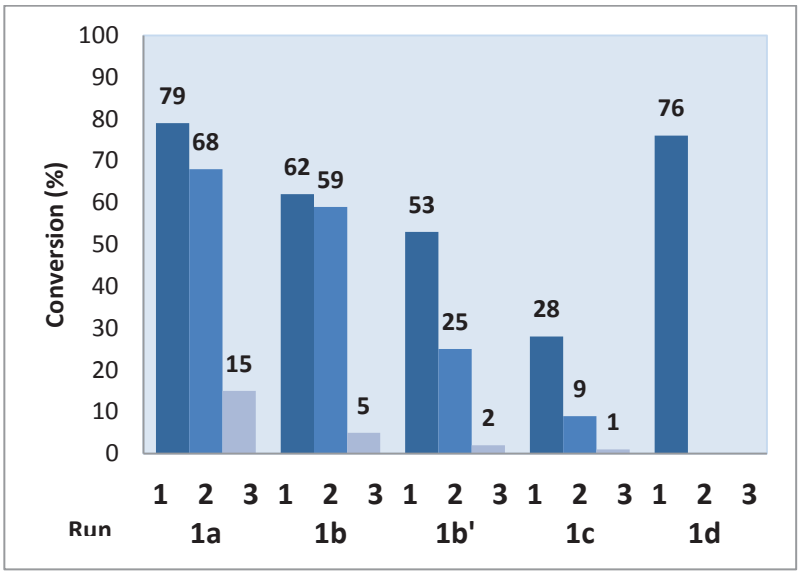

Figure 8. Results of the benzoin of condensation from benzaldehyde performed in THF at 80 °C for 24h in the presence of poly([NHC(H)][HCO_3]) **1**.

The first catalytic cycle led to benzoin in rather good yields (62-79%) with **1a-b'** and **1d** (See Figure 8). In contrast, a poor yield (28%) in benzoin was obtained with **1c** after the first run of catalysis. This might be ascribed to the poorer solubility of poly([NHC(H)][HCO_3]) **1c** in the reaction mixture compared to the other precursors, the corresponding poly(NHC) being also more hardly generated or prematurely deactivated. The slow kinetic of the reaction did not allow us to efficiently recycle the polymer pre-catalyst.

A significant decrease of the yield was also noted in the second catalytic cycle both for **1b'** and **1c** (25 and 9%, respectively), whereas the yield decreased only at the third run both with **1a** and **1b** (5 and 15%, respectively). Increasing the reaction time to 48h did not allow improving the generation of free poly(NHC)s **2** from **1**, as conversions were close to those obtained after 24h.

Overall, results of the benzoin condensation utilizing polymer precursors **1** are consistent with previous observations at LCPO when poly(NHC-CO_2) adduct homologues were employed:[46] the reaction is rather slow, yields drop after a few cycles, and polymer-supported pre-catalysts can be hardly recycled.

In conclusion, an easy synthetic access to air-stable and recyclable poly([NHC(H)][HCO_3])s **1** was provided for facile organocatalysis. Excellent catalytic activities could be achieved for the cyanosilylation and the transesterification reactions, whereas benzoin condensation requires longer reaction times, and did not allow efficiently

recycling the polymer-supported pre-catalysts, presumably owing to premature deactivation of poly(NHC)s under forcing conditions.

1.2. *N*-vinyl-3-alkylimidazolium-based PILs with carboxylate counter-anions for a use in organocatalysis

This section describes our preliminary investigations into the use of imidazolium-based PILs featuring carboxylate anions. A few research groups have indeed evidenced that organic acids could interact with NHCs.[51–55,80–84] "Classic" counter-anions (PF_6^-, BF_4^-, $CF_3SO_3^-$, TFSI) are unable to deprotonate the imidazolium ring to form the NHC.[85,86] In sharp contrast, anions derived from weak acids exhibits a sufficient basicity, which allows generating corresponding NHCs (Scheme 2).[52,53,84]

In 2006, Clyburne *et al.* have shown that free NHC as basic neutral compound (p*K*a values ranging from 22 to 24 in DMSO) can deprotonate weak acids such as phenol to produce a [cation···anion] pair that exhibited one of the shortest [C-H···O] hydrogen bonds (A, Scheme 9).[51] In 2010, Nyulàszi evidenced, for the first time, that anions of sufficient basicity (*e.g.* acetate) enabled a proton transfer in imidazolium-based ILs, providing an imidazole-2-ylidene derivative and an acid (acetic acid; B, Scheme 9).[52] The authors showed that the two species interacted to one with each other by hydrogen bonding or could be dissociated according to the pressure and the temperature. Further use of such a system for organocatalysis *via* NHC generation was then demonstrated.[55] In the meantime, Rogers *et al.* reported the chemisorption of carbon dioxide in imidazolium-based ILs with acetate counter-anions, establishing the principle of a NHC generation from an imidazolium featuring a carboxylate counter-anion (C, Scheme 9).[84]

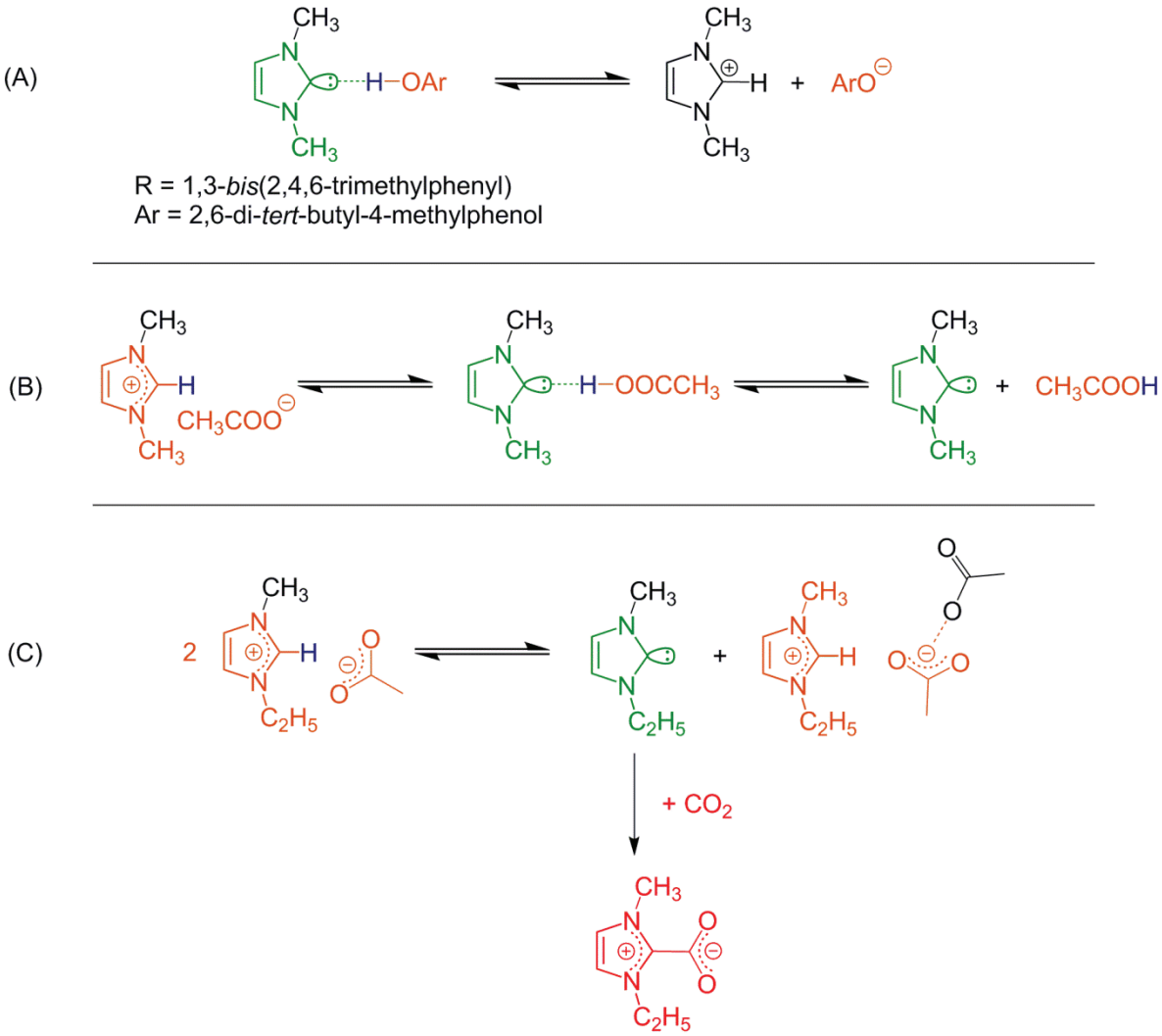

Scheme 9. (A) Deprotonation of a weak acid by NHC, adapted from reference 51. (B) Formation of NHC from imidazolium-based IL with acetate counter-anion, adapted for reference 52. (C) Proposed reaction of carbon dioxide and imidazolium-based ILs with acetate counter-anions, adapted from reference 84.

These pioneer works prompted us to design new IL monomers and related PILs thus possessing alkyl carboxylates as counter-anions. 1-Adamantane acetic acid and 10-undecanoic acid were selected as carboxylic acid-containing precursors, owing to their pronounced hydrophobic character.

1.2.1. Synthesis of poly(*N*-vinyl-3-butylimidazolium bromide-*co*-*N*-vinyl-3-butylimidazolium carboxylate)s

The synthesis of poly(*N*-vinyl-3-butylimidazolium bromide-*co*-*N*-vinyl-3-butylimidazolium carboxylate), denoted as poly([NHC(H)][Br]-*co*-[NHC(H)][R'COO]) **7**

where R' is an alkyl substituent (R' = 1-adamantyl **7a**, 10-undecyl **7b**), is shown in Scheme 10. IL monomers with halide counter-anions were first polymerized by FRP using AIBN as initiator, as described previously (see section 1.1.1).

The alkyl carboxylate salts were first prepared separately by simple deprotonation of the corresponding organic acid using *t*BuOK. As described above, anion metathesis reaction aimed at substituting the $RCOO^-$ for the Br^- anion was carried out at RT in dried methanol for 48h, with an excess of potassium carboxylate salts (2.5 eq.).[3–5,46,71] After dialysis, characterization of **7a** and **7b** by ^1H NMR spectroscopy revealed the presence of only 25 and 24% of 1-adamantyl carboxylates and 10-undecyl carboxylates as counter-anions, respectively (Figure 9 and Figure S15). In other words, anion exchange was not quantitative, and let to a statistical copolymer, denoted poly([NHC(H)][Br]-*co*-[NHC(H)][R'COO]) **7**, with both $RCOO^-$ and Br^- counter-anions. The bromide/carboxylate ratio was found close close to 3/1 both with the adamantyl and the undecyl substituents. We hypothesized that incomplete modification was due to the steric hindrance brought by the two alkyl carboxylates.

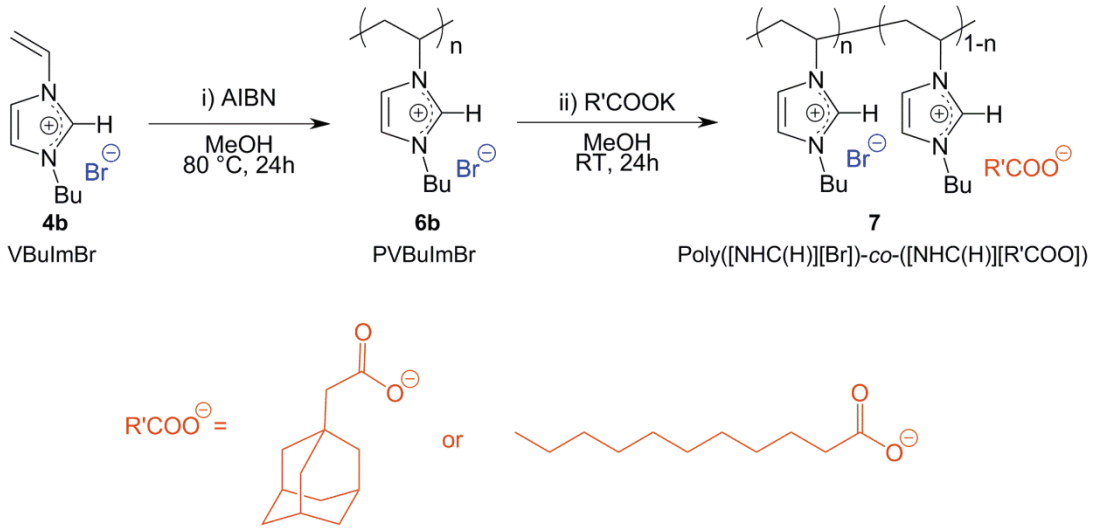

Scheme 10. Synthesis of poly([NHC(H)][Br]-*co*-[NHC(H)][R'COO]) **7** by FRP of VBuImBr **4b** followed by anion exchange exchange of PVBuImBr **6b**.

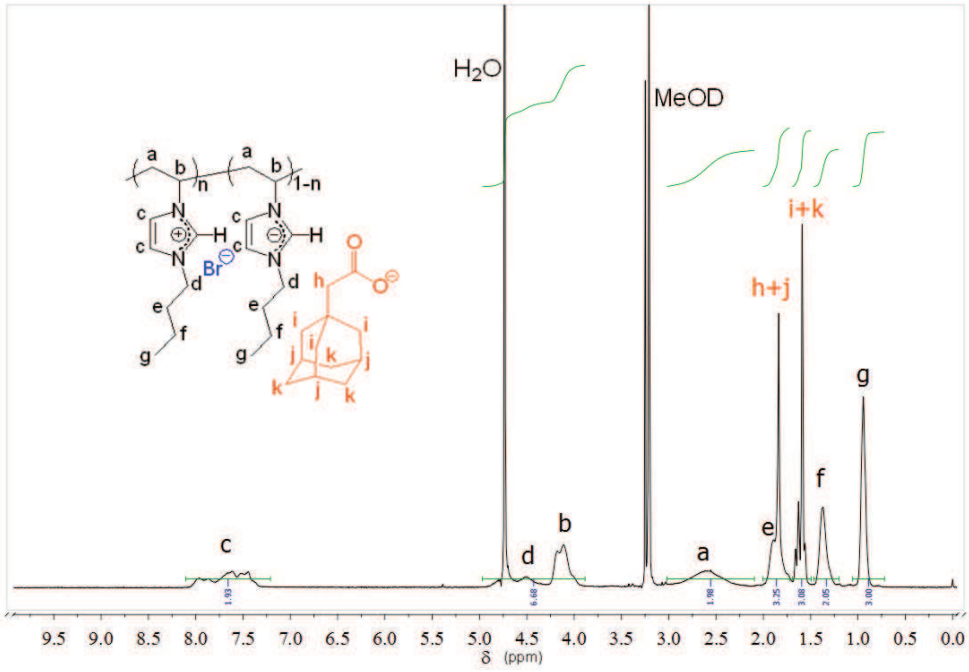

Figure 9. [1]H NMR spectrum of the poly([NHC(H)][Br]-*co*-[NHC(H)][AdamCOO]) **7a** in MeOD.

1.2.2. Use of poly(*N*-vinyl-3-butylimidazolium bromide-*co*-*N*-vinyl-3-butylimidazolium carboxylate)s as organocatalyst precursors

The potential of poly([NHC(H)][Br]-*co*-[NHC(H)][R'COO])s **7a** and **7b** as polymer-supported pre-catalysts was investigated for the benzoin condensation reaction, as a reference reaction of carbene catalysis. In both cases, the reaction was performed in DMF at 80 °C, in the presence of 3 mol% of **7a** or **7b** ([NHC(H)][R'COO] units). After 24h of reaction, 77 and 73% of conversion were obtained by analysis of the crude reaction mixture by [1]H NMR spectroscopy (Figure S10). These results are very promising when compared, for instance, to the previous results obtained with 10 mol% of poly([NHC(H)][HCO_3]s **1**. It is important to note that, in this case, organocatalyzed reactions took place under homogeneous conditions. Unfortunately, attempts to recycle the pre-catalysts were not successful, due to their solubility. A reaction carried out in THF where the polymer precursors **7** were insoluble, did not lead to benzoin.

Compared to previous PILs **1** with hydrogen carbonates counter-anions, polymer precursors **7** behaved as latent catalytic systems to generate poly(NHC)s. We are currently exploring the potential of these poly(NHC) precursors with other alkyl substituents with the perspective to manipulate the solubility of related PILs and recover the polymer-supports.

In summary, *N*-vinyl-3-alkylimidazolium-based PILs could be readily synthesized with specific counter-anions, including hydrogen carbonates or alkyl carboxylates, for a use in organocatalysis *via* the *in situ* generation of poly(NHC)s. Although efficient for catalyzing several reactions of molecular chemistry, the two types of polymer-supports showed some limitations, such as a premature deactivation owing to the forced conditions for the benzoin condensation or complicate recovery/recycling, in some cases. Another potential issue might be the close vicinity of NHC units to the polymer backbone which could restrict the accessibility of the substrates to the catalytic carbenic sites. In the next section, we show the use of other PIL precursors that are characterized by the presence of a spacer group between imidazolium units and the polymer backbone. Statistical poly(ionic liquid)-based copolymers (coPILs) of poly(*N*-vinylbenzylimidazolium)-type instead of a poly(*N*-vinylimidazolium) backbone have thus been designed, and have served as reactive polymer-supports for organocatalysis. We also show that such precursors can be used for post-polymerization modification (second part).

1.3. Polystyrene-based coPILs for a use in organocatalysis

1.3.1. Synthesis of poly(styrene)-*co*-poly(4-vinylbenzylbutylimidazolium chloride)

A similar statistical copolymer with a 2,6-diisopropylphenyl substituent on the imidazolium moiety was prepared by Lu *et al.* for its ability to trap carbon dioxide upon deprotonation of imidazolium units with a strong base (see Scheme 11).[63]

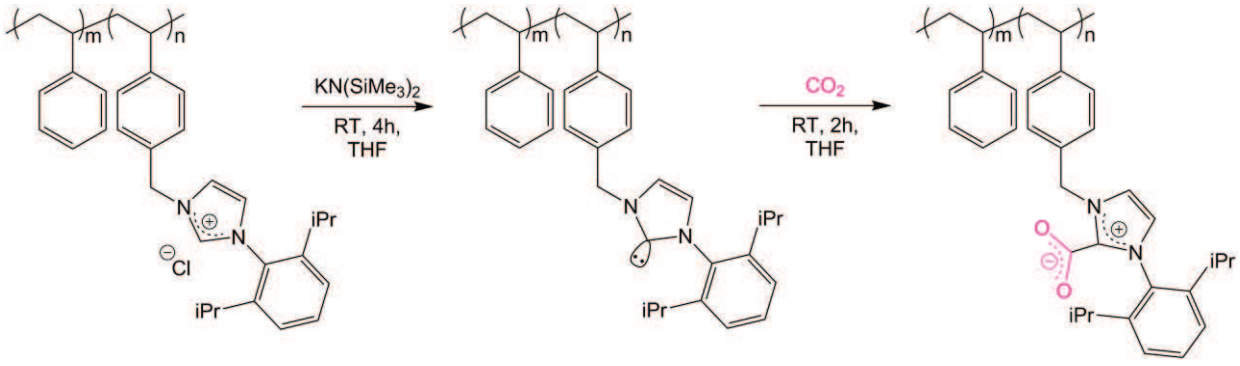

Scheme 11. Deprotonation of a statistical copoly(ionic liquid) with a strong base followed by the trapping of carbon dioxide, adapted from reference 63.

In the present work, the statistical coPIL **9** was synthesized by quaternization of a previously synthesized polystyrene-*co*-poly(4-vinylbenzyl chloride) **8** (PS-*co*-PVBnCl) statistical copolymer using *n*-butyl imidazole (see Scheme 12).[1–3,5,6,63,64]

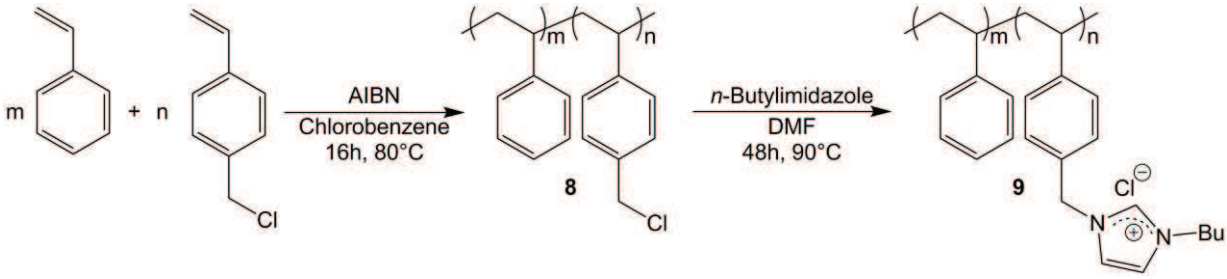

Scheme 12. Synthesis of PS-co-PVBnBuImCl **8** by FRcoP of styrene and 4-vinylbenzyl chloride (VBnCl), followed by quaternization of VBnCl units.

PS-*co*-PVBnCl was first obtained by conventional free-radical copolymerization in chlorobenzene at 80 °C using AIBN as a radical source. A copolymer exhibiting a unimodal molecular weight distribution was thus obtained ($\bar{M}_n$ = 30.0 kg/mol; $Đ$ = 1.65; see also Figure 10), as determined by SEC in THF.

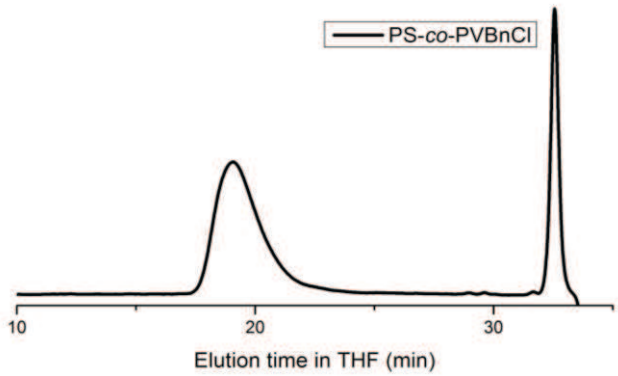

Figure 10. SEC trace in THF of PS-*co*-PVBnCl **8** obtained by FRP in chlorobenzene at 90 °C.

The styrene to 4-vinylbenzyl chloride molar ratio was set at 22/78 (Sty/VBnCl) in order to decrease the density of reactive functions, while maintaining a reasonable solubility. This composition was easily determined by comparing the intensity of signals corresponding to styrene and VBnCl units (total aromatics) to that of methylene protons in VBnCl, in the ^{1}H NMR spectrum of the obtained PS-*co*-PVBnCl copolymer (see equation in Figure 11).

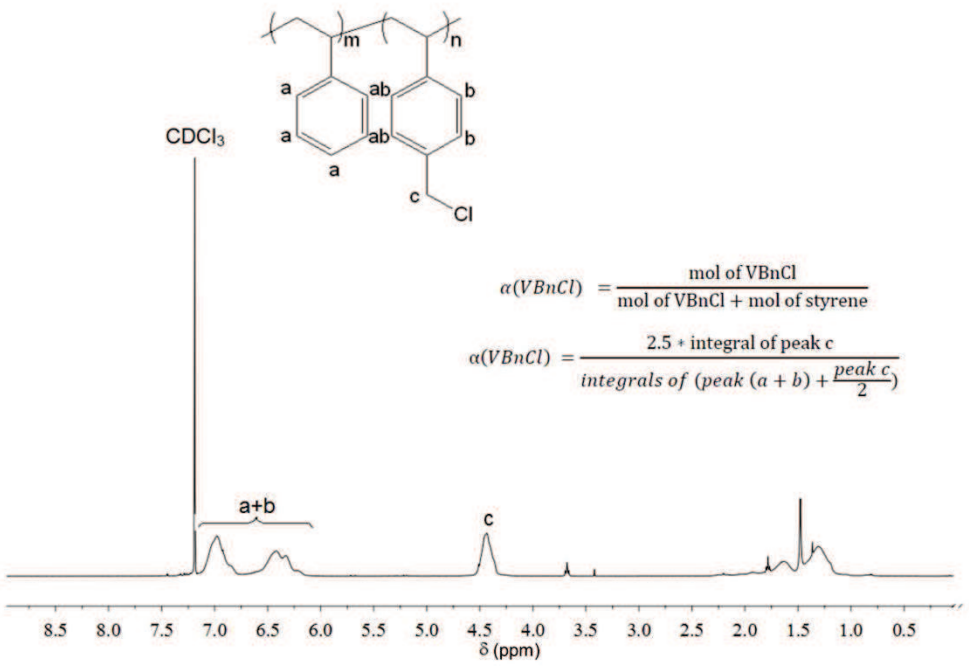

Figure 11. ^{1}H NMR spectrum of PS-*co*-PVBnCl **8** and equation to determine the mole fraction of VBnCl (α(VBnCl)) in the copolymer.

Then, quaternization of the VBnCl units, using an excess of *n*-butylimidazole in DMF at 90 °C for 48h (Scheme 12), allowed for a quantitative post-polymerization modification, as indicated by ^{1}H NMR analysis. This copolymer **9** was further characterized by ^{13}C NMR (Figure 12) and IR spectroscopy (see Figure S12), and by thermogravimetric analysis (TGA) (see Figure S13).

Characterization by ^{1}H NMR allowed stating on the quantitative reaction. Chemical shifts of protons of the methylene group –CH_2– from 4.4 to 5.4 ppm were observed, and characteristic signals of the butylimidazolium group were clearly detected (Figure 13).

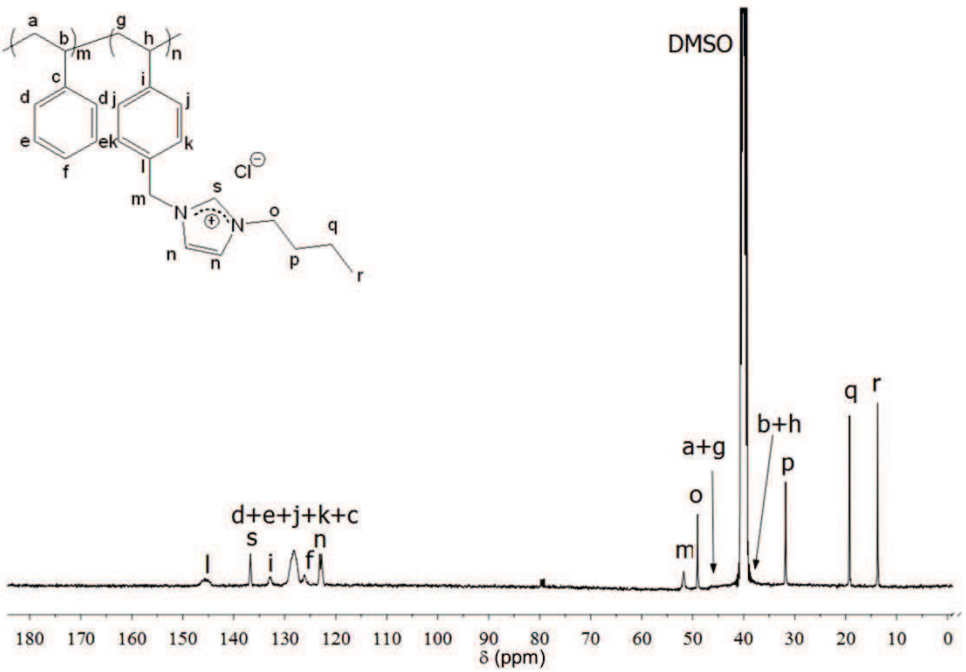

Figure 12. ^{13}C NMR spectrum of PS-*co*-PVBnBuImCl **9** in DMSO-d_6.

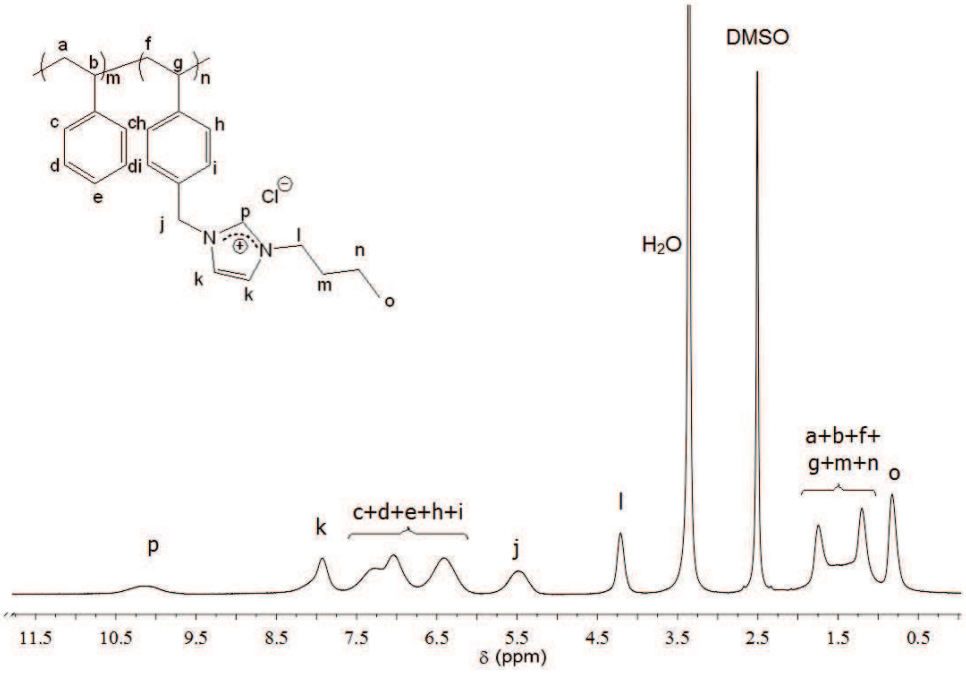

Figure 13. ^{1}H NMR spectrum of PS-*co*-PVBnBuImCl **9** in DMSO-d_6.

1.3.2. Synthesis of poly(styrene)-*co*-poly(4-vinylbenzylbutylimidazolium hydrogen carbonate)

In view of elaborating a reactive platform made of masked poly(NHC)s, a poly(styrene)-*co*-poly(4-vinylbenzylbutylimidazolium hydrogen carbonate) (PS-*co*-PVBnBuImHCO$_3$) **10**, incorporating HCO_3^- anions, was synthesized by anion metathesis of coPIL **9** using $KHCO_3$ in methanol (Scheme 13), following our previously reported procedure.[12–14,87]

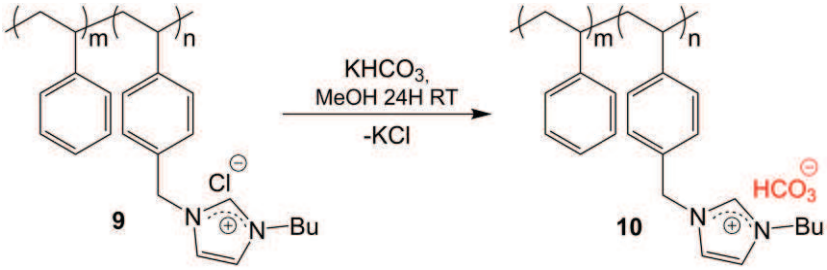

Scheme 13. PS-*co*-PVBnBuImHCO$_3$ **10** synthesized by anion exchange from PS-*co*-PVBnBuImCl **9**.

The novel PS-*co*-PVBnBuImHCO$_3$ **10** was characterized by ^{1}H, ^{13}C and DEPT 135 NMR spectroscopy, IR spectroscopy and TGA. Although chemical shifts of coPIL **10** were similar to those of the parent coPIL **9**, the presence of a characteristic signal at 161 ppm in the ^{13}C NMR spectrum of coPIL **10**, corresponding to the HCO_3^- quaternary carbon, attested to the efficiency of the anion exchange (Figure 14a).

In addition, DEPT 135 confirmed the expected structure (Figure 14b). The presence of the HCO_3^- counter-anion was further observed by IR spectroscopy with the appearance of new bands attributed to the hydrogen carbonate counter-anion (1650 and 1380 cm^{-1}) (Entries a in black and b in red, Figure S12). The extent of anion exchange was also evaluated by reacting an aqueous solution of coPIL **10** with $AgNO_3$; no AgCl precipitate was observed, in agreement with the absence of residual chloride.

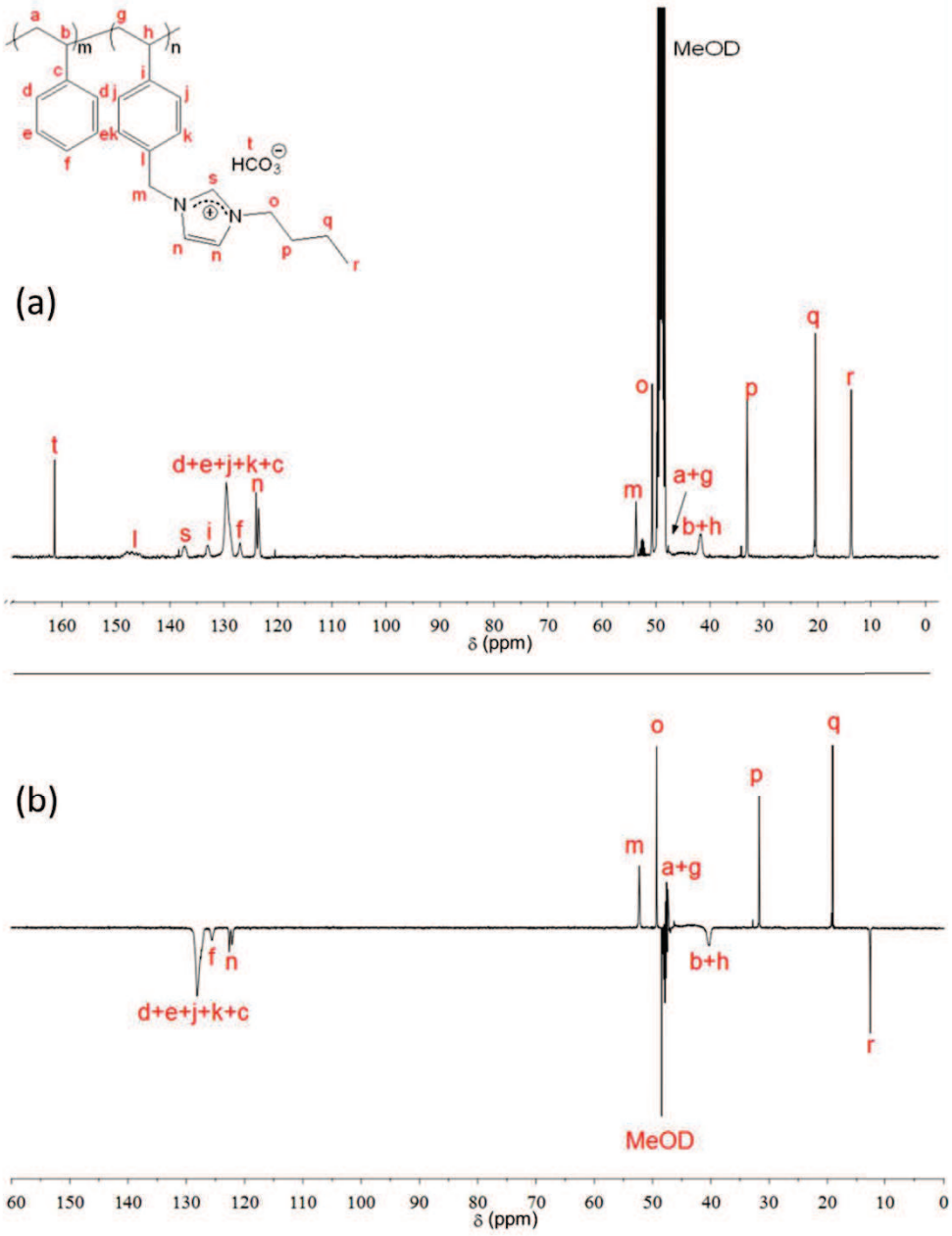

Figure 14. ^{13}C (a) and DEPT 135 (b) NMR spectra of the PS-*co*-PVBnBuImHCO$_3$ **10** in MeOD.

Interestingly, TGA of **10** showed a degradation profile in stages with consecutive weight losses that could be correlated to the different chemical parts of **10**. Accordingly, experimental weight losses (WL_{exp}) were found very close to expected values (WL_{calc}). As illustrated in Figure 25, indeed, the three weight losses detected at 30-300 °C, 300-575 °C and up to 575°C were ascribed to the loss of H_2O, CO_2 first, then of the butyl substituent of the imidazolium moiety (WL_{exp} = 33% *vs.* WL_{calc} = 35%), then of polystyryl backbone (WL_{exp} =

46% vs WL_{calc} = 45%) and, finally, of the imidazolium group (WL_{exp} = 21% vs WL_{calc} = 20%), respectively (Figure 15).

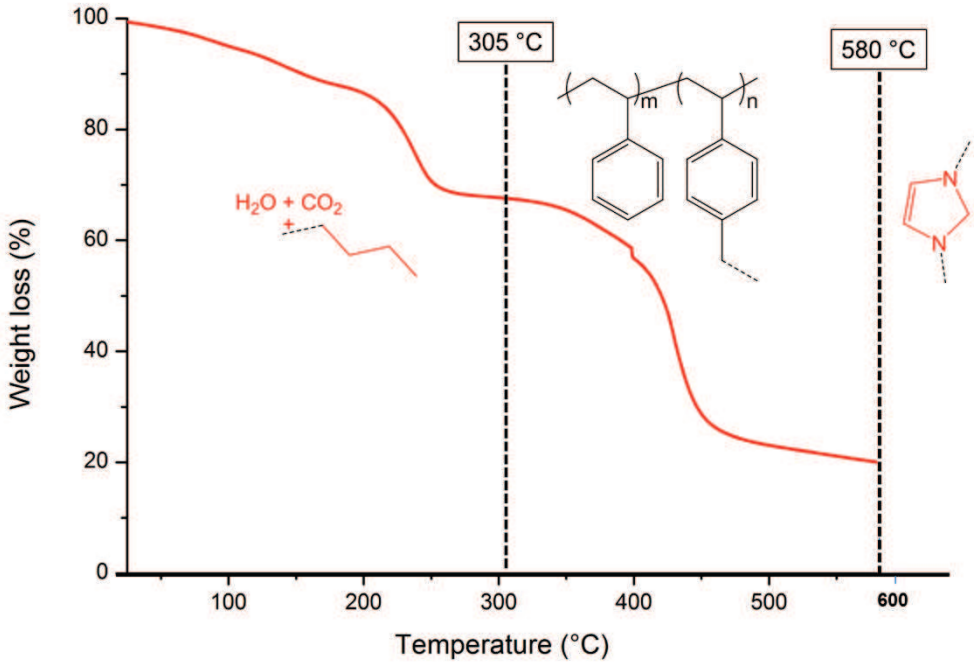

Figure 15. TGA curve of PS-*co*-PVBnBuImHCO$_3$ **10** under N_2 atmospher.

1.3.3. Organocatalysis using poly(styrene)-*co*-poly(4-vinylbenzylbutylimidazolium chloride or hydrogen carbonate)

1.3.3.1. Carbonatation reaction using poly(styrene)-*co*-poly(4-vinylbenzylbutylimidazolium chloride)

The catalytic activity of chloride anion-containing coPIL **9** was first evaluated in the cycloaddition of CO_2 and propylene oxide as a model substrate, affording propylene carbonate (Scheme 14). This reaction was recently shown to be catalyzed by PILs incorporating various counter-anions, such as Cl^-, BF_4^- or PF_6^-.[10,88,89] Mechanisms of this tested molecular reaction catalyzed by coPIL are depicted in the supporting information (See Scheme S4).

The coPIL **9** being insoluble in THF, its recycling was also investigated. The carbonatation reaction was performed in THF at 140 °C, in the presence of 3 mol% of **9** (VBnBuImCl units) with 2.5 MPa of CO_2. After each run, the solid catalyst was readily separated from the reaction mixture by filtration, washed, dried and reused for the next run. The filtrate was analyzed by ^{1}H NMR spectroscopy to identify the product and determine the conversion of the reaction (See Figure S11). Very good conversions were achieved during the

three successive cycles of organocatalysis (1st: 90; 2nd: 87; 3rd: 88%), attesting to an efficient recycling with no significant loss of catalytic activity of the polymer-supported catalyst **9** with the chloride anions.

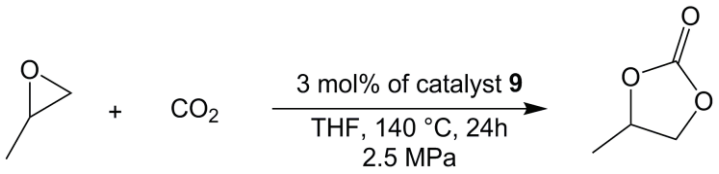

Scheme 14. Synthesis of propylene carbonate using PS-co-PVBnBuImCl **9** as catalyst.

1.3.3.2. Benzoin condensation using poly(styrene)-*co*-poly(4-vinylbenzylbutylimidazolium hydrogen carbonate)

To further illustrate the versatility of the coPIL platform, the polystyrene-based compound **10** was examined for its ability to behave as a masked poly(NHC) upon release of H_2O and CO_2, by analogy with the reactivity of both molecular and poly(*N*-vinyl)-type imidazolium hydrogen carbonate.[12,13] The potential of coPIL **10** as polymer-suported NHC organocatalyst was investigated in the benzoin condensation (Scheme 15).[13,17,75,76,87] The reaction was performed in THF at 80 °C, in the presence of 10 mol% of **10** ($VBnBuImHCO_3$ units) which were the same conditions applied for the catalytic evalutation of the poly(*N*-vinyl)-type imidazolium hydrogen carbonate **1**.

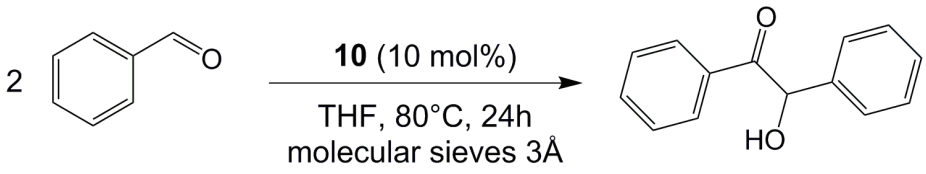

Scheme 15. Benzoin condensation using PS-*co*-PVBnBuImHCO$_3$ **10** as catalyst.

After 24h of reaction, 94% conversion was obtained by analysis of the crude reaction mixture by ^{1}H NMR (see Fig. S10), which compared well with the reactivity of molecular and polymeric *N*-vinyl-type imidazolium hydrogen carbonates previously reported.[13,14,46,87]

Figure 16 shows the increase of the benzoin conversion after optimization of the polymer structures. The catalytic efficiency was thus improved by the decrease of the imidazolium-based pre-catalyst density using the copolystyrenic PIL precursor **10** that proved more efficient than poly(*N*-vinyl)-type homologues carrying HCO_3^- or $RCOO^-$ as counter-anions (see section 1.1.2.3 and 1.2.2).

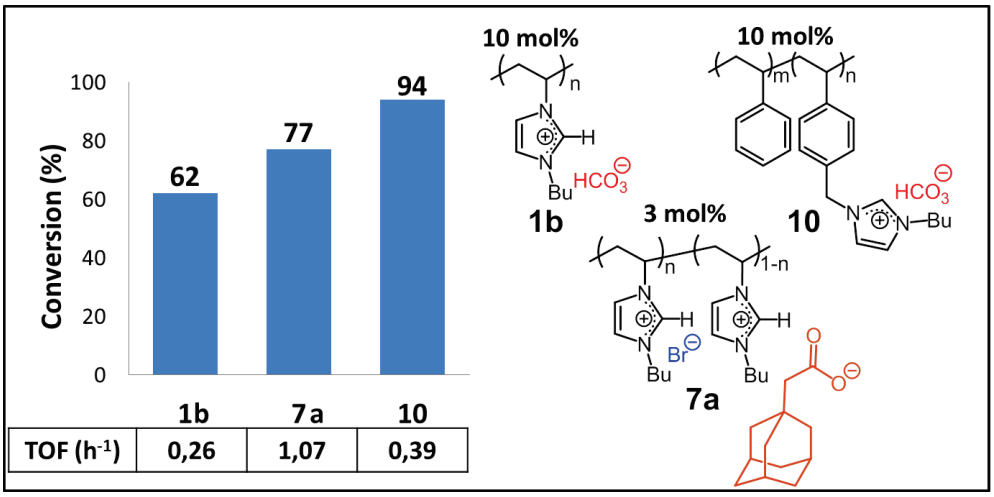

Figure 16. Comparison between conversions and turn-over frequency (TOF) of benzoin condensation reaction using our different pre-catalysts.

Further improvements could be expected, for instance, from using a polystyrene-based coPIL featuring carboxylate counter-anions. A statistical structure could also facilitate a quantitative anion exchange reaction, from bromide to carboxylate, which could not be achieved with a homopoly(*N*-vinyl) precursor, likely due to steric hindrance.

1.4. Mesoporous poly(ionic liquid)-based copolymer networks for a use in organocatalysis

As mentioned previously, we also investigated mesoporous copolymers in a monolithic form with a tunable IL content and a controllable porosity, for catalysis. These precursors were designed in the group of Dr. Jayin Yuan at Max Planck Institute (Potsdam, Germany).

Mesoporous polymers (pore sizes between 2 and 50 nm) have attracted huge research interest in the past 5 years due to their high surface area and meanwhile satisfactory mass/energy transfer, compared to microporous and macroporous systems.[90–92] The application scope of mesoporous polymers is very broad, including separation, adsorption, gas storage, porous carbon production and catalysis.[93–95] The direct copolymerization utilizing a cross-linking comonomer is a straightforward method to achieve mesoporous polymers, the porous structure of which depends on initial polymerization parameters, such as temperature, time, solvent, nature and amount of crosslinker or initiator.[96,97]

The incorporation of ILs into mesoporous polymers has received an increasing interest in recent years.[98–100] The high surface area provided by the porous polymer network, and the functionality of the ILs, can be synergistically combined in such a structure configuration.

For example, Xiao *et al.* reported the synthesis of mesoporous polymers that were surface-decorated with IL molecules *via* post-polymerization. In their approach, divinylbenzene (DVB) and *N*-vinylimidazole were firstly copolymerized under solvothermal conditions, forming a mesoporous network with Brunauer–Emmett–Teller specific surface area (S_{BET}) up to 670 m^2/g. The surface IL species were subsequently introduced *via* a quaternization reaction of imidazole groups, which was followed by anion exchange.[94] Ionic porous polymers obtained in this way were shown to efficiently catalyze the transesterification reaction for biodiesel production. Recently, Antonietti's group reported the synthesis of mesoporous polyelectrolyte networks with S_{BET} up to 310 m^2/g, *via* interpolyelectrolyte complexation in organic solvents.[101] Their application as polymer-supported catalysts for aerobic oxidation of hydrocarbons, CO_2 sorption and activation, and dye sorbent were demonstrated.

The mesoporous crosslinked PILs that were used in our work were obtained by copolymerization of an imidazolium-based IL monomer and DVB as crosslinker, under solvothermal conditions. Reaction conditions to achieve the PIL-based porous network (PILPNs), as well as their characterization and analysis *via* nitrogen sorption will not be discussed here, but can be found elsewhere.[102] We will only describe the synthesis of the PILPNs (Scheme 16) and their use as polymer-supported catalysts.As depicted in Figure 17, these PILPNs also served to access mesoporous carbon structures.

11

Scheme 16. Synthetic details of P(DVB-*y*EVIBr) **11** *via* copolymerization of DVB and *N*-ethyl-3-vinylimidazolium bromide (IL-EVIBr) under solvothermal reaction.

1.4.1. Copolymerization of *N*-vinyl-3-ethylimidazolium bromide monomers in presence of divinylbenzene

Figure 17 illustrates the general synthetic route to mesoporous PIL copolymer networks (PILPNs), and their subsequent applications as polymer-supported organocatalysts and for microporous carbons, respectively. For the sake of conciseness, the as-synthesized

copolymers are denoted as P(DVB-*co*-*y*IL), whereas y denotes the molar content of ILs in the monomer mixture. The preparation of the porous monoliths is based on the slightly procedure described by Xiao *et al*.[103]

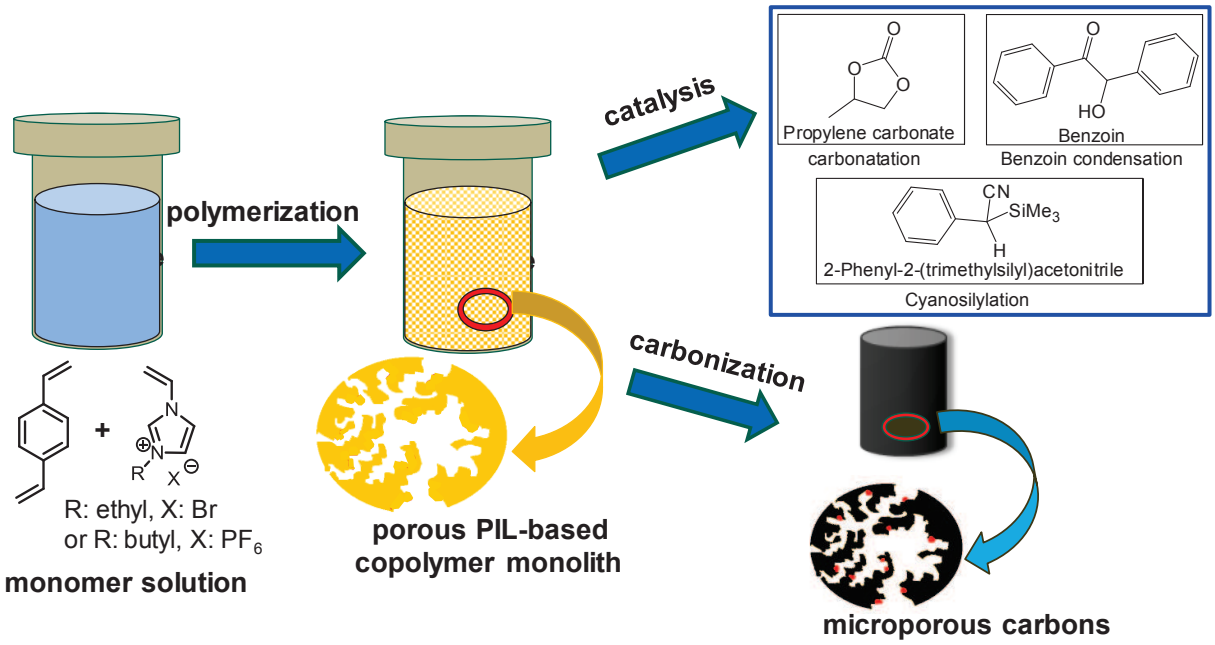

Figure 17. Illustration of the synthesis of mesoporous PIL copolymer networks and their application in catalysis and microporous carbon production.

In a typical procedure, DVB and a defined amount of IL (*N*-vinyl-3-ethylimidazolium bromide in our case typically 0.1 mol%) were mixed and dissolved in a given solvent, depending on the hydrophilicity/hydrophobicity of the employed IL comonomer. A homogeneous solution of comonomers was obtained and transferred to a Teflon stained autoclave. The reactor was then kept at either 180 °C for 24h in DMF. After cooling down, an adaptive columnar monolith was formed and immersed in the reaction solvent overnight to enable the extraction of any unreacted monomers. The purified monolith was dried in ambient conditions for 2 days to slowly evaporate the residual solvent, before it was completely dried at 80 °C under high vacuum (Figure 18A). This drying step was crucial to maintain the monolithic form.[104,105] The dried copolymer monoliths were then subjected to elemental analysis and nitrogen sorption measurements to characterize the composition and the pore feature, respectively.

N_2 sorption studies showed typical type-IV isotherms, giving a steep increase in a relative pressure range of 0.8 – 0.95, indicating the mesoporous characters (Figure S16). Characterization evidenced a S_{BET} value of 640 m²/g and a satisfactory pore volume (V_{total} =

1.07 cm^3/g). The SEM image in Figure 18C shows the particle morphology of P(DVB-0.1EVIBr).

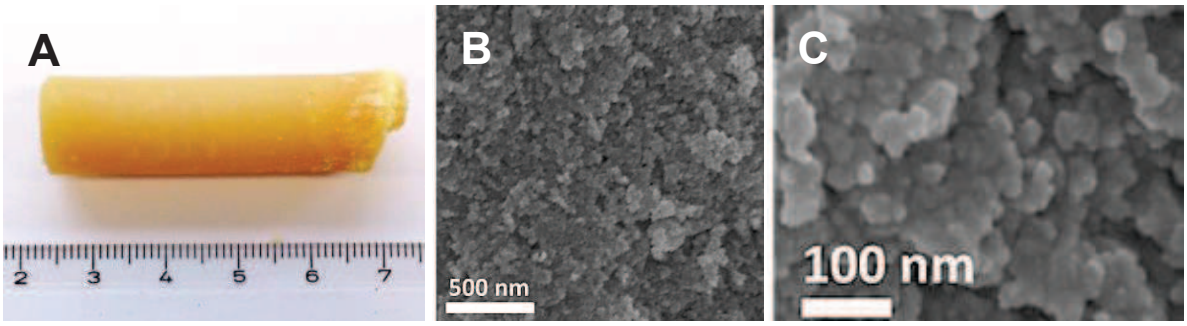

Figure 18. (A) photograph of a P(DVB-0.1EVIBr) **11** monolith. (B&C) SEM image and the enlarged view of a P(DVB-0.1EVIBr) monolith.

1.4.2. Synthesis of propylene carbonate using P(DVB-0.1EVIBr) as organocatalyst

The potential of these imidazolium-based mesoporous materials as polymer-supported (pre)catalysts in different reactions was then investigated. The catalytic activity of the P(DVB-0.1EVIBr) **11** copolymer was first evaluated towards cycloaddition between carbon dioxide and propylene oxide (Scheme 17). It is important to note that direct catalysis of this reaction by both molecular ILs and crosslinked PILs similar to ours were recently reported.[10,88,106,107] One advantage of the P(DVB-0.1EVIBr) monolithic precursor lies in the possibility to recycle and reuse it, after catalysis, owing to its nonsolubility in the reaction mixture.

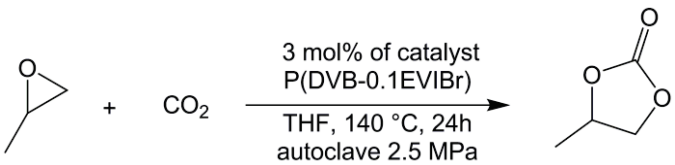

Scheme 17. Synthesis of propylene carbonate triggered by P(DVB-0.1EVIBr) **11** as polymer-supported catalyst (see also Scheme S4 for the reaction mechanism).

The organocatalyzed carbonatation reaction was performed in THF at 140 °C, in the presence of 3 mol% of polymer-supported catalyst (EVIBr units), at 2.5 MPa of CO_2. After each run, the solid catalyst was easily separated from the reaction mixture by simple filtration, allowing a recycling and a reuse for the next run. Formation of propylene carbonate was confirmed by ^1H NMR spectroscopy of the filtrate (see equation for the determination of the

conversion and corresponding ^{1}H NMR spectrum in Figure S11). Excellent conversions were obtained up to three cycles of organocatalysis, attesting to an efficient recycling with no significant loss of catalytic activity.

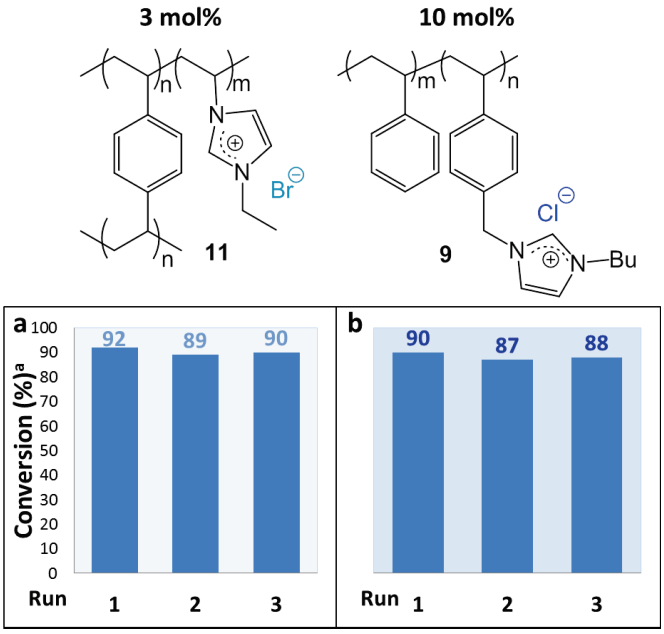

Figure 19. Results of the carbonatation of propylene oxide with carbon dioxide performed in THF at 140 °C for 24h under 2.5 MPa of pressure in the presence of P(DVB-0.1EVIBr) **11**, (a), compared with the use of **9** (b) (see Section 1.3.3.1).

As shown Figure 19, catalytic results obtained with **11** were excellent, related experiments also employed a lower catalytic amount compared to the non-crosslinked polymer-precursor **9** (see section 1.3.3.1), having similar structure. In addition, the synthesis of IL-based monolith **11** is faster and easier than that of coPIL **9**. Such mesoporous networks could be or practical use for continuous flow catalytic reactions.

1.4.3. Synthesis of crosslinked copoly(NHC) for organocatalysis

1.4.3.1. Synthesis of the cross-linked copoly(NHC) by deprotonation

The potential of P(DVB-0.1EVIBr) as precursors for polymer-supported NHCs was also studied. It is well-documented that the NHCs can be directly *in situ* generated by deprotonation of the acidic proton of imidazolium IL salt precursor using a strong base, in an aprotic solvent.[12,13,26,46] Following this strategy, P(DVB-0.1EVIBr) was treated by an excess of potassium bis(trimethylsilyl)amide (KHMDS) suspended in THF at -80 °C under an inert

atmosphere. This allowed generating the corresponding P(DVB-0.1EV(NHC)) **12** (Scheme 18). After 24h of stirring, excess of base and by-products were extracted by filtration and washed with dry THF.

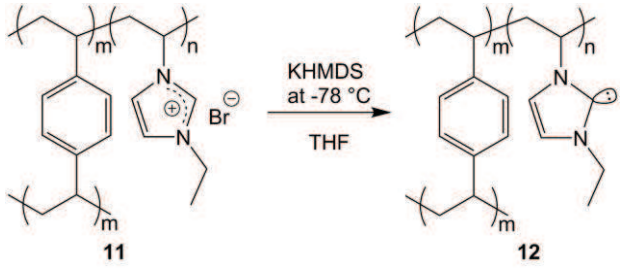

Scheme 18. Synthesis of the cross-linked copoly(*N*-heterocyclic carbene) P(DVB-0.1EV(NHC)) **12** by deprotonation of the P(DVB-0.1EVIBr) **11**.

1.4.3.2. Benzoin condensation and cyanosilylation reaction

The cross-linked P(DVB-0.1EV(NHC)) **12** was then investigated as polymer-supported NHC in both benzoin condensation (Scheme 19) and cyanosilylation reactions (Scheme 20). After the P(DVB-0.1EV(NHC)) was generated, the substrate (*i.e.* benzaldehyde, and trimethylsilyl cyanide) was added, and the reaction mixture was stirred for 1 or 24h, depending on the implemented reaction. Of particular interest, insolubility of the crosslinked polymer-supported catalyst allowed for its easy recycling up to 3 cycles. After each run, the solid catalyst was separated from the reaction mixture by filtration, washed and dried, and then reused for the next run.

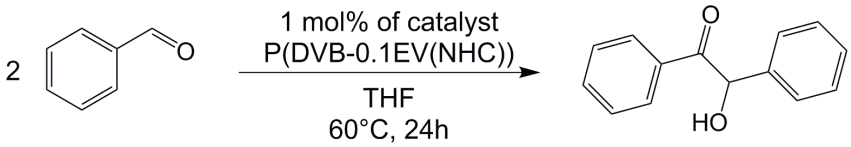

Scheme 19. Benzoin condensation using PDVB-0.1EV(NHC) **12** as supported catalyst.

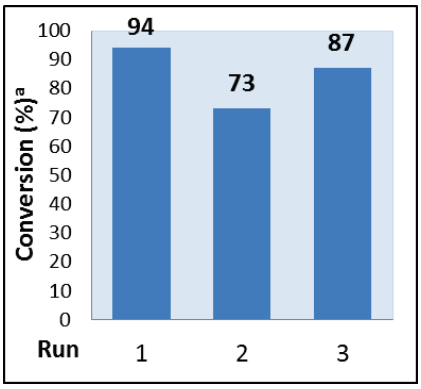

Figure 20. Results of the benzoin of condensation from benzaldehyde performed in THF at 60 °C for 24h in the presence of 1 mol% of EV(NHC) catalytic units in P(DVB-0.1EV(NHC)) **12**.

Benzoin condensation reactions (Scheme 19) were performed in THF at 60 °C, in the presence of 1 mol% of P(VDB-0.1 EV(NHC)) (EV(NHC) units). Benzoin formation was monitored by ^{1}H NMR spectroscopy of the filtrate (see equation used for the determination of the conversion in benzoin and ^{1}H NMR spectrum in Figure S10). Fairly good conversions were achieved, up to three cycles of organocatalysis (Figure 20), attesting to an efficient recycling while maintaining a high catalytic activity. The slight loss of efficiency could be ascribed to partial deactivation of NHC units, likely due to their sensitivity to trace impurities and the conditions reactions.

Overall, it is worth emphazing that results of the benzoin condensation utilizing cross-linked copoly(NHC)s **12** proved superior (higher TOF values) to those employing noncrosslinked homopoly(NHC)s generated either from *N*-vinyl- (**1** and **7**) (see section 1.1.1.3 and 1.2.2) or from styrene-based (**10**) (see section 1.3.3.2) imidazolium PILs (see Figure 21).

For instance, not only the first run provided excellent catalytic activity, but the two subsequent cycles also gave a high conversion (73-87%) (Figure 20), contrarily to our previous observations. This might be ascribed to the mesoporous and monolithic character of P(VDB-0.1EV(NHC)) which could better preserve the carbenic centers. In addition, lower catalytic amounts of P(DVB-0.1EV(NHC)) **12** (*i.e.* 1 mol%) were used compared to our previous systems (*i.e.* 3 or 10 mol%) while maintaining an excellent catalytic efficiency. However, it should be acknowledged that here poly(NHC)s were formed under rather harsh conditions, *i.e.* use of a strong base at low temperature, while use of polymeric NHC

progenitors (*i.e.* PILs and coPILs with HCO_3^- and $RCOO^-$ counter-anions) could deliver NHC units *in situ* under mild conditions (see Figure 21).

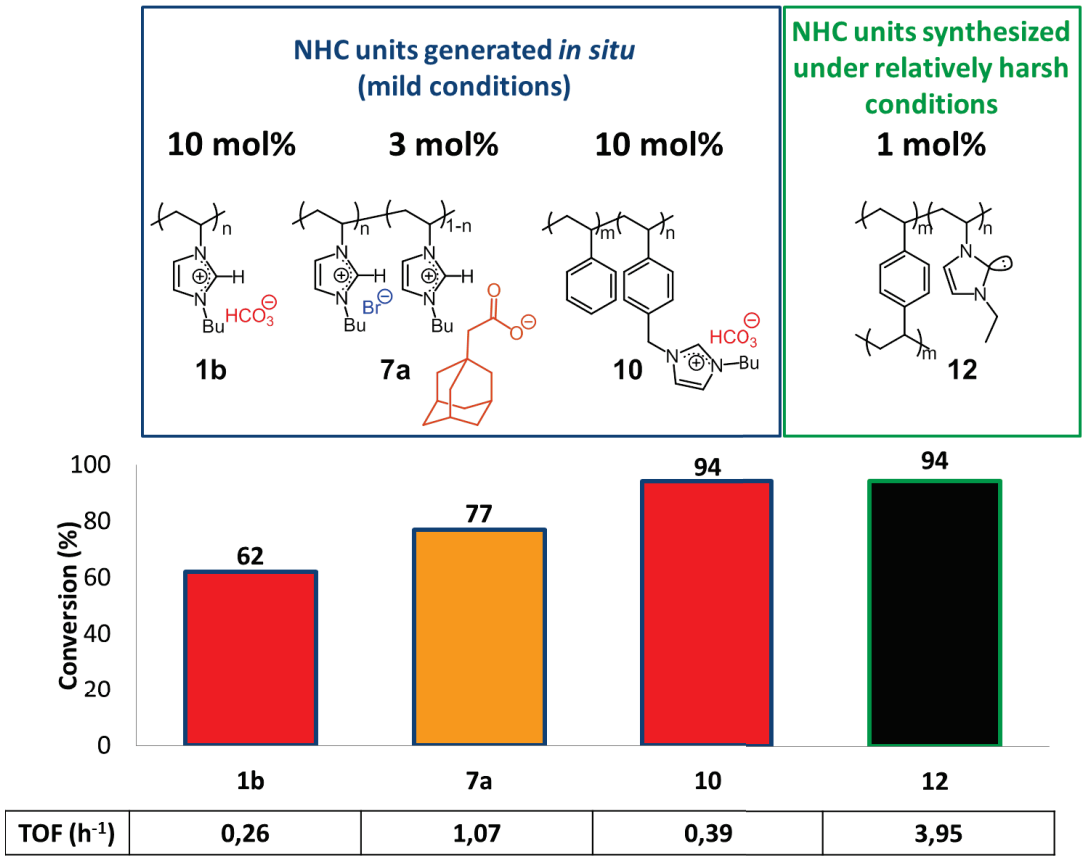

Figure 21. Comparison between conversions and TOF of benzoin condensation reaction using our different pre-catalysts.

Next, the catalytic potential of the P(DVB-0.1EV(NHC)) was investigated for the cyanosilylation of benzaldehyde with trimethylsilyl cyanide (TMSCN) (Scheme 20).[79,87] The reaction was carried out in THF in the presence of 0.5 mol% of EV(NHC) catalytic units, at 60 °C for 1h. Conversion was monitored by ^{1}H NMR spectroscopy of the filtrate (see equation and ^{1}H NMR spectrum in Figure S9). Excellent conversions were obtained after only 1h of stirring, up to 3 cycles (Figure 22), attesting to the efficiency and the recycling of the crosslinked polymer-supported catalyst.

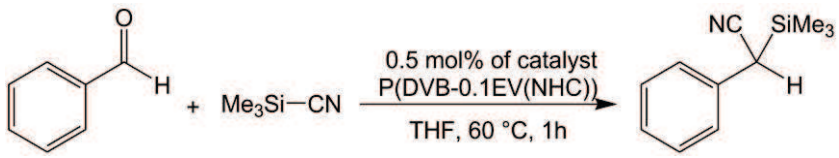

Scheme 20. Cyanosilylation using P(DVB-0.1EV(NHC)) **12** as supported catalyst.

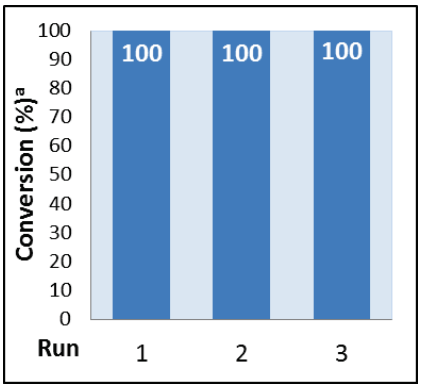

Figure 22. Results of the cyanosylilation reaction performed in THF at 60 °C for 1h in the presence of 0.5 mol% of EV(NHC) catalytic units in P(DVB-0.1EV(NHC)) **12**.

2. Post-polymerization modification using poly(styrene)-*co*-poly(4-vinylbenzylbutylimidazolium chloride or hydrogen carbonate)

In this part, we show that the statistical poly(*N*-vinylbenzyl imidazolium)-type coPILs **9** and **10** described above (see Scheme 13) can now serve as reactive polymer precursors for various quantitative post-chemical modifications, in addition of their use for organocatalysis discussed in the first part of this chapter.

Post-polymerization modification, referred to as polymer-analogous modification, is part of the common polymer chemistry toolbox.[108–110] This method consists in synthesizing new polymers by modification of naturally occurring macromolecules or preformed synthetic polymers. These precursors carry handles that can be converted into other functional groups, in a subsequent step of chemical modification.

Esterification of cellulose,[111,112] crosslinking of polyisoprene by vulcanization,[113] or methanolysis of poly(vinyl acetate)[114] are representative examples of post-polymerization modification reactions that are implemented at the industrial level. In recent years, various chemical reactions showing a very high chemoselectivity and/or orthogonality have been adapted to modify "tailor-made" chain-growth polymer precursors carrying handles, enabling the design of functional polymers that would be hardly accessible by a normal direct (co)polymerization technique.

A typical example is the nucleophilic substitution of polymeric activated esters, the synthesis of which can be achieved from miscellaneous monomers (*e.g.* *N*-(meth)acryloxysuccinimide,[115,116] pentafluorophenyl(meth)acrylate,[117] p-

nitrophenylacrylate,[118] etc.), either by (controlled) radical polymerization or by metal-catalyzed polymerization.

Many other reactive polymer precursors have served for polymer-analogous modification, for instance, polymers bearing anhydrides, isocyanates, oxazolones, epoxides, aldehydes or ketones that can be engaged in various chemical reactions.[119–121] Modification of preformed polymers by Michael-type addition reaction,[122] by thiol exchange, radical thiol reaction,[123,124] by the Huisgen 1,3-dipolar cycloaddition reaction,[125,126] or by palladium-catalyzed coupling and cross-coupling reactions[127,128] have also been reported.

2.1. Metallation from chloride-containing coPIL

Firstly, coPIL **9** was investigated as a precursor of a poly(NHC-Ag) complex **13**, by a simple metallation reaction. In molecular chemistry, NHC-Ag complexes are indeed easily synthesized from an imidazolium halide in presence of silver oxide, the latter reagent playing the role of both the base and the metallating agent.[32,33,129,130] The synthetic interest of such NHC-silver complexes lies in their ability to transfer the NHC fragment to other transition metals, hence they can serve as efficient masked NHCs.[130,131] Thus, by analogy with the synthesis of molecular NHC-Ag complexes, coPIL **9** was treated with Ag_2O in methylene chloride (Scheme 21). Mechanism of the metallation is depicted in the Annex (Scheme S5).[132]

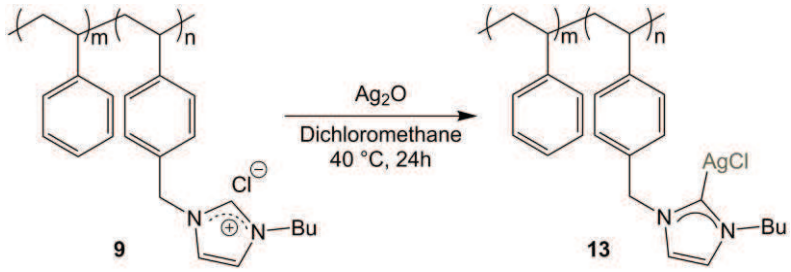

Scheme 21. Synthesis of PS-*co*-poly(NHC-Ag) complex **13** by metalation of PS-*co*-PVBnBuImCl **9** with Ag_2O.

The as-obtained PS-co-poly(NHC-Ag(I)Cl) complex, **13**, was isolated in good yields (~ 80%) after 24h of stirring at 40 °C. Copolymer **13** was completely characterized by ^{13}C NMR (Figure 23) and IR spectroscopy (Figure S12) and TGA (Figure S13). In particular, the signal due to the C_2H proton of the imidazolium moiety at 9.5-10.5 ppm completely vanished in the ^{1}H NMR spectrum, confirming that deprotonation by silver oxide took place. Moreover, the observation of a characteristic signal at 180 ppm in the ^{13}C NMR spectrum, downshifted by

138 ppm compared to that of C_2H in coPIL **9**, demonstrated the metallation of C_2 by Ag, and the formation of the targeted poly(NHC-Ag) complex **13** (Figure 23).

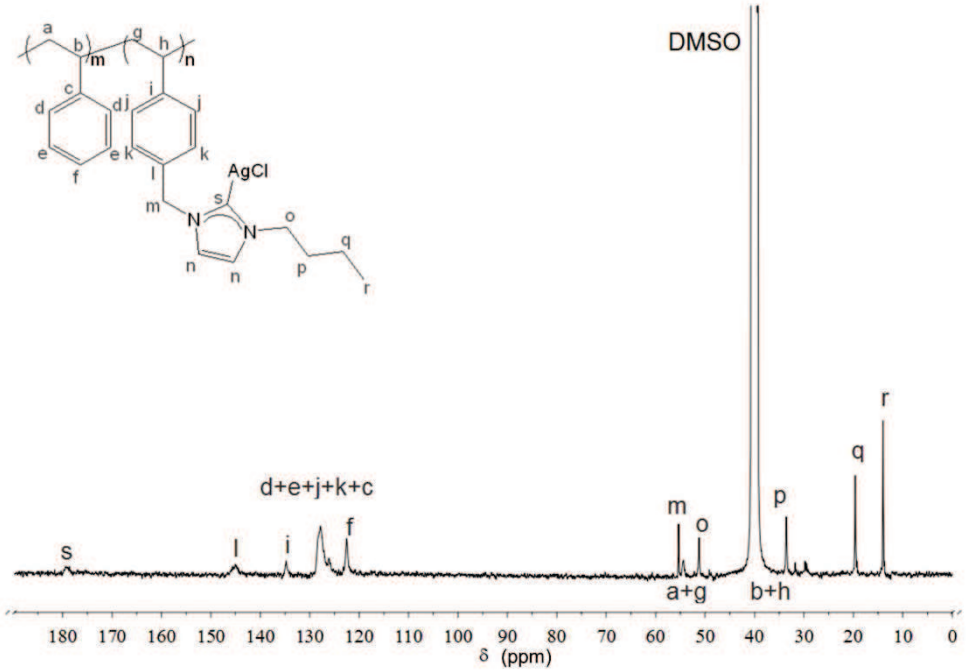

Figure 23. ^{13}C NMR spectrum of the PS-co-poly(NHC-Ag) complex **13** in DMSO-d_6.

2.2. Stoichiometric addition (CS_2, isothiocyanate)

Besides being powerful ligands for transition metals and organocatalysts for a variety of transformations, molecular NHCs were recently shown to react with small electrophilic organic molecules, including CO_2,[38] CS_2,[38,39] N_2O,[133] aldehydes,[134–137] esters,[137] ketenes[138–141] and isothiocyanate under true stoichiometric conditions.[39,142,143] Here, two model organic substrates, CS_2 and isothiocyanate, were investigated to highlight the stoichiometric reactivity of our coPIL **10** (Scheme 22).

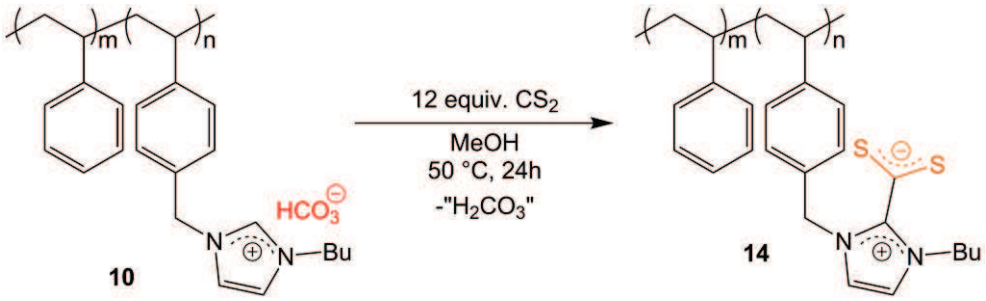

Scheme 22. Stoichiometric post-functionalization of PS-*co*-PVBnBuImHCO$_3$ **10** with CS_2 upon release of "H_2CO_3".

Thus, reaction of PS-*co*-PVBnBuImHCO$_3$ **10** with an excess of CS_2 (12 equiv.) in MeOH, at 50 °C for 24h, led to the corresponding polybetaine, PS-co-poly(azolium dithiolate) **14**, also denoted as PS-*co*-Poly(NHC-CS_2) adduct (**14**, Scheme 22). The structure of **14** was authenticated by ^{13}C, ^{1}H NMR, and IR spectroscopy (Figure S12) and by TGA (Figure 25). In particular, a diagnostic signal at 231 ppm, corresponding to the –CS_2 moiety could be observed in the ^{13}C NMR spectrum of **14** (Figure 24), in good agreement with data concerning molecular analogs reported in the literature.[39,75]

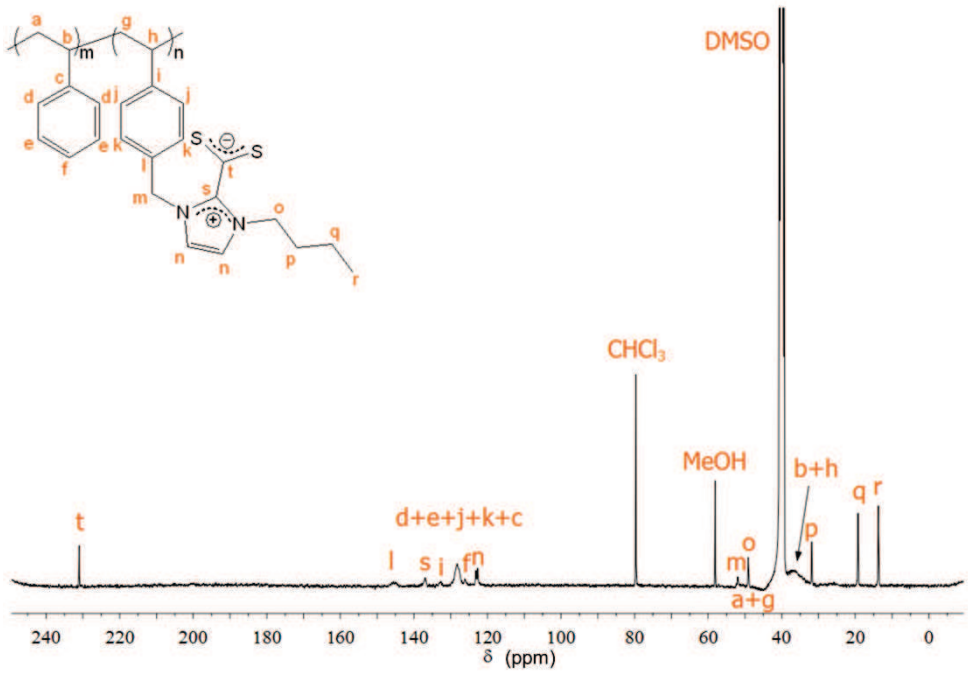

Figure 24. ^{13}C NMR spectrum of the PS-*co*-poly(NHC-CS_2) **14** in DMSO-d_6.

In addition, two bands at 1050 and 1250 cm^{-1}, corresponding to the symmetric and asymmetric stretching mode of CS_2, respectively, could be observed in the IR spectrum of **14**, while the concomitant disappearance of the characteristic band of the HCO_3^- counter-anion at 1650 and 1380 cm^{-1} were noted (Entries b in red and d in orange, Figure S12).

The chemical composition of **14** could be further established by TGA, where a good agreement between experimental and theoretical weight loss of carbon disulfide (WL_{exp} = 23% *vs.* WL_{calc} = 22%), butyl substituents (WL_{exp} = 15% *vs.* WL_{calc} = 16.5%), polystyryl backbone (WL_{exp} = 45% *vs.* WL_{calc} = 42.5%) and imidazole moieties (WL_{exp} = 17% *vs.* WL_{calc} = 19%) could be observed (Figure 25).

Importantly, although this reaction involving CS_2 has limited synthetic utility, it clearly establishes that coPIL **10** can quantitatively deliver the corresponding free copoly(NHC) in solution, in addition to affording the novel copolybetaine **14**.

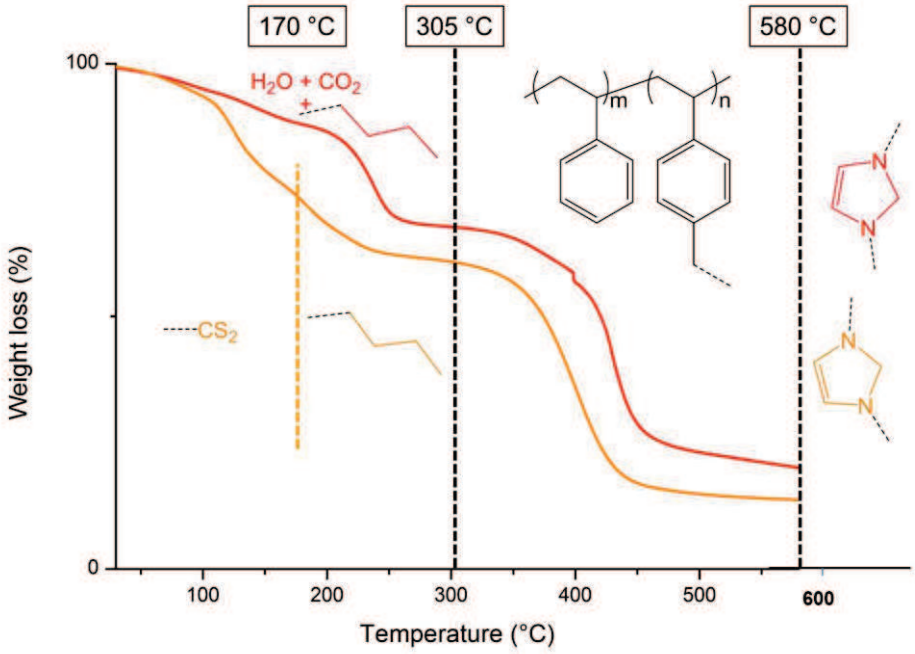

Figure 25. TGA curves of PS-*co*-PVBnBuImHCO$_3$ **10** (red) versus PS-*co*-Poly(NHC-CS$_2$) adduct **14** (orange).

Next, PS-*co*-PVBnBuImHCO$_3$ **10** was tested in the reaction with 2.5 equiv. of 3,5-(bistrifluoromethyl)phenyl isothiocyanate (R-NCS) in MeOH, at 60 °C for 24h (Scheme 23).

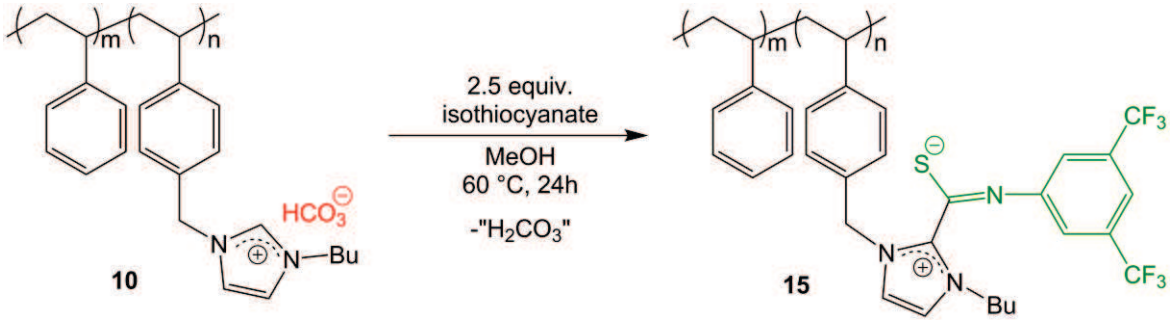

Scheme 23. Stoichiometric post-functionalization of PS-*co*-PVBnBuImHCO$_3$ **10** with 3,5-(bistrifluoromethyl)phenyl isothiocyanate upon release of "H_2CO_3".

The resulting polybetaine **15** was fully characterized by ^{19}F, ^{1}H, ^{13}C NMR, IR spectroscopy and TGA. In particular, analysis of **15** by ^{19}F NMR ($\delta(CF_3)$ = - 60 ppm), after several washings with toluene, supported the binding of the isothiocyanate onto the copolymer (Figure 26). Moreover, the two quaternary carbons of the N_2C-*C*(S)NR fragment

(s) and (t) could be distinguished at 156 and 182 ppm, respectively, in the ^{13}C NMR spectrum (Figure 26), attesting to the generation of copoly(NHC) from coPIL **10**, and subsequent reaction with the isothiocyanate.

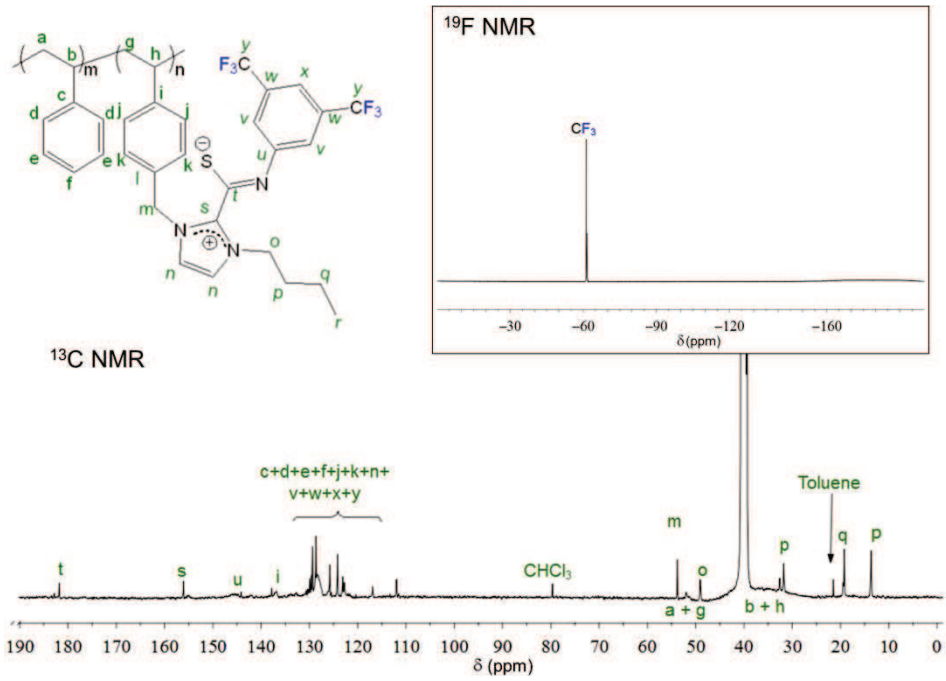

Figure 26. ^{13}C and ^{19}F NMR spectra of the PS-*co*-poly(NHC-RNCS) **15** in DMSO-d_6.

2.3. Stoichiometric transfer of Pd and Au from HCO_3^- containing coPIL

Having established that coPIL **10** was able to quantitatively react both with CS_2 and isothiocyanate, *via* the formation of the related copoly(NHC), yielding novel copolymers with a betaine-type structure, we turned our attention to the reactivity of coPIL **10** towards organometallic substrates. Indeed, this would give access to various copoly(NHC)-transition metal complexes from a single platform based on imidazolium hydrogen carbonate coPIL, by analogy with their molecular homologues.[20,29,144–146] Thus, the stoichiometric reaction of coPIL **10** was investigated with two representative metallic fragments: palladium allyl chloride dimer $[Pd(allyl)Cl]_2$ and chloro(dimethyl sulfide) gold(I) $Au(SMe_2)Cl$.

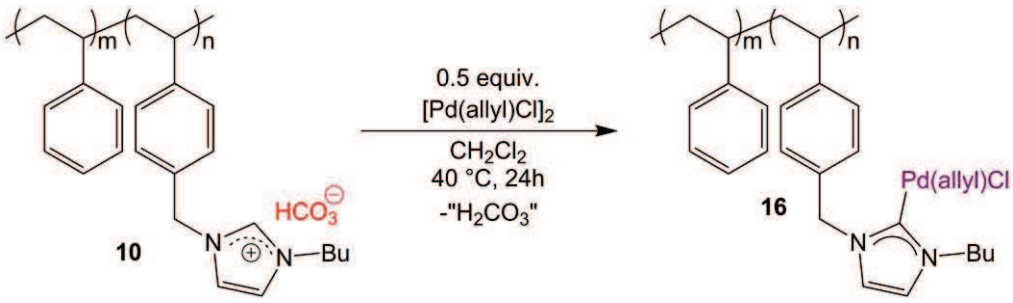

Scheme 24. Stoichiometric post-functionalization of PS-*co*-PVBnBuImHCO$_3$ **10** with [Pd(allyl)Cl]$_2$ upon release of "H_2CO_3".

Thus, **10** was first reacted with 0.5 equiv. of [Pd(allyl)Cl]$_2$ in methylene chloride (Scheme 24). The corresponding PS-*co*-poly(NHC-Pd(II)) complex **16** was isolated in excellent yield (>90%), after 24h of stirring at 40 °C and was fully characterized by ^{1}H, ^{13}C NMR and IR spectroscopy. In particular, the complete disappearance of the signal corresponding to the C*H* proton of the imidazolium moiety, at 9.5-10.5 ppm in the ^{1}H NMR spectrum, confirmed the release of H_2O and CO_2. In the corresponding ^{13}C NMR spectrum, the characteristic signal of the carbene center was observed at 179.8 ppm, in agreement with that observed for analogous palladium-NHC complexes (δ = 175.6-188.5 ppm).[14,16,147] In addition, the characteristic signals of the allyl group (δ(CH) = 114.8 ppm; δ(CH_2) = 71.6 ppm; δ(CH_2) = 48.5 ppm) could be detected (Figure 27).

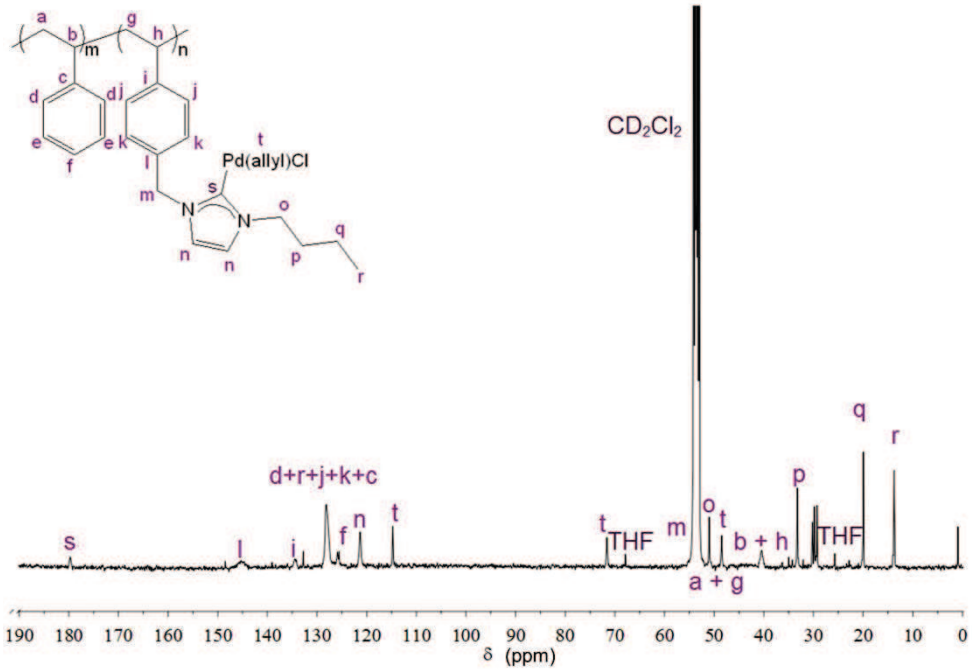

Figure 27. ^{13}C NMR spectrum of the PS-*co*-poly(NHC-Pd(allyl)Cl) **16** in CD_2Cl_2.

Similarly, the reaction of coPIL **10** with $Au(SMe_2)Cl$ was also successfully accomplished, giving excellent yield (87%) of the corresponding PS-*co*-poly(NHC-Au) complex **17**, after 24h of stirring in DMF at 50 °C (Scheme 25). The characteristic signal of the carbene center could be observed at 178.8 ppm in the ^{13}C NMR spectrum (Figure 28), confirming the carbene complex structure of **17**.

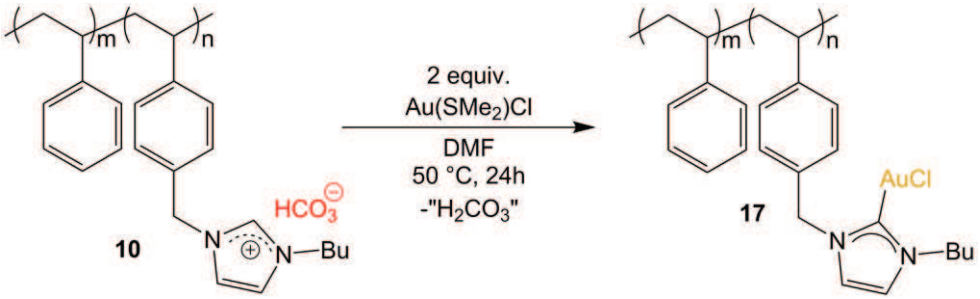

Scheme 25. Stoichiometric post-functionalization of PS-*co*-PVBnBuImHCO$_3$ **10** with $Au(SMe_2)Cl$ upon release of "H_2CO_3".

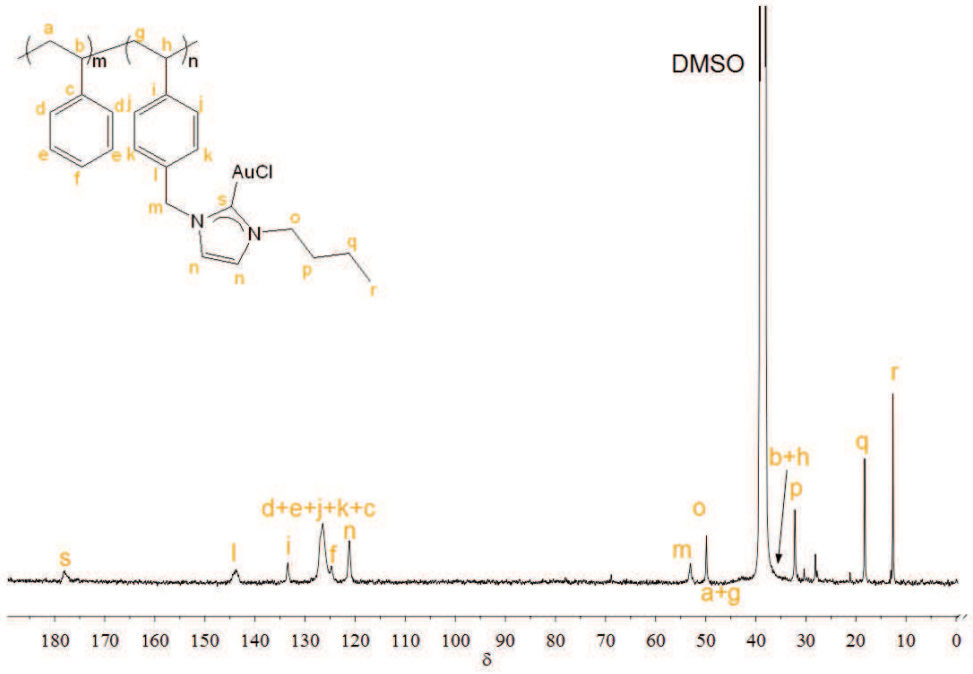

Figure 28. ^{13}C NMR spectrum of the PS-*co*-poly(NHC-AuCl) **17** in DMSO-d_6.

In summary, the efficiency of novel imidazolium-based PILs with either hydrogen carbonate and chloride counter-anions was demonstrated as poly(NHC) precursors for stoichiometric post-polymerization modifications with organic and organometallic substrates. Exploiting the imidazolium reactivity, an optimization of the polymer backbone was achieved, from a homopoly(ionic liquid) version to a statistical copolymeric version. Increasing the distance between the polymer backbone and the imidazolium *via* a spacer

group and introducing the NHC precursor units statistically along the polymer backbone, indeed, improved the NHC generation. A summary highlighting the use of coPILs **9** and **10**, for the purpose of organocatalysis and for post-chemical modification, is shown in Figure 29.

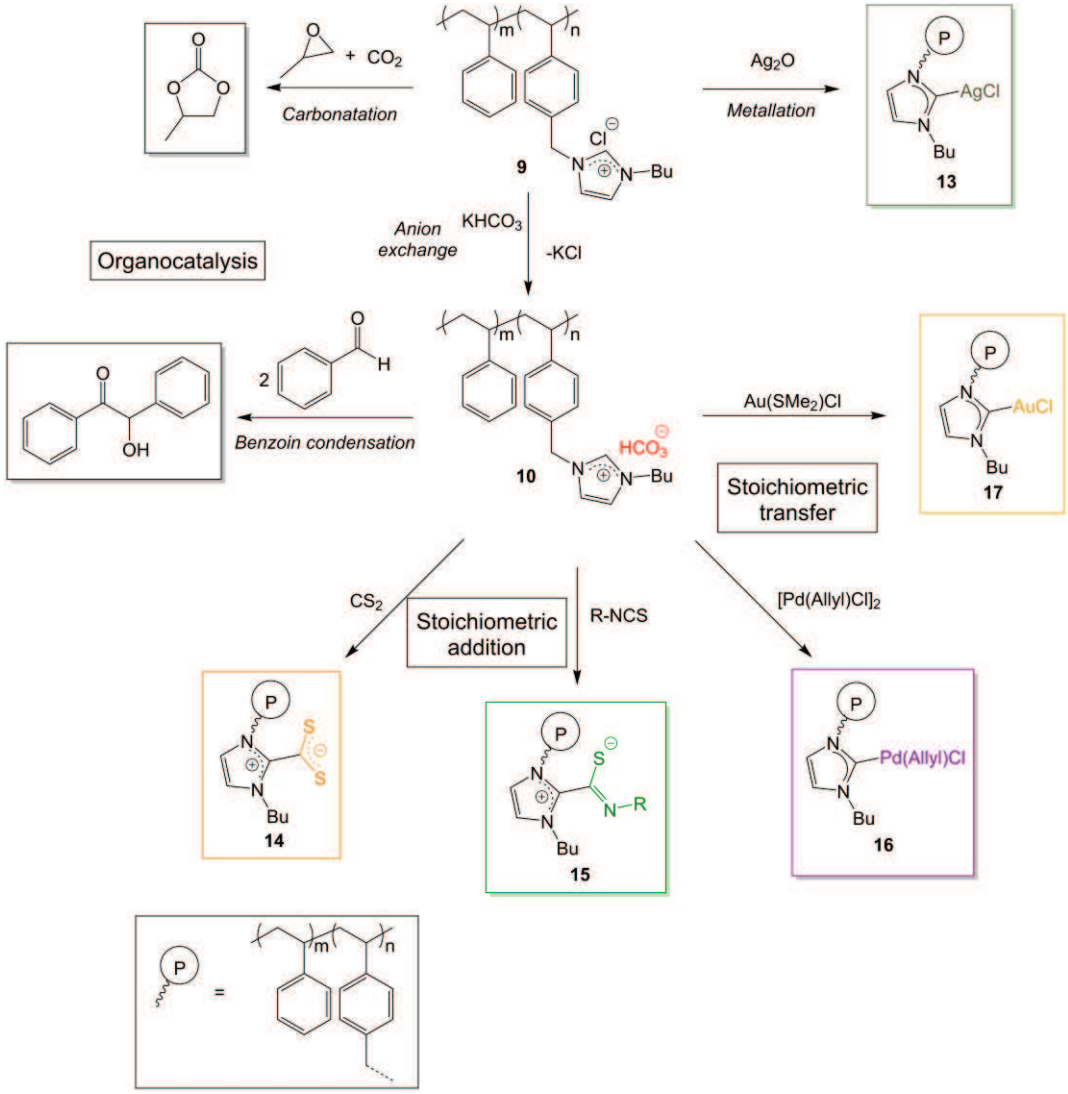

Figure 29. Copoly(ionic liquid)s, PS-*co*-PVBnBuImCl **9** and PS-*co*-PVBnBuImHCO$_3$ **10** for various post-polymerization modifications and for organocatalysis.

Conclusion

In this chapter, novel *N*-vinylimidazolium-based homopolymers, statistical styrenic-type copolymers and mesoporous copolymer networks were specifically designed by relatively simple synthetic methods utilizing free-radical copolymerization. Advantage of the intrinsic reactivity of the imidazolium moiety was taken through the use of all these novel poly(ionic liquid)s for organocatalytic reactions of molecular chemistry. The statistical styrenic-type coPIL precursor was also employed for quantitative post-chemical modification.

From poly(*N*-vinyl-3-alkyl imidazolium hydrogen carbonate)s, the *in situ* generation of related polymer-supported *N*-heterocyclic carbenes, poly(NHC)s, occured by a formal loss of "H_2CO_3" ($H_2O + CO_2$). Re-carboxylation of as-obtained poly(NHC)s allowed easily recycling the polymer precursors and reusing them for several organocatalytic cycles, especially for transesterification and cyanosilylation reactions. Excellent catalytic activities could be achieved for the latter reactions, whereas benzoin condensation required longer reaction times, and did not allow efficiently recycling the polymer-supported pre-catalysts, presumably owing to a premature deactivation of poly(NHC)s under forcing conditions.

Poly(*N*-vinylimidazolium bromide-*co*-*N*-vinylimidazolium carboxylate)s were synthesized for the first time, by partial anion exchange reaction from the parent poly(*N*-vinylimidazolium bromide), though this modification step proved incomplete, likely owing to steric hindrance issues. Analysis revealed around 25% of carboxylate counter-anions. Catalytic tests on the benzoin condensation reaction established the generation of the NHC units, and confirmed the anion exchange between the bromine ions and the carboxylates.

Copoly(ionic liquid)s (coPILs) based on poly(styrene)-*co*-poly(4-vinylbenzylbutylimidazolium) salts, consisting of either a chloride or a hydrogen carbonate counter-anion, PS-*co*-PVBnBuIm(Cl or HCO_3), were also achieved by quaternization of a preformed statistical PS-*co*-PVBnCl copolymer, in order to decrease the catalytic density. These coPILs featuring a spacer group between the polymer backbone and the imidazolium moiety represent a versatile platform of reactive polymers, due to the presence of imidazolium units statistically distributed along the polymer backbone. The two coPILs could be used as efficient polymer-supported organocatalysts for the synthesis of cyclic carbonate and the benzoin condensation as well. In the latter case, catalysis occurred *via* the generation of NHC units when using the hydrogen carbonate counter-anion.

In addition, a novel mesoporous polymer monolith, with adjustable contents of ionic liquid, high specific surface area and pore volumes were elaborated by a facile solvothermal copolymerization route. Such ionic mesoporous polymers, called PILPNs, were successfully applied as polymer-supported organic (pre)catalysts, either for the cyclocarbonatation of propylene oxide or for the benzoin condensation or for cyanosilylation, *via* generation of NHC units with a strong base.

Comparison of the catalytic performances of the four different imidazolium-based PILs described in this chapter, also showing the merits and drawbacks in each case, is summarized in Table 2.

Table 2. Comparison of imidazolium-based PILs used for the benzoin condensation reaction

	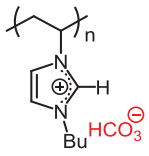	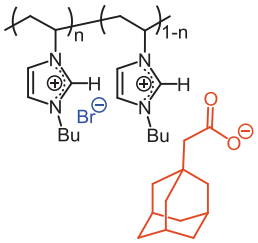	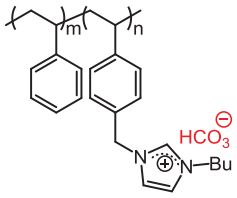	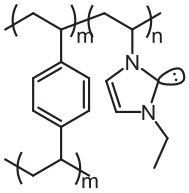
Catalytic amount (mol%)	10	3	10	1
Benzoin condensation conversion (%)	62	77	94	94
TOF (h^{-1})	0,26	1,07	0,39	3,95
Advantages	- Synthesis in 2 steps - Recycling	- Synthesis in steps - Homogeneous catalysis	- Excellent conversion - Low catalytic density along the polymer - Parent polymer easily characterized	- Excellent conversion - Low amount of catalyst -Low catalytic density - Synthesis in 2 steps - Recycling
Drawbacks	- Lower conversion	- No recycling	- Synthesis in 3 steps	- NHC generation by deprotonation with a strong base

Then, the polystyrene-based coPILs were post-functionalized by a variety of simple organic and organometallic substrates. This synthetic strategy opens avenues to the synthesis of novel polymers, such as polybetaines and poly(NHC-Met) complexes. Combined characterization methods, including NMR and IR spectroscopy as well as TGA allowed attesting to the expected structure of the polymer derivatives, after transfer of the NHC units either to organic substrates (*e.g.*, CS_2, RNCS) or to catalytically relevant transition metals (*e.g.*, Ag, Pd, Au).

This straightforward synthetic strategy might be generalized to access many other functional polymers *via* the copoly(NHC) generation occurring *in situ* from air-stable solid compounds.

These different imidazolium-based polymer precursors thus offer novel perspectives for various organocatalyzed reactions under various conditions, according to the chemical structure selected. For example, PILPNs could be developed for efficient organocatalysis under a continuous flow in a column system.

In addition, the stoichiometric post-chemical modifications of coPILs forming metallic poly(NHC)-adducts could be obviously used for organometallic catalysis (Heck reaction, Suzuki coupling, hydrogenation, oxidation etc.). Addition of electrophilic substrates could also be expanded to other molecular compounds which have been described to react with NHCs at stoichiometry (*e.g.* fullerenes or azides). These reactions could also be used for network synthesis using multifunctional electrophiles (*e.g.* bis-azides, bis-isothiocyanates, etc.).

In the next chapter of this manuscript, we show that *N*-vinylimidazolium-type PILs can also be engineered into well-defined block copolymer structures, through the use of a peculiar controlled radical polymerization method. Further investigations into the self-assembly, either in bulk or in solution, will be also described.

Experimental and supporting information

Materials.

N-Vinylimidazole (99%), 1-bromobutane (99%), 1-bromoethane (99%), 2-bromoethylbenzene (99%), 1-bromododecane (99%), 1-adamantaneacetic acid (98%) and 10-undecenoic acid (98%) were obtained from Alfa Aesar and used as received. Azobis(2-methylpropionitrile) (AIBN, 99%) was received from Aldrich and was purified by recrystallization from methanol. Styrene (>99%), divinylbenzene (DVB) (80% mixture of isomers), Silver oxide(I) (>99%), chloro(dimethylsulfide)gold(I) $Au(SMe_2)Cl$, Dimethylaminopropionitrile (DMAPN, 98%) and potassium persulfate (KPS, 99%) were purchased from Aldrich and used as received. 4-vinylbenzyl chloride (90%) were purchased from Acros and used as received. 3,5-(bistrifluoromethyl)phenyl isothiocyanate (98%) were purchased from TCI and used as received. Allylpalladium chloride dimer $[Pd(Allyl)Cl]_2$ (99%) were purchased from Strem and used as received. 4,4'-Azobis(4-cyanovaleric acid) (V-501, 99%) and 2,2'-azobis(4-methoxy-2,4-dimethyl valeronitrile) (V-70, 99%) were purchased from Wako chemicals used as received. Benzyl alcohol (Aldrich, 99%) and benzaldehyde (Aldrich, 99.5%) were distilled prior to use. Vinyl acetate (Aldrich, 99%) was dried over CaH_2 and distilled prior to use. Trimethylsilylcyanide (TMSCN, 98%) and potassium tert-butoxide (97%) from ABCR were used as received. Potassium bicarbonate ($KHCO_3$ 99.7%, Aldrich) was dried at 50 °C for 12h under vacuum prior to use. Tetrahydrofuran (THF) was distilled over Na/benzophenone. Dimethyl sulfoxide (DMSO 99.5%, Fischer) and ethyl acetate (99.7%, Aldrich) were used without further purification. MeOH was distilled over Na metallic before use. CO_2 (N-45, Air Liquide) was purified by passing through a click-on inline "super clean purifier" (SGT) prior to use.

Instrumentation.

^1H NMR, ^{13}C NMR, DEPT135 NMR and ^{19}F NMR spectra were recorded on a Bruker AC-400 spectrometer in appropriate deuterated solvents. Some ^{13}C measurements were performed at 298K on a Bruker Avance III 400 spectrometer operating at 100.7 MHz and equipped with a 5mm Bruker multinuclear direct cryoprobe-head. The 1D ^{13}C NMR data were obtained over 6144 scans with a 30° flip angle (90° pulse=9 μs), an acquisition time of 1.3s, a relaxation delay of 3s and 65k data points. Molar masses of water soluble PILs were determined by size exclusion chromatography (SEC) in H_2O/formic acid (0.3 M) as the eluent (0.6 mL/min) and with pyridine as a flow marker at 25 °C, using both refractometric (RI) and UV detectors (Varian). Analyses were performed using a PL-GPC50 plus integrated GPC System equipped

with PSS SUPREMA Max columns with pore sizes of 30 and 1000 Å respectively (connected in series), fitted with dual detectors (refractometry and UV). Calibration curve was done using Poly(2-vinylpyridine) as polymer standards. Molar masses of THF soluble polymer were determined by size exclusion chromatography (SEC) in THF as the eluent (1 mL/min) and with trichlorobenzene as a flow marker at 40 °C, using both refractometric (RI) and UV detectors (Varian). Analyses were performed using a three-column set of TSK gel TOSOH (G4000, G3000, G2000 with pore sizes of 20, 75, and 200 Å respectively, connected in series) calibrated with polystyrene standards. A Bruker Tensor 27 spectrometer was used for ATR-FTIR analysis. Thermogravimetric analyses (TGA) were performed using a TA instruments Q50 under a nitrogen atmosphere, from room temperature (10 °C/min) to 600 °C. The weight loss was recorded as a function of temperature. The specific surface area and pore size distribution were calculated using the Brunauer–Emmett–Teller (BET) equation, and the density functional theory (DFT) method (slit/cylinder. pores, QSDFT adsorption branch), respectively. Samples were degassed at 120 °C for 20h prior to the measurements.

Synthesis of *N*-vinyl-3-ethylimidazolium bromide VEtImBr (4a).

N-Vinyl-3-ethylimidazolium bromide ([NHC(H)][Br]) **4a** was prepared following a procedure already described. The monomer was recovered as a white solid (100% yield). ***N*-vinyl-3-butylimidazolium bromide VBuImBr (4b), *N*-vinyl-3-(1-phenylethyl)-imidazolium bromide VEtPhImBr (4c)** and ***N*-vinyl-3-dodecylimidazolium bromide VDodeImBr (4d)** were prepared following a similar procedure. NMR data were in accordance with those reported in the literature.

Synthesis of *N*-vinyl-3-ethylimidazolium hydrogen carbonate VEtImHCO$_3$ (2a).

A mixture of *N*-vinyl-3-ethylimidazolium bromide, **1a**, (1 g, 4.92 mmol) and 1.05 equiv of $KHCO_3$ (518 mg, 5.18 mmol) was dried at 60 °C under vacuum for 12h. Dry methanol (5 mL) was then added, and the resulting suspension was stirred for 24h at RT. After filtration of the suspension over Celite, methanol was evaporated under vacuum to yield a sticky solid. After trituration of the solid with acetone and filtration, **2a** was obtained as a yellowish powder and dried under dynamic vacuum (yield: 83%). The product was then stored under static vacuum. ^{1}H NMR (CD_3OD): δ 1.56 (d, C*H*$_3$-CH_2-, 3H), 4.39 (q, CH_3-C*H*$_2$- , 2H), 5.43 (dd, *H*CH=CH-N, 1H), 5.92 (dd, *H*CH=CH-N, 1H), 7.26 (dd, CH_2=C*H*-N, 1H), 7.78 (s, N-CH=C*H*-N, 1H), 8.00 (s, N-C*H*=CH-N, 1H). ^{13}C NMR (CD_3OD): δ 15.41 (*C*H_3-CH_2-), 52.8 (*C*H_2-CH_3), 109.9 (*C*H_2=CH-N), 120.8 (N-*C*H=CH-N), 124.1 (N-CH=*C*H-N), 129.9 (CH_2=*C*H-N), 136.1 (N-*C*H-N), 161.4 (H*C*O_3).

Synthesis of *N*-vinyl-3-butylimidazolium hydrogen carbonate VBuImHCO$_3$ (5b).

5b was prepared following a similar procedure to that used for the synthesis of **5a**. ^{1}H NMR (CD_3OD, Figure 1): δ 0.98 (t, C*H*$_3$-CH$_2$-CH$_2$-CH$_2$-, 3H), 1.32 (s, CH$_3$-C*H*$_2$-C*H*$_2$-CH$_2$-, 2H), 1.90 (t, CH$_3$-CH$_2$-C*H*$_2$-CH$_2$-, 2H), 4.27 (t,N-C*H*$_2$-CH$_2$-CH$_2$-CH$_3$, 2H), 5.4 and 4.9 (d, N-CH-C*H*$_2$, 2H), 7.25 (dd, N-C*H*=CH$_2$, 1H), 7.7 and 8.0 (d, C*H*=C*H*, 2H). ^{13}C NMR (CD_3OD, Figure 2): δ 13.57 (*C*H$_3$-CH$_2$-CH$_2$-CH$_2$-), 20.28 (CH$_3$-*C*H$_2$-CH$_2$-CH$_2$-), 37.72 (CH$_3$-CH$_2$-*C*H$_2$-CH$_2$-), 50.73 (CH$_3$-CH$_2$-CH$_2$-*C*H$_2$-), 109.9 (*C*H$_2$=CH-N), 120.8 (N-*C*H=CH-N), 124.1 (N-CH=*C*H-N), 129.9 (CH$_2$=*C*H-N), 135.1 (N-*C*H-N), 161.0 (H*C*O$_3$).

Synthesis of *N*-vinyl-3-(1-phenylethyl)imidazolium hydrogen carbonate VEtPhImHCO$_3$ (5c).

5c was prepared following a similar procedure as that used for the synthesis of **5a**. ^{1}H NMR (CD_3OD): δ 1.89 (d, C*H*$_3$-CH-, 3H), 5.42 (dd, *H*CH=CH-N, 1H), 5.83 (m, C*H*-(CH$_3$)(C$_5$H$_5$), 1H), 6.00 (dd, *H*CH=CH-N, 1H), 7.29 (dd, CH$_2$=C*H*-N, 1H), 7.43 (m, CH-C$_5$*H*$_5$, 5H), 8.00 (s, N-CH=C*H*-N, 1H), 8.25 (s, N-C*H*=CH-N, 1H), 9.84 (s, N-C*H*-N, 1H). ^{13}C NMR (DMSO-d_6): δ 19.36 (*C*H$_3$-CH-), 58.9 (*C*H-(CH$_3$)(C$_5$H$_5$)), 107.7 (*C*H$_2$=CH-N), 118.8 (N-*C*H=CH-N), 120.8 (N-CH=*C*H-N), 126.0 and 128.0 (CH-*C*$_5$H$_5$), 133.5 (CH$_2$=*C*H-N), 138.1 (N-*C*H-N), 158.3 (H*C*O$_3$).

Synthesis of *N*-vinyl-3-dodecylimidazolium hydrogen carbonate VDodeImHCO$_3$ (5d).

5d was prepared following a similar procedure to that used for the synthesis of **5a**. ^{1}H NMR (CD_3OD): δ 0.7 (t, C*H*$_3$(-CH$_2$-)$_{10}$CH$_2$-, 3H), 1.2-1.3 (m, CH$_3$(-C*H*$_2$-)$_9$CH$_2$-CH$_2$, 18H), 1.7 (q, CH$_3$(-CH$_2$-)$_9$C*H*$_2$-CH$_2$, 2H), 4.1 (t, CH$_3$(-CH$_2$-)$_9$CH$_2$-C*H*$_2$, 2H), 5.4 (dd, *H*CH=CH-N, 1H), 5.92 (dd, *H*CH=CH-N, 1H), 7.26 (dd, CH$_2$=C*H*-N, 1H), 7.78 (s, N-CH=C*H*-N, 1H), 8.00 (s, N-C*H*=CH-N, 1H). ^{13}C NMR (CD_3OD): δ 15.1 (*C*H$_3$-CH$_2$-CH$_2$(-CH$_2$-)$_7$CH$_2$-CH$_2$-), 24.9 (CH$_3$-*C*H$_2$-CH$_2$(-CH$_2$-)$_7$CH$_2$-CH$_2$-), 28.2 (CH$_3$-CH$_2$-*C*H$_2$(-CH$_2$-)$_7$CH$_2$-CH$_2$-), 31.2 (CH$_3$-CH$_2$-CH$_2$(-*C*H$_2$-)$_7$CH$_2$-CH$_2$-), 34.7 (CH$_3$(-CH$_2$-)$_9$*C*H$_2$-CH$_2$-), 54.2 (CH$_3$-CH$_2$-CH$_2$-*C*H$_2$-), 110.5 (*C*H$_2$=CH-N), 122.8 (N-*C*H=CH-N), 124.1 (N-CH=*C*H-N), 130.9 (CH$_2$=*C*H-N), 137.3 (N-*C*H-N), 161.4 (H*C*O$_3$).

Synthesis of PVBuImBr (6b) by polymerization of VBuImBr (4b).

In a typical experiment, a 10 mL Schlenk tube was flame dried and charged with 1g (4.3 mmol) of **4b**, 12.7 mg (0.08 mmol) of AIBN and 4 mL of methanol. The Schlenk tube was subjected to five freeze-thaw cycles and placed in a thermostated oil bath previously

maintained at 80 °C. The reaction was quenched after 3h by sudden cooling with liquid nitrogen. The resulting poly(*N*-vinyl-3-butylimidazolium) bromide (**6b**) was isolated by precipitation in acetone. After drying under vacuum, **6b** was obtained as a yellowish powder (Yield 95%). M_n = 25000 g.mol^{-1} (D = 1.45) by SEC in H_2O/acid formic (0.3 M) (see Figure 5). ^{1}H NMR (CD_3OD, see Figure S7): δ 8.9-9.3 (br, N-C*H*-N,1H), 7.3-7.8 (br, C*H*=C*H*, 2H), 3.9-4.5 (br,N-C*H*$_2$-CH$_2$-CH$_2$-CH$_3$, 2H), 4.4-4.8 (br, N-C*H*-CH$_2$, 1H), 2.4-3.0 (br, N-CH-C*H*$_2$, 2H), 1.7-2.1 (br, CH$_3$-CH$_2$-CH$_2$-CH$_2$-, 2H), 1.3-1.6 (br, CH$_3$-CH$_2$-C*H*$_2$-CH$_2$-, 2H), 0.9-1.2 (br, C*H*$_3$-CH$_2$-CH$_2$-CH$_2$-, 3H).

Synthesis of PVEtImHCO$_3$ (1a, R = ethyl) by polymerization of VEtImHCO$_3$.

In a typical experiment, a Schlenk tube was flame-dried and charged with 1 g (5.43 mmol) of **4a**, 24.3 mg (0.09 mmol) of KPS and 10 mL of DMSO. The Schlenk tube was subjected to five freeze-thaw cycles before adding 10.1 µL (0.09 mmol) of DMAPN under argon flow. The reaction mixture was stirred for 24h at room temperature. The obtained polymer was precipitated in acetone to remove residual monomer, filtrated and dried under vacuum. **1a** was recovered as a yellowish powder (Yield: 85%). M_n = 29000 g.mol^{-1} (D = 2.3) by SEC in H_2O/formic acid (0.3 M) (see also Figure 5). ^{1}H NMR (CD_3OD, see Figure S2) : 1.4-1.7 (C*H*$_3$-CH$_2$, 3H), 2.4-2.7 (*H*$_2$C-CH-N, 2H), 4.1-4.4(C*H*$_2$-CH$_3$, 2H), 4.4-4.7 (H$_2$C-C*H*-N, 1H), 7.4-8.0 (N-C*H*=C*H*-N, 2H). ^{13}C NMR (CD_3OD, see Figure S1) : δ 14.7 (*C*H$_3$-CH$_2$-), 40.9 (H$_2$C-*C*H-N), 58.3 (*C*H$_2$-CH$_3$),120.3 et 122.0 (N-*C*H=*C*H-N), 136.8 (N-*C*H-N), 160.9 (H*C*O$_3$).

Synthesis of PVBuImHCO$_3$ (1b, R = butyl) by polymerization of VBuImHCO$_3$.

1b was prepared following a similar procedure to that used for **1a** (Yield: 98%). M_n = 26200 g.mol^{-1} (D = 1.78) by SEC in H_2O/formic acid (0.3 M) (see also Figure 5). ^{1}H NMR (CD_3OD, see Figure 3) : 0.8-1 (br, C*H*$_3$-CH$_2$-CH$_2$-CH$_2$-, 3H), 1.2-1.4 (br, CH$_3$-C*H*$_2$-C*H*$_2$-CH$_2$-, 2H), 1.6-1.9 (br, CH$_3$-CH$_2$-C*H*$_2$-CH$_2$-, 2H), 2.1-2.4 (br, C*H*$_2$-CH-N, 1H), 3.7-4.1 (br, CH$_2$-C*H*-N, 1H), 4.2-4.7 (br,N-C*H*$_2$-CH$_2$-CH$_2$-CH$_3$, 2H), 7.5-8.0 (br, C*H*=C*H*, 2H), 9.5-10 (br, N-C*H*-N, 1H). ^{13}C NMR (CD_3OD, see Figure 4): δ 13.5 (*C*H$_3$-CH$_2$-CH$_2$-CH$_2$-), 20.28 (CH$_3$-*C*H$_2$-CH$_2$-CH$_2$-), 32.0 (CH$_3$-CH$_2$-*C*H$_2$-CH$_2$-), 42.2 (*C*H$_2$-CH-N), 50.7 (CH$_3$-CH$_2$-CH$_2$-*C*H$_2$-), 54.2 (CH$_2$-*C*H-N), 120.8-122.3 (N-*C*H=*C*H-N), 137.1 (N-*C*H-N), 159.0 (H*C*O$_3$).

Synthesis of $PVPhEtImHCO_3$ (1c, R= 1-phenylethyl) by polymerization of $VPhEtImHCO_3$.

1c was prepared following a similar procedure to that used for **1a** (Yield 95%). ^{1}H NMR (CD_3OD, see Figure S4) : 1.7-2.1 (br, C*H*$_3$-CH-, D3H), 2.3-3.3 (br, *H*$_2$C-CH-N, 2H), 4.6-5.1 (br, CH_2-C*H*-N, 1H), 5.3-5.6 (br, C*H*-(CH_3)(C_5H_5), 1H), 7.2-7.7 (br, CH-C_5H_5, N-CH=C*H*-N, N-C*H*=CH-N, 7H). ^{13}C NMR (CD_3OD, see Figure S3): 22 .3(*C*H_3-CH-), 41.4 (*C*H_2-CH-N), 60.2 (*C*H-(CH_3)(C_5H_5)), 61.9 (CH_2-*C*H-N), 121.5 (N-*C*H=*C*H-N), 128.7-136.3 (CH-*C*$_5$H$_5$), 139.8 (N-*C*H-N), 161.4 (H*C*O_3).

Synthesis of $PVDodeImHCO_3$ (1d, R = dodecyl) by polymerization of $VDodeImHCO_3$.

1d was prepared following a similar procedure to that used for **1a** (Yield: 68%). ^{1}H NMR (CD_3OD, see Figure S6) δ 0.7-0.8 (br, C*H*$_3$(-CH_2-)$_{10}$$CH_2$-3H), 1.2-1.1-1.4 (br, CH_3(-C*H*$_2$-)$_9$$CH_2$-$CH_2$, 18H), 1.7-2.0 (br, CH_3(-CH_2-)$_9$C*H*$_2$-CH_2, 2H), 2.-2.5 (br, C*H*$_2$-CH-N, 2H), 4.1-4.3 (br, CH_3(-CH_2-)$_9$$CH_2$-C*H*$_2$, 2H), 4.3-4.5 (br, CH_2-C*H*-N, 1H), 7.5-8.0 (br, C*H*=C*H*, 2H). ^{13}C NMR (CD_3OD, see Figure S5): δ 15.1 (*C*H_3-CH_2-CH_2(-CH_2-)$_7$$CH_2$-$CH_2$-), 24.9 ($CH_3$-*C*$H_2$-$CH_2$(-$CH_2$-)$_7$$CH_2$-$CH_2$-), 28.2 ($CH_3$-$CH_2$-*C*$H_2$(-$CH_2$-)$_7$$CH_2$-$CH_2$-), 31.2 ($CH_3$-$CH_2$-$CH_2$(-*C*$H_2$-)$_7$$CH_2$-$CH_2$-), 34.7 ($CH_3$(-$CH_2$-)$_9$*C*$H_2$-$CH_2$-), 44.2 (*C*$H_2$-CH-N), 54.2 ($CH_3$-$CH_2$-$CH_2$-*C*$H_2$-), 122.8-124.2 (N-*C*H=*C*H-N), 137.3 (N-*C*H-N), 162.2 (H*C*O_3).

Synthesis of $PVRImHCO_3$ via anion exchange of PVRImBr.

4 mmol of poly(*N*-vinyl-3-alkylimidazolium bromide) **6** were dissolved in dry methanol, and the resulting solution was added to a stirred solution of $KHCO_3$ (1.05 eq.), in methanol. The resulting suspension was stirred for 24h at RT. After filtration over Celite, methanol was evaporated under vacuum to yield a sticky solid. After trituration of the solid with acetone and filtration, poly(*N*-vinyl-3-alkylimidazolium hydrogen carbonate) **1** was obtained as a yellowish powder and dried under dynamic vacuum (Yield 95%). NMR data were in accordance with **1b'** (see Figure 3 and Figure 4).

Catalytic tests using PVRImHCO$_3$ salt precursors. All catalytic tests were carried out under a dry and inert atmosphere, at RT and at 80 °C, using Schlenk equipment.

Transesterification (see Scheme 6).

In a typical experiment, precursor **1** (0.5 mmol) was introduced in a Schlenk tube. The solid compound was allowed to stir for 1h under vacuum and the flask was then subjected to three Ar/vacuum cycles. A 5 mL portion of THF, 0.5 mL (5 mmol) of benzyl alcohol and 0.55 mL (6 mmol) of vinyl acetate were added. The reaction mixture was stirred for 2h at 80 °C. Note that a suspension was obtained under these conditions owing to the nonsolubility of precursor **1a-c**. After the reaction mixture was allowed cooling to RT, 1 atm of CO_2 was added, to favor the formation of poly(*N*-vinyl-3-alkylimidazolium carboxylate) **3** from the corresponding poly(NHC) **2** (see Scheme 1). After stirring for 30 min, the mixture was filtered under vacuum, and the filtrate was analyzed by ^{1}H NMR in $CDCl_3$. Conversion in benzyl acetate was calculated by ^{1}H NMR in $CDCl_3$ (Figure S8) by comparing the integral value of the −C*H*$_2$− benzyl alcohol signal (δ 4.5 ppm) to that of the −C*H*$_2$− benzyl acetate signal (δ 5 ppm). The recovered polymer was suspended in THF and reused for a next run of catalysis.

Cyanosilylation (see Scheme 7).

In a typical experiment, a Schlenk tube was charged with **1** (0.25 mmol), and the solid compound was allowed to stir for 1h under vacuum and the flask was then subjected to three Ar/vacuum cycles. A 5 mL portion of THF followed by 0.5 mL (5 mmol) of benzaldehyde and 0.75 mL of TMSCN (6 mmol) were added. The rest of the procedure was identical to that described above for the transesterification reaction. Conversion in α-trimethylsilyloxy-phenylacetonitrile was determined by ^{1}H NMR in $CDCl_3$ (Figure S9) by comparing the integral value of the aldehyde signal of benzaldehyde (δ 10 ppm) to that of the −C*H*− cyanide product (δ 5.5 ppm).

Benzoin condensation reaction (see Scheme 8).

In a typical experiment, **1** (0.5 mmol) and molecular sieves were introduced into a Schlenk tube. The solid mixture was allowed to stir for 1h under vacuum and the flask was then subjected to three Ar/vacuum cycles. A 5 mL portion of THF and then 0.5 mL (5 mmol) of benzaldehyde were added. The reaction mixture was stirred for 24h at 80 °C. The rest of the procedure was identical to that described above for the transesterification reaction. Benzoin conversion was determined by ^{1}H NMR in $CDCl_3$ (Figure S10) by comparing the integral

value of the aldehyde signal of benzaldehyde (δ 10 ppm) with that of the −C*H*− benzoin signal (δ 6 ppm).

Synthesis of poly(*N*-vinyl-3-butylimidazolium carboxylate-*co*-*N*-vinyl-3-butylimidazolium carboxylate)s by anion metathesis

Poly(*N*-vinyl-3-butylimidazolium bromide) **6** were dissolved in dry methanol, and the resulting solution was added to a stirred solution of RCOOK (2.5 eq.), in methanol. The resulting suspension was stirred at RT. After 48h, the solution was dialyzed in methanol for 1 day. Poly(*N*-vinyl-3-butylimidazolium carboxylate-*co*-*N*-vinyl-3-butylimidazolium carboxylate)s **7** was obtained as a yellowish powder after evaporation of methanol and dried under dynamic vacuum (Yield 60%). ^{1}H NMR of **7a** (adamantyl substituent) (CD_3OD, see Figure 9): δ 7.3-8.1 (br, C*H*=C*H*, 2H), 3.8-4.2 (br,N-CH_2-CH_2-CH_2-CH_3, 2H), 4.4-4.8 (br, N-C*H*-CH_2, 1H), 2.3-3.0 (br, N-CH-CH_2, 2H), 1.7-2.1 (br, CH_3-CH_2-CH_2-CH_2-, 2H; -CH_2-COO^- ; 2H; -C*H*-, 3H), 1.6-1.8 (br, -CH_2-, 12H), 1.3-1.6 (br, CH_3-CH_2-CH_2-CH_2-, 2H), 0.9-1.2 (br, CH_3-CH_2-CH_2-CH_2-, 3H). ^{1}H NMR of **13b** (decyl substituent) (CD_3OD, see Figure S15): δ 7.5-8.3 (br, C*H*=C*H*, 2H), 4.4-4.7 (br, N-C*H*-CH_2, 1H), 4.1-4.3 (br,N-CH_2-CH_2-CH_2-CH_3, 2H), , 2.3-3.0 (br, N-CH-CH_2, 2H), 2.2-2.3 (br, -CH_2-COO^-; 2H), 1.7-2.1 (br, CH_3-CH_2-CH_2-CH_2-, 2H), 1.6-1.7 (br, -CH_2-CH_2-COO^-, 2H), 1.3-1.5 (br, CH_3-CH_2-CH_2-CH_2-, 2H), 1.2-1.3 (br, -(CH_2)$_6$-CH_2-CH_2-COO^-, 12H), 0.9-1.2 (br, CH_3-CH_2-CH_2-CH_2-, 3H), 0.8-0.9 (br, CH_3-(CH_2)$_8$-COO^-, 3H).

Synthesis of polystyrene-co-poly(4-vinylbenzyl chloride) (PS-co-PVBnCl) by free radical copolymerization.

A 10 mL Schlenk tube was flame dried and charged with 1 g (9.6 mmol) of styrene, 4.4 g (28.8 mmol) of 4-vinylbenzyl chloride and 12 mL of chlorobenzene. 50 mg (0.32 mmol, 0.8 mol %) of AIBN was added to the stirred solution. The Schlenk tube was subjected to five freeze-thaw cycles and placed in a thermostated oil bath previously maintained at 80 °C. The reaction was quenched after 16h by sudden cooling with liquid nitrogen. The resulting PS-*co*-PCMS was isolated by precipitation in cold methanol. The white precipitate was filtered, washed with methanol and dried under vacuum. (Yield 75%). $\bar{M}_n$ = 30 kg.mol^{-1} ($Đ$ = 1.65) by SEC in THF (see Figure 10). The composition of the copolymer was calculated by ^{1}H NMR in $CDCl_3$ (see Figure 11). ^{1}H NMR ($CDCl_3$): δ = 6.2-7.3 (br, 11H; -C$_6$*H*$_5$, -C$_6$*H*$_4$), 4.2-4.3 (br, 2H; -CH_2-Cl), 1.3-1.8 (br, 6H; CH_2-CH-C_6H_5; CH_2-C*H*-C_6H_5; CH_2-CH-C_6H_4; CH_2-C*H*-C_6H_4).

Synthesis of polystyrene-*co*-poly(4-vinylbenzylbutylimidazolium chloride) (PS-*co*-PVBnBuImCl) 9 by quaternization.

2.5 g (14 mmol VBnCl units) Polystyrene-*co*-poly(4-vinylbenzyl chloride) and 4.34 g (2.5 equiv., 35 mmol) of *N*-butylimidazole were dissolved in dimethylformamide (DMF) (12 mL) and heated to 90 °C for 48h, during which time the solution became cloudy and yellow in color. The resulting PS-*co*-PVBnBuImCl was isolated by precipitation in cold diethyl ether. The white precipitate was filtered and stored in air. (Yield 95%). ^{1}H NMR (DMSO-d_6, see numbering of Figure 13): δ = 9.8-10.5 (br, 1H; N-C*H*-N), 7.5-8.3 (br, 2H; C*H*=C*H*), 6.2-7.3 (br, 9H; -C_6H_5, 5H; -C_6H_4), 5.1-5.5 (br, 2H; -CH_2-), 4.0-4.3 (br, 2H; N-CH_2-CH_2), 1-2.3 (br, 10H; CH_2-CH-C_6H_5; CH_2-C*H*-C_6H_5; CH_2-CH-C_6H_4; CH_2-C*H*-C_6H_4; CH_2-CH_2-CH_2; CH_2-CH_2-CH_3), 0.8-0.9 (br, 3H; CH_2-CH_2-CH_3). ^{13}C NMR (DMSO-d_6, see numbering of Figure 12): 144.0-147.1 (C_l), 136.8 (C_s), 132.8 (C_i), 127.2-130.1 ($C_{d,e,j,k,c}$), 126.2 (C_f), 122.9 (C_n), 51.8 (C_m), 49.0 (C_o), 47.1-48.2 ($C_{a,g}$), 39-41 ($C_{b,h}$), 31.8 (C_p), 19.2 (C_q), 13.7 (C_r).

Synthesis of polystyrene-*co*-poly(4-vinylbenzylbutylimidazolium hydrogen carbonate) (PS-*co*-PVBnBuImHCO$_3$) 10 *via* anion exchange.

This metathesis reaction was performed following the procedure described in the literature. 2 g (6.6 mmol VBnBuImCl units) were dissolved in 5 mL of dry methanol and the resulting solution was added to a stirred solution of $KHCO_3$ (1.05 eq.), in dry methanol. The resulting suspension was stirred for 24h at RT. After filtration, methanol was evaporated under vacuum. After trituration of the solid with acetone and filtration, PS-*co*-PVBnBuImHCO_3 was obtained as a yellowish powder, dried under dynamic vacuum at 40°C overnight and stored at air. (Yield 90%). ^{1}H NMR (CD_3OD, see Figure S14): δ = 7.2-7.6 (br, 2H; C*H*=C*H*), 6.20-7.3 (br, 9H; -C_6H_5; -C_6H_4), 5.1-5.4 (br, 2H; -CH_2-), 4-4 (br, 2H; N-CH_2-CH_2), 1-2.3 (br, 10H; CH_2-CH-C_6H_5; CH_2-C*H*-C_6H_5; CH_2-CH-C_6H_4; CH_2-C*H*-C_6H_4; CH_2-CH_2-CH_2; CH_2-CH_2-CH_3), 0.8-0.9 (br, 3H; CH_2-CH_2-CH_3). ^{13}C NMR (CD_3OD, see numbering of Figure 14): 161.3 (C_t), 144.9-147.2 (C_l), 138.1 (C_s), 133.0 (C_i), 128.2-131.1 ($C_{d,e,j,k,c}$), 127.0 (C_f), 123.6-124.0 (C_n), 53.7 (C_m), 50.7 (C_o), 48-49 ($C_{a,g}$), 41-43 ($C_{b,h}$), 33.1 (C_p), 20.5 (C_q), 13.8 (C_r).

Synthesis of propylene carbonate a using PS-*co*-PVBnBuImCl 9 as catalyst.

In a typical reaction, 76 mg (0.22 mmol VBnBuImCl units) of PS-*co*-PVBnBuImCl, 0.5 mL (7.2 mmol) of propylene oxide and 3 mL of dry THF were introduced into a stainless steel autoclave reactor. The autoclave was then transferred into a 140 °C preset oil bath. After 15 min, the autoclave was placed under 2.5 MPa of CO_2 and refilled 3 times during the 24h of reaction. Then, the autoclave was cooled to room temperature, depressurized and the resulting

mixture was dissolved in acetone before filtration to remove the catalyst. For recycling studies, the solid catalyst was washed, filtered off with acetone and dried under vacuum. Conversion was calculated by gravimetry and by ^{1}H NMR in $CDCl_3$ (see Figure S11), comparing the integral value of the -CH_3 signal of propylene oxide (δ = 1.31 ppm) with that of the -CH_3 signal of propylene carbonate (δ = 1.49 ppm).

Benzoin condensation using PS-co-PVBnBuImHCO$_3$ 10 or poly([NHC(H)][Br]-co-[NHC(H)][R'COO]) 7 as catalyst.

165 mg (0.5 mmol VBnBuImHCO$_3$ units) of PS-*co*-PVBnBuImHCO$_3$ (stored in a capped vial under air) and molecular sieves were introduced into a Schlenk tube. The powder was submitted to 30 min under vacuum and finally three Ar/vacuum cycles. THF (5 mL), previously distilled from Na/benzophenone, and then benzaldehyde (0.5 mL, 5 mmol) were added under inert atmosphere. The Schlenk tube was then transferred into a 80 °C preset oil bath. Conversion was calculated by ^{1}H NMR in $CDCl_3$ (Figure S10), comparing the integral value of the CHO signal of benzaldehyde (δ = 10 ppm) with the integral value of the α-hydroxy CH signal of benzoin (δ = 6 ppm); after 24 h, 94% conversion was obtained. The procedure were exactly similar using poly([NHC(H)][Br]-*co*-[NHC(H)][R'COO]) **7** as catalyst except the use of DMF as solvent and a lower amount of catalyst.

Copolymerization of IL monomers EVIBr and BVIPF$_6$ in presence of DVB

Targeted copolymers were designed as PDVB-*y*EVIBr and PDVB-*y*BVIPF$_6$ where *y* stands for the molar ratio of ionic liquid 1-ethyl-3-vinylimidazolium bromide (EVIBr) or ionic liquid 1-butyl-3-vinylimidazolium hexafluorophosphate (BVIPF$_6$) to DVB. In a typical synthesis of mesoporous copolymers of divinylbenzene (DVB) and EVIBr, 2.0 g of DVB was added into a solution containing 0.05 g of AIBN and 20 mL of DMF, followed by addition of 0.31 g of IL-EVIBr. After stirring at room temperature for 3h, the mixture was transferred into a Teflon autoclave and then solvothermally treated at 180 °C for 24h. After evaporation of the solvents at room temperature, the PDVB-0.1EVIBr sample with monolithic morphology was obtained. Similarly, the mesoporous copolymer of divinylbenzene (DVB) and BVIPF$_6$ was synthesized as follows. 2.0 g of DVB was added into a solution containing 0.05 g of AIBN and 20 mL of THF, followed by addition of 0.46 g of BVIPF$_6$. After stirring at room temperature for 3h, the mixture was transferred into a Teflon autoclave and then solvothermally treated at 100 °C for 24h. After evaporation of the solvents at room temperature, the PDVB-0.1BVIPF$_6$ sample in a monolithic morphology was obtained.

For comparison purpose, DVB and N-vinylimidazole (VI) were polymerized in DMF and THF according to an already reported procedure.

Synthesis of the cross-linked copoly(*N*-heterocyclic carbene) PDVB-0.1EV(NHC)

In a typical experiment, 1 g of PDVB-0.1EVIBr (0.50 mmol EVIBr units) (S_{BET} = 640 m²/g) was placed in a Schlenk tube that was previously flamed and dried under vacuum for 2h and subjected to three Ar/vacuum cycles before adding 15 mL of dry THF. The Schlenk tube was cooled at -80 °C, and 110 mg (0.55 mmol) of KHMDS previously dissolved in 55 mL of dry THF were introduced into the polymer solution. The reaction mixture was allowed to warm to room temperature and was stirred overnight. The resulting solid compound was filtered off under inert atmosphere and washed with dry THF to remove traces of residual reagents. The white solid obtained was stored under vacuum. (Yield 100%).

Catalysis experiments

Synthesis of propylene carbonate using PDVB-0.1EVIBr as crosslinked polymer-supported catalyst

In a typical reaction, 160 mg of PDVB-0.1EVIBr (0.081 mmol of EVIBr units) (S_{BET} = 640 m²/g), 0.2 mL (2.86 mmol) of propylene oxide and 3 mL of THF were introduced into a stainless steel autoclave reactor. The autoclave was transferred into a 140 °C preset oil bath. After 15 min, the autoclave was placed under 2.5 MPa of CO_2 and refilled 3 times during the reaction. After 24h of reaction and cooling down at room temperature, the mixture was filtered and the polymer-supported catalyst was washed with acetone, while the solution was concentrated under vacuum. Conversion was calculated by gravimetric analysis and by ^{1}H NMR in $CDCl_3$ by comparing the integral value of the -C*H*$_3$ signal of propylene oxide (δ = 1.31 ppm) with the integral of the -C*H*$_3$ signal of propylene carbonate (δ = 1.49 ppm) from an aliquot withdrawn before the filtration (see Figure S11).

Benzoin condensation using PDVB-0.1EV(NHC) as catalyst

In a typical reaction, 100 mg of cross-linked PDVB-0.1EV(NHC) (0.05 mmol NHC units) (stored under inert atmosphere) was introduced into a Schlenk tube. The powder was submitted to 30 min under vacuum and finally three Ar/vacuum cycles. THF (5 mL), previously distilled from Na/benzophenone, and then benzaldehyde (0.5 mL, 5 mmol) were added under inert atmosphere. The Schlenk tube was then transferred into a 60 °C preset oil bath. After stirring for 24h, the suspension, due to the non-solubility of the cross-linked catalyst, was filtered off under vacuum, and the filtrate was analyzed by ^{1}H NMR in $CDCl_3$ to obtain the conversion. Conversion was calculated (Figure S10), comparing the integral value

of the aldehyde signal of benzaldehyde (δ = 10 ppm) with the integral value of the α-hydroxy C*H* signal of benzoin (δ = 6 ppm). The recovered cross-linked copoly(NHC)s was washed with dry THF and suspended in THF and reused for a next run of catalysis.

Cyanosilylation using PDVB-0.1EV(NHC) as catalyst

In a typical reaction, 50 mg (0.025 mmol NHC units) of cross-linked PDVB-0.1EV(NHC) (stored under inert atmosphere) was introduced into a Schlenk tube. The powder was submitted to 30 min under vacuum and finally three Ar/vacuum cycles. THF (5 mL), previously distilled from Na/benzophenone, and then benzaldehyde (0.5 mL, 5 mmol) and TMSCN (0.75 mL, 6 mmol) were added under inert atmosphere. The Schlenk tube was then transferred into a 60 °C preset oil bath. After stirring for 1h, the suspension, due to the non-solubility of the cross-linked catalyst, was filtered off under vacuum, and the filtrate was analyzed by ^{1}H NMR in $CDCl_3$ to obtain the conversion. Conversion was calculated (Figure S9), comparing the integral value of the aldehyde signal of benzaldehyde (δ = 10 ppm) with the integral value of the -C*H*- signal of cyanide (δ = 5.5 ppm). The recovered cross-linked copoly(NHC)s was washed with dry THF and suspended in THF and reused for a next run of catalysis.

Synthesis of PS-co-poly(NHC-Ag) complex 13

100 mg (0.33 mmol VBnBuImCl units) of PS-*co*-PVBnBuImCl and 76.5 mg (0.33 mmol) of Ag_2O were introduced in a dried and flamed Schlenk tube. Powders were submitted to 30 min under vacuum and finally three Ar/vacuum cycles. Dry methylene chloride (5 mL) was added under Argon and the Schlenk tube transferred into an oil bath at 40°C for 24h under stirring. The solution was filtered to remove residuals Ag_2O and AgCl. These salts were further extracted with hot methylene chloride and volatiles were removed under vacuum. The resulting brown powder was dried and stored under vacuum (Yield 80%). ^{1}H NMR (DMSO-d_6): δ = 7.2-7.6 (br, 2H, C*H*=C*H*), 6.2-7.3 (br, 9H; -C_6H_5; -C_6H_4), 5.1-5.4 (br, 2H; -CH_2-), 3.9-4.2 (br, 2H; N-CH_2-CH_2), 1-1.95 (br, 10H; CH_2-CH-C_6H_5; CH_2-C*H*-C_6H_5; CH_2-CH-C_6H_4; CH_2-C*H*-C_6H_4; CH_2-C*H*$_2$-CH_2; CH_2-C*H*$_2$-CH_3), 0.75-0.95 (br, 3H; CH_2-CH_2-C*H*$_3$). ^{13}C NMR (DMSO-d_6, see numbering of Figure 23): 178.9 (C_s), 145.2 (C_l), 134.7 (C_i), 124.7-127.9 ($C_{d,e,j,k,c}$), 123.2 (C_f), 121.6-122.6 (C_n), 55.4 (C_m), 54.3 ($C_{a,g}$), 51.2 (C_o), 41.3-43.8 ($C_{b,h}$), 33.6 (C_p), 19.4 (C_q), 13.8 (C_r).

Synthesis of PS-*co*-Poly(NHC-CS_2) adduct 14

50 mg (0.15 mmol $VBnBuImHCO_3$ units) of PS-*co*-$PVBnBuImHCO_3$ (stored in a capped vial under air) and molecular sieves were introduced into a Schlenk tube. Dry methanol (5 mL) and 137 mg (12 equiv., 1.8 mmol) of carbon disulfide (CS_2) were added under inert atmosphere. The Schlenk tube was then transferred into a 50 °C preset oil bath. The solution was stirred for 24h. After removal the volatile under vacuum, the resulting yellowish solid was washed. After being dried at 40 °C for 24h, **14** was obtained as a yellowish powder. (yield 92%). ^{1}H NMR (DMSO-d_6): δ = 7.5-7.8 (br, 2H; C*H*=C*H*), 6.0-7.7 (br, 9H; -C_6H_5; -C_6H_4), 5.2-5.8 (br, 2H; -CH_2-), 4.0-4.3 (br, 2H; N-CH_2-CH_2), 1.0-2.0 (br, 10H; CH_2-CH-C_6H_5; CH_2-C*H*-C_6H_5; CH_2-CH-C_6H_4; CH_2-C*H*-C_6H_4; CH_2-CH_2-CH_2; CH_2-CH_2-CH_3), 0.8-1.0 (br, 3H; CH_2-CH_2-CH_3). ^{13}C NMR (DMSO-d_6, see numbering of Figure 24): 231.0 (C_t), 145.2 (C_l), 137.9 (C_s), 132.6 (C_i), 126.8-131.5 ($C_{d,e,j,k,c}$), 126.2 (C_f), 122.7-123.2 (C_n), 49.1 (C_m), 47.2 ($C_{a,g}$), 42.6 (C_o), 37-39 ($C_{b,h}$), 30.1 (C_p), 20.2 (C_r), 13.7 (C_r).

Synthesis of PS-co-poly(NHC-RNCS) 15

70 mg (0.21 mmol $VBnBuImHCO_3$ units) of PS-*co*-$PVBnBuImHCO_3$ (stored in a capped vial under air) and molecular sieves were introduced into a Schlenk tube. Compounds were submitted to 30 min under vacuum and finally three Ar/vacuum cycles. Dry MeOH (5 mL) was added under inert atmosphere. Then, 143 mg (2.5 equiv., 0.53 mmol) of 3,5-(bistrifluoromethyl)phenyl isothiocyanate (R-NCS) was added and the Schlenk tube was transferred into a 60 °C preset oil bath. The solution was stirred for 24h and then poured in toluene and washed twice before filtration. A yellow-white powder was removed and dried under vacuum. (Yield 72%). ^{1}H NMR (DMSO-d_6): δ = 7.5-7.8 (br, 3H; C*H*=C*H*; $C_2(CF_3)CH$), 6.0-7.7 (br, 11H; -C_6H_5; -C_6H_4-; -C_6H_3-), 5.2-5.8 (br, 2H; -CH_2-), 4.0-4.3 (br, 2H; N-CH_2-CH_2), 1.0-2.0 (br, 10H; CH_2-CH-C_6H_5; CH_2-C*H*-C_6H_5; CH_2-CH-C_6H_4; CH_2-C*H*-C_6H_4; CH_2-CH_2-CH_2; CH_2-CH_2-CH_3), 0.8-1.0 (br, 3H; CH_2-CH_2-CH_3). ^{13}C NMR (DMSO-d_6, see numbering of Figure 26): 181.8 (C_t), 156.1 (C_s), 145.0 (C_u), 138.1 (C_i), 116.1-130.0 ($C_{c,d,e,f,j,k,n,v,w,x,y}$), 53.8 ($C_m$), 52.0 ($C_{a,g}$), 49.1 ($C_o$), 37.0-39.3 ($C_{b,h}$), 32.6 ($C_p$), 19.3 ($C_q$), 13.7 ($C_r$).

Synthesis of PS-*co*-poly(NHC-Pd(II)) complex 16

160 mg (0.48 mmol $VBnBuImHCO_3$ units) of PS-*co*-$PVBnBuImHCO_3$ (stored in a capped vial under air), 105 mg (0.6 equiv., 0.29 mmol) of palladium allyl chloride dimer

$[Pd(Allyl)Cl]_2$ and molecular sieves were introduced into a Schlenk tube. Compounds were submitted to 30 min under vacuum and finally three Ar/vacuum cycles. Dry CH_2Cl_2 (5 mL) was added under inert atmosphere and the Schlenk tube was then transferred into a 40 °C preset oil bath. The solution was stirred for 24h and then poured in diethyl ether to precipitate **16** as a grey powder. (Yield 81%) ^{1}H NMR (CD_2Cl_2): δ = 7.5-7.8 (br, 2H; C*H*=C*H*), 6.0-7.7 (br, 9H; -C_6H_5;-C_6H_4-), 5.2-5.8 (br, 3H; -CH_2-; CH_{allyl}), 4.0-4.2 (br, 2H; N-CH_2-CH_2), 2.9-3.2 (br, 4H, C$H_{2,\ allyl}$), 1.0-2.0 (br, 10H; CH_2-CH-C_6H_5; CH_2-C*H*-C_6H_5; CH_2-CH-C_6H_4; CH_2-C*H*-C_6H_4; CH_2-CH_2-CH_2; CH_2-CH_2-CH_3), 0.8-1.0 (br, 3H; CH_2-CH_2-CH_3). ^{13}C NMR (CD_2Cl_2, see numbering of Figure 27): 178.0 (C_s), 143.9 (C_l), 133.4 (C_i), 125.9-130.2 ($C_{d,r,j,k,c}$), 124.7 (C_f), 121.5-123.3 (C_n), 114.8 (C_t), 71.6 (C_t), 53.0 (C_m), 49.8 (C_o), 49.0 ($C_{a,g}$), 48.5 (C_t), 37-39 ($C_{b,h}$), 32.2 (C_p), 18.3 (C_p), 13.0 (C_r).

Synthesis of PS-co-poly(NHC-AuCl) complex 17

100 mg (0.30 mmol VBnBuImHCO$_3$ units) of PS-*co*-PVBnBuImHCO$_3$ (stored in a capped vial under air), 175 mg (2 equiv, 0.60 mmol) of chloro(dimethylsulfide)gold(I) Au(SMe$_2$)Cl and molecular sieves were introduced into a Schlenk tube. Compounds were submitted to 30 min under vacuum and finally three Ar/vacuum cycles. Dry DMF (5 mL) was added under inert atmosphere and the Schlenk tube was then transferred into a 50 °C preset oil bath. The solution was stirred for 24h and then filtered. A yellow powder was obtained and dried under vacuum for 24h at 40 °C. (Yield 87%) ^{1}H NMR (DMSO-d_6): δ = 7.5-7.8 (br, 2H; C*H*=C*H*), 6-7.7 (br, 9H; -C_6H_5;-C_6H_4), 5.2-5.8 (br, 2H; -CH_2-), 4.0-4.3 (br, 2H; N-CH_2-CH_2), 1.0-2.0 (br, 10H; CH_2-CH-C_6H_5; CH_2-C*H*-C_6H_5; CH_2-CH-C_6H_4; CH_2-C*H*-C_6H_4; CH_2-CH_2-CH_2; CH_2-CH_2-CH_3), 0.8-1.0 (br, 3H; CH_2-CH_2-CH_3). ^{13}C NMR (DMSO-d_6, see numbering of Figure 28): 178.0 (C_s), 143.9 (C_l), 133.4 (C_i), 126-130 ($C_{d,e,j,k,c}$), 124.7 (C_f), 121-123 (C_n), 53.0 (C_m), 49.8 (C_o), 49.0 ($C_{a,g}$), 37-39 ($C_{b,h}$), 32.2 (C_p), 18.3 (C_q), 13.0 (C_r).

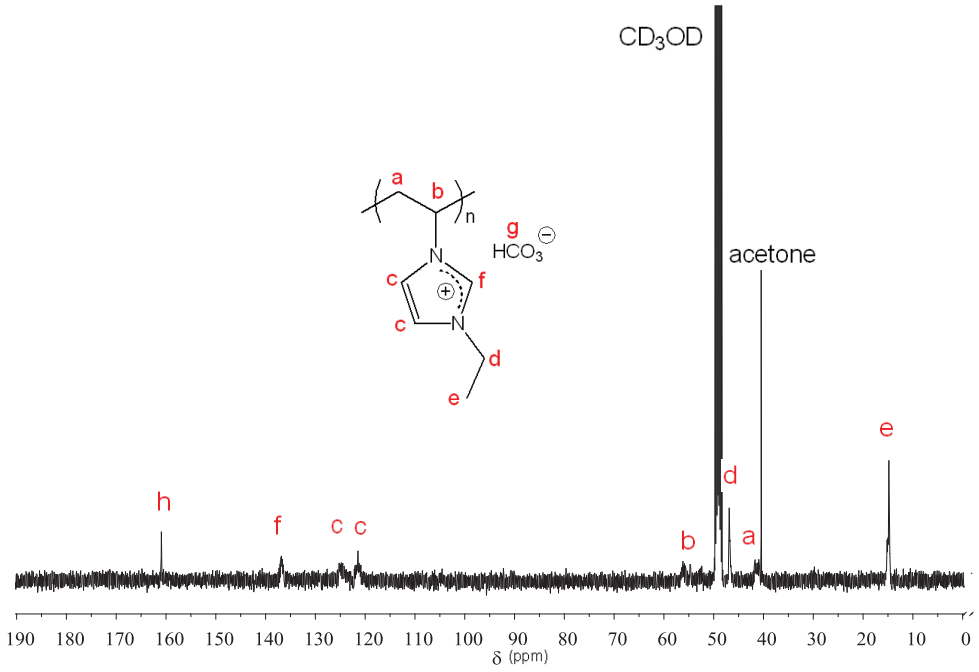

Figure S1. ^{13}C NMR spectrum of poly(*N*-vinyl-3-ethylimidazolium hydrogen carbonate) **1a** in CD_3OD.

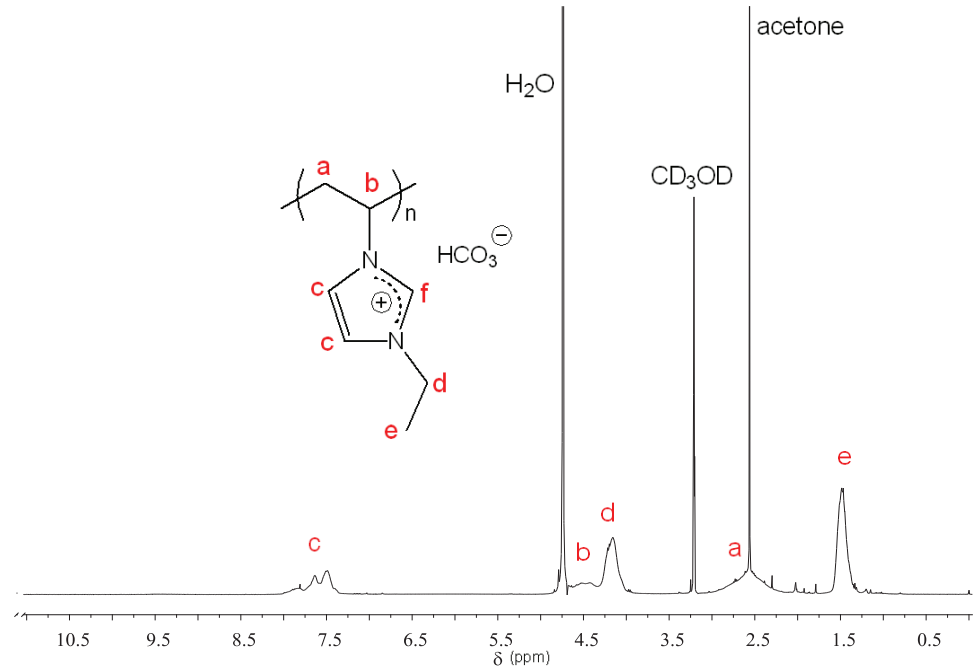

Figure S2. ^{1}H NMR spectrum of poly(*N*-vinyl-3-ethylimidazolium hydrogen carbonate) **1a** in CD_3OD.

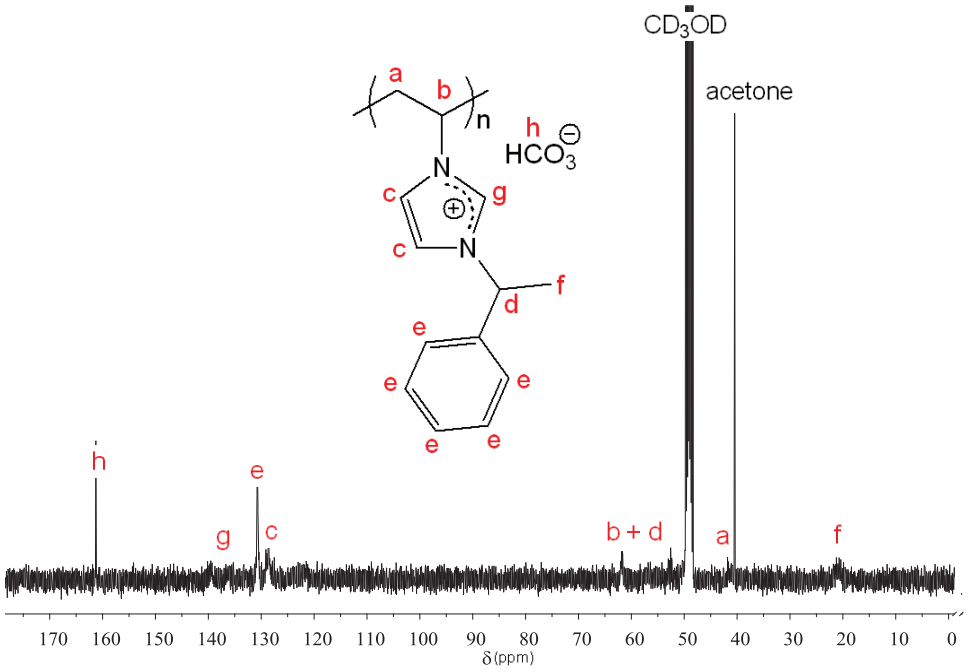

Figure S3. ^{13}C NMR spectrum of poly(*N*-vinyl-3-ethylphenylimidazolium hydrogen carbonate) salt **1c** in CD_3OD.

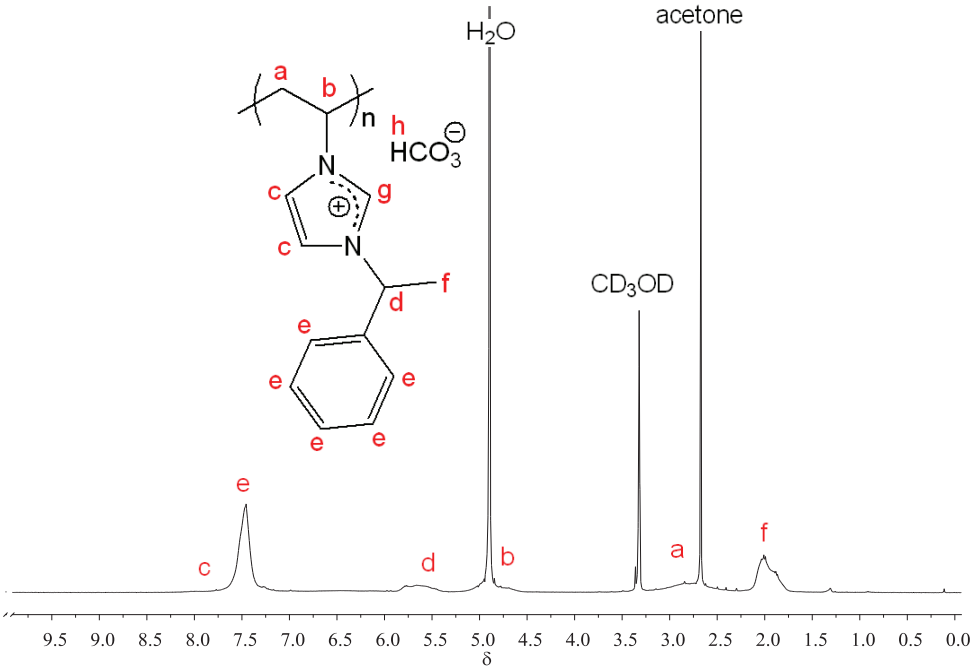

Figure S4. ^{1}H NMR spectrum of poly(*N*-vinyl-3-ethylphenylimidazolium hydrogen carbonate) salt **1c** in CD_3OD.

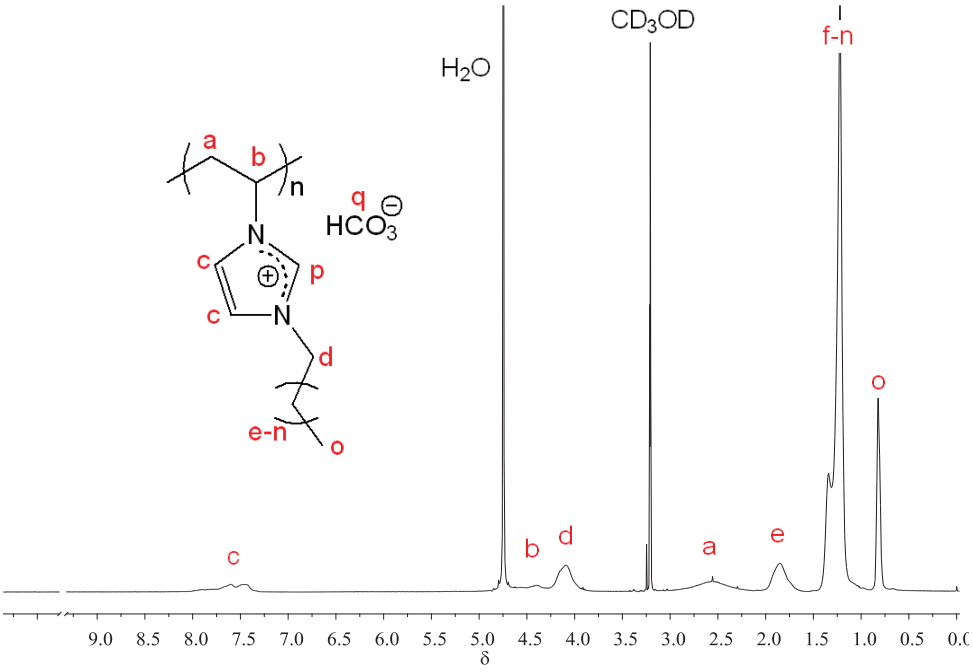

Figure S5. ^{13}C NMR spectrum of poly(*N*-vinyl-3-dodecylimidazolium hydrogen carbonate) salt **1d** in CD_3OD.

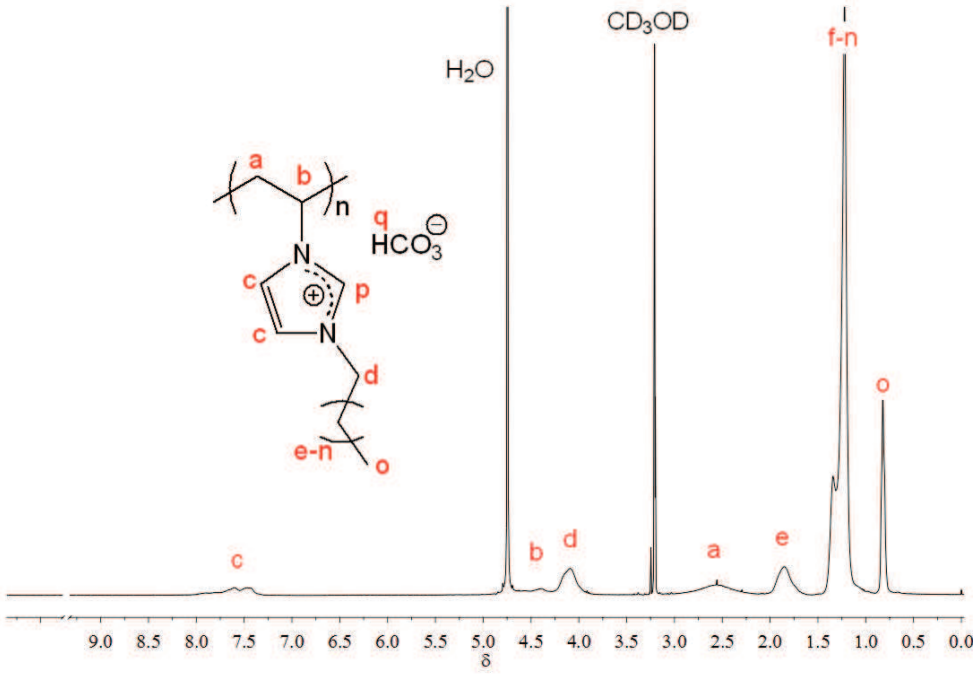

Figure S6. ^{1}H NMR spectrum of poly(*N*-vinyl-3-dodecylimidazolium hydrogen carbonate) salt **1d** in CD_3OD.

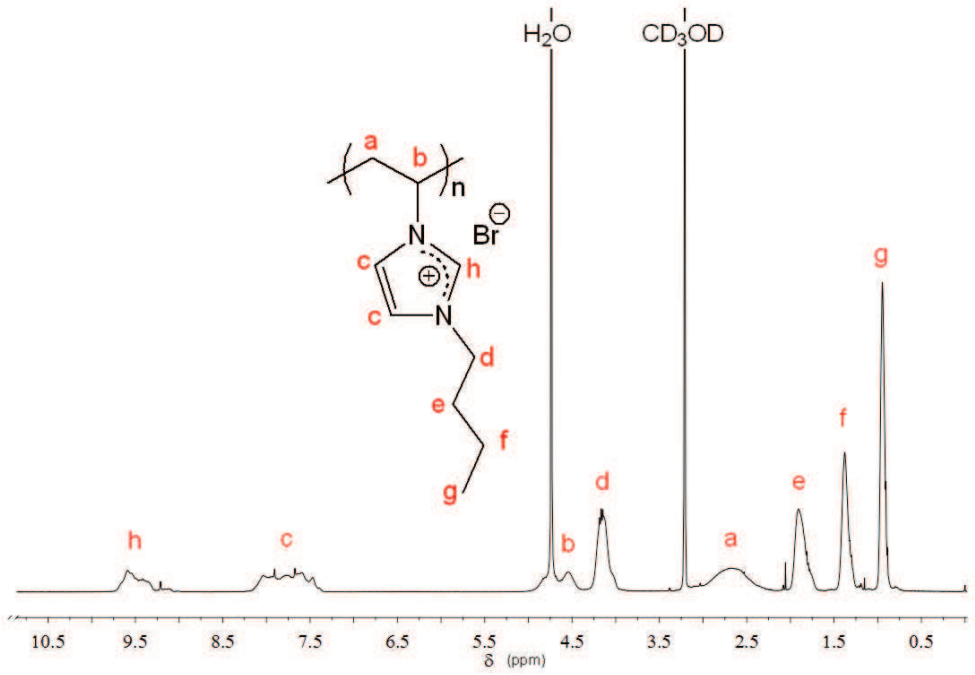

Figure S7. ^{1}H NMR spectrum of poly(*N*-vinyl-3-butylimidazolium bromide) **6b** in CD_3OD.

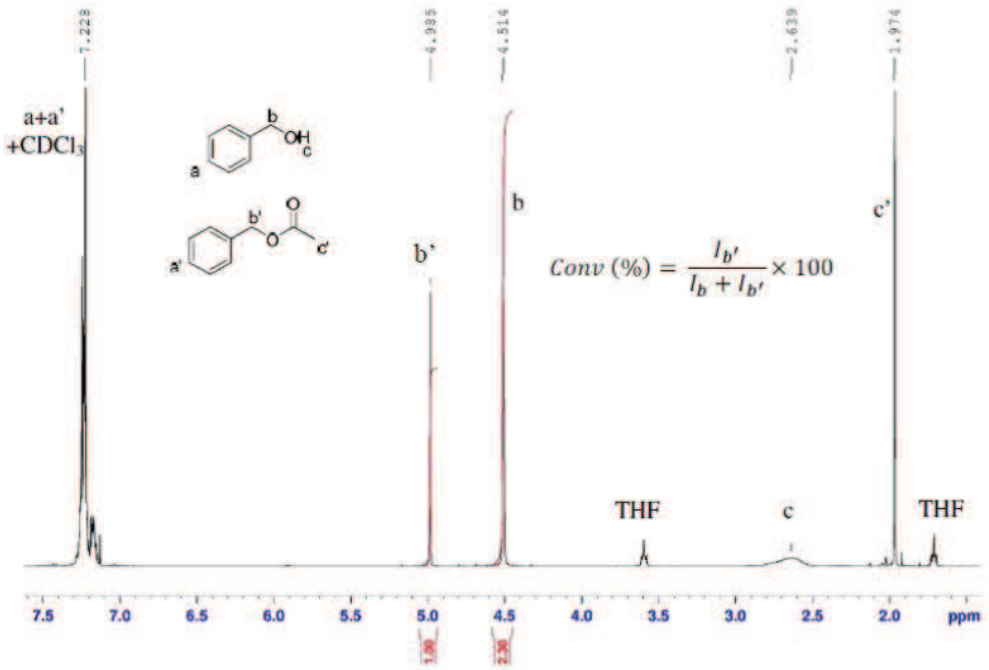

Figure S8. ^{1}H NMR spectrum in $CDCl_3$ to determine the conversion during the transesterification reaction between benzyl alcohol and vinyl acetate in THF.

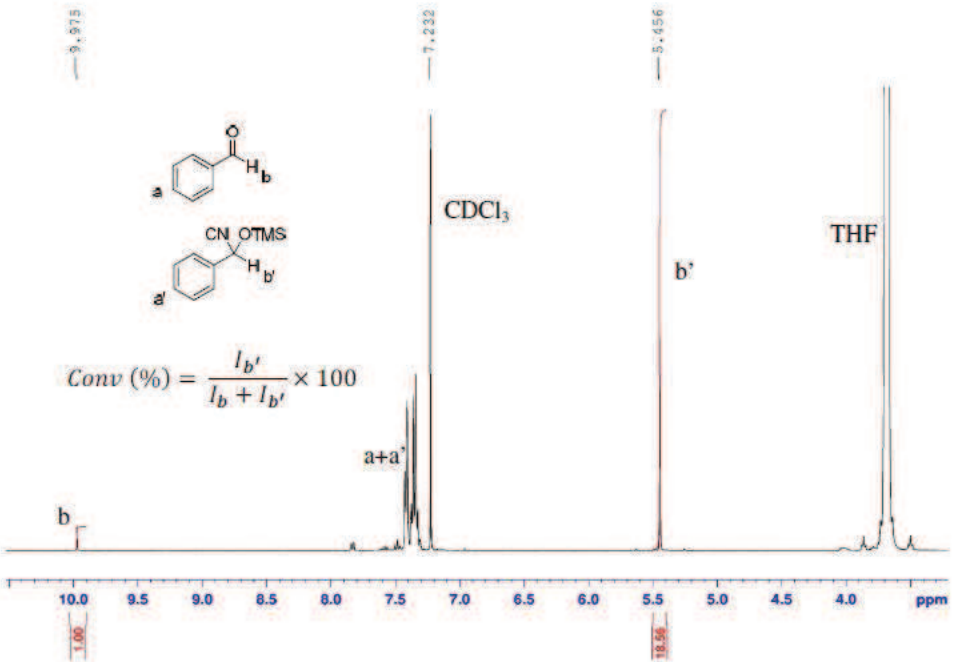

Figure S9. ^{1}H NMR spectrum in $CDCl_3$ to determine the conversion during cyanosilylation reaction of benzaldehyde in THF.

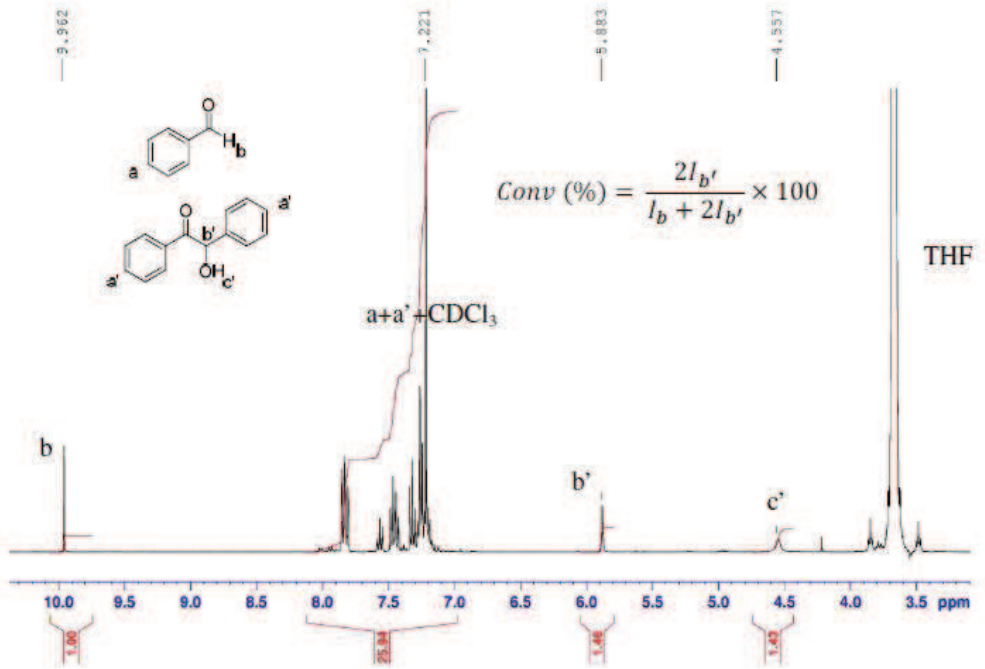

Figure S10. ^{1}H NMR spectrum in $CDCl_3$ to determine the conversion during the benzoin condensation reaction in THF.

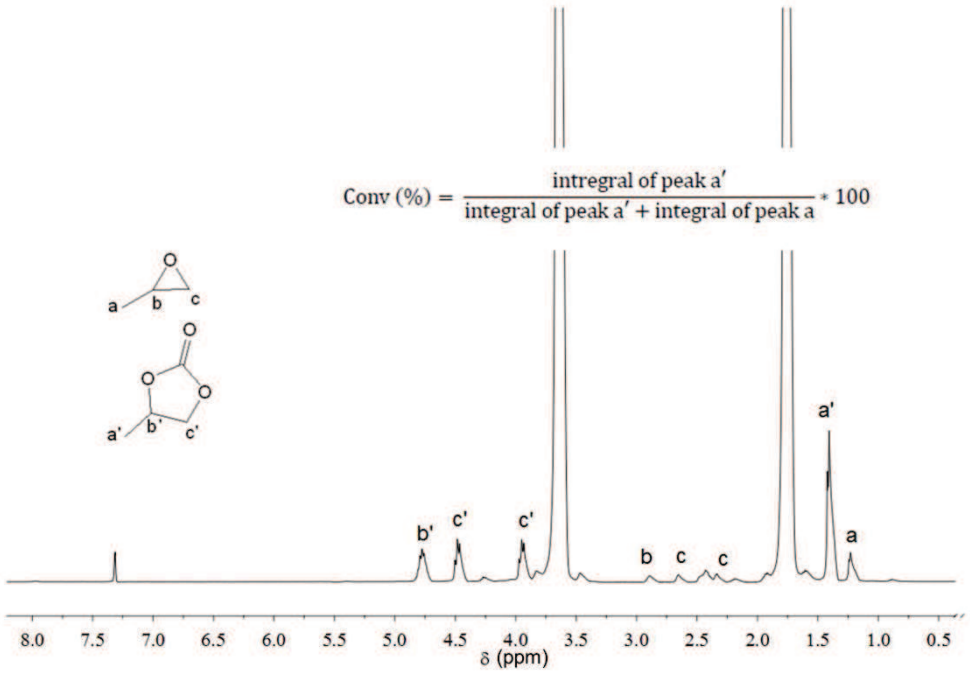

Figure S11. ^{1}H NMR spectrum in $CDCl_3$ and equation used to determine the conversion during the carbonatation reaction in THF.

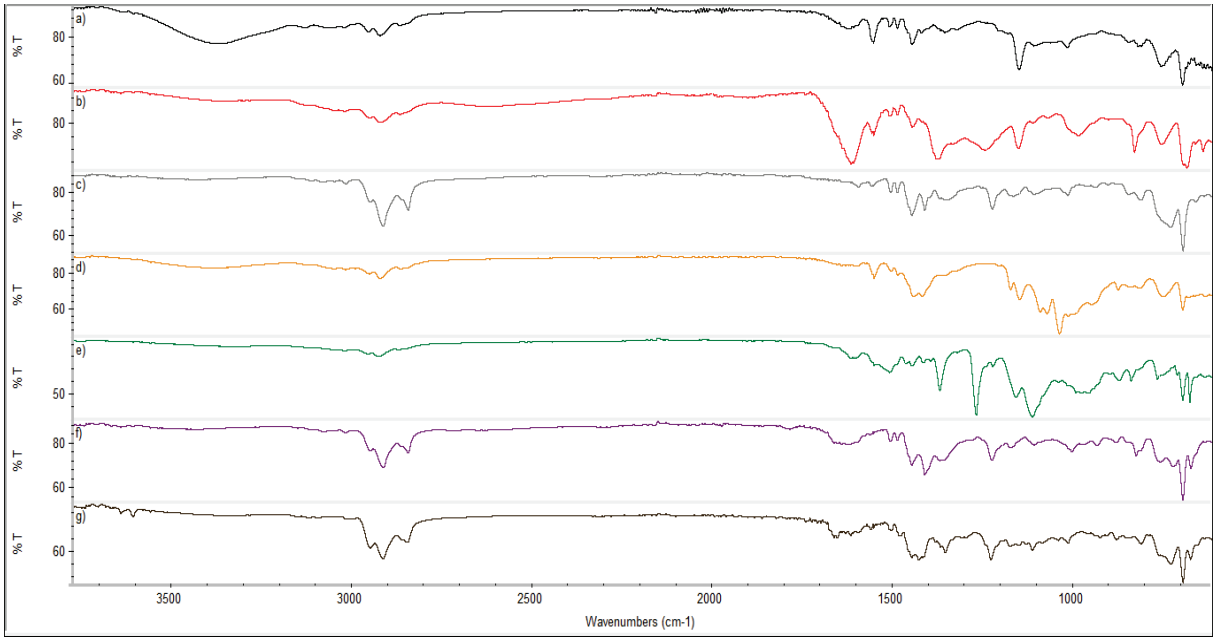

Figure S12. IR spectra of a) PS-*co*-PVBnBuImCl **9**, b) PS-*co*-PVBnBuImHCO_3 **10**, c) PS-*co*-poly(NHC-Ag(I)) complex **13**, d) PS-co-poly(NHC-CS_2) **14**, e) PS-co-poly(NHC-RNCS) **15**, f) PS-co-poly(NHC-Pd(allyl)Cl) **16** and g) PS-co-poly(NHC-AuCl) **17**.

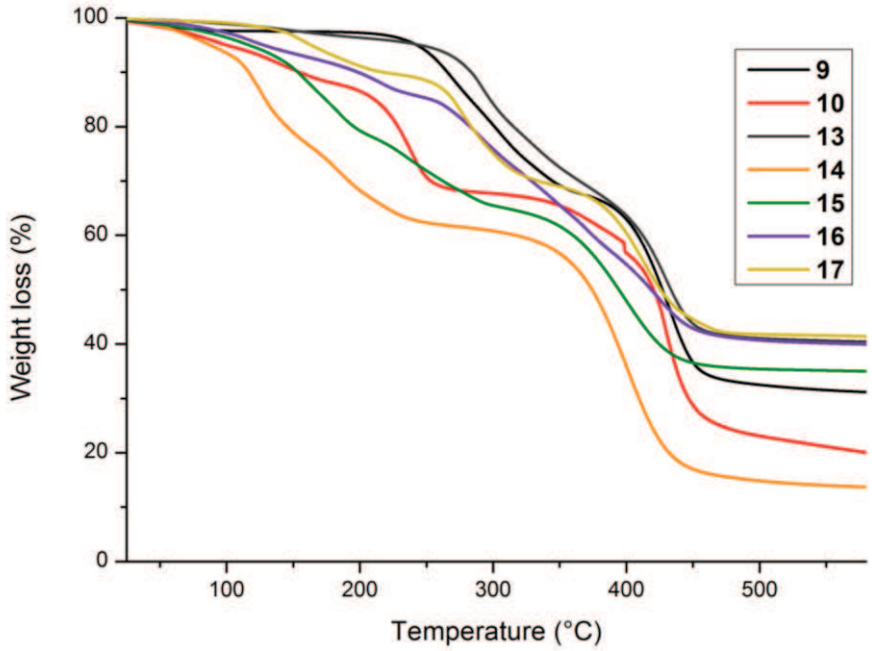

Figure S13. TGA curves of the thermal degradation of PS-*co*-PVBnBuImCl **9** (black), PS-*co*-PVBnBuImHCO$_3$ **10** (red), PS-*co*-poly(NHC-Ag(I)) complex **13** (grey), PS-co-poly(NHC-CS$_2$) **14** (orange), PS-co-poly(NHC-RNCS) **15** (green), PS-co-poly(NHC-Pd(allyl)Cl) **16** (violet) and g) PS-co-poly(NHC-AuCl) **17** (dark yellow).

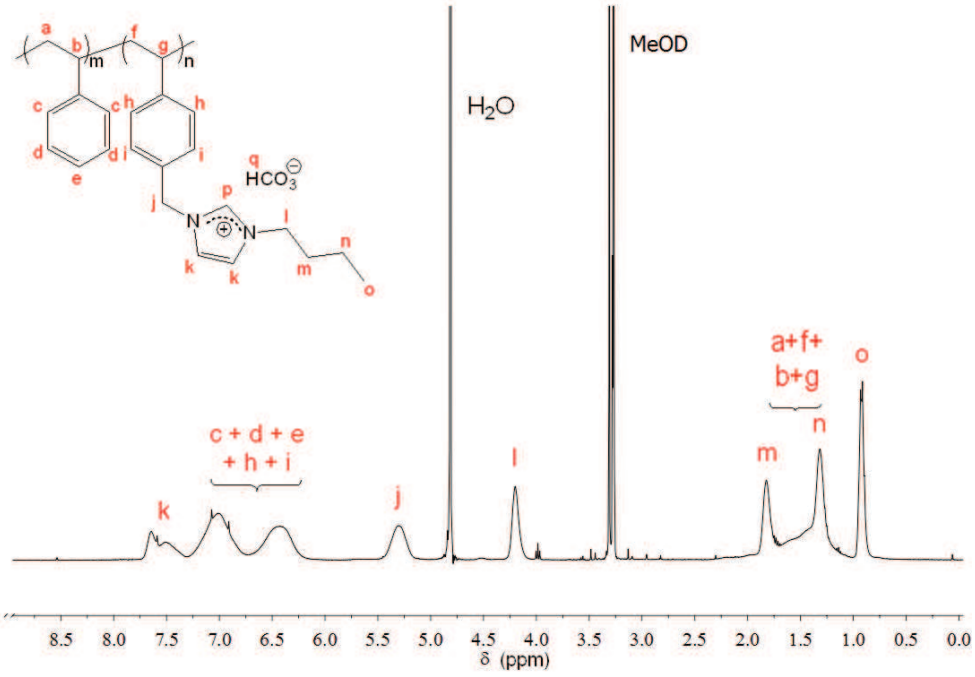

Figure S14. ^{1}H NMR spectrum of the PS-*co*-PVBnBuImHCO$_3$ **10** in MeOD.

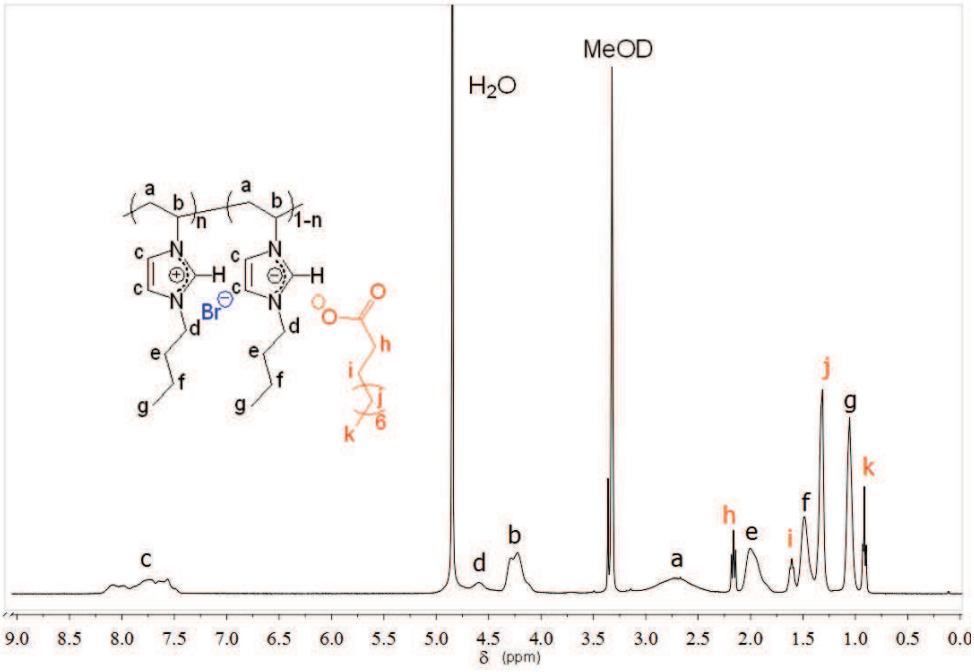

Figure S15. [1]H NMR spectrum of the poly([NHC(H)][Br]-*co*-[NHC(H)][decylCOO]) **7b** in MeOD.

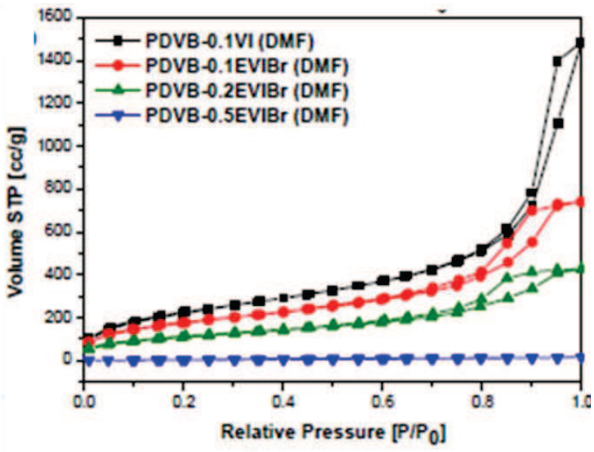

Figure S16. Nitrogen adsorption/desorption isotherms of PDVB-0.1EVIBr (red circle).

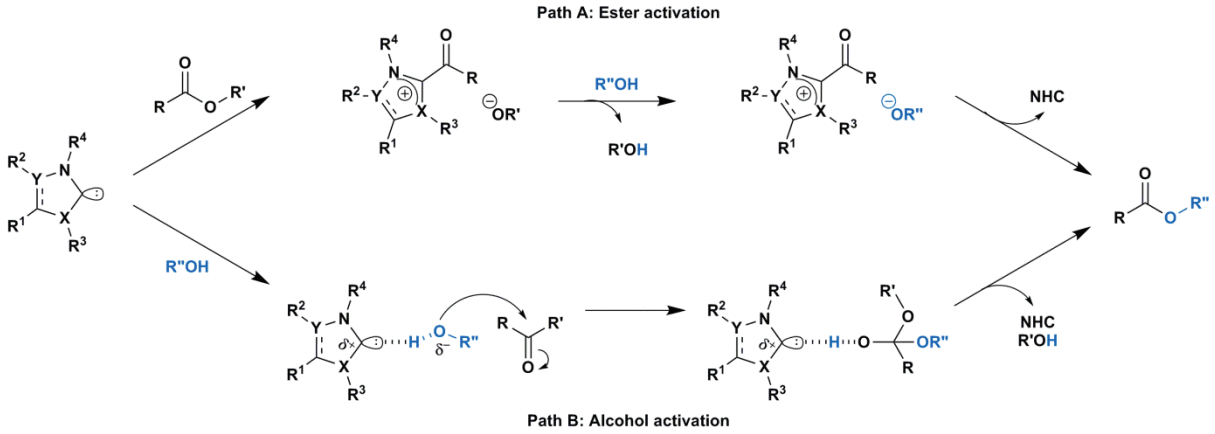

Scheme S1. Mechanism of the NHC-catalyzed transesterification reaction (ester *vs*. alcohol activation).

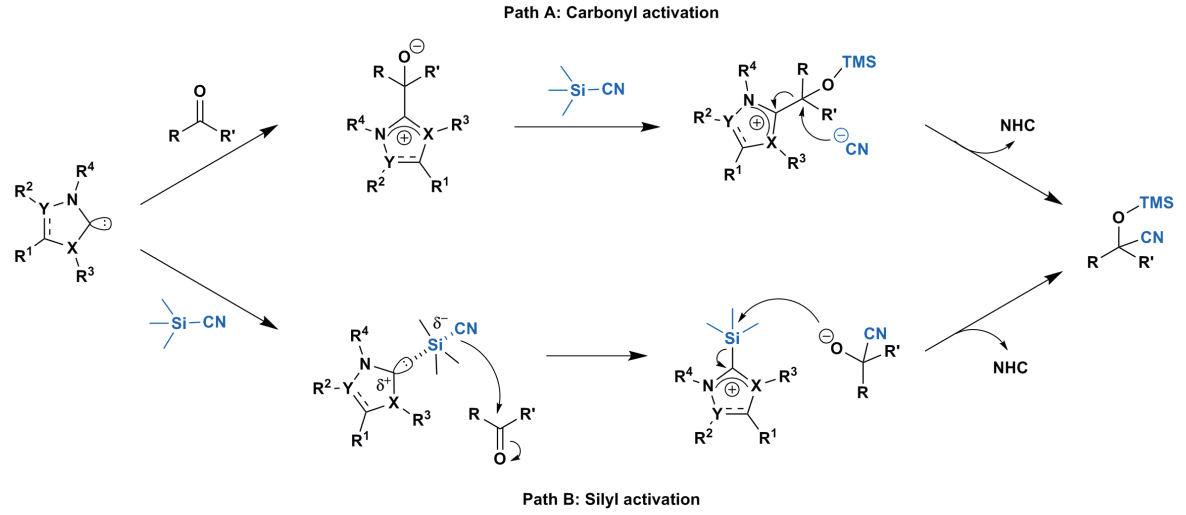

Scheme S2. Mechanism of the NHC-catalyzed cyanosilylation reaction (carbonyl *vs*. silyl activation).

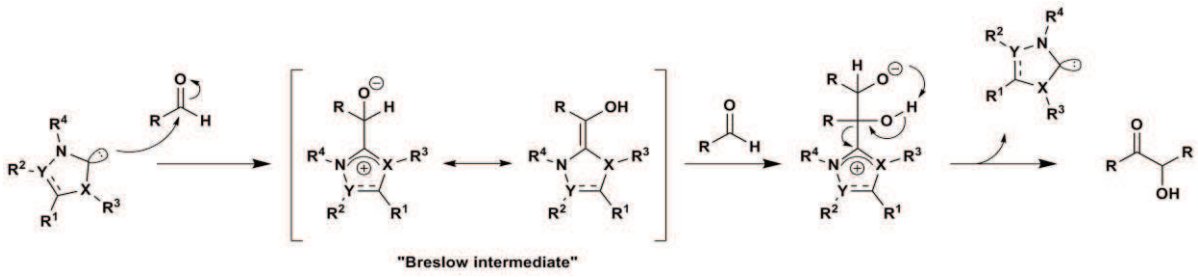

Scheme S3. Mechanism of the NHC-catalyzed benzoin condensation reaction.

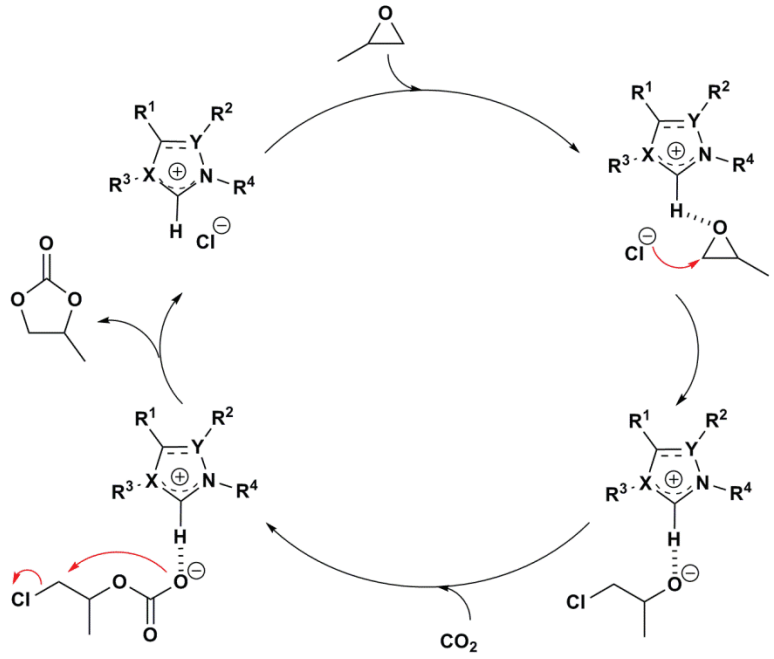

Scheme S4. Mechanism of the cycloaddition reaction between propylene oxide and carbon dioxide.

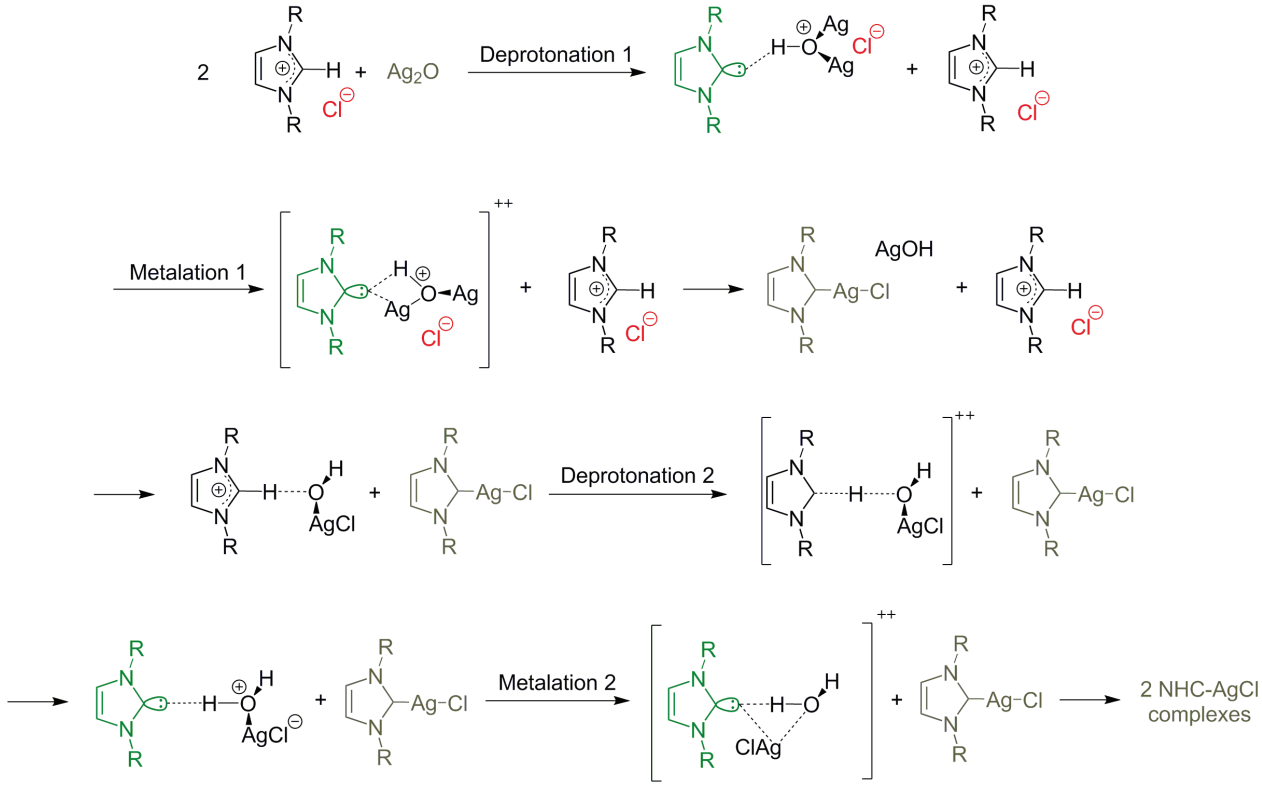

Scheme S5. Mechanism for formation of two silver NHC products upon treating imidazolium chloride with Ag_2O.[132]

References

1. Yuan, J.; Mecerreyes, D.; Antonietti, M. *Prog. Polym. Sci.* **2013**, *38*, 1009–1036.
2. Mecerreyes, D. *Prog. Polym. Sci.* **2011**, *36*, 1629–1648.
3. Lu, J.; Yan, F.; Texter, J. *Prog. Polym. Sci.* **2009**, *34*, 431–448.
4. Green, M. D.; Long, T. E. *Polym Rev* **2009**, *49*, 291–314.
5. Anderson, E. B.; Long, T. E. *Polymer* **2010**, *51*, 2447–2454.
6. Yuan, J.; Antonietti, M. *Polymer* **2011**, *52*, 1469–1482.
7. Hallett, J. P.; Welton, T. *Chem. Rev.* **2011**, *111*, 3508–3576.
8. De María, P. *Angew. Chemie Int. Ed.* **2008**, *47*, 6960–6968.
9. Myles, L.; Gore, R. G.; Gathergood, N.; Connon, S. J. *Green Chem.* **2013**, *15*, 2740–2746.
10. Ghazali-Esfahani, S.; Song, H.; Paunescu, E.; Bobbink, F. D.; Liu, H.; Fei, Z.; Laurenczy, G.; Bagherzadeh, M.; Yan, N.; Dyson, P. J. *Green Chem.* **2013**, *15*, 1584–1589.
11. Xiong, Y.; Wang, Y.; Wang, H.; Wang, R.; Cui, Z. *J. Appl. Polym. Sci.* **2012**, *123*, 1486–1493.
12. Fèvre, M.; Pinaud, J.; Leteneur, A.; Gnanou, Y.; Vignolle, J.; Taton, D.; Miqueu, K.; Sotiropoulos, J.-M. *J. Am. Chem. Soc.* **2012**, *134*, 6776–6784.
13. Fèvre, M.; Coupillaud, P.; Miqueu, K.; Sotiropoulos, J.-M.; Vignolle, J.; Taton, D. *J. Org. Chem.* **2012**, *77*, 10135–10144.
14. Fevre, M.; Vignolle, J.; Taton, D. *Polym. Chem.* **2013**, *4*, 1995–2003.
15. Benhamou, L.; Chardon, E.; Lavigne, G.; Bellemin-Laponnaz, S.; César, V. *Chem. Rev.* **2011**, *111*, 2705–2733.
16. Bourissou, D.; Guerret, O.; Gabbaï, F. P.; Bertrand, G. *Chem. Rev.* **1999**, *100*, 39–92.
17. Powell, A. B.; Suzuki, Y.; Ueda, M.; Bielawski, C. W.; Cowley, A. H. *J. Am. Chem. Soc.* **2011**, *133*, 5218–5220.
18. Hock, S. J.; Schaper, L.-A.; Herrmann, W. A.; Kuhn, F. E. *Chem. Soc. Rev.* **2013**, *42*, 5073–5089.
19. Crabtree, R. H. *Coord. Chem. Rev.* **2007**, *251*, 595.
20. Díez-González, S.; Marion, N.; Nolan, S. P. *Chem. Rev.* **2009**, *109*, 3612–3676.
21. Marion, N.; Díez-González, S.; Nolan, S. P. *Angew. Chemie Int. Ed.* **2007**, *46*, 2988–3000.
22. Enders, D.; Niemeier, O.; Henseler, A. *Chem. Rev.* **2007**, *107*, 5606–5655.
23. Moore, J.; Rovis, T. In *Asymmetric Organocatalysis SE - 18*; List, B., Ed.; Topics in Current Chemistry; Springer Berlin / Heidelberg, **2009**; Vol. 291, pp. 118–144.
24. Kiesewetter, M. K.; Shin, E. J.; Hedrick, J. L.; Waymouth, R. M. *Macromolecules* **2010**, *43*, 2093–2107.
25. Fèvre, M.; Vignolle, J.; Gnanou, Y.; Taton, D. In *Polymer Science: A Comprehensive Reference*; Editors-in-Chief:; Matyjaszewski, K.; Möller, M., Eds.; Elsevier: Amsterdam, **2012**; pp. 67–115.
26. Fevre, M.; Pinaud, J.; Gnanou, Y.; Vignolle, J.; Taton, D. *Chem. Soc. Rev.* **2013**, *42*, 2142–2172.
27. Glorius, F. In *N-Heterocyclic Carbenes in Transition Metal Catalysis SE - 1*; Topics in Organometallic Chemistry; Springer Berlin / Heidelberg, **2007**; Vol. 21, pp. 1–20.
28. Dröge, T.; Glorius, F. *Angew. Chemie Int. Ed.* **2010**, *49*, 6940–6952.
29. De Frémont, P.; Marion, N.; Nolan, S. P. *Coord. Chem. Rev.* **2009**, *253*, 862–892.
30. Denk, M. K.; Rodezno, J. M.; Gupta, S.; Lough, A. J. *J. Organomet. Chem.* **2001**, *617-618*, 242–253.
31. Hollóczki, O.; Terleczky, P.; Szieberth, D.; Mourgas, G.; Gudat, D.; Nyulászi, L. *J. Am. Chem. Soc.* **2010**, *133*, 780–789.

32. Wang, H. M. J.; Lin, I. J. B. *Organometallics* **1998**, *17*, 972–975.
33. Lin, J. C. Y.; Huang, R. T. W.; Lee, C. S.; Bhattacharyya, A.; Hwang, W. S.; Lin, I. J. B. *Chem. Rev.* **2009**, *109*, 3561–3598.
34. Coulembier, O.; Lohmeijer, B. G. G.; Dove, A. P.; Pratt, R. C.; Mespouille, L.; Culkin, D. A.; Benight, S. J.; Dubois, P.; Waymouth, R. M.; Hedrick, J. L. *Macromolecules* **2006**, *39*, 5617–5628.
35. Nyce, G. W.; Csihony, S.; Waymouth, R. M.; Hedrick, J. L. *Chem. – A Eur. J.* **2004**, *10*, 4073–4079.
36. Coulembier, O.; Delva, X.; Hedrick, J. L.; Waymouth, R. M.; Dubois, P. *Macromolecules* **2007**, *40*, 8560–8567.
37. Coulembier, O.; Moins, S.; Dubois, P. *Macromolecules* **2011**, *44*, 7493–7498.
38. Delaude, L. *Eur. J. Inorg. Chem.* **2009**, *2009*, 1681–1699.
39. Delaude, L.; Demonceau, A.; Wouters, J. *Eur. J. Inorg. Chem.* **2009**, *2009*, 1882–1891.
40. Van Ausdall, B. R.; Glass, J. L.; Wiggins, K. M.; Aarif, A. M.; Louie, J. *J. Org. Chem.* **2009**, *74*, 7935–7942.
41. Bridges, N. J.; Hines, C. C.; Smiglak, M.; Rogers, R. D. *Chem. – A Eur. J.* **2007**, *13*, 5207–5212.
42. Voutchkova, A. M.; Appelhans, L. N.; Chianese, A. R.; Crabtree, R. H. *J. Am. Chem. Soc.* **2005**, *127*, 17624–17625.
43. Voutchkova, A. M.; Feliz, M.; Clot, E.; Eisenstein, O.; Crabtree, R. H. *J. Am. Chem. Soc.* **2007**, *129*, 12834–12846.
44. Sauvage, X.; Demonceau, A.; Delaude, L. *Macromol. Symp.* **2010**, *293*, 28–32.
45. Naik, P. U. P. U.; Petitjean, L.; Refes, K.; Picquet, M.; Plasseraud, L. *Adv. Synth. Catal.* **2009**, *351*, 1753–1756.
46. Pinaud, J.; Vignolle, J.; Gnanou, Y.; Taton, D. *Macromolecules* **2011**, *44*, 1900–1908.
47. Pawar, G. M.; Buchmeiser, M. R. *Adv. Synth. Catal.* **2010**, *352*, 917–928.
48. Duong, H. A.; Cross, M. J.; Louie, J. *Org. Lett.* **2004**, *6*, 4679–4681.
49. Bantu, B.; Pawar, G. M.; Decker, U.; Wurst, K.; Schmidt, A. M.; Buchmeiser, M. R. *Chem. – A Eur. J.* **2009**, *15*, 3103–3109.
50. Bantu, B.; Pawar, G. M.; Wurst, K.; Decker, U.; Schmidt, A. M.; Buchmeiser, M. R. *Eur. J. Inorg. Chem.* **2009**, *2009*, 1970–1976.
51. Canal, J. P.; Ramnial, T.; Dickie, D. A.; Clyburne, J. A. C. *Chem. Commun.* **2006**, 1809–1818.
52. Holloczki, O.; Gerhard, D.; Massone, K.; Szarvas, L.; Nemeth, B.; Veszpremi, T.; Nyulaszi, L. *New J. Chem.* **2010**, *34*, 3004–3009.
53. Liu, D.; Zhang, Y.; Chen, E. Y.-X. *Green Chem.* **2012**, *14*, 2738–2746.
54. Rodriguez, H.; Gurau, G.; Holbrey, J. D.; Rogers, R. D. *Chem. Commun.* **2011**, *47*, 3222–3224.
55. Kelemen, Z.; Holloczki, O.; Nagy, J.; Nyulaszi, L. *Org. Biomol. Chem.* **2011**, *9*, 5362–5364.
56. Akiyama, R.; Kobayashi, S. *Chem. Rev.* **2009**, *109*, 594–642.
57. Barbaro, P.; Liguori, F. *Chem. Rev.* **2008**, *109*, 515–529.
58. Ikegami, S.; Hamamoto, H. *Chem. Rev.* **2009**, *109*, 583–593.
59. Lu, J.; Toy, P. H. *Chem. Rev.* **2009**, *109*, 815–838.
60. Buchmeiser, M. R. *Chem. Rev.* **2008**, *109*, 303–321.
61. Bergbreiter, D. E.; Tian, J.; Hongfa, C. *Chem. Rev.* **2009**, *109*, 530–582.
62. Yang, Y. C.; Bergbreiter, D. E. *Pure Appl. Chem.* **2013**, *85*, 493–509.

63. Zhou, H.; Zhang, W.-Z.; Wang, Y.-M.; Qu, J.-P.; Lu, X.-B. *Macromolecules* **2009**, *42*, 5419–5421.
64. Green, O.; Grubjesic, S.; Lee, S.; Firestone, M. A. *Polym. Rev.* **2009**, *49*, 339–360.
65. Texter, J. *Macromol. Rapid Commun.* **2012**, *33*, 1996–2014.
66. Marcilla, R.; Alberto Blazquez, J.; Rodriguez, J.; Pomposo, J. A.; Mecerreyes, D. *J. Polym. Sci. Part A Polym. Chem.* **2004**, *42*, 208–212.
67. Zhao, F.; Meng, Y.; Anderson, J. L. *J. Chromatogr. A* **2008**, *1208*, 1–9.
68. Kim, T.; Suh, M.; Kwon, S. J.; Lee, T. H.; Kim, J. H. J. E.; Lee, Y. J.; Hong, M.; Suh, K. S. *Macromol. Rapid Commun.* **2009**, *30*, 1477–1482.
69. Naik, P. U.; Refes, K.; Sadaka, F.; Brachais, C.-H.; Boni, G.; Couvercelle, J.-P.; Picquet, M.; Plasseraud, L. *Polym. Chem.* **2012**, *3*, 1475–1480.
70. He, H.; Zhong, M.; Adzima, B.; Luebke, D.; Nulwala, H.; Matyjaszewski, K. *J. Am. Chem. Soc.* **2013**, *135*, 4227–4230.
71. Jaeger, W.; Bohrisch, J.; Laschewsky, A. *Prog. Polym. Sci.* **2010**, *35*, 511–577.
72. Madhavan, N.; Jones, C. W.; Weck, M. *Acc. Chem. Res.* **2008**, *41*, 1153–1165.
73. Nyce, G. W.; Lamboy, J. A.; Connor, E. F.; Waymouth, R. M.; Hedrick, J. L. *Org. Lett.* **2002**, *4*, 3587–3590.
74. Grasa, G. A.; Güveli, T.; Singh, R.; Nolan, S. P. *J. Org. Chem.* **2003**, *68*, 2812–2819.
75. Hans, M.; Wouters, J.; Demonceau, A.; Delaude, L. *European J. Org. Chem.* **2011**, *35*, 7083–7091.
76. Breslow, R. *J. Am. Chem. Soc.* **1958**, *80*, 3719–3726.
77. Herrmann, W. A.; Goossen, L. J.; Köcher, C.; Artus, G. R. J. *Angew. Chemie Int. Ed. English* **1996**, *35*, 2805–2807.
78. Song, J. J.; Gallou, F.; Reeves, J. T.; Tan, Z.; Yee, N. K.; Senanayake, C. H. *J. Org. Chem.* **2006**, *71*, 1273–1276.
79. Tan, M.; Zhang, Y.; Ying, J. Y. *Adv. Synth. Catal.* **2009**, *351*, 1390–1394.
80. Cowan, J. A.; Clyburne, J. A. C.; Davidson, M. G.; Harris, R. L. W.; Howard, J. A. K.; Küpper, P.; Leech, M. A.; Richards, S. P. *Angew. Chemie Int. Ed.* **2002**, *41*, 1432–1434.
81. Sohn, S. S.; Rosen, E. L.; Bode, J. W. *J. Am. Chem. Soc.* **2004**, *126*, 14370–14371.
82. Thomas, M.; Brehm, M.; Hollóczki, O.; Kirchner, B. *Chem. – A Eur. J.* **2014**, *20*, 1622–1629.
83. McCrary, P. D.; Beasley, P. A.; Gurau, G.; Narita, A.; Barber, P. S.; Cojocaru, O. A.; Rogers, R. D. *New J. Chem.* **2013**, *37*, 2196–2202.
84. Gurau, G.; Rodríguez, H.; Kelley, S. P.; Janiczek, P.; Kalb, R. S.; Rogers, R. D. *Angew. Chemie Int. Ed.* **2011**, *50*, 12024–12026.
85. Earle, M. J.; Esperanca, J. M. S. S.; Gilea, M. A.; Canongia Lopes, J. N.; Rebelo, L. P. N.; Magee, J. W.; Seddon, K. R.; Widegren, J. A. *Nature* **2006**, *439*, 831–834.
86. Strasser, D.; Goulay, F.; Kelkar, M. S.; Maginn, E. J.; Leone, S. R. *J. Phys. Chem. A* **2007**, *111*, 3191–3195.
87. Coupillaud, P.; Pinaud, J.; Guidolin, N.; Vignolle, J.; Fèvre, M.; Veaudecrenne, E.; Mecerreyes, D.; Taton, D. *J. Polym. Sci. Part A Polym. Chem.* **2013**, *51*, 4530–4540.
88. Roshan, K. R.; Mathai, G.; Kim, J.; Tharun, J.; Park, G.-A.; Park, D.-W. *Green Chem.* **2012**, *14*, 2933–2940.
89. Kozak, J. A.; Wu, J.; Su, X.; Simeon, F.; Hatton, T. A.; Jamison, T. F. *J. Am. Chem. Soc.* **2013**, *135*, 18497–18501.
90. Polarz, S.; Smarsly, B. *J. Nanosci. Nanotechnol.* **2002**, *2*, 581–612.
91. Smarsly, B.; Grosso, D.; Brezesinski, T.; Pinna, N.; Boissière, C.; Antonietti, M.; Sanchez, C. *Chem. Mater.* **2004**, *16*, 2948–2952.

92. Kuemmel, M.; Grosso, D.; Boissière, C.; Smarsly, B.; Brezesinski, T.; Albouy, P. A.; Amenitsch, H.; Sanchez, C. *Angew. Chemie Int. Ed.* **2005**, *44*, 4589–4592.
93. Liu, F.; Kong, W.; Qi, C.; Zhu, L.; Xiao, F.-S. *ACS Catal.* **2012**, *2*, 565–572.
94. Yang, J.; Qiu, L.; Liu, B.; Peng, Y.; Yan, F.; Shang, S. *J. Polym. Sci. Part A Polym. Chem.* **2011**, *49*, 4531–4538.
95. Zhang, Y.-L.; Liu, S.; Liu, S.; Liu, F.; Zhang, H.; He, Y.; Xiao, F.-S. *Catal. Commun.* **2011**, *12*, 1212–1217.
96. Wei, S.; Lu, D.-X.; Sun, J.; He, Y.; Zhu, L.; Zhang, Y.-L.; Xiao, F.-S. *Colloids Surfaces A Physicochem. Eng. Asp.* **2012**, *414*, 327–332.
97. Zhang, Y.; Wei, S.; Liu, F.; Du, Y.; Liu, S.; Ji, Y.; Yokoi, T.; Tatsumi, T.; Xiao, F.-S. *Nano Today* **2009**, *4*, 135–142.
98. Wilke, A.; Yuan, J.; Antonietti, M.; Weber, J. *ACS Macro Lett.* **2012**, *1*, 1028–1031.
99. Liu, F.; Zuo, S.; Kong, W.; Qi, C. *Green Chem.* **2012**, *14*, 1342–1349.
100. Coman, S. M.; Florea, M.; Parvulescu, V. I.; David, V.; Medvedovici, A.; Vos, D. De; Jacobs, P. A.; Poncelet, G.; Grange, P. *J. Catal.* **2007**, *249*, 359–369.
101. Zhao, Q.; Yin, M.; Zhang, A. P.; Prescher, S.; Antonietti, M.; Yuan, J. *J. Am. Chem. Soc.* **2013**, *135*, 5549–5552.
102. Kuzmicz, D.; Coupillaud, P.; Men, Y.; Vignolle, J.; Vendraminetto, G.; Ambrogi, M.; Taton, D.; Yuan, J.; Vendraminetto, Giordano Ambrogi, M. *Polymer* **2014**, *55*, 3423–3430.
103. Liu, F.; Li, W.; Sun, Q.; Zhu, L.; Meng, X.; Guo, Y.-H.; Xiao, F.-S. *ChemSusChem* **2011**, *4*, 1059–1062.
104. Fontanals, N.; Maria Marcé, R.; Galià, M.; Borrull, F. *J. Polym. Sci. Part A Polym. Chem.* **2004**, *42*, 2019–2025.
105. Xiong, Y.; Wang, Y.; Wang, H.; Wang, R. *Polym. Chem.* **2011**, *2*, 2306–2315.
106. Watile, R. A.; Deshmukh, K. M.; Dhake, K. P.; Bhanage, B. M. *Catal. Sci. Technol.* **2012**, *2*, 1051–1055.
107. Ema, T.; Miyazaki, Y.; Taniguchi, T.; Takada, J. *Green Chem.* **2013**, *15*, 2485–2492.
108. Roth, P. J.; Wiss, K. T.; Theato, P. In *Polymer Science: A Comprehensive Reference*; Matyjaszewski, K.; Möller, M., Eds.; Elsevier: Amsterdam, **2012**; pp. 247–267.
109. Gauthier, M. A.; Gibson, M. I.; Klok, H.-A. *Angew. Chemie Int. Ed.* **2009**, *48*, 48–58.
110. Hawker, C. J.; Wooley, K. L. *Science* **2005**, *309*, 1200–1205.
111. Fumagalli, M.; Ouhab, D.; Boisseau, S. M.; Heux, L. *Biomacromolecules* **2013**, *14*, 3246–3255.
112. Gu, Y.; Jerome, F. *Chem. Soc. Rev.* **2013**, *42*, 9550–9570.
113. Maisonneuve, L.; Lebarbe, T.; Grau, E.; Cramail, H. *Polym. Chem.* **2013**, *4*, 5472–5517.
114. Liu, J.; Detrembleur, C.; Hurtgen, M.; Debuigne, A.; De Pauw-Gillet, M.-C.; Mornet, S.; Duguet, E.; Jerome, C. *Polym. Chem.* **2014**, *5*, 77–88.
115. O'Reilly, R. K.; Hawker, C. J.; Wooley, K. L. *Chem. Soc. Rev.* **2006**, *35*, 1068–1083.
116. Breul, A. M.; Hager, M. D.; Schubert, U. S. *Chem. Soc. Rev.* **2013**, *42*, 5366–5407.
117. Barz, M.; Tarantola, M.; Fischer, K.; Schmidt, M.; Luxenhofer, R.; Janshoff, A.; Theato, P.; Zentel, R. *Biomacromolecules 9*, 3114–3118.
118. Zupan, M.; Krajnc, P.; Stavber, S. *J. Polym. Sci. Part A Polym. Chem.* **1998**, *36*, 1699–1706.
119. Kakuchi, R.; Theato, P. In *Functional Polymers by Post-Polymerization Modification*; Wiley-VCH Verlag GmbH & Co. KGaA, **2012**; pp. 45–64.
120. Prescher, J. A.; Bertozzi, C. R. *Nat Chem Biol* **2005**, *1*, 13–21.
121. Maynard, H. D.; Broyer, R. M.; Kolodziej, C. M. In *Click Chemistry for Biotechnology and Materials Science*; John Wiley & Sons, Ltd, **2009**; pp. 53–68.

122. Gevrek, T. N.; Arslan, M.; Sanyal, A. In *Functional Polymers by Post-Polymerization Modification*; Wiley-VCH Verlag GmbH & Co. KGaA, **2012**; pp. 119–151.
123. Singha, N. K.; Schlaad, H. In *Functional Polymers by Post-Polymerization Modification*; Wiley-VCH Verlag GmbH & Co. KGaA, **2012**; pp. 65–86.
124. Kolb, H. C.; Finn, M. G.; Sharpless, K. B. *Angew. Chemie Int. Ed.* **2001**, *40*, 2004–2021.
125. Huisgen, R. *Angew. Chemie* **1963**, *75*, 604–637.
126. Debets, M. F.; van Berkel, S. S.; Dommerholt, J.; Dirks, A. (Ton) J.; Rutjes, F. P. J. T.; van Delft, F. L. *Acc. Chem. Res.* **2011**, *44*, 805–815.
127. Itoh, T.; Mase, T. *J. Org. Chem.* **2006**, *71*, 2203–2206.
128. Sessions, L. B.; Cohen, B. R.; Grubbs, R. B. *Macromolecules* **2007**, *40*, 1926–1933.
129. Garrison, J. C.; Youngs, W. J. *Chem. Rev.* **2005**, *105*, 3978–4008.
130. Lin, I. J. B.; Vasam, C. S. *Coord. Chem. Rev.* **2007**, *251*, 642–670.
131. Naumann, S.; Buchmeiser, M. R. *Catal. Sci. Technol.* **2014**, *4*, 2466–2479.
132. Hayes, J. M.; Viciano, M.; Peris, E.; Ujaque, G.; Lledós, A. *Organometallics* **2007**, *26*, 6170–6183.
133. Tskhovrebov, A. G.; Vuichoud, B.; Solari, E.; Scopelliti, R.; Severin, K. *J. Am. Chem. Soc.* **2013**, *135*, 9486–9492.
134. Berkessel, A.; Yatham, V. R.; Elfert, S.; Neudörfl, J.-M. *Angew. Chemie Int. Ed.* **2013**, *52*, 11158–11162.
135. Berkessel, A.; Elfert, S.; Etzenbach-Effers, K.; Teles, J. H. *Angew. Chemie Int. Ed.* **2010**, *49*, 7120–7124.
136. Berkessel, A.; Elfert, S.; Yatham, V. R.; Neudörfl, J.-M.; Schlörer, N. E.; Teles, J. H. *Angew. Chemie Int. Ed.* **2012**, *51*, 12370–12374.
137. Bugaut, X.; Glorius, F. *Chem. Soc. Rev.* **2012**, *41*, 3511–3522.
138. Maji, B.; Mayr, H. *Angew. Chemie Int. Ed.* **2013**, *52*, 11163–11167.
139. Hans, M.; Wouters, J.; Demonceau, A.; Delaude, L. *Chem. – A Eur. J.* **2013**, *19*, 9668–9676.
140. Reynolds, T. E.; Stern, C. A.; Scheidt, K. A. *Org. Lett.* **2007**, *9*, 2581–2584.
141. Izquierdo, J.; Orue, A.; Scheidt, K. A. *J. Am. Chem. Soc.* **2013**, *135*, 10634–10637.
142. Norris, B. C.; Sheppard, D. G.; Henkelman, G.; Bielawski, C. W. *J. Org. Chem.* **2010**, *76*, 301–304.
143. Li, J.-Q.; Liao, R.-Z.; Ding, W.-J.; Cheng, Y. *J. Org. Chem.* **2007**, *72*, 6266–6269.
144. Viciu, M. S.; Navarro, O.; Germaneau, R. F.; Kelly, R. A.; Sommer, W.; Marion, N.; Stevens, E. D.; Cavallo, L.; Nolan, S. P. *Organometallics* **2004**, *23*, 1629–1635.
145. De Frémont, P.; Scott, N. M.; Stevens, E. D.; Nolan, S. P. *Organometallics* **2005**, *24*, 2411–2418.
146. Baker, M. V; Barnard, P. J.; Berners-Price, S. J.; Brayshaw, S. K.; Hickey, J. L.; Skelton, B. W.; White, A. H. *J. Organomet. Chem.* **2005**, *690*, 5625–5635.
147. Jensen, D. R.; Sigman, M. S. *Org. Lett.* **2002**, *5*, 63–65.

Chapter 3

Poly(ionic liquid)-based Block Copolymers by Cobalt-Mediated Radical Polymerization: Synthesis, Self-Assembly and Applications

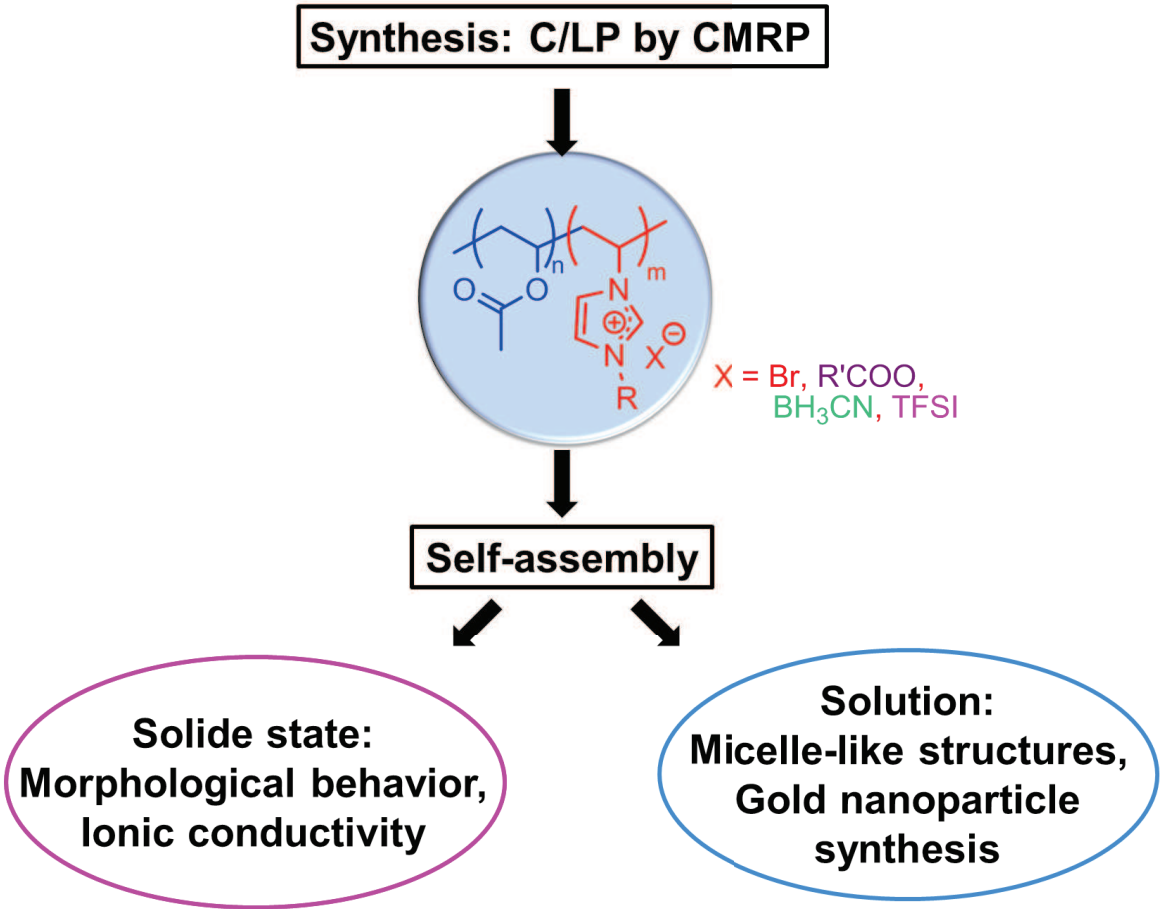

Keywords: Poly(ionic liquid)s, Block copolymers, Imidazolium, Self-assembly, Conductivity, Gold nanoparticles.

Abstract: A new family of imidazolium-based poly(ionic liquid) block copolymers (PIL BCPs) has been developed. Synthesis of poly(vinyl acetate)-*b*-poly(*N*-vinyl-3-alkylimidazolium bromide), referred to as PVAc-*b*-PIL(Br), is achieved by sequential cobalt-mediated radical polymerization (CMRP), following two methods. The first method uses a specifically designed alkyl-cobalt initiator. The second method employs the *bis*(acetylacetonato)cobalt(II) ($Co(acac)_2$) as controlling agent in conjunction with 2,2'-azobis(4-methoxy-2,4-dimethyl valeronitrile) (V-70) as a radical source, both reagents being commercially available. Comparison of the two synthetic strategies shows that the former provides a better control over molar masses, dispersities and chain-end fidelity *via* a reversible deactivation radical polymerization (RDRP) process whereas a degenerative transfer (DT) process characterizes the method utilizing $Co(acac)_2$ and V-70. Combined characterization techniques, including ^{1}H NMR, DOSY NMR, TGA, DSC, SAXS and TEM have established the formation of PIL BCPs in almost all cases.

The ability of these compounds to generate ordered self-assembled mesostructures at the solid state is also evidenced in this chapter. In particular PIL(Br or TFSI) and PVAc blocks show a high degree of incompatibility, giving rise to a strong microphase separation by forming well-ordered lamellae and hexagonally packed cylinders in the composition range investigated. Ionic conductivity measurements lead to different values in the range of $\sim 10^{-10}$ to $\sim 10^{-4}$ S/cm, depending on sample preparation, equipment, and the overall measurement conditions. Importantly, these values are significantly higher than that of the homoPIL homologue, confirming that phase segregation into ordered mesophases from PIL BCP strongly enhance the ionic transport properties.

Self-assembling properties in solution of these novel PIL BCPs can also be manipulated, in particular through both anion exchange and post-chemical modification of the PVAc block into poly(vinyl alcohol) (PVA). For instance, the amphiphilic PVAc-*b*-PIL(Br) self-assembles into micelle-like structures in a selective solvent (water or THF), as does the poly(vinyl alcohol)-b-poly(*N*-vinyl-3-butylimidazolium carboxylate-co-bis(trifluorosulfonyl) imide) (PVA-*b*-PIL(RCOO-*co*-TFSI)). The latter compound can finally serve both as stabilizer and reducing agent, *via* the introduction of cyanoborohydride (BH_3CN^-) counter-anions, to achieve gold nanoparticles in aqueous solution in the form of gold nanoplates such as nanocubes and hexagonal or octahedral nanoplates, depending on the molar ratio between the BH_3CN^- counter-anion and the gold complex (*i.e.* $HAuCl_4$).

Part of these results have been published in the following papers:

- *C. Detrembleur, A. Debuigne, M. Hurtgen, C. Jérome , J. Pinaud, M. Fèvre, P. Coupillaud, J. Vignolle, D. Taton. "Synthesis of 1-Vinyl-3-Ethylimidazolium-Based Ionic Liquid (Co)polymers by Cobalt-Mediated Radical Polymerization." Macromolecules* ***2011****, 43, 6397-6404.*
- *P. Coupillaud, M. Fèvre, A-L. Wirotius, K. Aissou, G. Fleury, A. Debuigne, C. Detrembleur, D. Mecerreyes, J. Vignolle, D. Taton. "Precision Synthesis of Poly(Ionic Liquid)-Based Block Copolymers by Cobalt-Mediated Radical Polymerization and Preliminary Study of Their Self-Assembling Properties." Macromol. Rapid Comm,* ***2014****, 35,422-430.*

Chapter 3

Poly(ionic liquid)-based Block Copolymers by Cobalt-Mediated Radical Polymerization: Synthesis, Self-Assembly and Applications

Table of Contents

Introduction

Engineering of block copolymers (BCPs) is a multidisciplinary field spanning macromolecular chemistry, theoretical calculations and physics of polymer materials.[1–3] Some BCPs are practically used in our daily life, *e.g.* as compatibilizers, viscosity modifiers, dispersants, etc. Their potential in other areas, including drug delivery, nanoscale lithography in microelectronics is also being extensively investigated.[4–12]

The success of BCPs is due to their self-assembling properties, either in the solid state or in a selective solvent of one block, which provides a wide range of morphologies in the submicron size range.[13–16] Precision polymer chemistry,[17,18] involving controlled/living polymerization techniques, has reached such maturity that a great variety of BCP architectures and compositions can now be achieved.

As emphasized in the bibliographic chapter of this manuscript, most of poly(ionic liquid) block copolymers (PIL BCPs) reported so far, are based on imidazolium-type PIL. Only a handful of studies have focused on their self-assembly in solution,[19–23] giving rise to micelle-like nanostructures, which can be triggered by a simple ion exchange (this relates to the ionic sensitivity of PILs).[24–27] Other physicochemical studies include the synthesis of magnetic materials,[28,29] carbon dioxide capture and,[30–32] more recently, formation of nanostructured films by self-assembly at the solid state in correlation with ionic conductivity measurements.[33–42]

In 2011, in collaboration with the group of Dr. C. Detrembleur in CERM (Liège, Belgium), we have introduced a new family of PIL BCPs based on poly(*N*-vinyl-3-ethylimidazolium bromide) (PVEtImBr) and poly(vinyl acetate) (PVAc) (see section 2.1.4., chapter 1).[43] Synthesis of these compounds was achieved by sequential cobalt-mediated radical polymerization (CMRP) in solution (Scheme 1, Route A).[44] In addition to PVAc-*b*-PVEtImBr diblock copolymers, symmetric PVAc-*b*-PVEtImBr-*b*-PVAc triblock copolymers issued from the irreversible and selective radical coupling of parent diblocks, in the presence of isoprene as coupling agent, were obtained.[45]

Though straightforward, the aforementioned method however required the prior synthesis of an alkyl-cobalt(III) adduct as a mediating agent (**a**, Scheme 1). Use of a commercially available controlling agent, namely, *bis*(acetylacetonato)cobalt(II) ($Co(acac)_2$; **b**, Scheme 1) in conjunction with 2,2'-azobis(4-methoxy-2,4-dimethylvaleronitrile) (V-70; **c**, Scheme 1) to grow PVAc chains in a controlled fashion by CMRP is yet possible.[46]

In the present chapter, we describe that crossing over from a CMRP-derived PVAc to a PIL based on *N*-vinyl-3-butylimidazolium allows for an easy access to PVAc-*b*-PIL BCPs (Scheme 1, Route B), as an alternative to CMRP utilizing the alkyl-cobalt(III) adduct (**a**). Both synthetic routes will be discussed in the first part.

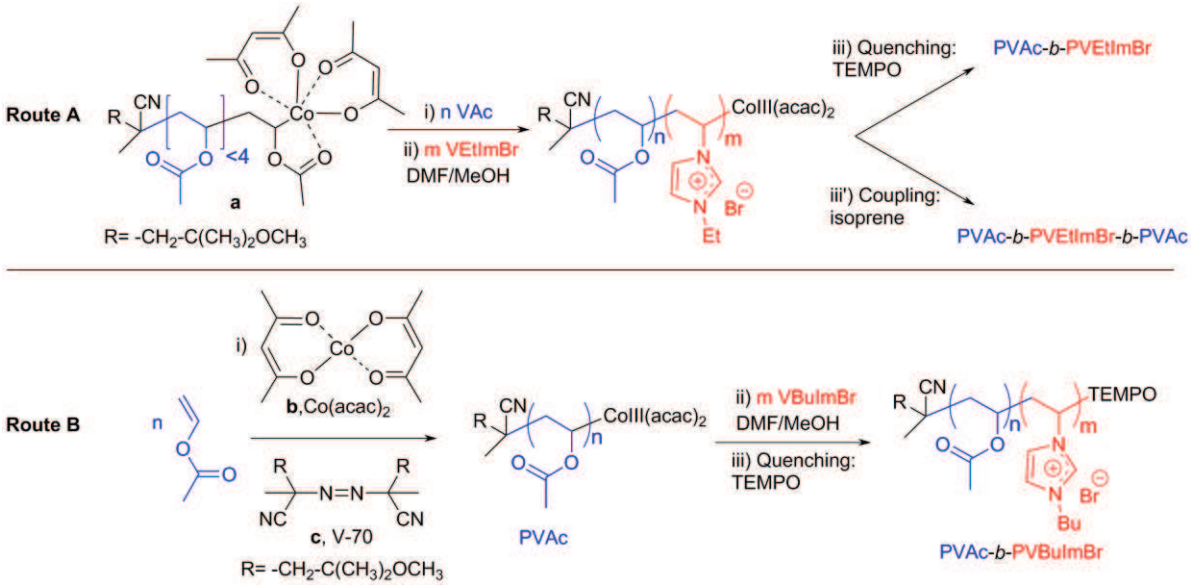

Scheme 1. Route A. Synthesis of PVAc-*b*-PVEtImBr and PVAc-*b*-PVEtImBr-*b*-PVAc by sequential CMRP using alkyl-cobalt(III) adduct (**a**) as a mediating agent as previously reported.[43] Route B. Synthesis of PVAc-*b*-PVBuImBr by sequential CMRP using $Co(acac)_2$ (**b**) and V-70 (**c**).

The second part of this chapter will show different nanostructures that can be achieved by self-assembly, either in bulk or in solution, from our PIL BCPs. Morphologies in bulk have been examined by different characterization techniques, including synchrotron small-angle X-ray spectroscopy (SAXS), transmission electron microscopy (TEM), differential scanning calorimetry (DSC) and thermogravimetric analysis (TGA). The ionic conductivity properties of some PIL BCPs, featuring the bis(trifluorosulfonyl) imide (TFSI) counter-anions, have also been determined using electrochemical impedance spectroscopy (EIS) in collaboration with both Dr. A. Serghei and Pr. E. Drockenmuller at IMP, University of Lyon, and Dr. K. Aïssou and Dr. G. Fleury at LCPO, University of Bordeaux.

Due to their amphiphilic character, PVAc-*b*-PVBuImBr BCPs have also been engineered in selective solvents to micelle-like nanostructures. Subsequent chemical modification of the PVAc block has also allowed us to achieve PIL BCP with a poly(vinyl alcohol) (PVA) nonionic block.

PVA-*b*-PIL carrying cyanoborohydride counter-anions (BH_3CN^-) has also been employed as both polymeric stabilizers and reducing agents for the synthesis of gold colloidal nanoparticles.

1. Synthesis of poly(vinyl acetate)-*b*-poly(*N*-vinyl-3-alkylimidazolium bromide) by CMRP

This section describes two synthetic route to PVAc-*b*-PIL(Br) PIL BCPs, as illustrated in Scheme 1. The CMRP of *N*-vinyl-3-ethylimidazolium bromide using the specifically alkyl-cobalt controlling agent was investigated in a previous collaboration between the group of Liège and our group.[43] This study established the conditions the best suited to achieve a good control over molar masses and dispersities. Thus, well-defined PVAc-*b*-PVEtImBr PIL BCPs were synthesized from a CMRP-derived PVAc-$Co(acac)_2$ initiator, in a mixture of DMF and MeOH (2/1: v/v) at 30 °C.

Based on this, a series of new PVAc-*b*-PVEtImBr and PVAc-*b*-PVBuImBr (Route A, Scheme 1) was synthesized at LCPO, using the alkyl-cobalt that was provided by our collaborators in Liège. In parallel, attempts to synthesize PIL BCPs by CMRP without resorting to the alkyl-cobalt initiator, but using the commercially available $Co(acac)_2$ (**b)** and the V-70 (**c**, Route B, Scheme 1), have been realized. Results of CMRP obtained from both routes, and comparison of the two methods, are presented hereafter.

1.1. PVAc-*b*-PIL(Br) synthesis using the alkyl-cobalt as initiator

Controlled cobalt-mediated radical polymerization (CMRP) utilizing the alkyl-cobalt (**a**) (Scheme 1) can be applied to non-conjugated vinyl monomers, as vinyl acetate (VAc) and *N*-vinylpyrrolidone (NVP).[44] A proper selection of the polymerization conditions, in particular the temperature and the use of coordinating solvents, allows fine-tuning CMRP from the same controlling agent. Extension of CMRP to conjugated vinyl monomers, such as acrylonitrile[47] and alkyl acrylates,[48] and to the preparation of unprecedented related copolymers has been reported.[43,45,49,50]

Synthesis of the novel series of PVAc-*b*-PIL(Br) block copolymers was achieved by sequential CMRP of VAc and VEtImBr or VBuImBr in the presence of alkyl-cobalt (**a**) (Scheme 1). First, a poly(vinyl acetate) end-capped by $Co(acac)_2$, PVAc-$Co(acac)_2$ was prepared by CMRP of VAc at 30 °C in bulk, following established experimental conditions.[43]

After a few hours of reaction, about 50% of VAc conversion were reached (Table 1). After removal of residual monomer under vacuum, the resulting PVAc-Co(acac)$_2$ was employed as a macroinitiator for CMRP of IL monomers in methanol at 30 °C.

Characterization of our PIL compounds by SEC proved very challenging. In our previous works, poly(*N*-vinyl-3-ethylimidazolium bromide) and corresponding PVAc-*b*-PIL(Br) BCPs could be analyzed by SEC in DMF. A typical SEC trace is shown in Figure 1a. As mentioned earlier in this document, Matyjaszewski *et al.* recently established a general method for measuring molar masses of PILs, by adding 10 mM of LiTFSI in the THF as eluent, and analyzed PILs with TFSI counter-anions.[51] By this technique, interactions between PIL blocks and the columns could seemingly be avoided.

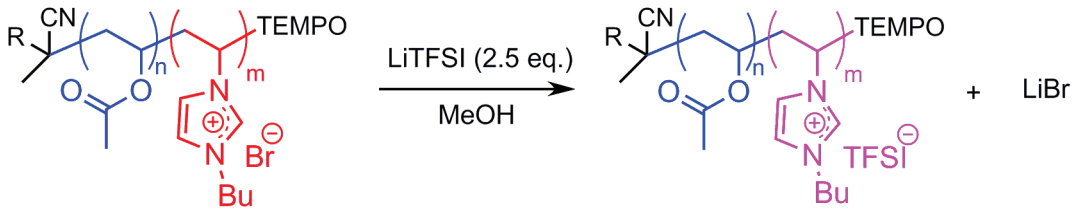

Scheme 2. Anion exchange from bromide to bis(trifluorosulfonyl) imide on PVAc-*b*-PIL(Br).

Such conditions have been set up in POLYMAT in the group of D. Mecerreyes in San-Sebastian. Consequently, anion metathesis, substituting the bis(trifluorosulfonyl) imide (TFSI) for the bromine (Br^-) anion was systematically preformed with our PIL BCPs, before analysis by SEC (Scheme 2) at POLYMAT. The as-obtained PILs with TFSI counter-anions were soluble in THF, the anion exchange reaction being quantitative and well-documented.[52]

Table 1. Synthesis of PVAc and PIL BCPs using the alkyl-cobalt initiator.

Entry	Sample	Polymer	[I][a]/ [VAc]	[PVAc]/ [IL(Br)]	DMF/ MeOH	T (°C)	t (h)	Conv. (%)[b]	$M_{n,th}$ (g.mol^{-1})[b]	$M_{n,exp}$, SEC(THF) (g.mol^{-1})/$Đ$[d]	$M_{n,exp}$, SEC(THF/LiTFSI) (g.mol^{-1})/$Đ$[e]	$M_{n,PIL(Br)}$ (g.mol^{-1})[f]	$M_{n,PIL\ BCP(Br)}$ (g.mol^{-1})	n:m[h]	PIL(Br) wt (%)
1[i]		PVAc	1/96	-	-	40	5.5	50	4000	4000/1.05	n.d.[j]	-	-	-	-
2[i]	**1(Br)**	PVAc-*b*-PVEtImBr	-	1/22	3/2	30	8	90	4000	n.d.[j]	n.d.[j]	4000	8000	40:15	50
3		PVAc	1/96	-	-	30	5.5	44	3700	3400/1.05	5000/1.08	-	-	-	-
4	**2(Br)**	PVAc-*b*-PVEtImBr	-	1/20	3/2	30	7	75	3000	n.d.[j]	13600/1.12	3000	6400	40:15	47
5		PVAc	1/224	-	-	30	9.5	46	9200	8400/1.16	10500/1.12	-	-	-	-
6	**3(Br)**	PVAc-*b*-PVBuImBr	-	1/43	3/2	30	8.7	23	2300	n.d.[j]	19600/1.17	2300	10700	98:10	21
7		PVAc	1/339	-	-	30	9.5	40	12000	9500/1.10	11100/1.10	-	-	-	-
8	**4(Br)**	PVAc-*b*-PVBuImBr	-	1/22	3/2	30	8.7	70	3500	n.d.[j]	19000/1.20	3700	13200	110:16	28

[a] Alkyl-cobalt initiator concentration. [b] Monomer conversion determined by ^{1}H NMR. [c] Theoretical M_n of the corresponding block obtained by ^{1}H NMR. [d] M_n obtained By SEC in THF. [e] M_n obtained by SEC in THF with 10 mM of LiTFSI after anion exchange from bromide to TFSI on the PIL BCPs. [f] M_n Obtained by ^{1}H NMR spectroscopy. [h] n = number of VAc units; m = number of IL units. [i]Polymers synthesized by Detrembleur *et al.* in Liège in 2011.[43] [j] not determined.

Block copolymerization proved effective, as attested by SEC traces of copolymer samples showing a shift towards the higher molar masses, compared to the SEC trace of the PVAc macroinitiator (Figure 1). No peak due to unreacted PVAc chain precursor is visible. Though, a slight shoulder in the high molar mass can be noted. This side peak was attributed to coupling reactions that occurred during workup, or upon quenching the reaction as already observed for other CMRP-derived polymers previously reported.[44,50,53] The dispersity of copolymers remained low ($Đ$ ~ 1.08-1.20), attesting to an effective crossover reaction.

These observations are thus consistent with a controlled process and the formation of well-defined PVAc-*b*-PIL BCPs. One can also note that the dispersity of PIL BCPs carrying the butyl substituent on the imidazolium ring is slightly higher than that of PIL BCPs with the ethyl group. This could be due to some differences in the kinetics of the CMRP between the two monomers (*e.g.* different equilibrium constant between active and dormant species).

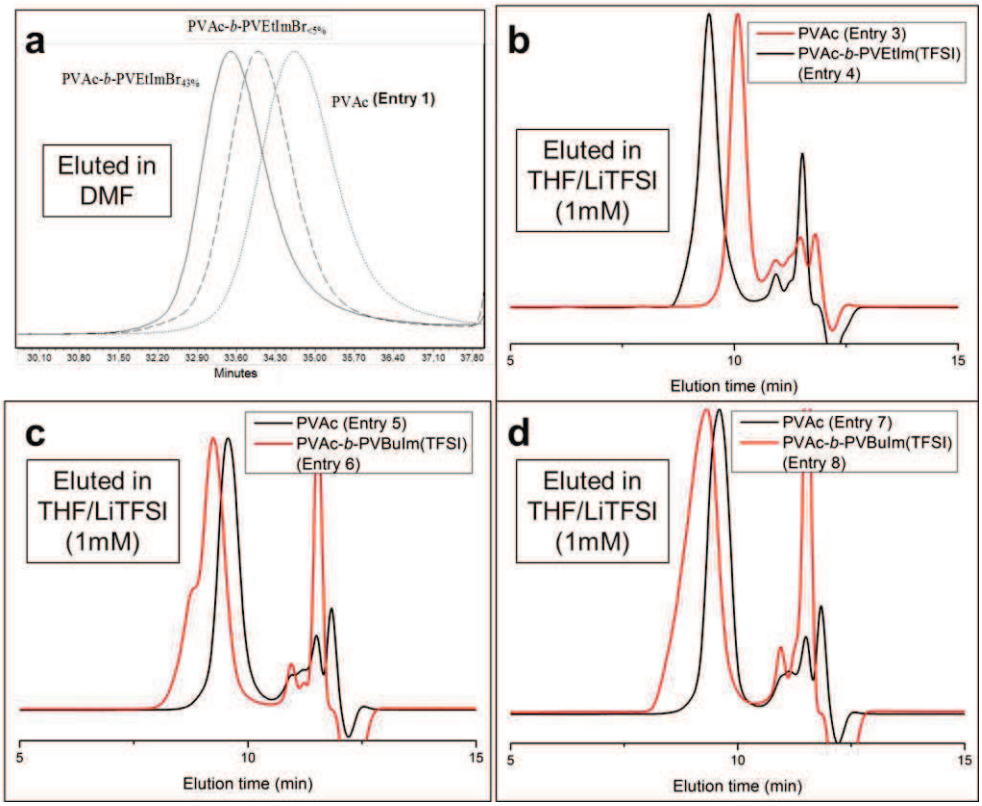

Figure 1. SEC traces of PVAc-*b*-PIL PIL BCPs: **a)** SEC traces of PVAC-Co(acac)$_2$ and PVAc-*b*-PVEtImBr **1(Br)**. Experiments achieved in 2011 in Liège.[43] **b)** SEC traces of PVAC-Co(acac)$_2$ and PVAc-*b*-PVEtIm(TFSI) **2(TFSI)**. **c)** SEC traces of PVAC-Co(acac)$_2$ and PVAc-*b*-PVBuIm(TFSI) **3(TFSI)**. **d)** SEC traces of PVAC-Co(acac)$_2$ and PVAc-*b*-PVBuIm(TFSI) **4(TFSI)**.

Characterization by ^{1}H NMR of compounds obtained after purification by dialysis against MeOH revealed the presence of characteristic signals of both blocks. The composition of the

PVAc-*b*-PIL(Br) could thus be determined, by comparing the intensity of methine proton of PVAc (4.8 ppm) with that of protons -CH_3 of the ethyl (1.4 ppm), or butyl substituent (0.8 ppm), or protons characteristic of the imidazolium ring (8.0 ppm) (Figure 2). Representative results are provided in Table 1.

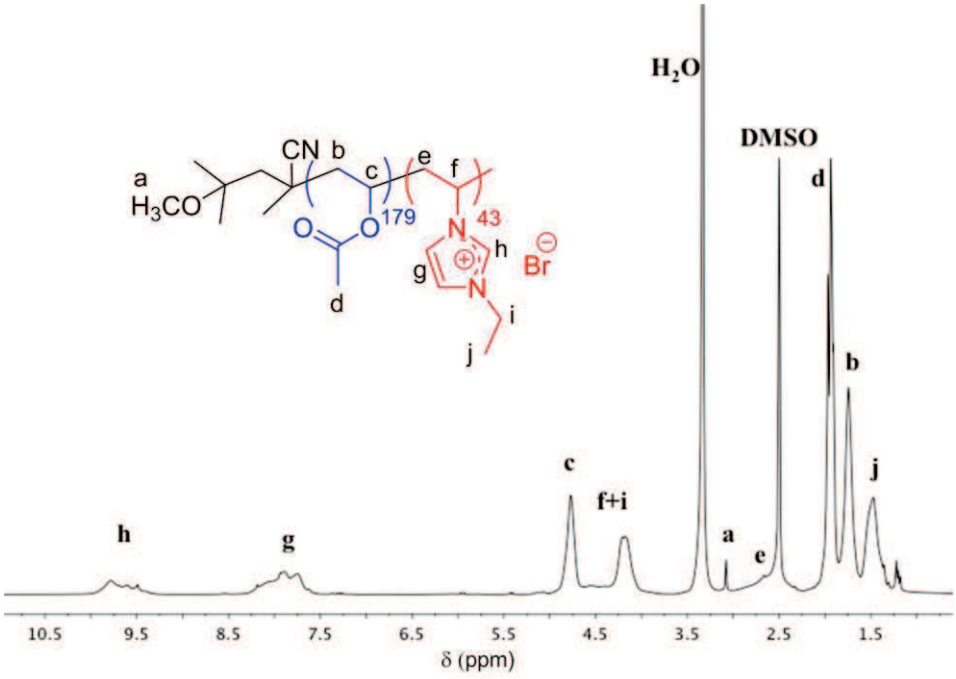

Figure 2. ^{1}H NMR spectrum of PVAc-*b*-PVEtImBr **1(Br)** (Table 1) in DMSO-δ_6.

From a mechanistic point of view, the team of Liège has established that control of CMRP utilizing the alkyl-cobalt (**a**) (Scheme 1) is ensured by the occurrence of a reversible deactivation radical polymerization (RDRP) process, as shown in Scheme 3.[44,46,54] Upon homolytic cleavage, the carbon-cobalt bond of adduct (**a**) (Scheme 1) releases both the alkyl radical and the cobalt (II) complex serving as initiating fragment and terminator, respectively. Chelation by the carbonyl group of the last VAc unit with the Co complex provides an extra stabilization to the Co-C bond. DMF can also play the role of a ligand to facilitate the cleavage of the Co-C and favor the propagation step (Scheme 3).[47,54] A degenerative transfer (DT) process can also operate under other conditions (see discussion further).

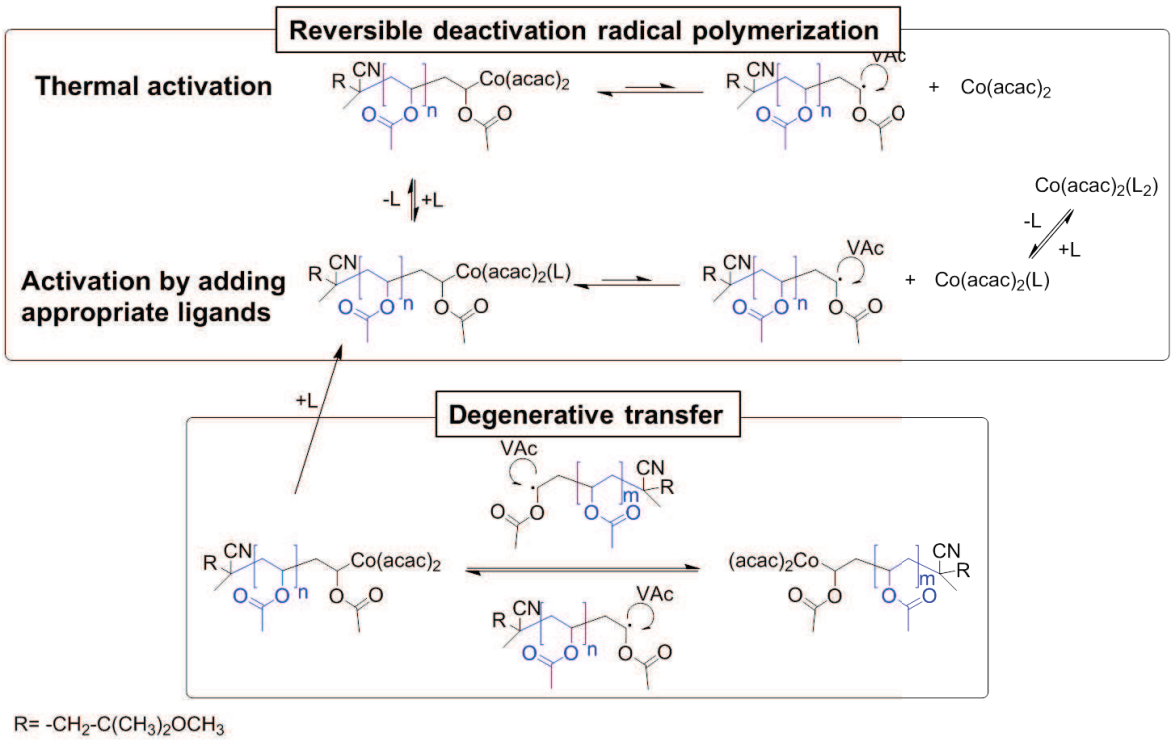

Scheme 3. Mechanisms of reversible deactivation radical polymerization (RDRP) and degenerative chain transfer (DT) in the CMRP of VAc initiated by a model cobalt adduct.

1.2. PVAc-*b*-PIL(Br) synthesis using $Co(acac)_2$ and V-70 as initiator

A series of poly(vinyl acetate)-*b*-poly(*N*-vinyl-3-butylimidazolium bromide), PVAc-*b*-PVBuImBr, PIL BCP was synthesized by sequential CMRP using a bi-component system consisting of $Co(acac)_2$ (**b**) and V-70 (**c**), both of these reagents being commercially available (Scheme 1, Route B).

In a typical procedure, a PVAc macroinitiator end-capped by $Co(acac)_2$ (PVAc-$Co(acac)_2$) was first prepared by CMRP of VAc at 30 °C in bulk, using an excess of V-70 as the radical source and $Co(acac)_2$ as the mediating agent ([V-70]/[$Co(acac)_2$] = 6.5/1). A well-defined PVAc-$Co(acac)_2$ (M_w/M_n < 1.2) was thus obtained, as determined by SEC in THF calibrated with polystyrene standards. Molar masses of PVAc measured by SEC were slightly higher than theoretical values, which might be explained by the linear PS standards used for SEC calibration (Table 2). The residual monomer was thoroughly removed under vacuum, before adding VBuImBr in a mixture of MeOH/DMF at 0 °C. After a few hours, the reaction was quenched with TEMPO (Scheme 4), to avoid any further radical coupling between the copolymer chains.

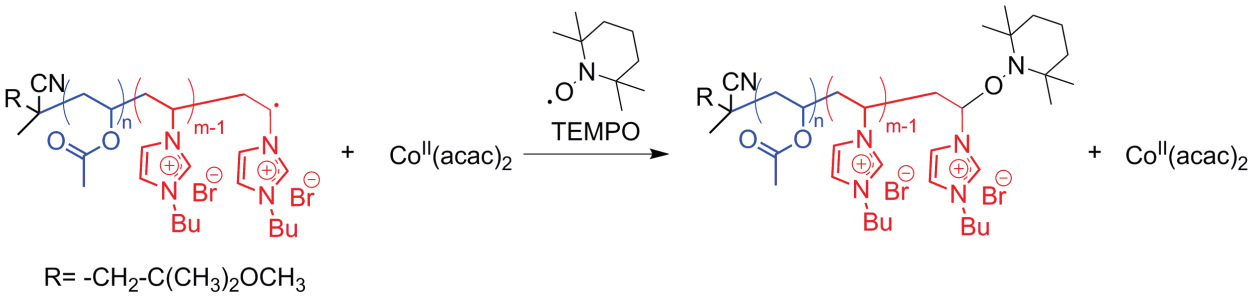

Scheme 4. PIL BCPS quenching with TEMPO.

The composition of the PVAc-*b*-PVBuImBr BCP was again determined by ^{1}H NMR, as described previously (Table 2). Characterization by ^{1}H NMR of the compound purified by dialysis against MeOH revealed the presence of characteristic signals of both blocks, using DMSO-δ_6 or CD_2Cl_2, two good solvents for both the PVAc and the PVBuImBr block.

Results of SEC characterization obtained after anion exchange, from bromide to TFSI, of PIL BCPs **5-11** are also summarized in Table 2 (see also Figure 3).

The first PVAc block was generally well-defined ($Đ$ < 1.2). However, shapes of molar masses distribution obtained after crossing-over from PVAc to the PIL block by CMRP showed a certain loss of control. In particular, dispersities slightly increased when using a longer PVAc (PIL BCPs **8**, **9**, **10** and **11**, see also Entry 7-14, Table 2). Samples **5** and **6** arising from entries 1-4, that were, using a PVAc precursor of ~5000 g.mol^{-1} also gave relatively poor defined BCPs. In contrast, compounds **7** showed a shift towards the higher molar masses with no unreacted PVAc chains left. The shoulder in the high molar masses region observed in some cases, likely resulted from radical irreversible coupling reactions, as already explained previously (Figure 3, PIL BCPs **6**, **8**, **10**).

Table 2. Synthesis of PIL BCPs using the $Co(acac)_2$ and the V-70.

Entry	Sample	Polymer	[$Co(acac_2)$] / [VAc]	[PVAc]/ [IL(Br)]	DMF/ MeOH	t (h)	Conv. (%)[a]	$M_{n,th}$ ($g.mol^{-1}$)[b]	$M_{n,exp}$, SEC(THF) ($g.mol^{-1}$)/$Đ$[c]	$M_{n,exp}$, SEC(THF/LiTFSI) ($g.mol^{-1}$)/$Đ$[d]	$M_{n,PIL(Br)}$ ($g.mol^{-1}$)[e]	$M_{n,PIL\ BCP}$ ($g.mol^{-1}$)	n:m[f]	PIL(Br) wt (%)
1		PVAc	1/115	-	-	65	50	4400	4500/1.11	4800/1.28	-	-	-	-
2	**5(Br)**	PVAc-*b*-PIL(Br)	-	1/43	3/2	3	75	7500	n.d.[g]	16900/1.51	9700	14000	50:42	69
3		PVAc	1/115	-	-	66	59	5800	5700/1.15	6200/1.27	-	-	-	-
4	**6(Br)**	PVAc-*b*-PIL(Br)	-	1/87	3/2	2	68	13600	n.d.[g]	25700/1.76	14300	19900	65:62	72
5		PVAc	1/115	-	-	69	48	4700	5000/1.20	5700/1.30	-	-	-	-
6	**7(Br)**	PVAc-*b*-PIL(Br)	-	1/108	3/2	10	94	23400	n.d.[g]	30900/1.32	21200	25900	54:92	82
7		PVAc	1/287	-	-	50	30	7300	7500/1.25	6700/1.27	-	-	-	-
8	**8(Br)**	PVAc-*b*-PIL(Br)	-	1/43	3/2	2	90	4000	n.d.[g]	20200/1.38	8300	15600	84:36	53
9		PVAc	1/287	-	-	50	57	14200	14500/1.20	n.d.[g]	-	-	-	-
10	**9(Br)**	PVAc-*b*-PIL(Br)	-	1/65	3/2	2	41	6200	n.d.[g]	20100/1.21	11800	26000	163:51	45
11		PVAc	1/287	-	-	50	62	15600	15700/1.22	15800/1.29	-	-	-	-
12	**10(Br)**	PVAc-*b*-PIL(Br)	-	1/87	3/2	2	43	8600	n.d.[g]	23900/1.31	4200	19800	179:18	21
13		PVAc	1/281	-	-	48	64	15600	18300/1.10	19100/1.30	-	-	-	-
14	**11(Br)**	PVAc-*b*-PIL(Br)	-	1/89	3/2	2	41	6200	n.d.[g]	28300/1.39	9900	25500	179:43	39

[a] Monomer conversion determined by ^1H NMR. [b] Theoretical M_n of the corresponding block obtained by ^1H NMR. [c] M_n obtained By SEC in THF. [d] M_n obtained by SEC in THF with 10 mM of LiTFSI after anion exchange from bromide to TFSI on the PIL BCPs. [e] M_n Obtained by ^1H NMR spectroscopy. [f] n = number of VAc units; m = number of IL units. [g] not determined.

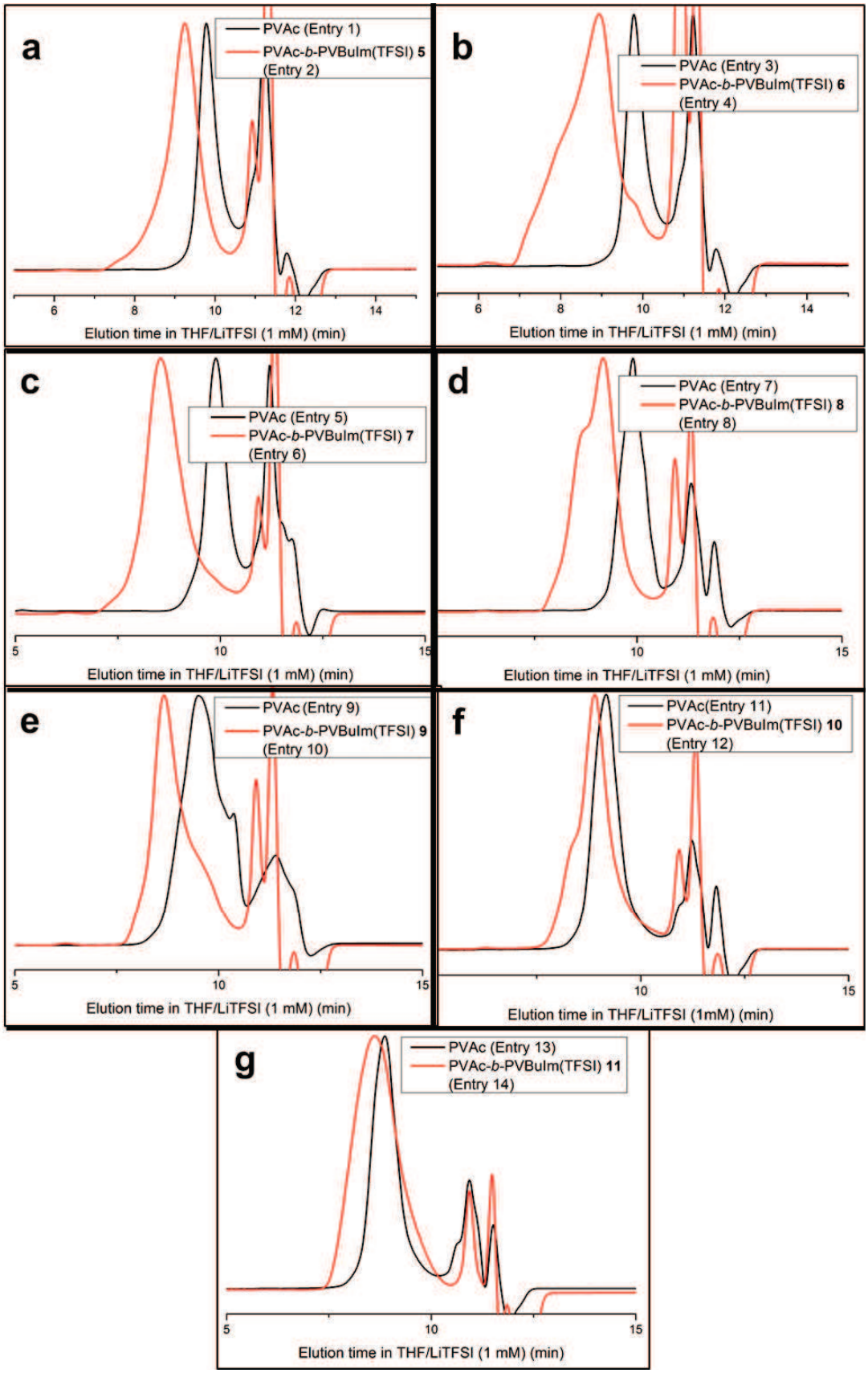

Figure 3. SEC traces of polymers **5-11** eluted in a mixture THF/LiTFSI (10 mM).

As a general trend, it can be stated that samples grown by CMRP using commercially available $Co(acac)_2$ and V-70 as bi-component system showed a less well-defined structure than BCPs obtained from the pre-synthesized alkyl-cobalt (**a**). This might be explained by the excess of radical initiators (V-70) that is needed and that causes a change of the polymerization mechanism, from a reversible deactivation radical polymerization (RDRP) to a degenerative transfer (DT) process, as highlighted in Scheme 3.[44,46,54]

In the latter case, growing polymer radicals are temporarily deactivated by reacting with dormant polymer chains terminated by a C-Co group. Control over this DT process is not as optimal as that prevailing in CMRP by a RDRP process.[44,46,54] However, DT allows maintaining a reasonable level of control.[44]

Note also that our PIL BCPs were synthesized before the procedure by Matyjaszewski *et al.* for SEC characterization was established.[51]

In order to validate our synthetic strategies and, in particular, the efficiency of the crossing-over reaction, characterization of our samples by diffusion ordered spectroscopy (DOSY) 2D NMR was attempted. This technique is based on the Pulsed Gradient Spin Echo NMR experiment, and has already proven useful to evidence BCP formation (Figure 4).[31,55–60] The NMR analysis by DOSY of a block copolymer of general structure X-*b*-Y can indeed reveal the presence of residual X and/or Y homopolymers. The pure X-*b*-Y block copolymer is expected to give rise to a single diffusion coefficient (technically speaking, this is reflected by a unique horizontal straight line). Any deviation would reveal the presence of residual (A or B) homopolymers.

In our case, DOSY NMR experiments were performed on a few PIL BCPs. A representative DOSY NMR spectrum of PVAc-*b*-PVBuImBr **11(Br)** is shown in Figure 4. This DOSY map of **11(Br)** is a two-dimensional correlation showing chemical shifts and diffusion coefficients on the horizontal and vertical axes, respectively.

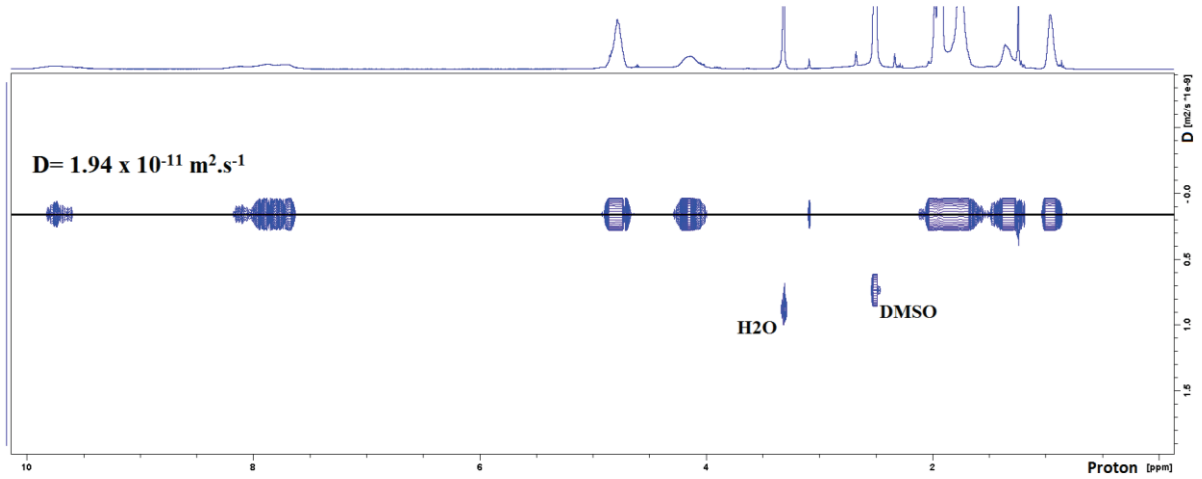

Figure 4. 400MHz 2D DOSY NMR spectrum obtained at 298K in DMSO-δ_6 solution of the copolymer **11(Br)**.

NMR signals due to compounds of different sizes can be clearly distinguished. The ^{1}H NMR spectrum exhibits signals corresponding to both the PVAc block (δ= 4.79; 1.96-1.76 ppm) and the PVBuImBr block (δ=9.72; 7.87; 4.15; 1.37; 0.97 ppm). ^{1}H NMR signals of PVAc and PVBuImBr give rise to the same diffusion coefficient, *i.e.* 1.94 x 10^{-11} $m^2.s^{-1}$, attesting to the effective covalent linkage of the PVBuImBr and the PVAc blocks. To make sure that these was no residual PVBuImBr or PVAc, dilute DMSO solutions of a PVAc (M_n = 10000 $g.mol^{-1}$) and a PVBuImBr (M_n = 10000 $g.mol^{-1}$) were also analyzed by DOSY NMR and were compared to the block copolymer sample (Figure 5-6).

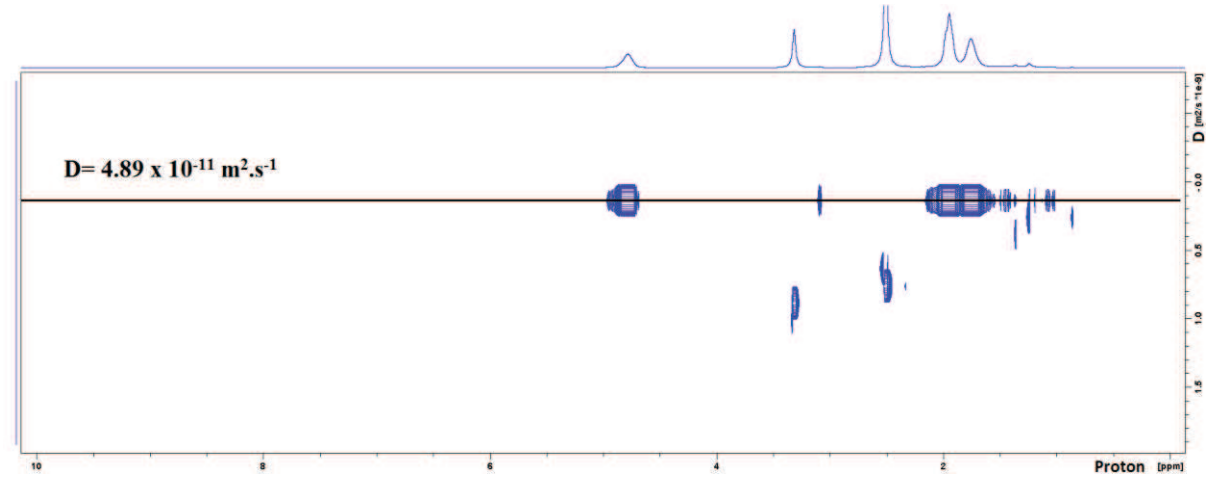

Figure 5. 400 MHz 2D DOSY NMR spectra obtained at 298K in DMSO-δ_6 solution of block PVAc.

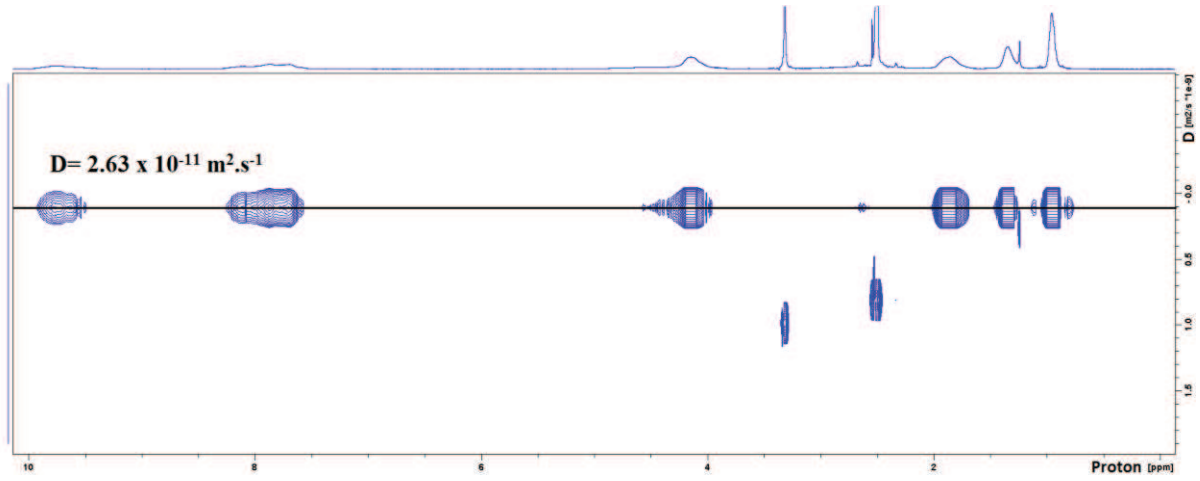

Figure 6. 400 MHz 2D DOSY NMR spectra obtained at 298K in DMSO-δ_6 solution of block PVBuImBr.

The diffusion coefficients of PVAc and PVBuImBr were found to be 4.89 x 10^{-11} $m^2.s^{-1}$ and 2.63 x 10^{-11} $m^2.s^{-1}$, respectively. One can thus conclude that no residual PVAc or PVBuImBr homopolymer was present on the DOSY map of the block copolymer, while the decrease in the diffusion coefficient indicated an increase in the average aggregation size due to the formation of the PVAc-*b*-PVBuImBr PIL BCP. Hence, PVAc-*b*-PVBuImBr BCP **11(br)** formed with a minimum amount -if any- of homopolymer contaminant.

In conclusion, synthesis of rather well-defined poly(vinyl acetate)-*b*-poly(*N*-vinyl-3-alkylimidazolium bromide) diblock copolymers could thus be achieved by sequential cobalt-mediated radical polymerization, using either a mono-component controlling agent (Route A; Scheme 1) or a bi-component system based on *bis*(acetylacetonato)cobalt(II) and a radical source (Route B, Scheme 1). Route A provides a better control over molar masses, dispersities and crossover efficiencies between the PVAc and the PIL block than Route B. However, Route A requires the prior synthesis of the alkyl-cobalt initiator, while Route B employs simple commercially available reagents.

2. Morphological behavior and conductivity of PVAc-*b*-PIL at the solid state

As emphasized in chapter 1 of this manuscript, imidazolium-based PIL BCPs can lead to phase-separated ordered nanostructures by self-assembly at the solid state. The self–assembling properties of our block copolymers were thus investigated, by combining different techniques, such as TGA, DSC, TEM as well as SAXS. The ionic conductivity of some of these ionic compounds with TFSI counter-anions was also evaluated.

2.1. Morphological behavior

As emphasized in the bibliographic chapter (chapter 1), formation of nanostructured morphologies at the solid state dramatically influences the transport properties of PIL BCPs. A preliminary study of the $PVAc_{179}$-*b*-$PVBuImBr_{43}$ **11(Br)**, that was synthesized according to route B Scheme 1, was carried out, before investigations of a more complete series of PIL BCPs, spanning the composition range of 21-82 wt% PIL(Br) (Table 2).

The metathesis reaction was readily accomplished first by reacting PVAc-*b*-PVBuImBr with LiTFSI in MeOH, yielding the PVAc-*b*-PVBuIm(TFSI), as previously described. TGA and DSC analysis of all our PIL BCPs showed a similar thermal stability and a glass transition temperature of ~ 40 °C for the PVAc block, and of ~ 190 °C and ~ 57 °C for compounds with a Br^- and a TFSI counter-anion, respectively. These results are consistent with other reported data where ILs and PILs had a lower T_g, as well as a higher thermal stability than their counterparts with bromine anions.[52,61]

Typical analysis by DSC of PVAc-*b*-PVBuImBr **11(Br)** is shown in Figure 7, where two glass transition temperatures (T_g ~ 42 °C and 191 °C) are noted, indicative of a phase segregation at the solid state. In the case of PVAc-*b*-PVBuIm(TFSI), the T_g of the PVAc was again detected at approximately 42 °C, and the second T_g value was observed at 57.2 °C,[61] which corresponded to the PVBuIm(TFSI).

The thermal degradation profile of both PIL BCPs is provided in Figure 7b. As expected, compound with Br^- anions exhibited a slightly lower thermal stability (decomposition temperature, T_d, determined by 5 wt% loss), compared to its homologue with the bulkier TFSI anions (initial weight loss at 285 °C *vs*. 295 °C).[52]

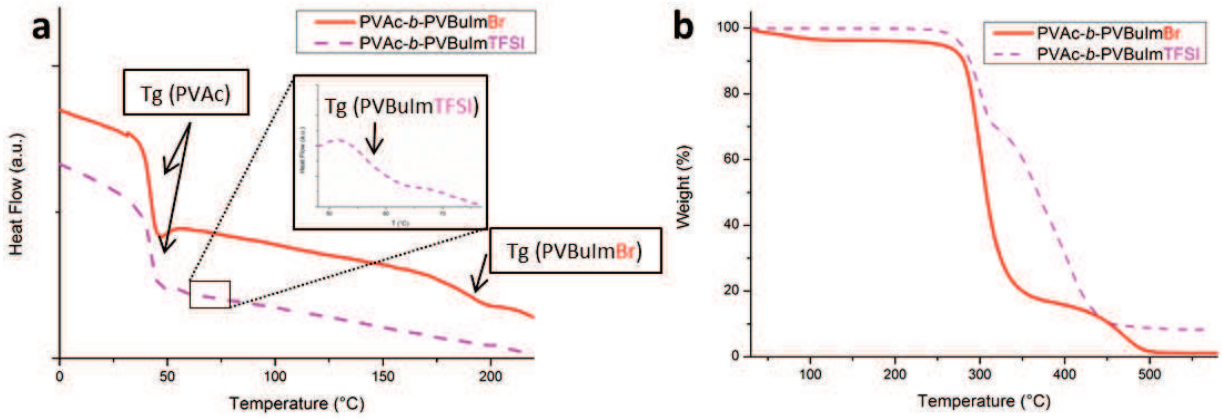

Figure 7. (a) DSC and TGA (b) curves of $PVAc_{179}$-*b*-$PVBImBr_{43}$ **11(Br)** (red/solid) and $PVAc_{179}$-*b*-$PVBIm(TFSI)_{43}$ **11(TFSI)** (pink/dash).

The solid-state morphology of the two PIL BCPs copolymers **11(Br)** and **11(TFSI)** was then investigated by temperature-dependent synchrotron small-angle X-ray scattering (SAXS) at the ESRF Grenoble (collaboration with Dr. G. Fleury and Dr. K. Aïssou from the LCPO) and transmission electron microscopy (TEM).

These combined techniques revealed the formation of well-structured nanodomains in the form of lamellar phases, in both cases, as illustrated in Figure 8. Note that these observations were made from thin solid sample cut from raw materials of the two BCPs without any thermal annealing.

Self-assembly in bulk of other families of PIL BCPs discussed in chapter 1 have demonstrated the importance of sample preparation on morphologies.[31,39,42] Attempts to obtain thin films by spin-coating following by thermal or solvent annealing were not successful in our case. Indeed, optical microscopy evidenced partial dewetting hampering viable measurements (see Figure S1).

SAXS patterns of $PVAc_{179}$-*b*-$PVBuImBr_{43}$ **11(Br)** obtained in a 30-260 °C range temperatures showed the presence of four-order peaks located at q/q^* ratios of 1, 2, 3, 4 (where q^* is the position of the primary scattering wave vector, q_{100}). This series of reflections is consistent with a layered periodic symmetry of a highly ordered lamellar organization, consisting here of alternating PVAc and PVBuImBr layers. A characteristic interdomain spacing of $2\pi/q^* \approx 39$ nm was determined.[62,63]

The observation of both several higher-order reflections in the SAXS pattern and relatively high interdomain spacing (in comparison with more traditional uncharged BCPs) indicated a significant degree of long-range order, due to a strong microphase separation between the two blocks. Similar observations were recently described for other charged and uncharged PIL BCP architectures, where PIL chains exhibit a high degree of chain-stretching leading to rather large domain spacings.[39,42] Hence, PVAc and PVBuImBr might be strongly incompatible (large Flory-Huggins χ_{12} parameter, that is the degree of incompatibility of the two blocks).[62–64]

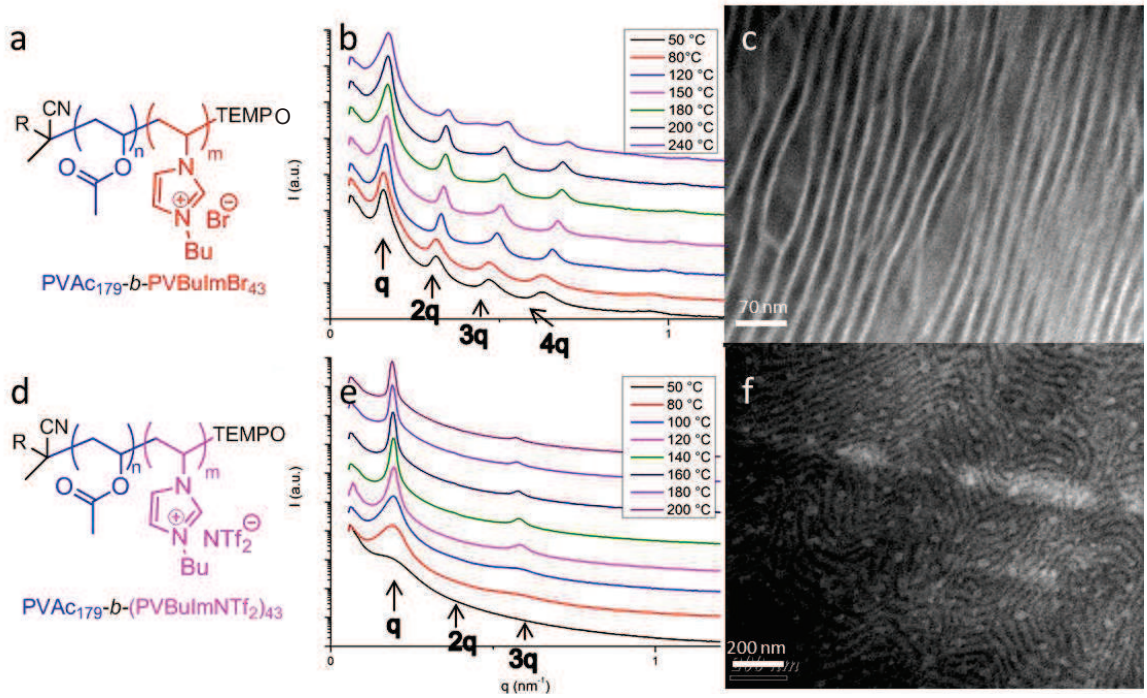

Figure 8. SAXS (b) and TEM micrograph (c) of $PVAc_{179}$-*b*-$PVBuImBr_{43}$ **11(Br)** (a). SAXS (e) and TEM micrograph (f) of and $PVAc_{179}$-*b*-$PVBuIm(TFSI)_{43}$ **11(TFSI)** (d).

Temperature-dependent X-ray scattering indicated no change in morphology for the temperature range of 30−200 °C. Therefore, no order-order or order-disorder transitions were observed and only minor deviations in domain spacing in this temperature range was noted. However, a peak appeared at a position √7q when increasing temperature up to 260 °C. This could be attributed to a morphological change of the mesostructure, from a lamellar phase to another non identified microphase-separated structure, owing to a decrease of the χ_{12} with the temperature.

In the 30−200 °C temperature range, TEM images of **11(Br)** clearly indicated a microphase-separated bulk morphology with a characteristic lamellar organization. Two different contrast levels were observable in TEM images, with the darkest regions corresponding to PVBuImBr microdomains, while PVAc lamellae appeared white due to the lower density of this polymer. The measured interdomain spacing was around 35 nm, which was roughly in accordance with the SAXS data (ca. 39 nm).

TEM also attested to some morphological differences when annealing a film above 200 °C for only 10 min (Figure 9). Visualization of a distinct morphology could not be clearly established, however, TEM pictures seemingly indicating the presence of a blend composed of both layered structure and a hexagonally packed structure that could be tentatively attributed to hexagonal perforated lamellae. A few papers from the PIL BCP literature have

reported such a coexistence of lamellae and hexagonally packed cylinders, in a range of composition of 34-40 wt% PIL.[42,65–68]

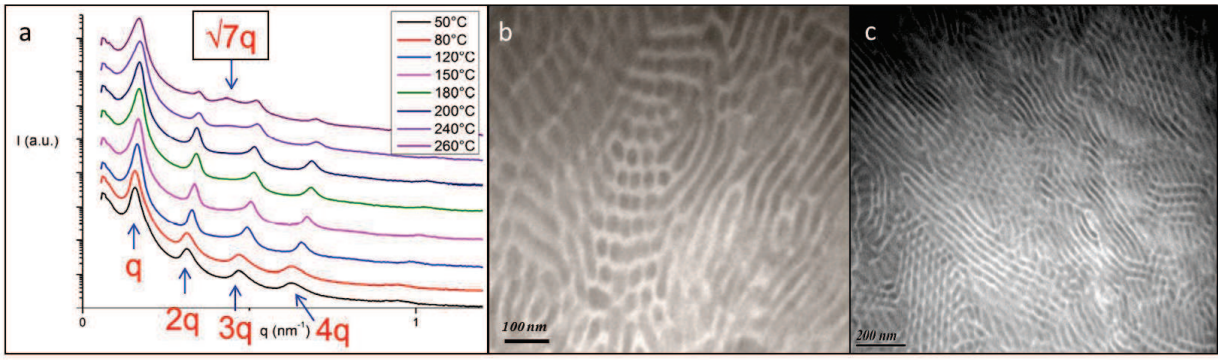

Figure 9. SAXS measurements of **11(Br).** (b and c) TEM micrograph after thermal annealing at 200 °C for 10 min of **11(Br)**.

TEM characterization of the $PVAc_{179}$-*b*-$PVBuIm(TFSI)_{43}$ PIL BCP **11(TFSI)** obtained after anion exchange also showed a lamellar mesostructure, which was corroborated by SAXS data. Both a broad and a minor peak at low temperature, at q/q^* ratios of 1 and 3 only, was indeed observed. The major peak at $q/q^* = 1$ sharpened as the temperature was increased.

Interestingly, suppression of the second order reflection in this sample, over a large temperature range, strongly suggested a symmetric volume fraction ($f_v \approx 0.5$) for this particular block copolymer.[39,42,62,63,69,70] Since the density of both PVBuImBr and PVBuIm(TFSI) homopolymers is not known, we could not directly correlate the weight fraction values of our PIL BCPs (here X = 38.8% and 52.9%, before and after anion exchange, as determined by ^{1}H NMR from the sample with Br^- anions) to volume fractions (f_v). However, assuming that $f_v = 0.5$ for this particular $PVAc_{179}$-*b*-$PVBuIm(TFSI)_{43}$, a rough estimate of the density of $PVBuIm(TFSI)_{43}$ gave a value of 1.38 $g.cm^{-3}$. Knowing this value of density of this PIL is particularly interesting for the determination of the volumic fraction (see Table 3) and for the design of other BCPs by CMRP. Unfortunately, such a calculation was not possible for PIL BCP samples consisting of the bromide anions.

In this case, the characteristic period determined from SAXS data, $2\pi/q \approx 32$ nm, was smaller than that obtained for the parent $PVAc_{179}$-*b*-$PVBuImBr_{43}$ (39 nm). This might be explained by a conformational change of the PIL block after anion exchange. Note that the latter result contrasts with previous observations made from other PIL BCP compounds, where larger anions gave a higher domain spacing.[29]

Analysis of the other PIL BCPs (**6**, **7**, **8**, **9**, **10** and **11)** featuring either a Br^- or a TFSI

counter-anion, showed either a lamellae (Lam) or a hexagonally packed cylindrical (Hex) morphology, as summarized in Figure 10. In other words, neither spheres on a body-centered-cubic lattice nor the bicontinuous gyroid mesophase were observed with the range of composition of our samples (see Table 3). Identification of a well-identified mesophase was also difficult in some cases using the SAXS experiments from Nanostar-U instrument (Bruker AXS) (Centre de Recherche Paul Pascal, Pessac, France), despite a χ_{12} parameter that is probably high for the PIL BCPs.

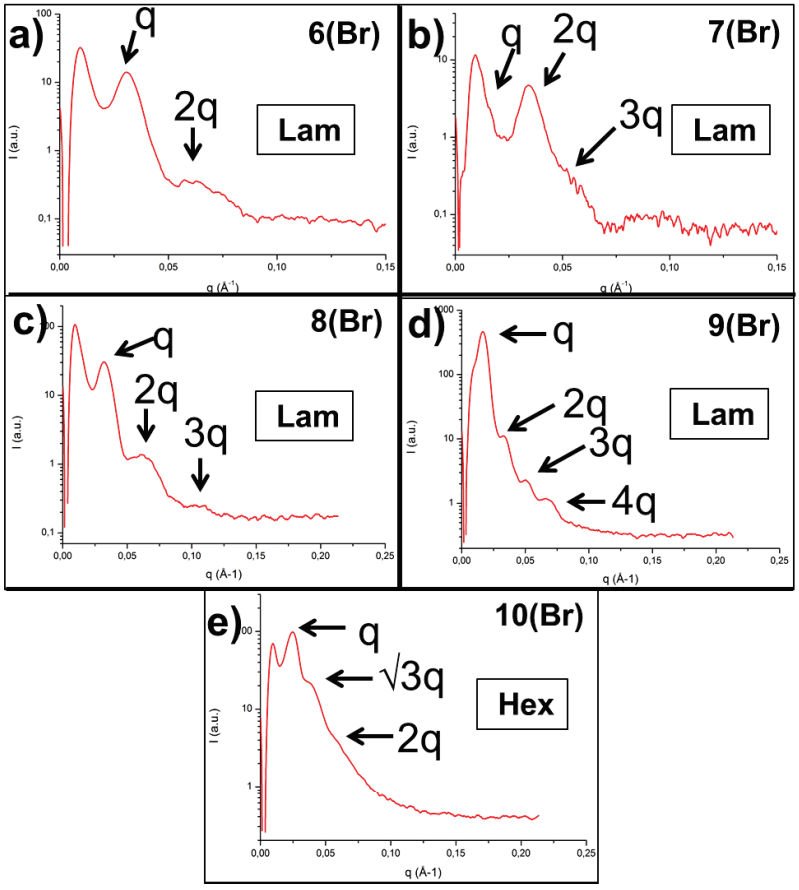

Figure 10. SAXS measurements of PVAC-*b*-PIL(Br): a) **6(Br)**; b) **7(Br)**; c) **8(Br)**; d) **9(Br)**; e) **10(Br)** achieved in CRPP, Bordeaux.

The series of reflections in Figure 10 are consistent with a layered periodic symmetry of a highly ordered lamellar organization. Domain spacings (d_{100}) for samples **7 (Br)** and **11(Br)** were very similar ~ 39 nm. This result was not expected, considering the PIL weight fraction that differed significantly from one sample to another (82 and 39 wt%, respectively). However, an intermediate weight fraction of 45 wt% of PIL for sample **9(Br)** exhibited a characteristic period of 27 nm. The characteristic lamellar period, as determined from SAXS data, of both samples **6(Br)** (72 wt% of PIL) and **8(Br)** (53 wt% of PIL) was found equal to

14 nm. However, it was not possible to draw conclusions about the influence of the PIL weight fraction on the lamellar domain sizes.

Compound **10(Br)** with a composition of 21 wt% in PIL revealed diffraction reflections that were consistent with hexagonally packed cylinders, at q/q^* ratios of 1, √3, 2. The inter-cylinder distance ($2d_{100}/\sqrt{3}$) was found to be 22 nm. The presence of this BCP morphology was consistent with our previous findings regarding compound **11(Br)** whose change in morphology with temperature, from lamellae to hexagonally packed cylinders, was noted.

It is highly likely that there is a range of composition, *i.e.* between 21 and 33 wt% in PIL, where lamellae and hexagonally packed cylinders may coexist.[71] From a theoretically point of view, however, and considering that PIL BCPs would behave as nonionic coil-coil regular BCPs, the composition region located between lamellae and hexagonally packed cylinders should be occupied, at equilibrium, by the bicontinuous gyroid phase.[14,69] Coexistence of Lam and Hex phases,[42,65–68] or the presence of metastable hexagonally perforated lamellae phase has already been reported for other PIL BCPs (see chapter 1).[69,72,73] Hence, absence of the gyroid phase could be explained by a high segregation regime,[74] owing to the conformational asymmetry between PVAc and PIL blocks. However, another possible explanation is the fact that our samples would exhibit a rather broad molar mass distribution, as discussed previously.[75] Spheres on a body-centered-cubic lattice were not observed because this morphology would have required a higher asymmetric composition (PIL weight fraction < 20 wt% of PIL).

Table 3. Morphological behavior of CMRP-derived PIL BCPs

Entry	n:m[a]	$M_{n,PVAc}$ (g.mol^{-1})[b]	$M_{n,PIL(Br)}$ (g.mol^{-1})[c]	$M_{n,PIL\ BCP}$ (g.mol^{-1})	PIL wt (%)	f_{PIL}[d]	Morphological behavior[e]
6(Br)	65:62	5600	14300	19900	72	n.d.[f]	Lam
6(TFSI)	-	-	26700	32300	83	83	n.d.[f]
7(Br)	54:92	4700	21200	25900	82	n.d.[f]	Lam
7(TFSI)	-	-	39700	44400	89	89	n.d.[f]
8(Br)	84:36	7300	8300	15600	53	n.d.[f]	Lam
8(TFSI)	-	-	15500	22800	57	68	n.d.
9(Br)	163:51	14200	11800	26000	45	n.d.[f]	Lam
9(TFSI)	-	-	22000	36200	61	57	Lam
10(Br)	179:18	15600	4200	19800	21	n.d.[f]	Hex
10(TFSI)	-	-	7800	23400	33	30	Hex
11(Br)	179:43	15600	9900	25500	39	n.d.[f]	Lam (+Hex)
11(TFSI)	-	-	18300	33800	53	50	Lam

[a] n = number of VAc units; m = number of IL units [b] M_n obtained By SEC measurement in THF. [c] M_n Obtained by ^{1}H NMR spectroscopy. [d] Volume fraction of the PIL BCP using a density of 1.38 g.cm^{-3} for the PIL block: $f_{PIL} = (M_{n,PIL(TFSI)}/1.38)/((M_{n,PVAc})/1.19)+(M_{n,PIL(TFSI)}/1.38))$. [e] Morphological behavior determined by SAXS and/or TEM. [f] not determined.

Unfortunately, the lack of contrast between the PIL(TFSI) block and PVAc block did not allow us to conclude about the morphological behavior, except for PIL BCPs **9(TFSI)** and **11(TFSI)**. The composition ratio of these two samples is very similar, with a PIL weight fraction of 61%. SAXS data and TEM images showed the existence of a lamellar mesostructure, but no second order reflection (Figure 11), again suggesting a symmetric volume fraction close to $f_v \approx 0.5$. Note again that this SAXS equipment is not as powerful as the synchrotron used in ESRF, Grenoble. Here, the characteristic period determined from SAXS data is also smaller than their parent PVAc-*b*-PIL(Br) (22 *vs* 27 nm respectively), in agreement with our previous results from sample **11(TFSI)**.

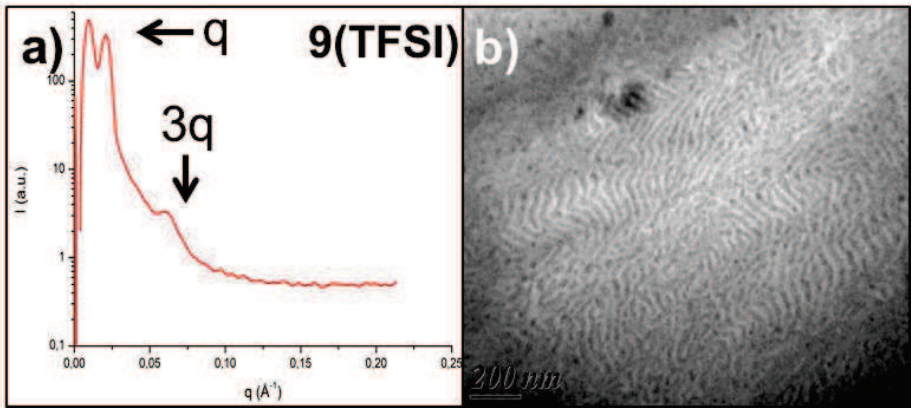

Figure 11. (a) SAXS measurements of $PVAc_{163}$-*b*-$PVBuIm(TFSI)_{51}$ **9(TFSI)**. (b) TEM micrograph of $PVAc_{163}$-*b*-$PVBuIm(TFSI)_{51}$ **9(TFSI)**.

Finally, SAXS experiments were also performed with both the di- and symmetric triblock copolymers, PVAc-*b*-PVEtImBr **1(Br)** and PVAc-*b*-PVEtImBr-*b*-PVAc, which were previously reported.[43] The symmetric PVAc-*b*-PVEtImBr-*b*-PVAc triblock copolymers were synthesized radical coupling of parent PVAc-*b*-PVEtImBr diblocks, in the presence of isoprene as coupling agent (Scheme 1, Route A). The weight fraction in PIL of these triblocks is 50%. The presence of well-defined peaks at q/q^* ratios of 1, 2, 3, 4 in a temperature range of 30-220 °C again unambiguously indicated that both architectures self-organized in bulk into lamellae, with a very similar phase behavior (Figure 13).[76,77] However, a small difference in interdomain spacings (11.1 vs. 10.4 nm, for the triblock and its parent diblock sample, respectively) was determined, which is consistent with predictions by Matsen et al., as illustrated Figure 12.[76] Indeed, the presence of end segments in diblock copolymers slightly decreases the degree of segregation. "*Consequently, triblock melts remain ordered to higher temperatures than their diblock counterparts.*"[76]

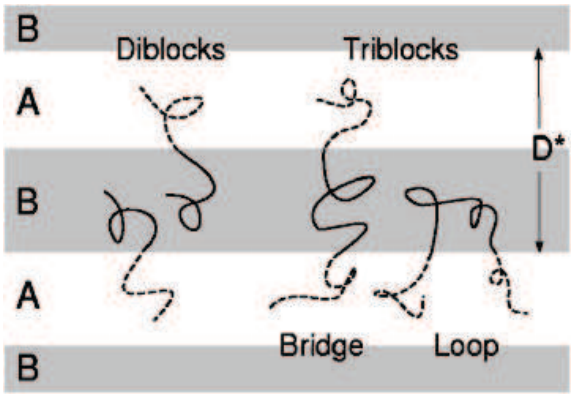

Figure 12. Schematic illustration of lamellar morpholgy induced by the phase segregation of di- and triblock copolymers, adapted from reference 76.

This was verified in our systems, where the triblock sample exhibited more detectable reflections at high temperature. In addition, triblock copolymers are expected to provide better mechanical at the solid state, due to possible physical network connecting the nanodomains.[77]

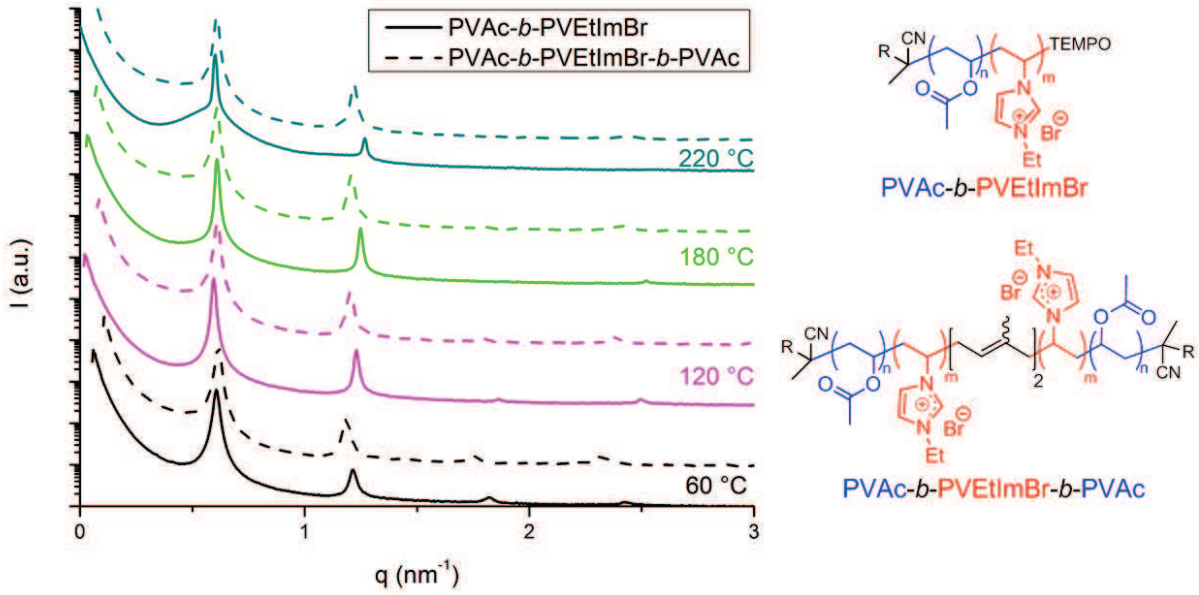

Figure 13. SAXS of $PVAc_{46}$-*b*-$PVEtImBr_{20}$ **1(Br)** (solid) and $PVAc_{46}$-*b*-$PVEtImBr_{52}$-*b*-$PVAc_{46}$ (dash).

2.2. Conductivity measurements

The potential of PVAc-*b*-PIL as single-ion conductors at the solid state was then explored. Here we provide our preliminary results regarding their ionic conductivity, without a thorough optimization. As previously discussed in chapter 1, external parameters have a strong influence on the ionic conductivity, which includes the relative humidity, the temperature or the use of exogenous ILs. Use of self-assembled BCPs for transport properties allows developing mechanically robust nanostructured materials, providing PIL domains as connecting paths for ion conduction. Whether microphase segregation can favor ionic conductivity properties or not, is still an open debate in the current literature. In addition, comparison is hard to be made because some values from the literature were likely obtained in presence of residual monomer, and/or under relative humidity.[33–35,37–42,67,78,79]

The ionic conductivity of our PIL BCPs was evaluated both at LCPO, in collaboration with Dr. G. Fleury and Dr. K. Aïssou, and with Dr. A. Serghei and Pr. E. Drockenmuller at IMP, Lyon. In LCPO, we measured the temperature dependence of the anhydrous ionic conductivity σ* (ω, *T*) of PVAc-*b*-PVBuIm(TFSI) by electrical impedance spectroscopy (EIS).

Polymers **7**, **8**, **9**, **10** and **11** with TFSI counter-anions (Table 2) were first solvent casted onto an indium tin oxide (ITO) glass substrate, and annealed 10 min at 65 °C. Copolymer **6** was only solvent-casted but not annealed. Then, an aluminium electrode thick was placed on top of the polymer film, as illustrated in Figure 14. In this case, σ* (ω, *T*) was measured in the 100 – 10^6 Hz frequency range, under isothermal conditions, with temperatures ranging from 90 °C to RT and increments of 10 °C under an inert nitrogen atmosphere.

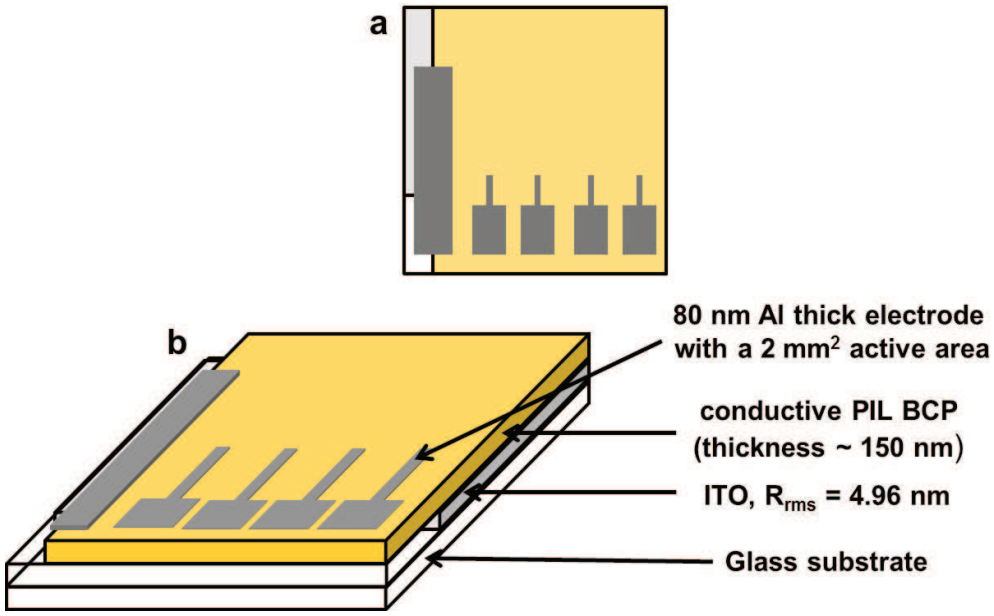

Figure 14. Illustration of the cell stacking for the PIL BCP ionic conductivity measurements.

The PIL BCP resistance R_{film} was extracted from the impedance spectra fitted by means of an equivalent electrical randle circuit that is displayed in Figure 16. The equivalent circuit is composed of the electrode resistance $R_{contact}$ in series with a high-frequency capacitance which is in parallel with PIL BCP resistance, R_{film}, in series with the blocking electrode/electrolyte interfaces noted W. Finally, the conductivity was calculated following equation 1. Film thicknesses were measured after ionic conductivity measurements by AFM, as illustrated in Figure 15.

$$\sigma_{DC} = \frac{1}{R_{film}} * \frac{L}{S} \qquad (1)$$

σ : ionic conductivity (S/cm)
R_{film} : resistivity (ohms)
L : film thickness (cm)
S : Electrode contact surface (cm²)

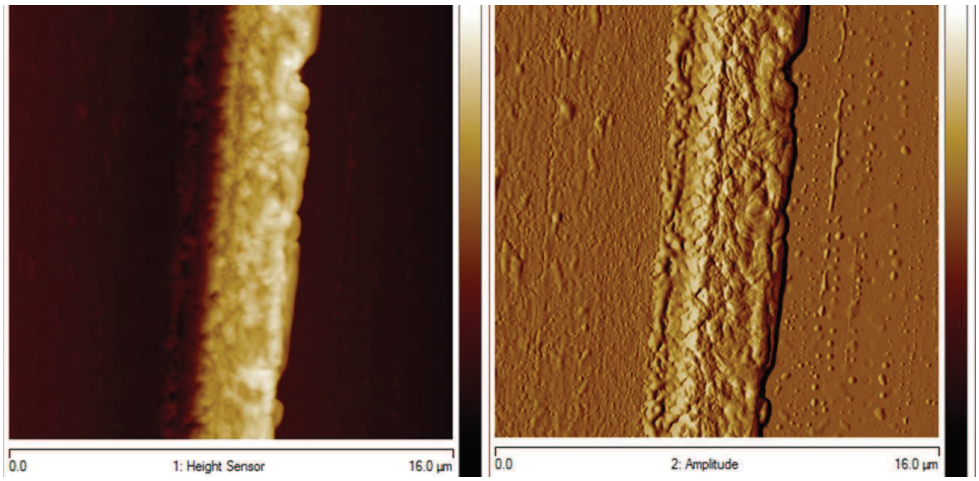

Figure 15. AFM images enabling the film thickness measurement of sample **9**, L = 110 nm.

Direct current conductivity (σ_{DC}) values were obtained from the plateau in the domains considered for PVAc-*b*-PVBuIm(TFSI) are reported as a function of inverse temperature (Figure 16).

Under such conditions, ionic conductivity of sample **6** (σ_{DC} = 3.10^{-8} S/cm at 30 °C) was found significantly higher, by 1-2 orders of magnitude than that of the other copolymers. However, no significant difference could be noted between copolymers **6** and **7**, for instance, which are yet of different composition.

Since samples were also analyzed by GISAXS at the synchrotron in Grenoble, this could have degraded the film homogeneity. In addition, dewetting of some samples was noted after measurements, which could explain the rather low ionic conductivity.

Values of σ_{DC} for all of the prepared PIL BCPs range from $\sim 10^{-10}$ to $\sim 10^{-4}$ S cm^{-1}, but it was rather difficult to draw a clear relationship between these values and the composition of the samples. However, our results are in the same range of the ionic conductivity for other PIL BCPs reported in the literature (σ_{DC} between 10^{-9}-10^{-4} S/cm; see chapter1).

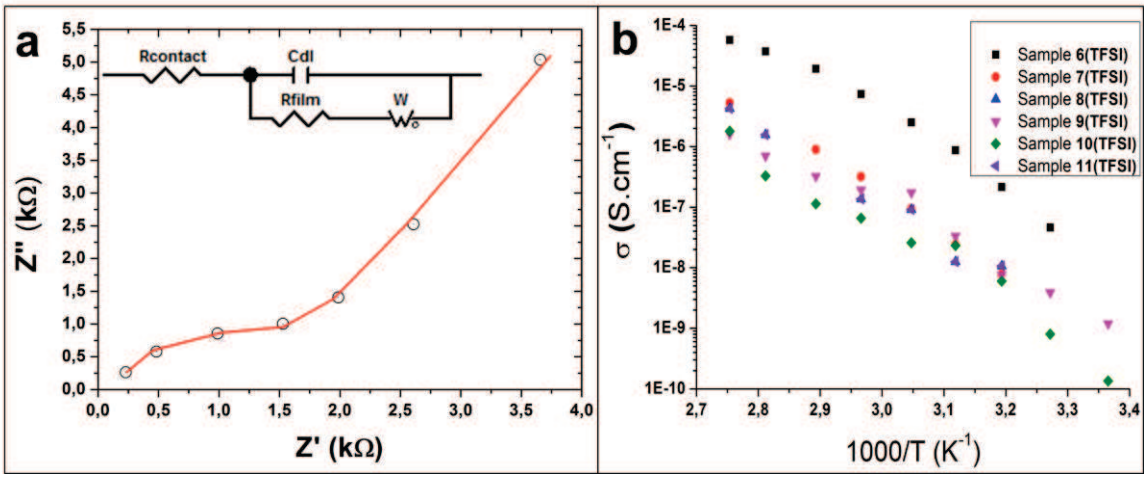

Figure 16. a) Imaginary impedance *vs* real impedance at 90 °C for $PVAc_{65}$-*b*-$PVBuIm(TFSI)_{62}$ **6(TFSI)**; b) Conductivity *vs* inverse temperature for PIL BCPs with TFSI counter-anions.

Ionic conductivity of copolymer **6(TFSI)** followed a Vogel-Fulcher-Tammann (VFT) dependence, evidencing correlation between the charge transport of the ionic species and the molecular mobility of the polymer matrix. Temperature-dependent ionic conductivities reported in Figure 16 were thus fitted with the VFT equation 2, where σ_∞ is the ionic conductivity in the limit of high temperatures, B is the fitting parameter related to the activation energy of ionic conduction, and T_0 is the Vogel temperature which ranges from 30 to 70K below the *Tg*.

$$\sigma_{DC} = \sigma_\infty \times e^{\left(\frac{-B}{T-T_0}\right)} \quad (2)$$

Table 4. VFT equation values of the PIL BCP **6(TFSI)** (results from Bordeaux).

Sample	σ_{DC} at 30 °C (S/cm)	σ_∞ (S/cm)	B (K)	T_O (K)
6(TFSI)	3.10^{-8}	1101	1.01	280

Surprisingly, the temperature-dependent ionic conductivity of many of our PIL BCPs followed an Arrhenius behavior, instead of a VFT dependence, similar to that reported for hydrated homoPILs.[80] The Arrhenius activation energies determined for PIL BCPs **7**, **8**, **9**, **10** and **11** with TFSI counter-anions are 12.7, 11.4, 8.31, 10.58, 11.36 kJ/mol respectively. The Arrhenius behavior eventually involved the presence of humidity or hydrated PIL BCPs rather than hydrophobic PILs that would exhibit a VFT behavior. This could be due to long exposure in air atmosphere of our samples during the GISAXS measurements.

In contrast to the temperature-dependent ionic conductivity of hydrophobic PILs obeying a VFT behavior, the ionic conductivity of hydrophilic PILs dramatically depends on the level of hydration.

To gain a further insight into the ionic transport porperties of our compounds, we sent the $PVAc_{174}$-*b*-$PVBuIm(TFSI)_{74}$ **12(TFSI)** sample to Pr. E. Drockenmuller and Dr. A. Serghei at IMP (Lyon). The sample was solvent casted onto a platinum electrode and annealed at 110 °C in vacuum for ca. 24 hours, in order to eliminate solvent residues and adsorbed moisture. The second platinum electrode was placed on top using 20 μm thick Teflon spacers to build-up a measurement cell in a parallel plate configuration with a well-defined separation distance. The sample was annealed again at 110 °C in the cryostat of the dielectric spectrometer under a flow of pure nitrogen. The complex conductivity function $\sigma^*(\omega,T) = \sigma'(\omega,T) + i\sigma''(\omega,T)$ was continuously monitored during this second thermal annealing to ensure that PIL BCP **12** was stable within the annealing conditions and that a constant value of σ_{DC} was attained before starting the measurements. This annealing procedure ensured the removal of all volatiles and the preparation of well-equilibrated samples, which led to stable and reproducible experimental results.

The complex conductivity function was then measured in a very rigorous manner, *i.e.*, in a broad frequency range (10 MHz – 0.1 Hz), under isothermal conditions and at different temperatures. The measurements were carried out under a flow of pure nitrogen, and the temperature stability was controlled within an absolute error of ± 0.1 K. The applied voltage was low (0.1 V) in order to exclude any possible non-linear effects that could take place at the interface with the measurement electrodes. After completing the measurements in the temperature range between 110 °C and - 20 °C in steps of 10 °C, several temperature points were re-measured to ensure that the experimental results were stable and reproducible.

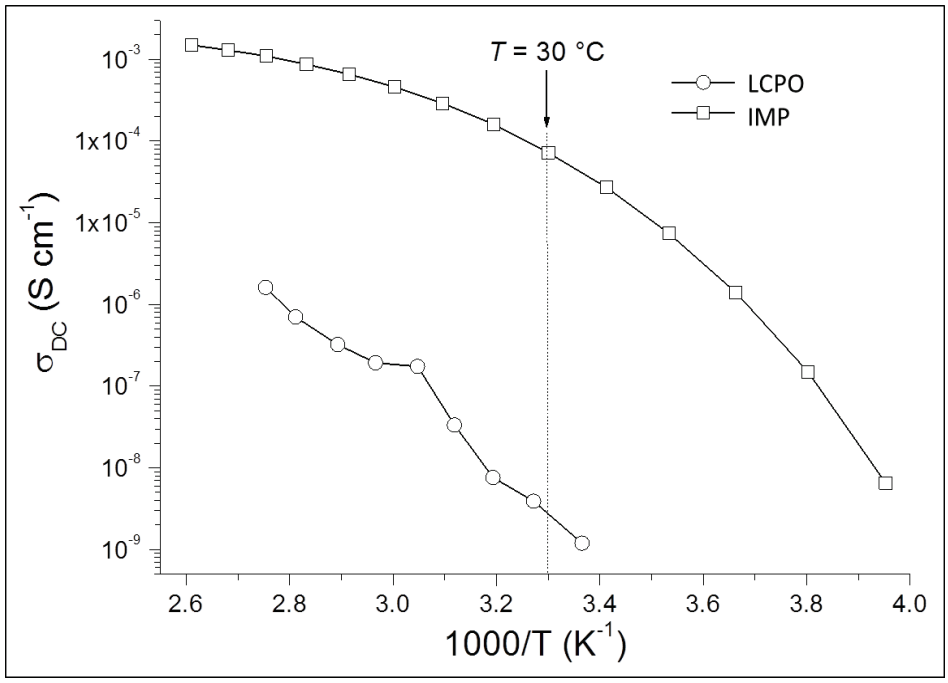

Figure 17. Comparison of Conductivities *vs* inverse temperature for PVAc-*b*-PVBuIm(TFSI) **12** measured in LCPO and IMP by EIS.

The values of σ_{DC} were derived from the plateau of σ' *vs* frequency spectra in the temperature range of -20 °C to 110 °C. These values were reported as a function of the inverse temperature, as depicted in Figure 17.

To our surprise, the ionic conductivity of sample **12(TFSI)**, σ_{DC} at 30 °C ~ 8.10^{-5} S/cm was ca. 4 order of magnitudes higher than the value that was determined at LCPO (σ_{DC} at 30 °C ~ 2.10^{-9} S/cm). This certainly reflected the influence of the sample preparation of the measurement. Results obtained by this second procedure are thus extremely promising and compare well with the highest values of σ_{DC} reported in the literature for other PIL BCPs.[33,39,42,79]

It is interesting to note that this ion-conductive $PVAc_{161}$-*b*-$PVBuIm(TFSI)_{74}$ **12(TFSI)**, which was not described in the previous section due to its close composition with the $PVAc_{163}$-*b*-$PVBuIm(TFSI)_{51}$ **9(TFSI)**, also exhibited a lamellar morphology with a nanodomain period around 26 nm (Figure 18).

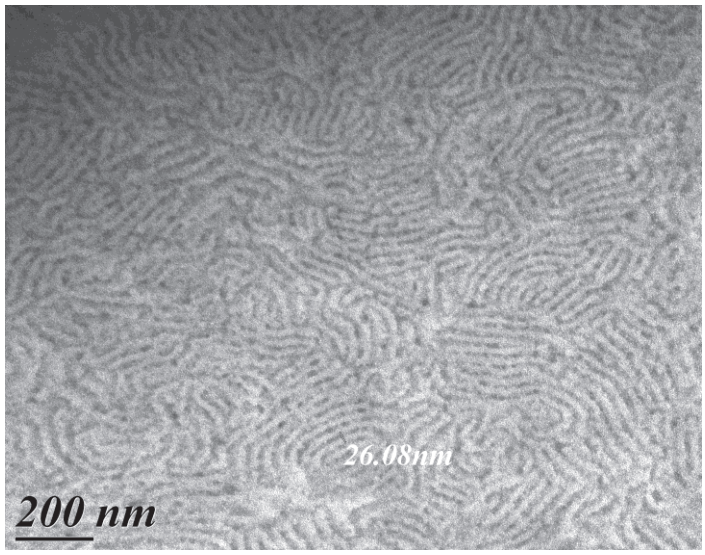

Figure 18. TEM image of the $PVAc_{161}$-*b*-$PVBuIm(TFSI)_{74}$ **12(TFSI)**.

Taking into account these results, we can hypothesize that nanodomain formation by self-assembly allows for enhanced ionic conductivity, compared to homopolymer homologues. A value of ~ 2.5 x 10^{-11} S/cm at 25 °C was reported by Vygodkii. for the homopolymer PVEtIm(TFSI).[81] In addition, ionic conductivity of copolymer **12(TFSI)** followed a Vogel-Fulcher-Tammann (VFT) with values reported in Table 5.

Table 5. VFT equation values of the PIL BCP **12(TFSI)** (Results from Lyon).

Sample	σ_{DC} at 30 °C (S/cm)	σ_∞ (S/cm)	*B*	T_O
12(TFSI)	8.10^{-5}	1.02	523	276

Both sample preparation and nanostructuration thus play an important role in the ion-conductive performances, as already emphasized in chapter 1.[42,80]

The rather low ionic conductivity, as determined at the LCPO, might be due to the difficulty encountered for solvent casting the sample on a glass substrate with ITO. Indeed attempts to analyze the morphological behavior of these PIL BCPs, requiring thin film formation by spin coating, failed. GISAXS, AFM, TEM did not give reliable results compared to SAXS obtained on raw materials, or TEM after cryo-cut. At the IMP in Lyon, the sample was simply deposed on aluminium electrode, followed by thermal annealing to remove the solvent and humidity. This sample preparation procedure thus seemed to provide a more homogeneous sample at the solid state.

3. Self-assembling properties of PIL BCPs in solution

The self-assembling properties in solution of several PIL BCPs described above were also examined. Anion metathesis between the bromine and the bis(trifluorosulfonyl) imide (TFSI) counter-anion on the PIL allowed us to manipulate these solution properties, by switching from hydrophilic ones to hydrophobic polymers.[52]

Various counter-anions were introduced, including bromides, carboxylates, bis(trifluorosulfonyl) imides and cyanoborohydrides, while post-chemical modification of the PVAc block into a poly(vinyl alcohol) (PVA) block by methanolysis allowed us to derive PVA/PIL BCPs.[25,26]

3.1.Self-assembly in solution of PVAc-*b*-PIL(Br)

The PVAc-*b*-PVBuImBr **11(Br)** (Table 2) copolymer that was prepared by CMRP using the bi-component based $Co(acac)_2$ and V-70 was studied. Formation of micelle-like structures could be evidenced by NMR in THF-d_8 and D_2O, that were, selective solvents of PVAc and PVBuImBr, respectively (Figure 19). For instance, the ^1H NMR spectrum in THF-d_8 showed intense peaks corresponding to the protons of PVAc, while peaks due to the protons of the PIL block were weakly intense. The reverse situation was noted in D_2O, where protons of PVAc could not be detected, whereas peaks of PVBuImBr clearly appeared.

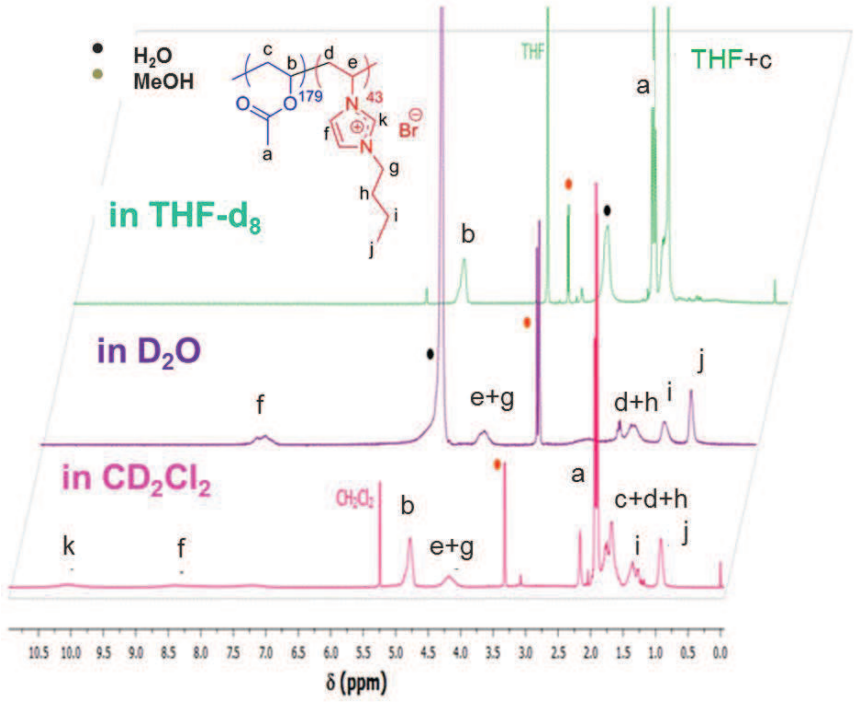

Figure 19. ^{1}H NMR spectrum of PVAc-*b*-PVBuImBr **11(Br)** self-assembly in CD_2Cl_2 (pink), D_2O (purple) and THF-d_8 (green).

Further analyses by dynamic light scattering (DLS) and transmission electron microscopy (TEM) confirmed that this PVAc-*b*-PVBuImBr compound self-assembled into stable and well-defined nanoparticles of different morphologies, depending on the solvent (Figure 20).

The hydrodynamic radius (R_H) of aggregates formed in THF was around 37 nm, as determined by DLS, while TEM images of a THF solution evidenced large compound micelles, corresponding to aggregated spherical micelles with PIL blocks forming the multiple cores of these aggregates.

As visualized by TEM (Figure 20b), the same compound was found to self-assemble into polymeric vesicles (also referred to as polymersomes) in water, with PVAc blocks forming the hydrophobic membrane. The R_H value, as determined by DLS in water, was found to be 175 nm with a relatively uniform size distribution. Considering that amphiphilic $PVAc_{179}$-*b*-$PVBuImBr_{43}$ **11(Br)** has a hydrophilic weight fraction (f) of 38.8%, observation of polymersomes is consistent with the empirical rule proposed by Discher and Eisenberg (polymeric vesicles are generally generated from block copolymers with f around 35±10%).[82]

A schematic representation of nanoparticles, as a result of the self-assembly in solution of $PVAc_{179}$-*b*-$PVBuImBr_{43}$ **11** is shown in Figure 20.

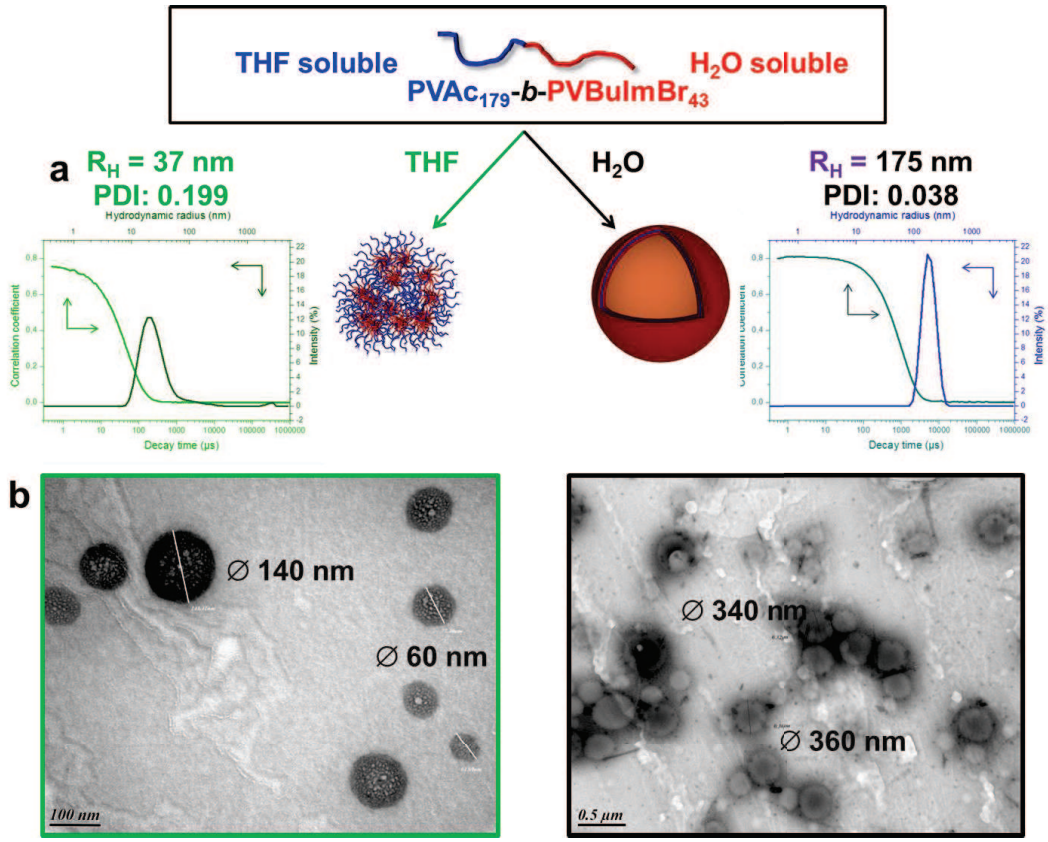

Figure 20. Self-assembly in solution of PVAc-*b*-PVBuImBr **11(Br)**. (a) DLS measurements in THF (green) and H_2O (purple). (b) TEM micrographs of PVAc-*b*-PVBuImBr **11(Br)** in THF (green) and H_2O (purple).

3.2. Self-assembling properties of PVA-*b*-PIL

3.2.1. Methanolysis of PVAc-*b*-PVBuImBr

Chemical modification into PVA was carried out following a well-established procedure.[83] Methanolysis of the PVAc into PVA, using an excess of hydrochloric acid (HCl, 2 eq.) in MeOH at RT for 24h, allowed for a quantitative post-polymerization modification of the $PVAc_{163}$-*b*-$PVBuImBr_{51}$ **9(Br)** into a doubly hydrophilic BCP, PVA_{163}-*b*-$PVBuImBr_{51}$ **13(Br)** (Scheme 5).

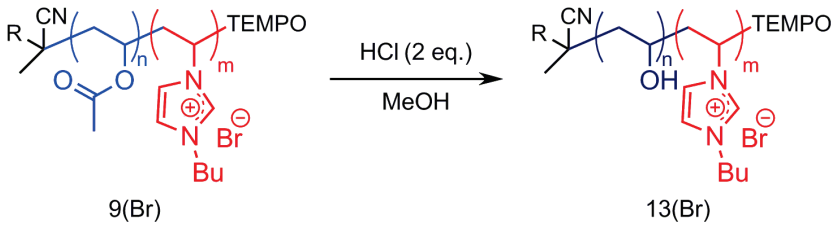

Scheme 5. Synthesis of PVA-*b*-PIL(Br) **13(Br)** by methanolysis of PVAc-*b*-PIL(Br) **9(Br)**.

Characterization by ^{1}H NMR allowed stating on the quantitative reaction. Chemical shifts of the proton of the polymer backbone –*CH*-, from 4.5 to 3.8 ppm, were indeed observed, and the disappearance of characteristic signals of the methyl group –CH_3 due to acetate moieties was clearly evidenced (Figure 21).

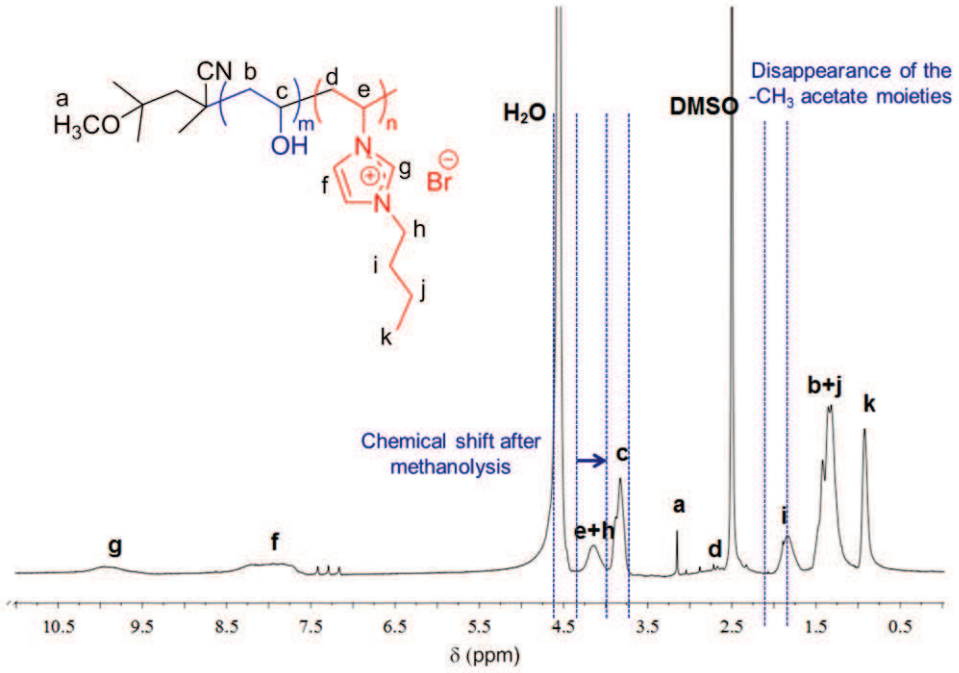

Figure 21. ^{1}H NMR spectrum of PVA-*b*-PVBuImBr **13(Br)** in DMSO-δ_6.

3.2.2. Self-aggregation in solution of PVA-*b*-PIL

The ionic responsiveness of this PIL BCP based on PVA was investigated. With bromide (Br^-) as counter-anion, this PIL BCP was highly soluble in water. The double hydrophilic PVA_{163}-*b*-$PVBuImBr_{51}$ **13(Br)** was next transformed into an amphiphilic PVA_{163}-*b*-$PVBuIm(R'COO)_{51}$ **14** by anion exchange, R' being the hydrophobic adamantyl group, as described above. In contrast to classic anion metathesis (see section 1.1 or in chapter 2 for other examples), the exchange between Br^- and $R'COO^-$ was carried out in pure water. However, and as already discussed in chapter 2, the anion metathesis was not quantitative with such bulky carboxylate counter-anions (~ 27%). The targeted PIL BCP did not precipitate but remained water-soluble, presumably owing to the presence of stabilizing PVA blocks forming the shell of a micelle-like structure.

The self-assembled aggregates were further investigated by DLS and TEM (Figure 23 and Figure 24a). Formation of polymeric vesicles (polymersomes) by self-assembly in solution was expected, considering the hydrophilic weight fraction of this amphiphilic BCP, and on

the basis of the empiric rule of Discher and Eisenberg.[82] Amphiphilic $PVAc_{151}$-*b*-$PVBuIm(R'COO)_{51}$ PIL BCP would have a hydrophilic weight fraction (f) of 29.3% after quantitative anion exchange in agreement with f around 35±10%.

The hydrodynamic radius (R_H) of the aggregates formed in water was found to be 14.2 nm by DLS (Entry A black curve, Figure 23b), with relatively narrow distribution of relaxation times (PDI = 0.176).

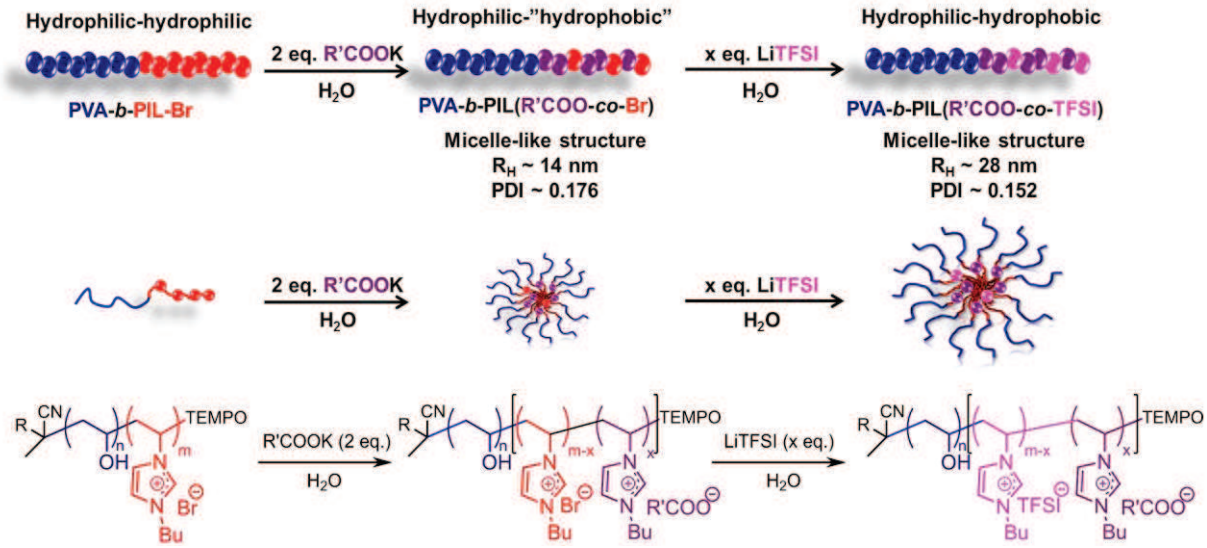

Figure 22. Illustration of size and shape variation induced by the ionic responsiveness of the PVA-*b*-PIL(Br) and their chemical structure.

Thus, after dialysis, the ionic responsiveness of the PIL BCP was investigated by adding LiTFSI (0.3, 0.7 or 1 eq. of IL units) in order to exchange with bromide counter-anions. It is believed that partial anion exchange eventually led to an IL-based copolymer exhibiting a random distribution of Br^-, $R'COO^-$ in the PIL block.

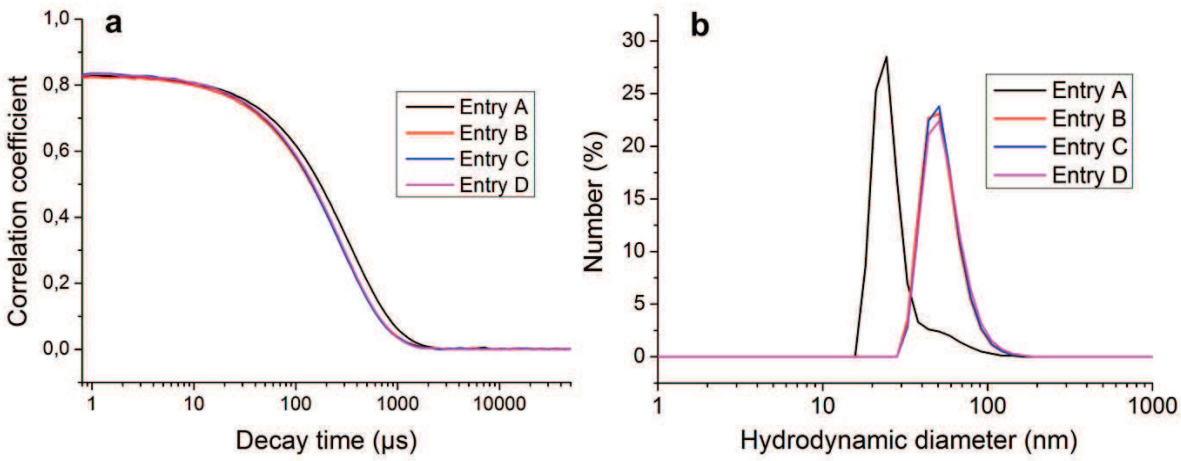

Figure 23. DLS measurements in H_2O of PIL BCP **14** (See Table 6).

Table 6. DLS measurements of PIL BCP **14**.

Reagent added	**A: 2 eq. R'COOK**	**B: A + 0.3 eq. LiTFSI**	**C: A + 0.7 eq. LiTFSI**	**D: A + 1 eq. LiTFSI**
R_H (nm)	**14.2**	**26.9**	**27.6**	**27.7**
PDI	**0.176**	**0.174**	**0.155**	**0.126**

As shown in Figure 23b, the hydrodynamic radius of aggregates formed in water was found to be around 27 nm by DLS, after addition of 0.3 eq. of LiTFSI (entry B), which was twice higher compared to that of the parent PIL BCP **13(Br)**. Further addition of 0.7 and 1 equivalent of LiTFSI to the micellar solution did not increase the size further, which might be explained by the saturation of the micelle-like structures in the hydrophobic core.

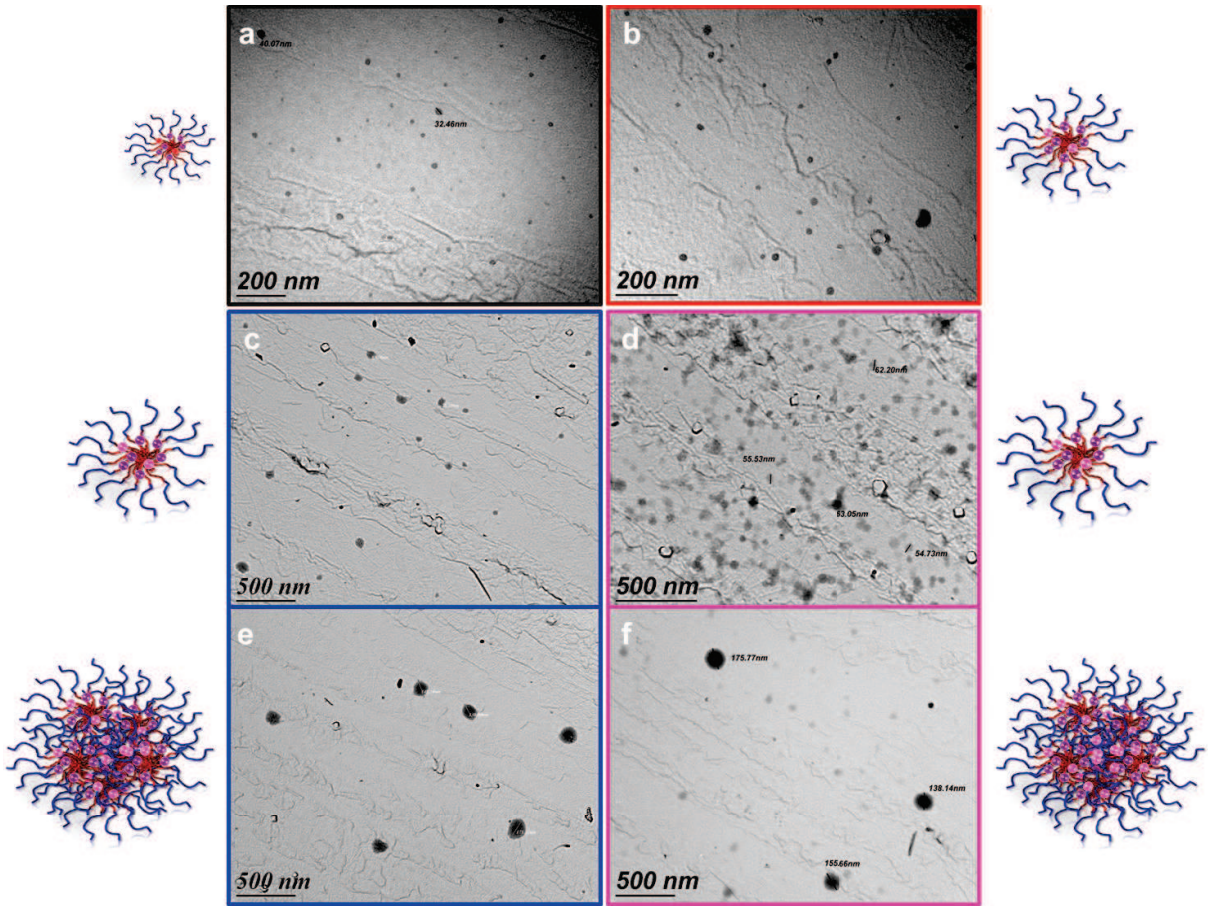

Figure 24. TEM images and schematic illustration of PVA-*b*-PIL BCPs: a) Entry A (Table 6); b) Entry B (Table 6); c) Entry C (Table 6); d) Entry D (Table 6); e) Entry C (Table 6); f) Entry D (Table 6).

TEM images obtained from aqueous solutions of this PIL BCP revealed the formation of aggregated micelles, a rather good correlation in the size between DLS and TEM techniques being found (Figure 24). For instance, the hydrophilic weight fraction of PVA-*b*-PVBuIm(R'COO-*co*-TFSI) **14** were in a range of 26-30% and observations of micelle-like structures are consistent with the prediction of Discher and Eisenberg.[82]

Interestingly, bigger objects, with a R_H in a range of 75-120 nm (TEM images (e) and (f), Figure 24) that could not be detected by DLS measurements were observed by TEM, for samples resulting from the addition of 0.7 and 1 eq. of LiTFSI. Analysis by static light scattering (SLS) in water did not give reliable results, likely because of the formation of big micellar aggregates. One can also hypothesize that TFSI counter-anions partially replaced the carboxylate counter-anions, forming bigger objects.

As illustrated in Figure 22, the hydrophobic content in amphiphilic PVA-*b*-PIL BCPs can be adjusted by varying the extent of the anion exchange, from partial to complete modification. The size and shape of the corresponding aggregates can thus be manipulated.

Furthermore, both the anion exchange and the self-assembly into micelle-like structures occurred simultaneously.

Perspectives of this work would be to achieve core-shell structures for organocatalysis within PIL-based hydrophobic cores of the micelles dispersed that could further generate poly(NHC)s in aqueous media.[84–87] Indeed the micellar system could be composed of a similar block copolymer with a hydrophilic ionic or neutral block as a shell to stabilize the nanostructure in water, while the core would be a statistical PIL block composed of a mixture of carboxylate counter-anions and TFSI to facilitate the self-assembly and protect the active catalytic entities.

4. PVA-*b*-PIL block copolymers as stabilizers and reducing agents for the elaboration of gold nanoparticles

Recently, a few studies have reported the use of ILs acting simultaneously as solvent, stabilizer and reducing agent for the synthesis of metal colloid nanoparticles.[88–90] On this basis, it was tempting to use our PIL BCPs as polymeric surfactants for colloidal dispersion. Some examples have already shown the use of homoPILs for the dispersion-stabilization of silica nanoparticles, carbon nanotubes or graphenes and poly(3,4-ethylenedioxythiophene) (PEDOT).[91–96] The counter-anion can also be used as a true active species, for instance, for the purpose of catalysis (see chapter 1 and also one example in chapter 2, for the use of some of our PILs for carbonatation).[97,98]

In addition, a few reports have evidenced excellent affinity between the PVA and gold nanoparticles.[99–101] Poly(vinyl alcohol) was reported as a good stabilizer of Au nanoparticles, and can meantime be used as reducing agent after few days at room temperature.[99,101,102]

In Polymat (San-Sebastian, Spain), Mecerreyes *et al.* have established that cationic imidazolium-based PILs, bearing specific counter-anions, can be used as oxidizing or reducing agents.[103] Thus cyanoborohydride anion (BH_3CN^-)-containing PILs have been used to achieve gold nanoparticles in aqueous dispersions. Reduction of Au^+ ions to metallic Au(0) occurs thanks to the reducing BH_3CN^- anion, while the cationic PIL backbone allows avoiding the macroprecipitation. It is interesting to note that no specific shape of the nanoparticles has been noted.

We thus looked at PVA-*b*-PIL BCP as both polymeric stabilizer and reducing agent for the preparation of gold nanoparticle synthesis, *via* a combination BH_3CN^- and TFSI as counter-anions (Figure 25).

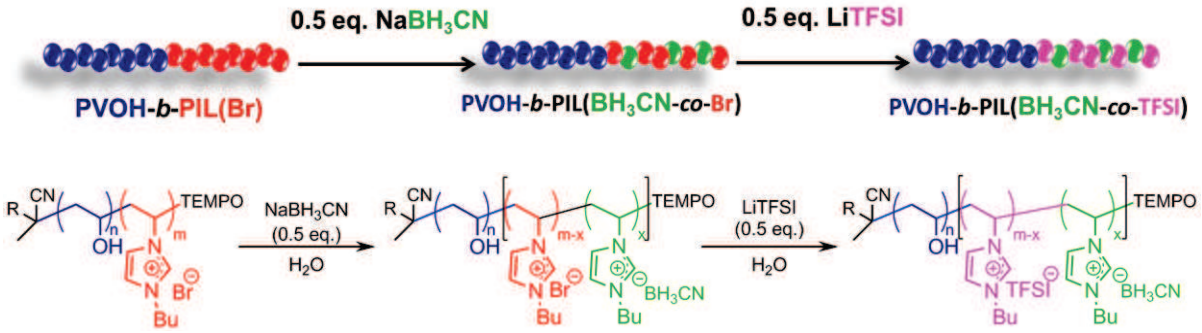

Figure 25. Illustration of the anion exchange between bromide, cyanoborohydride and bis(trifluorosulfonyl) imide counter-anions, and resulting chemical structures.

The PVA_{163}-*b*-$PVBuImBr_{51}$ BCP **13** was again used for this purpose. The anion exchange reaction was carried out in a 2-step sequence. First, anion metathesis was achieved in water, from bromide to cyanoborohydride, using a default of BH_3CNNa (0.5 eq.), in contrast to the use of an excess of carboxylate ions described previously. After dialysis, addition of LiTFSI (0.5 eq.) on the PVA-*b*-PVBuIm(Br-*co*-BH_3CN) copolymer was applied, which quickly formed a micellar solution containing the as-obtained PVA-*b*-PVBuIm(BH_3CN-*co*-TFSI) (**15**) (colourless solution on the left, Figure 26).

Analyses by DLS and TEM of the resulting aqueous solution confirmed that the sample **15** self-assembled into stable and well-defined nanoparticles in water (Figure 20). The hydrodynamic radius (R_H) of aggregates thus formed was around 26 nm. TEM images of a water solution evidenced large compound micelles. However, nano-objects did not proved stable during the drying process on the TEM grid, which could explain their bigger size. Nevertheless, the micelle-like structure formation confirmed the ionic responsiveness of the parent PIL BCP, after dialysis.

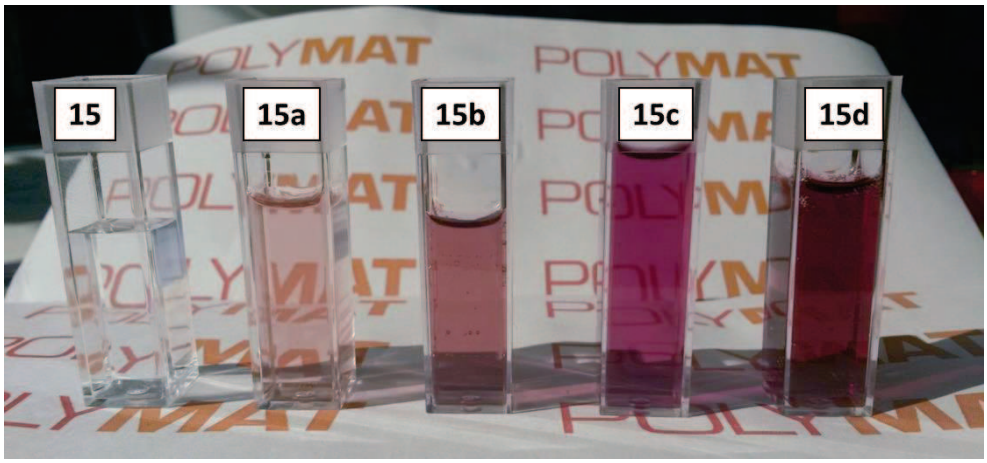

Figure 26. Photograph gold nanoparticles dispersions stabilized by the PIL BCP with various $HAuCl_4$ content. (Respectively **a** = 0.9, **b** = 1.5, **c** =3 and **d** > 3 eq. of reducing agent units).

Following the procedure established in a previous work at Polymat,[103] an aqueous solution of $HAuCl_4$ salt (**a** = 0.9, **b** = 1.5 and **c** =3 eq. of reducing agent units) was added under stirring to the colloidal solution of the PIL BCP. The solution turned pink instantaneously as commonly observed for gold nanoparticle dispersions.[103,104] The coloration is due to the nanoparticle plasmonic resonance. UV-visible spectrum of the dispersion **15c** confirmed the presence of the plasmon band at 523 nm corresponding to the presence of gold nanoparticles smaller than 20 nm (Figure 28). Surprisingly, DLS measurements of the solution after addition of the gold complex did not evidence significant change in the micelle-like structure size.

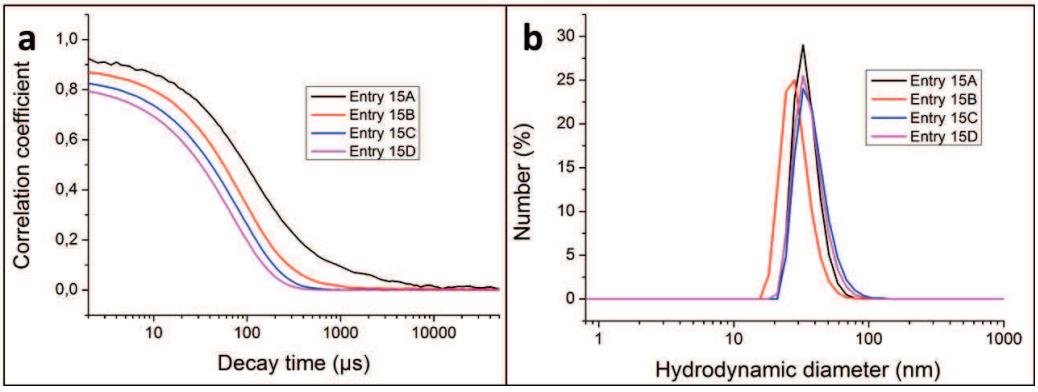

Figure 27. DLS measurements of PVA-*b*-PVBuIm(BH_3CN-*co*-TFSI) **15**.

Originally, we expected a growth of the nanoparticle inside the core-shell structure induced by the PVA-*b*-PVBuIm(BH_3CN-*co*-TFSI) **15** that could increase the nanostructure size. We observed by UV-visible spectroscopy suggested the formation of small gold nanoparticles, similar to those observed in POLYMAT using a PVEtIm(BH_3CN) homoPIL.[103]

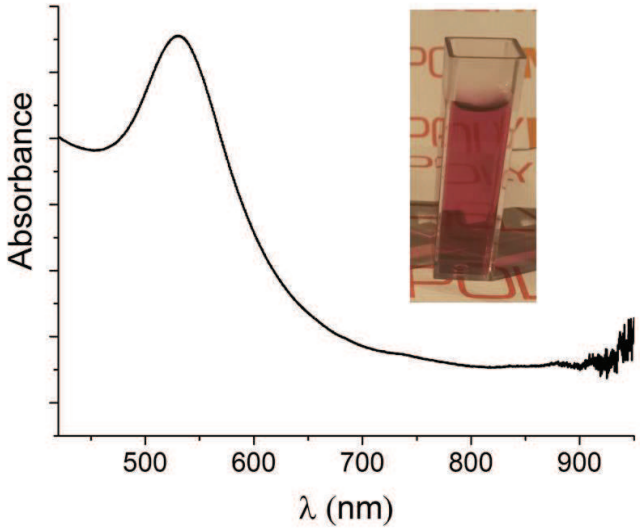

Figure 28. UV-visible spectrum of the gold nanoparticles dispersions **15c** prepared with the PIL BCP **15** as reactant and stabilizer.

However, TEM images showed the formation of anisotropic gold nanoparticles that depended as of the ratio between gold and reducing agent (Figure 29). With a default of gold (0.9 eq. of BH_3CN), we observed the formation of gold nanocubes, while bigger shapes, such as hexagonal or octahedral nanoplates with an excess of $HAuCl_4$ were identified (Figure 29).

The fact that core-shell micelles were not observed was probably due to the PVA block playing the role of polymeric stabilizer,[102] that also impacted on the growth of the gold nanoparticles (Figure 29e). These preliminary results thus suggested that the molar ratio PIL BCP to gold is a key factor to produce shaped gold nanoparticles. Further experiments should be investigated at POLYMAT, to better understand the role played by the PVA-*b*-PIL in comparison to the homoPIL homologues.[103]

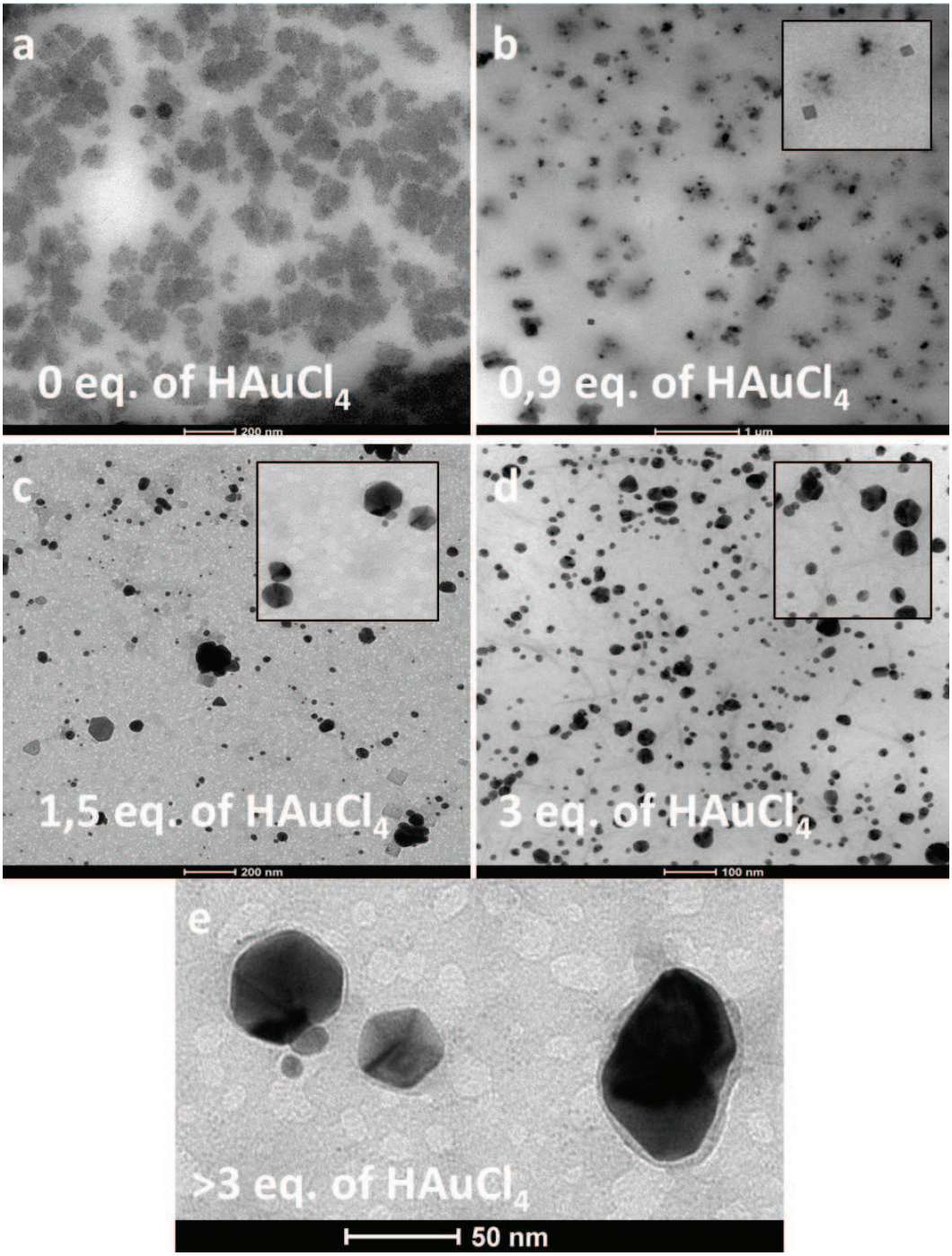

Figure 29. TEM images of gold nanoparticle dispersions.

Conclusion

A novel family of imidazolium-based poly(ionic liquid) block copolymers (PIL BCPs), namely poly(vinyl acetate)-*b*-poly(*N*-vinyl-3-alkylimidazolium bromide), denoted PVAc-*b*-PIL(Br), was designed. Synthesis was achieved by sequential cobalt-mediated radical polymerization (CMRP), either using a pre-synthesized alkyl-cobalt initiator or by directly making use of *bis*(acetylacetonato)cobalt(II) controlling agent and V-70 as a radical source, both reagent being commercially available. Comparison of the two synthetic strategies suggested that the use of the alkyl-cobalt induced a reversible deactivation radical polymerization (RDRP) process, providing an excellent control of the polymerization. The second method utilizing $Co(acac)_2$ and V-70 proceeded by a degenerative transfer (DT) process, which allowed maintaining a relatively good control over molar masses, dispersities and chain-end fidelity.

The ability of these PIL BCPs to generate ordered self-assembled mesostructures at the solid state was also established in this chapter. Compounds constituted of bromine (Br^-) or bistrifluorosulfnonyl) imide (TFSI) anions and PVAc seemingly exhibited a high degree of incompatibility, giving rise to strong microphase separation, owing to both their charged and their uncharged character. Lamellar and hexagonally packed cylinder morphologies were clearly identified according to the weight ratio between the two blocks. Preliminary investigation into the ionic conductivity of some of these PIL BCPs yielded rather σ_{DC} values ($\sim 10^{-5}$ S/cm) that compare well with the highest values reported for other PIL BCP systems. However, ionic conductivity measurements were demonstrated to dramatically depend on the sample preparation. Measurements determined in the LCPO were 3-4 orders of magnitude lower than at the IMP, likely owing to a partial dewetting of the thin film (2.10^{-9} *vs* 8.10^{-5} S/cm at 30 °C, respectively). In both cases, values prove much higher than the conductivity measured from a homoPIL homologue (σ_{DC} at 30 °C ~ 8.10^{-5} S/cm *vs* 1.10^{-11} S/cm). More investigations would be needed, however so as to evidence the influence of the nanostructuration on the ionic conductivity properties.

More generally speaking, the possibility for fine-tuning the length of both blocks, as well as the nature of the counter-anion, makes PIL BCPs a versatile platform for manipulating the ionic conductivity by varying the size and the shape of nanodomains.

Self-assembling properties in solution of these PIL BCPs were also manipulated thanks to both the anion exchange reaction and to the post-chemical modification of the PVAc block.

Thus, the amphiphilic PVAc-*b*-PIL(Br) compound showed the formation of micelle-like structures in a selective solvent (water or THF). The PVAc block was subsequently methanolyzed into poly(vinyl alcohol) (PVA), forming a double hydrophilic block copolymer, PVA-*b*-PIL(Br), which proved ionic responsive in aqueous solution. A poly(vinyl alcohol)-*b*-[poly(*N*-vinyl-3-butylimidazolium carboxylate)-*co*-poly(*N*-vinyl-3-butylimidazolium bis(trifluorosulfonyl) imide)], denoted as PVA-*b*-PIL(RCOO-*co*-TFSI), was thus synthesized by anion exchange and was shown to generate a core-shell structure in aqueous media.

Advantage of PIL BCPs was finally taken to both stabilizers and reducing agents, *via* the borocyanohydride (BH_3CN) counter-anions, to access gold nanoparticles in aqueous solution. The core-shell structure of the PVA-*b*-PIL(BH_3CN-*co*-TFSI) attested to stabilizing effect of the two blocks. These PIL BCPs enabled the growth of gold nanoplates, such as nanocubes and hexagonal or octahedral nanoplates, depending on the molar ratio between the reducing agent BH_3CN^- and the gold complex.

As summarized in Figure 30, this work may open perspectives owing to the modularity provided by the different parameters of the PIL BCP structure:

i. Synthesis of novel PIL BCPs by CMRP by changing the nonionic block. For instance, *N*-vinylpyrrolidone (NVP), *N*-vinylimidazole (NVIm), acrylonitrile (AN), can be readily polymerized by CMRP in a controlled fashion. Hence, new functionalities with tunable mechanical properties may be introduced in view of developing ionic conducting materials with optimal properties.

ii. Imidazolium-based PILs could be easily modified by varying the alkyl substituent on the imidazolium ring, *e.g.* with hydrophilic or hydrophobic alkyl groups. Various counter-anions could also be introduced, from hydrophilic ones to hydrophobic ones to tune the solubility/viscosity of PIL BCPs.

iii. Investigations into redox counter-anions such as perrhenate (ReO_4^-), nitrate (NO_3^-), tungstate (WO_4^{2-}), persulfate ($S_2O_8^{2-}$), or hydrosulfite ($S_2O_4^{2-}$) could be implemented to achieve conducting PEDOT dispersions. Magnetic properties could also be provided by $Fe_3Br_{10}^-$ counter-anions, so as to develop nanostructured magnetic materials.

iv. Obviously, the ability of the imidazolium-based PIL, precursors for generating poly(*N*-heterocyclic carbene)s (poly(NHC)s) or poly(NHC-metal adduct)s as highlighted in chapter 2 could be applied for further organic or organometallic

catalysis in self-assembled structures in aqueous solution.

v. Concerning the self-assembling properties at the solid state, PIL triblock copolymers could be better exploited to provide better mechanical properties at the solid state than diblock homologues while exhibiting a similar ionic conductivity.

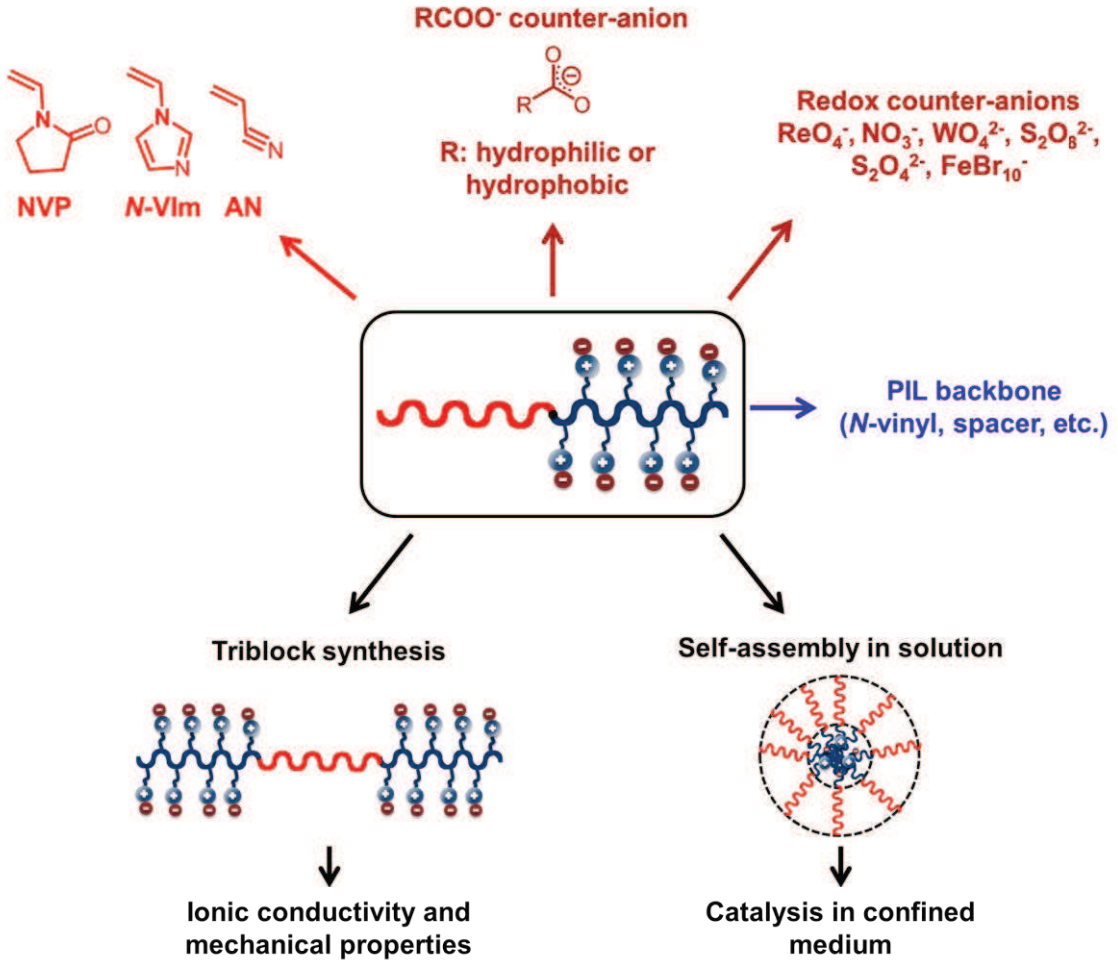

Figure 30. Schematic representation of perspectives offered by these imidazolium-based PIL BCPs.

Experimental and supporting information

Materials.

2,2'–Azo-bis-(4-methoxy-2,4-dimethyl valeronitrile) (V-70) (Wako) and cobalt(II) acetylacetonate ($Co(acac)_2$) (Alfa Aesar), 2,2,6,6-tetramethylpiperidine-1-oxy (TEMPO) (98%, Aldrich), hydrochloric acid 37% (Aldrich), gold(III) chloride (Aldrich), sodium cyanoborohydride (95%, Aldrich), lithium bis(trifluoromethanesulfonyl) imide (99%, TCI), 1-adamantaneacetic acid (98%, Alfa Aesar) were used as received. Vinyl acetate (>99%, Aldrich) was dried over calcium hydride before being distilled under reduced pressure and stored under argon. 1-vinylimidazole (99%) and 1-bromobutane (99%) were obtained from Alfa Aesar and used as received. Methanol (MeOH) was distilled over Na before use. Dimethylformamide (DMF) was dried over calcium hydride and distilled prior to use. MeOH (≥99.8%, Aldrich) for dialysis or the anion exchange, DMF (≥99.7%, Scharlau) used for the quaternization of the 1-vinylimidazole and diethyl ether (anhydrous, Baker) were used without further purification. Membrane Spectra/Por (cut-off: 1000 Da) was used for dialysis.

Instrumentation.

All DOSY (Diffusion Ordered Spectroscopy) measurements were performed at 298 K on a Bruker Avance III 400 spectrometer operating at 400.33 MHz and equipped with a 5 mm Bruker multinuclear z-gradient direct cryoprobe-head capable of producing gradients in the z direction with strength 53.5 $G.cm^{-1}$. For each sample, 3 mg was dissolved in 0.4 ml of DMSO-d_6 for internal lock and spinning was used to minimize convection effects. The DOSY spectra were acquired with the *ledbpgp2s* pulse program from Bruker topspin software. The duration of the pulse gradients and the diffusion time were adjusted in order to obtain full attenuation of the signals at 95% of maximum gradient strength. The values were 2.5 ms for the duration of the gradient pulses and 300 ms for the diffusion time. The gradients strength was linearly incremented in 32 steps from 5% to 95% of the maximum gradient strength. A delay of 10 s between echoes was used. The data were processed using 8192 points in the F2 dimension and 64 points in the F1 dimension using the Bruker topspin software. Field gradient calibration was accomplished at 25 °C using the self-diffusion coefficient of H_2O+D_2O at 19.0 x 10^{-10} $m^2.s^{-1}$. Molar masses were determined by size exclusion chromatography (SEC) in THF as the eluent (1 mL/min) and with trichlorobenzene as a flow marker at 40 °C, using both refractometric (RI) and UV detectors (Varian). Analyses were performed using a three-column set of TSK gel TOSOH (G4000, G3000, G2000 with pore

sizes of 20, 75, and 200 Å respectively, connected in series) calibrated with polystyrene standards. Thermogravimetric analyses (TGA) were performed using a TA instruments Q50 under a nitrogen atmosphere, from room temperature (10 °C/min) to 600 °C. The weight loss was recorded as a function of temperature. Differential scanning calorimetry (DSC) measurements were carried out with a Q1000 apparatus from TA Instruments. DSC experiments were performed with aluminum sealed pans. A constant heating/cooling rate of 10 °C/min and gas purging (N_2) at a flow rate of 100 mL/min was used for all experiments. Transmission Electron Microscopy (TEM) images were recorded on a Hitachi H7650 microscope working at 80 kV equipped with a GATAN Orius 11 Megapixel camera. Thin solid samples were prepared by cryomicrotomy at -150 °C to observe the self-assembly in bulk. The usual thickness was around 50 nm. Block copolymers samples were stained with ruthenium tetroxide (RuO_4) vapor, and the PIL block was preferencially stained. Samples for the self-assembly in solution were prepared by spraying a 27.5 mg/mL solution of the block copolymer onto a copper grid (200 mesh coated with carbon) using a homemade spray tool. SAXS experiments were performed on the Dutch-Belgian Beamline (DUBBLE) at the European Synchrotron Radiation Facility (ESRF) station BM26B in Grenoble, France. A *Pilatus 1M* detector was used for recording the two-dimensional scattering images and a 2500 mm sample-to-detector distance was chosen. The energy of the x-ray beam was 11 keV, which corresponds to a wavelength of 1.127Å, and the scattering vector range covered was $0.2 < q < 3$ nm^{-1}, where the magnitude of the scattering vector is $q = (4\pi/\lambda)\sin\theta$, 2θ being the scattering angle. The two-dimensional images were radially averaged around the center of the primary beam in order to obtain the isotropic SAXS intensity profiles. The scattering pattern from a specimen of silver behenate was used for the calibration of the wavevector scale of the scattering curves. Finally, the data were normalized to the intensity of the incident beam in order to correct for primary beam intensity fluctuations. The second SAXS profiles were acquired in transmission on a Nanostar-U instrument (Bruker AXS) with a copper anode source. The resulting 2-D images are found to be isotropic, and the data are azimuthally averaged to yield curves of the scattering intensity versus $q = (4\pi/\lambda) \sin\theta$, where $\lambda = 1.54$ Å is the wavelength of the Cu Kα radiation and θ is half the scattering angle. UV-visible measurements were achieved on a SHIMADZU UV-2550.

Dynamic light scattering (DLS) was used to obtain the average size of the particles right after by using a Malvern ZetaSizer NanoZS instrument with 90° backscattering measurements at 25°C. 5.5 mg of PVAc-*b*-PVBuImBr were dissolved in 0.2 mL of MeOH and added (15

$mL.h^{-1}$) to 5 mL of water or THF under stirring. Three measurements were conducted and averaged for all the samples. ^1H NMR experiments for the self-assembly in solution were performed in a NMR tube. 1-2 mg of PVAc-*b*-PVBuImBr were dissolved in 50 µL MeOH, and added to 0.45 mL of D_2O or THF-d_8.

DLS was used to obtain the average size of the gold nanoparticles right after by using a Malvern Zetasizer Nano intrusment with 110° backscattering measurements at 25 °C, in Polymat, Spain. The gold nanoparticles TEM grids were prepared by deposition of a drop of sample solution on a Formvard film copper grid. The samples were examined in a Transmission electron Microscope, TECNAI G220 TWIN(FEI), operating at an acceleration Voltage of 200 keV in a bright-field image mode.

Synthesis of PVAc-*b*-PVEtImBr and PVAc-*b*-PVEtImBr-*b*-PVAc block copolymers by sequential CMRP using alkylcobalt(III) adduct 1

The synthesis of these copolymers was described in our previous report.

Synthesis of 1-vinyl-3-butylimidazolium bromide VBuImBr

1-Vinyl-3-butylimidazolium bromide (VBuImBr) was synthesized following the procedure described in the literature.[54, 55] The monomer was recovered as a white solid (100% yield). NMR data were in accordance with those reported in the literature.

Synthesis of the poly(vinyl acetate) macroinitiator end-capped with $Co(acac)_2$

A Schlenk tube was flame-dried and charged with 49.5 mg (0.19 mmol) of **2**, 387 mg (1.26 mmol) of **3**. The tube was placed in an ice bath under dynamic vacuum for 2h and subjected to three Ar/vacuum cycles. 5 mL (54.3 mmol) of dry VAc were introduced, and the reaction was stirred for 42h at 30 °C. An aliquot was withdrawn for calculating the conversion by ^1H NMR in $CDCl_3$ (64% conversion, $M_{n,theo}$ = 15,600 g/mol) and for analysis by SEC using THF (M_n = 18,300 g/mol; M_w/M_n = 1.10). Residual monomer was removed under vacuum at RT. ^1H NMR (400 MHz, $CDCl_3$, δ): 4.9 (br, 1H; C*H*O), 2 (br, 3H; CH_3), 1.8 (br, 2H; CH_2).

Synthesis of PVAc-*b*-PVBuImBr-$Co(acac)_2$ diblock copolymer

The flask containing the PVAc-$Co(acac)_2$ macroinitiator was cooled to 0 °C under argon and 8 mL DMF at 0 °C was added to dissolve the macroinitiator. A degassed solution of VBuImBr (3.92 g, 17.0 mmol) in a mixture of DMF/MeOH (8 mL/8 mL) was added and the polymerization occurred at 30 °C under stirring. Aliquots were regularly withdrawn for

calculating the conversion by ^{1}H NMR in CD_2Cl_2. The sample was quenched by adding an excess of TEMPO after 15 h (53% conversion). The final product was precipitated in diethyl ether. After re-dissolution in methanol, the product was dialyzed against methanol for 48 h and finally dried at 40 °C in vacuum for 24h. The composition of the copolymer was calculated by ^{1}H NMR in CD_2Cl_2: $PVAc_{(15600)}$-*b*-$PVBuImBr_{(9900)}$. ^{1}H NMR (400 MHz, CD_2Cl_2, δ): 10.2 (br, 1H; N-C*H*-N), 8.45 (br, 2H; C*H*=C*H*), 4.8 (br, 1H; CH_2-C*H*-O), 4.2 (br, 1H; CH_2-C*H*-N; br, 2H; N-CH_2-CH_2), 1.5-2 (br, 2H; CH_2-CH_2-CH_2; br, 2H; CH_2-CH-O; br, 2H; CH_2-CH-N), 1.3 (br, 2H; CH_2-CH_2-CH_3), 0.8 (br, 3H; CH_2-CH_2-CH_3).

Synthesis of PVAc-*b*-PVBuIm(Tf_2N) diblock copolymer by anion exchange

This metathesis reaction was performed following the procedure described in the literature. 300 mg (3.85 x 10^{-4} mol VBuImBr units) of PVAc-*b*-PVBuImBr were dissolved in 5 mL of MeOH. The resulting solution was added to a stirred solution of lithium bis(trifluorosulfonyl) imide $(CF_3SO_2)_2NLi$ (442 mg, 1.54 x 10^{-3} mol), previously dissolved in 5 mL of MeOH. 3.5 mL of water was added to force the precipitation after 30 min. The mixture was poured in 100 mL of water and the corresponding PVAc-*b*-PVBuIm(Tf_2N) was removed by filtration and dried under vacuum at 40 °C overnight. (80% yield).

Synthesis of PVA-*b*-PVBuImBr diblock copolymer by methanolysis

In a typical experiment, 1g (6.35 x 10^{-3} mol VAc units) of PVAc-*b*-PVBuImBr **18(Br)** were dissolved in 5 mL of MeOH. The resulting solution was added to a stirred solution of hydrochloric acid HCl 37% (3 mL, 13 x 10^{-3} mol). The reaction mixture was stirred for 24h at room temperature and then the solvent was removed under dynamic vacuum. The yellowish powder was dried under vacuum at 35 °C overnight. (90% yield).). ^{1}H NMR (400 MHz, DMSO-d_6, δ): 10.2 (br, 1H; N-C*H*-N), 8.45 (br, 2H; C*H*=C*H*), 4.2 (br, 1H; CH_2-C*H*-N; br, 2H; N-CH_2-CH_2), 3.8 (br, 1H; CH_2-C*H*-OH), 1.5-2 (br, 2H; CH_2-CH_2-CH_2; br, 2H; CH_2-CH-O; br, 2H; CH_2-CH-N), 1.3 (br, 2H; CH_2-CH_2-CH_3), 0.8 (br, 3H; CH_2-CH_2-CH_3).

Preparation of PVA-*b*-PVBuIm(RCOO-*co*-TFSI) diblock copolymer by anion exchange

In a typical experiment, 30mg (44 x 10^{-6} mol VBuImBr units) of PVA-*b*-PVBuImBr **13(Br)** were dissolved in 3 mL of water. 2 eq. of potassium carboxylate were dissolved in water and added to the PIL BCP solution. The solution was stirred for 2h and the dialyzed for one day. Then, a solution containing x eq. of LiTFSI was added on the micellar solution and stirred for few hours before filtration (0.45 μm).

Preparation of PVA-*b*-PVBuIm(BH_3CN-*co*-TFSI) diblock copolymer by sequential anion exchange

10 mg of PVA-*b*-PVBuImBr (14.5×10^{-6} mol VBuImBr units) of PVA-*b*-PVBuImBr **13(Br)** were dissolved in 2 mL of water and sequentially 0.5 aq. Of $NaBH_3CN$ and 0.5 eq. of LiTFSI were added to the solution under stirring. Then, gold complex solution was added on the PIL BCP solution under stirring. Solution became pink instantaneously.

Figure S1. Microscopic images of sample **11(TFSI)**: a) before annealing; b) after thermal annealing; c) after GISAXS and ionic conductivity measurements.

References

1. Bates, F. S.; Hillmyer, M. A.; Lodge, T. P.; Bates, C. M.; Delaney, K. T.; Fredrickson, G. H. *Science* **2012**, *336*, 434–440.
2. Whitesides, G. M.; Grzybowski, B. *Science* **2002**, *295*, 2418–2421.
3. Giacomelli, C.; Schmidt, V.; Aissou, K.; Borsali, R. *Langmuir* **2010**, *26*, 15734–15744.
4. Pan, D.; Turner, J. L.; Wooley, K. L. *Chem. Commun.* **2003**, 2400–2401.
5. Okhapkin, I.; Makhaeva, E.; Khokhlov, A. In *Conformation-Dependent Design of Sequences in Copolymers I*; Khokhlov, A., Ed.; Springer Berlin Heidelberg, **2006**; Vol. 195, pp. 177–210.
6. Ruokolainen, J.; Mäkinen, R.; Torkkeli, M.; Mäkelä, T.; Serimaa, R.; Brinke, G. ten; Ikkala, O. *Science* **1998**, *280*, 557–560.
7. Lin, Y.; Boker, A.; He, J.; Sill, K.; Xiang, H.; Abetz, C.; Li, X.; Wang, J.; Emrick, T.; Long, S.; Wang, Q.; Balazs, A.; Russell, T. P. *Nature* **2005**, *434*, 55–59.
8. Meng, F.; Zhong, Z.; Feijen, J. *Biomacromolecules* **2009**, *10*, 197–209.
9. Ruiz, R.; Kang, H.; Detcheverry, F. A.; Dobisz, E.; Kercher, D. S.; Albrecht, T. R.; de Pablo, J. J.; Nealey, P. F. *Science* **2008**, *321*, 936–939.
10. Bates, F. S.; Fredrickson, G. H.; Hucul, D.; Hahn, S. F. *AIChE J.* **2001**, *47*, 762–765.
11. Gamys, C. G.; Schumers, J.-M.; Mugemana, C.; Fustin, C.-A.; Gohy, J.-F. *Macromol. Rapid Commun.* **2013**, *34*, 962–982.
12. Gohy, J.-F.; Zhao, Y. *Chem. Soc. Rev.* **2013**, *42*, 7117–7129.
13. Klok, H. A.; Lecommandoux, S. *Adv. Mater.* **2001**, *13*, 1217–1229.
14. Bates, F. S.; Fredrickson, G. H. *Phys. Today* **1999**, *52*, 32–38.
15. Yu, B.; Li, B.; Sun, P.; Chen, T.; Jin, Q.; Ding, D.; Shi, A.-C. *J. Chem. Phys.* **2005**, *123*, 234902–234908.
16. Ding, J.; Liu, G.; Yang, M. *Polymer* **1997**, *38*, 5497–5501.
17. Lutz, J.-F. *Nat Chem* **2010**, *2*, 84–85.
18. Lutz, J.-F.; Ouchi, M.; Liu, D. R.; Sawamoto, M. *Science* **2013**, *341*.
19. Stancik, C. M.; Lavoie, A. R.; Achurra, P. A.; Waymouth, R. M.; Gast, A. P. *Langmuir* **2004**, *20*, 8975–8987.
20. Stancik, C. M.; Lavoie, A. R.; Schütz, J.; Achurra, P. A.; Lindner, P.; Gast, A. P.; Waymouth, R. M. *Langmuir* **2003**, *20*, 596–605.
21. Mori, H.; Yahagi, M.; Endo, T. *Macromolecules* **2009**, *42*, 8082–8092.
22. Mori, H.; Ebina, Y.; Kambara, R.; Nakabayashi, K. *Polym J* **2012**, *44*, 550–560.
23. Karjalainen, E.; Chenna, N.; Laurinmaki, P.; Butcher, S. J.; Tenhu, H. *Polym. Chem.* **2013**, *4*, 1014–1024.
24. Texter, J.; Vasantha, V. A.; Crombez, R.; Maniglia, R.; Slater, L.; Mourey, T. *Macromol. Rapid Commun.* **2012**, *33*, 69–74.
25. Vijayakrishna, K.; Jewrajka, S. K.; Ruiz, A.; Marcilla, R.; Pomposo, J. A.; Mecerreyes, D.; Taton, D.; Gnanou, Y. *Macromolecules* **2008**, *41*, 6299–6308.
26. Vijayakrishna, K.; Mecerreyes, D.; Gnanou, Y.; Taton, D. *Macromolecules* **2009**, *42*, 5167–5174.
27. Yuan, J.; Schlaad, H.; Giordano, C.; Antonietti, M. *Eur. Polym. J.* **2011**, *47*, 772–781.
28. Carrasco, P. M.; Tzounis, L.; Mompean, F. J.; Strati, K.; Georgopanos, P.; Garcia-Hernandez, M.; Stamm, M.; Cabañero, G.; Odriozola, I.; Avgeropoulos, A.; Garcia, I. *Macromolecules* **2013**, *46*, 1860–1867.

29. Carrasco, P. M.; Ruiz de Luzuriaga, A.; Constantinou, M.; Georgopanos, P.; Rangou, S.; Avgeropoulos, A.; Zafeiropoulos, N. E.; Grande, H.-J.; Cabañero, G.; Mecerreyes, D.; Garcia, I. *Macromolecules* **2011**, *44*, 4936–4941.
30. Nguyen, P. T.; Wiesenauer, E. F.; Gin, D. L.; Noble, R. D. *J. Memb. Sci.* **2013**, *430*, 312–320.
31. Wiesenauer, E. F.; Edwards, J. P.; Scalfani, V. F.; Bailey, T. S.; Gin, D. L. *Macromolecules* **2011**, *44*, 5075–5078.
32. Gu, Y.; Lodge, T. P. *Macromolecules* **2011**, *44*, 1732–1736.
33. Sudre, G.; Inceoglu, S.; Cotanda, P.; Balsara, N. P.; Copolymers, A. B. *Macromolecules* **2013**, *46*, 1519–1527.
34. Green, M. D.; Wang, D.; Hemp, S. T.; Choi, J.-H.; Winey, K. I.; Heflin, J. R.; Long, T. E. *Polymer* **2012**, *53*, 3677–3686.
35. Green, M. D.; Choi, J.-H.; Winey, K. I.; Long, T. E. *Macromolecules* **2012**, *45*, 4749–4757.
36. Gao, R.; Wang, D.; Heflin, J. R.; Long, T. E. *J. Mater. Chem.* **2012**, *22*, 13473–13476.
37. Ye, Y.; Choi, J.-H.; Winey, K. I.; Elabd, Y. A. *Macromolecules* **2012**, *45*, 7027–7035.
38. Ye, Y.; Sharick, S.; Davis, E. M.; Winey, K. I.; Elabd, Y. A. *ACS Macro Lett.* **2013**, 575–580.
39. Choi, J.-H.; Ye, Y.; Elabd, Y. A.; Winey, K. I. *Macromolecules* **2013**, *46*, 5290–5300.
40. Chanthad, C.; Masser, K. A.; Xu, K.; Runt, J.; Wang, Q. *J. Mater. Chem.* **2012**, *22*, 341–344.
41. Schneider, Y.; Modestino, M. A.; McCulloch, B. L.; Hoarfrost, M. L.; Hess, R. W.; Segalman, R. A. *Macromolecules* **2013**, *46*, 1543–1548.
42. Weber, R. L.; Ye, Y.; Schmitt, A. L.; Banik, S. M.; Elabd, Y. A.; Mahanthappa, M. K. *Macromolecules* **2011**, *44*, 5727–5735.
43. Detrembleur, C.; Debuigne, A.; Hurtgen, M.; Jérôme, C.; Pinaud, J.; Fèvre, M.; Coupillaud, P.; Vignolle, J.; Taton, D. *Macromolecules* **2011**, *44*, 6397–6404.
44. Debuigne, A.; Poli, R.; Jérôme, C.; Jérôme, R.; Detrembleur, C. *Prog. Polym. Sci.* **2009**, *34*, 211–239.
45. Debuigne, A.; Jérôme, C.; Detrembleur, C. *Angew. Chemie Int. Ed.* **2009**, *48*, 1422–1424.
46. Debuigne, A.; Caille, J.-R.; Detrembleur, C.; Jérôme, R. *Angew. Chemie Int. Ed.* **2005**, *44*, 1101–1104.
47. Debuigne, A.; Michaux, C.; Jérôme, C.; Jérôme, R.; Poli, R.; Detrembleur, C. *Chem. – A Eur. J.* **2008**, *14*, 7623–7637.
48. Wayland, B. B.; Peng, C.-H.; Fu, X.; Lu, Z.; Fryd, M. *Macromolecules* **2006**, *39*, 8219–8222.
49. Piette, Y.; Debuigne, A.; Bodart, V.; Willet, N.; Duwez, A.-S.; Jerome, C.; Detrembleur, C. *Polym. Chem.* **2013**, *4*, 1685–1693.
50. Debuigne, A.; Warnant, J.; Jérôme, R.; Voets, I.; de Keizer, A.; Cohen Stuart, M. A.; Detrembleur, C. *Macromolecules* **2008**, *41*, 2353–2360.
51. He, H.; Zhong, M.; Adzima, B.; Luebke, D.; Nulwala, H.; Matyjaszewski, K. *J. Am. Chem. Soc.* **2013**, *135*, 4227–4230.
52. Mecerreyes, D. *Prog. Polym. Sci.* **2011**, *36*, 1629–1648.
53. Debuigne, A.; Detrembleur, C.; Jérôme, C.; Junkers, T. *Macromolecules* **2013**, *46*, 8922–8931.

54. Debuigne, A.; Champouret, Y.; Jérôme, R.; Poli, R.; Detrembleur, C. *Chem. – A Eur. J.* **2008**, *14*, 4046–4059.
55. Viel, S.; Mazarin, M.; Giordanengo, R.; Phan, T. N. T.; Charles, L.; Caldarelli, S.; Bertin, D. *Anal. Chim. Acta* **2009**, *654*, 45–48.
56. Bakkour, Y.; Darcos, V.; Li, S.; Coudane, J. *Polym. Chem.* **2012**, *3*, 2006–2010.
57. Dong, S.; Zheng, B.; Zhang, M.; Yan, X.; Ding, X.; Yu, Y.; Huang, F. *Macromolecules* **2012**, *45*, 9070–9075.
58. Matos, I.; Ascenso, J.; Lemos, M.; Fan, Z.; Yuan, J.; Farinha, J.; Lemos, F.; Gonçalves da Silva, A. P. S.; Marques, M. *J. Polym. Res.* **2013**, *20*, 1–16.
59. Lefay, C.; Glé, D.; Rollet, M.; Mazzolini, J.; Bertin, D.; Viel, S.; Schmid, C.; Boisson, C.; D'Agosto, F.; Gigmes, D.; Barner-Kowollik, C. *J. Polym. Sci. Part A Polym. Chem.* **2011**, *49*, 803–813.
60. Guinaudeau, A.; Coutelier, O.; Sandeau, A.; Mazières, S.; Nguyen Thi, H. D.; Le Drogo, V.; Wilson, D. J.; Destarac, M. *Macromolecules* **2014**, *47*, 41–50.
61. Green, M. D.; Salas-de la Cruz, D.; Ye, Y.; Layman, J. M.; Elabd, Y. A.; Winey, K. I.; Long, T. E. *Macromol. Chem. Phys.* **2011**, *212*, 2522–2528.
62. Helfand, E.; Wasserman, Z. R. *Macromolecules* **1976**, *9*, 879–888.
63. Leibler, L. *Macromolecules* **1980**, *13*, 1602–1617.
64. Benoit, H.; Hadziioannou, G. *Macromolecules* **1988**, *21*, 1449–1464.
65. Hajduk, D. A.; Gruner, S. M.; Rangarajan, P.; Register, R. A.; Fetters, L. J.; Honeker, C.; Albalak, R. J.; Thomas, E. L. *Macromolecules* **1994**, *27*, 490–501.
66. Sakurai, S.; Momii, T.; Taie, K.; Shibayama, M.; Nomura, S.; Hashimoto, T. *Macromolecules* **1993**, *26*, 485–491.
67. Mai, S.-M.; Fairclough, J. P. A.; Terrill, N. J.; Turner, S. C.; Hamley, I. W.; Matsen, M. W.; Ryan, A. J.; Booth, C. *Macromolecules* **1998**, *31*, 8110–8116.
68. Pitet, L. M.; Hillmyer, M. A. *Macromolecules* **2009**, *42*, 3674–3680.
69. Matsen, M. W.; Bates, F. S. *Macromolecules* **1996**, *29*, 7641–7644.
70. Matsen, M. W.; Bates, F. S. *J. Chem. Phys.* **1997**, *106*, 2436–2448.
71. Scalfani, V. F.; Wiesenauer, E. F.; Ekblad, J. R.; Edwards, J. P.; Gin, D. L.; Bailey, T. S. *Macromolecules* **2012**, *45*, 4262–4276.
72. Hajduk, D. A.; Takenouchi, H.; Hillmyer, M. A.; Bates, F. S.; Vigild, M. E.; Almdal, K. *Macromolecules* **1997**, *30*, 3788–3795.
73. Matsen, M. W. *J. Phys. Condens. Matter* **2002**, *14*, R21.
74. Hamley, I. W.; O'Driscoll, B. M. D.; Lotze, G.; Moulton, C.; Allgaier, J.; Frielinghaus, H. *Macromol. Rapid Commun.* **2009**, *30*, 2141–2146.
75. Matsen, M. W. *Phys. Rev. Lett.* **2007**, *99*, 148304.
76. Matsen, M. W.; Thompson, R. B. *J. Chem. Phys.* **1999**, *111*, 7139–7146.
77. Hadziioannou, G.; Skoulios, A. *Macromolecules* **1982**, *15*, 258–262.
78. Nykaza, J. R.; Ye, Y.; Elabd, Y. A. *Polymer* **2014**, *55*, 3360–3369.
79. Bouchet, R.; Maria, S.; Meziane, R.; Aboulaich, A.; Lienafa, L.; Bonnet, J.-P.; Phan, T. N. T.; Bertin, D.; Gigmes, D.; Devaux, D.; Denoyel, R.; Armand, M. *Nat Mater* **2013**, *12*, 452–457.
80. Weber, R. L.; Ye, Y.; Banik, S. M.; Elabd, Y. A.; Hickner, M. A.; Mahanthappa, M. K. *J. Polym. Sci. Part B Polym. Phys.* **2011**, *49*, 1287–1296.
81. Vygodskii, Y. S.; Mel'nik, O. A.; Lozinskaya, E. I.; Shaplov, A. S.; Malyshkina, I. A.; Gavrilova, N. D.; Lyssenko, K. A.; Antipin, M. Y.; Golovanov, D. G.; Korlyukov, A. A.; Ignat'ev, N.; Welz-Biermann, U. *Polym. Adv. Technol.* **2007**, *18*, 50–63.
82. Discher, D. E.; Eisenberg, A. *Science* **2002**, *297*, 967–973.

83. Pichot, C.; Guillot, J.; Guyot, A. *J. Macromol. Sci. Part A - Chem.* **1974**, *8*, 1073–1086.
84. Bosman, A. W.; Janssen, H. M.; Meijer, E. W. *Chem. Rev.* **1999**, *99*, 1665–1688.
85. Lu, A.; Cotanda, P.; Patterson, J. P.; Longbottom, D. A.; O'Reilly, R. K. *Chem. Commun.* **2012**, *48*, 9699–9701.
86. Cotanda, P.; Lu, A.; Patterson, J. P.; Petzetakis, N.; O'Reilly, R. K. *Macromolecules* **2012**, *45*, 2377–2384.
87. Marguet, M.; Bonduelle, C.; Lecommandoux, S. *Chem. Soc. Rev.* **2013**, *42*, 512–529.
88. Srour, H.; Rouault, H.; Santini, C. C.; Chauvin, Y. *Green Chem.* **2013**, *15*, 1341–1347.
89. Helgadottir, I. S.; Arquillière, P. P.; Bréa, P.; Santini, C. C.; Haumesser, P.-H.; Richter, K.; Mudring, A.-V.; Aouine, M. *Microelectron. Eng.* **2013**, *107*, 229–232.
90. Campbell, P. S.; Lorbeer, C.; Cybinska, J.; Mudring, A.-V. *Adv. Funct. Mater.* **2013**, *23*, 2924–2931.
91. Marcilla, R.; Curri, M. L.; Cozzoli, P. D.; Martínez, M. T.; Loinaz, I.; Grande, H.; Pomposo, J. A.; Mecerreyes, D. *Small* **2006**, *2*, 507–512.
92. Soll, S.; Antonietti, M.; Yuan, J. *ACS Macro Lett.* **2012**, *1*, 84–87.
93. Fukushima, T.; Kosaka, A.; Ishimura, Y.; Yamamoto, T.; Takigawa, T.; Ishii, N.; Aida, T. *Sci.* **2003**, *300* , 2072–2074.
94. Pozo-Gonzalo, C.; Marcilla, R.; Salsamendi, M.; Mecerreyes, D.; Pomposo, J. A.; Rodríguez, J.; Bolink, H. J. *J. Polym. Sci. Part A Polym. Chem.* **2008**, *46*, 3150–3154.
95. Kim, T.; Suh, M.; Kwon, S. J.; Lee, T. H.; Kim, J. H. J. E.; Lee, Y. J.; Hong, M.; Suh, K. S. *Macromol. Rapid Commun.* **2009**, *30*, 1477–1482.
96. Hong, S. H.; Tung, T. T.; Huyen Trang, L. K.; Kim, T. Y.; Suh, K. S. *Colloid Polym. Sci.* **2010**, *288*, 1013–1018.
97. Bourissou, D.; Guerret, O.; Gabbaï, F. P.; Bertrand, G. *Chem. Rev.* **1999**, *100*, 39–92.
98. Roshan, K. R.; Mathai, G.; Kim, J.; Tharun, J.; Park, G.-A.; Park, D.-W. *Green Chem.* **2012**, *14*, 2933–2940.
99. Murphy, C. J.; Orendorff, C. J. *Adv. Mater.* **2005**, *17*, 2173–2177.
100. Pérez-Juste, J.; Rodríguez-González, B.; Mulvaney, P.; Liz-Marzán, L. M. *Adv. Funct. Mater.* **2005**, *15*, 1065–1071.
101. Porel, S.; Singh, S.; Radhakrishnan, T. P. *Chem. Commun.* **2005**, 2387–2389.
102. Longenberger, L.; Mills, G. *J. Phys. Chem.* **1995**, *99*, 475–478.
103. Gracia, R.; Vijayakrishna, K.; Mecerreyes, D. *React. Funct. Polym.* **2014**, *79*, 54–58.
104. Li, N.; Zhao, P.; Astruc, D. *Angew. Chemie Int. Ed.* **2014**, *53*, 1756–1789.

General Conclusion and Perspectives

This thesis work aimed at expanding the scope of imidazolium-based poly(ionic liquid)s (PILs) and their related PIL block copolymers (BCPs). The first objective was to develop novel air-stable and reactive imidazolium-based PILs of various polymer structures for the purpose of organocatalysis and for post-chemical modification as well. Taking benefit of the intrinsic reactivity of the imidazolium moiety of PILs had been so far under exploited before this work. Another objective was to design a novel family of well-defined PIL BCPs based on poly(vinyl acetate) and poly(*N*-vinyl-3-alkylimidazolium bromide) and, for this purpose, we resorted to the sequential cobalt-mediated radical polymerization (CMRP). The self-assembling properties both in solution and at the solid state of these PIL BCPs were investigated, which evidenced a high degree of incompatibility between the PVAc and the PIL blocks.

The first point was addressed through the elaboration of four different imidazolium-based PILs with halide, hydrogen carbonate or carboxylate counter-anions for a use in organocatalysis: poly(*N*-vinyl-3-alkylimidazolium hydrogen carbonate)s (poly([NHC(H)][HCO_3])s); poly(*N*-vinyl-3-butylimidazolium bromide-*co*-poly(*N*-vinyl-3-butylimidazolium carboxylate)s (poly([NHC(H)][Br]-*co*-[NHC(H)][RCOO])s); poly(styrene)-*co*-poly(4-vinylbenzylbutylimidazolium chloride or hydrogen carbonate)s (PS-*co*-PVBnBuIm(Cl or HCO_3)s); poly(divinylbenzene-0.1*N*-vinyl-3-ethylimidazolium bromide) (P(DVB-0.1EVIBr)) mesoporous network (PILPN). These new PILs were used as organocatalyst for the carbonatation reaction *via* their halide counter-anion or as poly(NHC) precursors for selected organocatalyzed reactions with excellent conversions depending of the polymer structure. In this chapter, advantages and drawbacks of each structure were discussed, the PS-*co*-PVBnBuIm(HCO_3) exhibited the best catalytic efficiency but cannot be recycled, in contrast to the poly([NHC(H)][HCO_3])s. The PILPN obtained excellent results and maintained good efficiency after few cycles but required a deprotonation by a strong base to generate the NHC units due to the polymer network.

The specific polystyrene-type coPILs exhibited excellent catalytic results owing to the distance between the imidazolium and the polymer backbone and the low catalytic density by their statistical character. Thanks to this structure, we succeeded stoichiometric addition reactions with electrophile substrates (CS_2, isothiocyanates and metallic complexes) to transform the coPIL precursor into a new polymeric compound.

These different imidazolium-based polymer precursors offer novel perspectives for various organocatalyzed reactions or organometallic catalysis (Heck reaction, Suzuki coupling, etc.) owing to the post-chemical modifications forming poly(NHC)-adducts, according to the chemical structure. Furthermore, addition of electrophilic substrates which react with NHCs at stoichiometry such as fullerenes, or azides, or multifunctional electrophiles (*e.g.* bis-azides, bis-isothiocyanates, etc.) for network synthesis, could be expanded using coPILs to develop new organic compounds.

Regarding on PIL BCPs, synthesis of poly(vinyl acetate)-*b*-poly(*N*-vinyl-3-alkylimidazolium bromide), (PVAc-*b*-PIL(Br)) by sequential cobalt-mediated radical polymerization (CMRP) *via* two synthetic strategies using the alkyl-cobalt initiator or directly the *bis*(acetylacetonato)cobalt(II) and the V-70 as radical source was described. Comparison between the two synthetic strategies and their influence on the polymerization control evidenced that the use of the alkyl-cobalt initiator induced a reversible deactivation radical polymerization (RDRP) process which exhibited an excellent control although this initiator requires complex synthesis and purification. In contrast, the degenerative transfer (DT) process using the $Co(acac)_2$ and V-70 exhibited lower control but maintained a relative good control.

Then, we discussed the morphological behavior of the PIL BCPs with bromine or bis(trifluorosulfonyl)imide (TFSI) counter-anions. The high degree of incompatibility enabled a strong microphase separation between the blocks. Lamellar and hexagonally packed cylinder morphologies were observed according to the weight ratio between the two blocks. Evaluation of ionic conductivity properties exhibited relatively good values compared to the imidazolium-based PIL BCPs from the literature. Comparison between the two techniques of measurement between the LCPO and the IMP (thin film *vs* raw materials in bulk) evidenced the important role of the sample preparation and the measurement conditions. It was concluded that morphological observations and ionic conductivity measurements required raw materials in bulk.

Self-assembly properties were manipulated thanks to the anion exchange reaction with various counter-anions and by post-chemical modification. A Proper choice in selective solvent and the ionic responsiveness of the PIL BCPs were exploited to form micelle-like structure. The amphiphilic PVAc-*b*-PIL(Br) evidenced the formation of micelle-like structure in selective solvent (water or THF). A poly(vinyl alcohol)-*b*-[poly(*N*-vinyl-3-butylimidazolium carboxylate)-*co*-poly(*N*-vinyl-3-butylimidazolium bis(trifluorosulfonyl)

imide)) (PVA-*b*-PIL(R'COO-*co*-TFSI)) was synthesized by methanolysis of the PVAc block followed by sequential anion exchange forming a core-shell structure. PIL BCPs were also used as stabilizers and reducing agents utilizing the borocyanohydride (BH_3CN^-) counter-anions to synthesize gold nanoparticles in aqueous solution. The core-shell structure of a PVA-*b*-PIL(BH_3CN-*co*-TFSI) evidenced the role of stabilizer of the two blocks. The PIL BCPs as micelle-like structures enabled the growth of gold nanoplates such as nanocubes and hexagonal or octahedral nanoplates according to the molar ratio between the reducing agent counter-anion BH_3CN^- and the gold complex.

This PhD work offers promising perspectives for these imidazolium-based PIL BCPs exploiting the modularity provided by the different parameters of the PIL BCP structure. CMRP could be used to develop novel PIL BCPs by changing the nonionic block (NVP, NVIm, AN) in a controlled fashion to tune mechanical properties. Synthesis of triblock copolymers while exhibiting similar ionic conductivity with their diblock homologues could be also better exploited. In addition, the reactivity of the imidazolium ring, the alkyl substituent (hydrophilic or hydrophobic) and the various counter-anions open promising perspectives for further organic or organometallic catalysis in self-assembled structures in solution, or nanostructured magnetic materials.

Título: Polímeros Líquidos Iónicos (PILs) Reactivos y Nanoestructuras a Partir de Copolímeros de Bloque Compuesto de un Bloque de PIL

Resumen: El objetivo de esta tesis fue el desarrollo de polímeros de ingeniería iónicos líquidos (pils) y tipo imidazolio una nueva familia de copolímeros de bloques relacionados. Lager tipo imidazolio fueron utilizados como reactivos para la catálisis orgánica y modificación química de polímeros después de la polimerización. Varios compuestos (homopolímeros, copolímeros aleatorios de tipo estireno, polímeros reticulados) estable en el aire, contra de la realización diversos aniones (bromuros, bicarbonatos, carboxilatos), han sido especialmente diseñadas utilizando estrategias de síntesis relativamente simple. Se utilizó la generación de carbenos N-heterocíclicos soportado sobre polímeros (poli (NHC) s) para comparar el rendimiento catalítico de estos precursores de referencia a través de reacciones de catálisis orgánica. Específicamente, los copolímeros de tipo estireno también se pueden funcionalizar sustratos por polimerización posterior estequiométricamente con diferentes electrófilos (por ejemplo, metales CS2, isotiocianato, de transición).
Una nueva familia de copolímero de bloque que contiene un poli (acetato de vinilo) y un bloque de poli (bromuro de N-vinil-3-alquilimidazolio) se sintetizó en CMRP. La capacidad de estos compuestos a auto-ensamblan en varias mesoestructuras como entonces se demostró solución en masa. Mediciones de conductividad iónica han demostrado la influencia de las condiciones de preparación y medición de la muestra en los valores obtenidos. El comportamiento en solución por el bloque PIL reactividad de iones, y la modificación química del bloque hidrófobo de poli (acetato de vinilo) hidrófilo poli (alcohol vinílico) permitió la formación de nanoestructuras diferentes micelares.
Palabras clave: polímeros líquidos iónicos, copolímeros de bloque, imidazolio, catálisis orgánica, Cambiar post-polimerización, auto-ensamblaje, conductividad iónica, las nanopartículas de oro.

POLYMAT
Basque Country University (UPV/EHU)
Joxe Mari Korta Center - Avda. Tolosa,
7220018, Donostia-San Sebastian, SPAIN

Titre : Polymères Liquides Ioniques (PIL) Réactifs et Nanostructures à Partir de Copolymères à Blocs Composés d'un Bloc PIL

Résumé : L'objectif de ce travail de thèse a été de développer l'ingénierie des polymères liquides ioniques (PILs) de type imidazolium ainsi qu'une nouvelle famille de copolymères à blocs apparentés.

Des PILs type imidazolium ont été utilisés en tant que polymères réactifs pour la catalyse organique et la modification chimique par post-polymérisation. Divers composés (homopolymères, copolymères statistiques de type styrénique, polymères réticulés) stables à l'air, portant divers contre-anions (bromures, hydrogénocarbonates, carboxylates), ont été spécialement conçus *via* des stratégies de synthèse relativement simples. La génération de carbènes *N*-hétérocycliques supportés sur polymères (poly(NHC)s) a permis de comparer les performances catalytiques de tous ces précurseurs à travers des réactions de référence de la catalyse organique. Spécifiquement, les copolymères statistiques type styrénique peuvent également être fonctionnalisés de manière stœchiométrique par post-polymérisation avec différents substrats électrophiles (*e.g.* CS_2, isothiocyanate, métaux de transition).

Une nouvelle famille de copolymère à blocs contenant un bloc poly(acétate de vinyle) et un bloc de type poly(bromure de *N*-vinyl-3-alkylimidazolium), a été synthétisé par CMRP. La capacité de ces composés à s'auto-assembler en diverses mésostructures en masse comme en solution a ensuite été démontrée. Des mesures de conductivité ionique ont montré l'influence de la préparation des échantillons et des conditions de mesures sur les valeurs obtenues. Le comportement en solution par la réactivité ionique du bloc PIL et la modification chimique du bloc hydrophobe poly(acétate de vinyle) en hydrophile poly(alcool vinylique) ont permis la formation de différentes nanostructures micellaires.

Mots clés : Polymères liquides ioniques, Copolymères à blocs, Imidazolium, catalyse organique, Modification post-polymérisation, Auto-assemblage, Conductivité ionique, nanoparticules d'or.

Title: Reactive Poly(ionic liquid)s (PILs) and Nanostructures from PIL-based Block Copolymers

Abstract: The aim of this PhD work is to expand the scope of engineered imidazolium-based poly(ionic liquid)s (PILs) and their related PIL-block copolymers (PIL BCPs).

The use of the imidazolium-based PILs as true reactive polymers for organocatalysis and post-chemical modification is first described. Miscellaneous air-stable PIL derivatives featuring various counter-anions (*e.g.* bromides, hydrogen carbonates, carboxylates), including homopolymers, statistical copolymers of styrenic-type and crosslinked copolymer networks have been specifically designed by relatively simple synthetic strategies. The generation of related polymer-supported *N*-heterocyclic carbenes, poly(NHC)s, enables comparing the catalytic performances in selected organocatalyzed reactions. Specific polystyrene-based coPILs can be also stoichiometrically derivatized by post-chemical modification using various electrophilic substrates (*e.g.* CS_2, isothiocyanate, transition metals).

A novel family of imidazolium-based PIL BCPs, namely poly(vinyl acetate)-*b*-poly(*N*-vinyl-3-alkylimidazolium bromide)s synthesized by CMRP, is then described. The ability of these compounds to self-assemble into various types of mesostructures in bulk or in solution has been demonstrated. Ionic conductivity measurements evidenced the influence of sample preparation and measurement conditions. The behavior in solution evidenced *via* the ionic responsiveness of the PIL block but also by post-chemical modification of the hydrophobic poly(vinyl acetate) block into hydrophilic poly(vinyl alcohol) the formation of various micelle-like nanostructures.

Keywords: Poly(ionic liquid)s, Block copolymers, Imidazolium, Organocatalysis, Post-polymerization modification, Self-assembly, Ionic conductivity, Gold nanoparticles

---

Laboratoire de Chimie des Polymères Organiques
UMR 5629
16 avenue Pey-Berland
F-33607 Pessac